

https://dspace.org/

Design and development of a novel 3D bioprinted bone tissue engineered drug delivery scaffold for the treatment of Bone Fractures

Kondiah, Pariksha Jolene

2019

https://hdl.handle.net/10539/34135

Kondiah, P. J. Design and development of a novel 3d bioprinted bone tissue engineered drug delivery scaffold for the treatment of bone fractures. University of the Witwatersrand; Johannesburg: 2019

Downloaded from a DSpace repository. https://dspace.org/

DESIGN AND DEVELOPMENT OF A NOVEL 3D BIOPRINTED BONE TISSUE ENGINEERED DRUG DELIVERY SCAFFOLD FOR THE TREATMENT OF BONE FRACTURES

PARIKSHA JOLENE KONDIAH

A thesis submitted to the Faculty of Health Sciences, University of the Witwatersrand, in fulfilment of the requirements for the degree of
Doctor of Philosophy



Supervisors:
Professor Viness Pillay
Department of Pharmacy and Pharmacology, Faculty of Health Sciences,
University of the Witwatersrand, South Africa

Professor Yahya E. Choonara
Department of Pharmacy and Pharmacology, Faculty of Health Sciences,
University of the Witwatersrand, South Africa

Johannesburg
2019

DECLARATION

I, Pariksha Jolene Kondiah, declare that this thesis is my own work. It has been submitted for the degree of Doctor of Philosophy in the Faculty of Health Sciences at the University of the Witwatersrand, Johannesburg, South Africa. It has not been submitted before for any degree or examination at this or any other University.

.....

Signed on the ….. day of July 2019

RESEARCH OUTPUTS

Publications

1. Pariksha J. Kondiah, Yahya E. Choonara, Pierre P. D. Kondiah, Thashree Marimuthu, Pradeep Kumar, Lisa C. du Toit and Viness Pillay**.** A Review of Injectable Polymeric Hydrogel Systems for Application in Bone Tissue Engineering. *Molecules* 2016, *21*, 1580.

2. Pariksha J. Kondiah, Yahya E. Choonara, Pierre P.D. Kondiah, Pradeep Kumar, Thashree Marimuthu, Lisa C. du Toit, Viness Pillay. Development of an Injectable Pseudo-Bone Thermo-Gel for Application in Small Bone Fractures. *International Journal of Pharmaceutics* 2017, *520*, 39-48.

International Research Presentations

1. Development of an injectable tissue engineered thermo-gel drug delivery system for application in small bone fractures. Pariksha J. Kondiah, Pierre P. D. Kondiah, Pradeep Kumar, Thashree Marimuthu, Lisa C. du Toit, Yahya E. Choonara and Viness Pillay. 5th Nano Today Conference, Waikoloa Beach Marriott, Hawaii, USA, December 6th-10th, 2017**.** Poster presentation.

2. Design and evaluation of a 3D bioprinted implantable drug delivery scaffold for application in bone tissue engineering. Pariksha J. Kondiah, Pierre P. D. Kondiah, Pradeep Kumar, Thashree Marimuthu, Lisa C. du Toit, Yahya E. Choonara and Viness Pillay. 7th International Conference on Mechanics of Biomaterials and Tissues, Waikoloa Hawaii, USA, 10-14th December 2017. Oral presentation.

ANIMAL ETHICS DECLARATION

I hereby confirm that the following study entitled "*Design and Development of a Novel 3D Bioprinted Bone Tissue Engineered Drug Delivery Scaffold for The Treatment of Bone Fractures*" has received approval from the Animal Ethics Committee of the University of the Witwatersrand with ethics clearance number 2017/11/75D (Appendix 7.1).

PATENT FILED

Treatment of bone fractures and tissue engineering. Pariksha Jolene Kondiah, Viness Pillay, Yahya Essop. Choonara, Pierre Pavan Demarco Kondiah, Pradeep Kumar, Lisa Claire. du Toit, Thashree Marimuthu. Patent provisionally filed.

DEDICATION

This thesis is dedicated to the Lord of the Universe, Bhagawan Sri Sathya Sai Baba, for without Him nothing is possible.

ACKNOWLEDGEMENTS

My greatest appreciation to my Beloved Lord, Bhagawan Sri Sathya Sai Baba, for His abundant love and grace, and for guiding and guarding me through this journey.

My deepest gratitude to my amazing parents, Roshan and Joan Kondiah, and to my absolutely wonderful brothers, Pierre and Sailesh Kondiah, for your infinite love and support.

To my Supervisors, Professor Viness Pillay and Professor Yahya Choonara, my heartfelt thanks to you for your continuous guidance and supervision.

To Professor Lisa du Toit, Dr. Thashree Marimuthu and Dr. Pradeep Kumar, my sincerest appreciation for your wisdom and help through this academic path.

A sincere thank you to Professor Kennedy Erlwanger for your expertise, passion, dedication and commitment. Your scientific advice, effort and time invested in my research is greatly appreciated.

A special thanks to The Central Animal Services Unit, Kleinbooi Mohlabi and Mduduzi Sithole for their assistance during the *in vivo* investigations of my study.

ABSTRACT

Reconstruction of complicated bone defects remain a significant challenge, especially in patients with insufficient horizontal and vertical bone dimensions. Injury, age-related bone defects, and pathological disorders are a few of the most common impairments related to bone fractures. This generally results in an extensive healing time, and in some cases, relapses occur due to the therapy not reaching the specific site of fracture. Although autogenous bone grafts are predominantly deemed the gold standard for bone repair, their use is restricted due to increased donor site morbidity and graft resorption, as well as limited bone availability. Therefore, bone tissue engineered 3D constructs customized for patient-specific needs are being manifested as pseudo-bone scaffolds to improve bone repair and regeneration, as well as to increase bone cell and tissue differentiation. In this study, a 3D bioprinted pseudo-bone drug delivery scaffold was fabricated to display matrix strength, matrix resilience, as well as porous morphology, of healthy human bone. Polymers employed for formulating the 3D scaffold comprised of polypropylene fumarate (PPF), free radical polymerized polyethylene glycol- polycaprolactone (PEG-PCL-PEG) and pluronic (PF127). Simvastatin was incorporated into the 3D bioprinted scaffolds, to further promote bone healing and repair properties. The 3D bioprinted scaffold was characterized for its chemical, morphological, mechanical, *in vitro* and *in vivo* properties, for evaluation of its behavior for application as an implantable technology. Computer Aided Design (CAD) software was employed, for developing the 3D bioprinted scaffold. Further optimization of the bioink formulation was undertaken using MATLAB® software employing artificial neural networks (ANN). The 3D bioprinted scaffolds, evaluated as 39 design formulations using MATLAB® software, comprised of variables of PPF ($8\%^{w}/_{v}$ – $20\%^{w}/_{v}$) and PF127 ($14\%^{w}/_{v}$ – $16\%^{w}/_{v}$). These design scaffold formulations were studied in response to duration of release of simvastatin and the degree of thermo-gelation of the bioink formulation. It was observed that with incremental increases in the concentration of PPF at constant PF127 levels, a comparatively greater concentration of simvastatin was released for the formulations. This can be attributed to the increasing incompatibility created by the hydrophobic chain regions of PPF encapsulating simvastatin, a biopharmaceutics classification system (BCS) class 2 drug, at higher concentrations. The ANN-optimized 3D bioprinted scaffold displayed significant properties as a controlled release platform, demonstrating drug release over 20 days. The 3D bioprinted scaffold further displayed formation of a pseudo-bone matrix using a human clavicle bone model, induced with a butterfly fracture. The strength of the pseudo-bone matrix, evaluated for its Matrix Hardness (MH) and Matrix Resilience (MR), was determined to be as strong as healthy human clavicle bones, having a MH of 99% and a MR of 98%. Due to the porous nature of the 3D bioprinted scaffold, the strain distribution experienced by the scaffold ranged up to 13.2% over 60 sec, with a young's modulus of 26,5 Mpa. Ex-vivo cytology studies determined distinct MG-63 cells with greater density within the 3D scaffold matrix, observing filopodias growth around the entire scaffold architecture. At day-30, it was clearly noticed that cells employed the larger surface area of the scaffold, reaching confluence and covering almost the entire surface of the scaffold. MTT assay for determining cell viability over 30 days, demonstrated a positive cell density after cell seeding occurred. Biodegradation analysis of the 3D bioprinted scaffolds reflected a gradual loss in polymer mass, with an initial 18% loss with 10 days of evaluation. It was also reflected that the scaffold maintained its circular morphology throughout the degradation process, with at least over half of the mass degraded within 20 days. *In vivo* studies using New Zealand White Rabbits (NZW) confirmed that the nasal bones, after being induced with a nasal fracture and treated with the 3D bioprinted scaffold, demonstrated greater evidence of bone healing and new bone formation. Treatment with simvastatin displayed considerable bone growth and proliferation, compared to unloaded simvastatin 3D bioprinted scaffolds. In comparison to the control defect where no treatment was administered, it was observed that an increased rate of bone healing and regeneration occurred by administration of the 3D bioprinted scaffold. This result was supported by both by X-ray and histological analysis. Evaluation of the nasal bone induced fracture observed after treatment of the statin-loaded 3D bioprinted scaffold after 4 weeks, resulted in sample area of focal nasal bone regeneration, with mild periosteal reaction typical of new bone formation and prominent osteoblastic activity. Furthermore, evaluation of the nasal bone induced fracture observed after treatment of the non-statin-loaded 3D bioprinted scaffold after 4 weeks, reflected focal defects visible in the nasal bone with granulation tissue observed. It can thus be proved that the 3D bioprinted drug delivery scaffold has significant potential for application in bone fracture treatment, with substantial benefits for new growth and repair.

TABLE OF CONTENTS

DECLARATION i

RESEARCH OUTPUTS ii

ANIMAL ETHICS DECLARATION iii

PATENT FILED iv

DEDICATION v

ACKNOWLEDGEMENTS vi

ABSTRACT vii

LIST OF FIGURES xiii

LIST OF TABLES xvii

LIST OF ABBREVIATIONS xviii

CHAPTER 1 1

INTRODUCTION 1

1.1 Background into Bone Tissue Engineering 1

1.2. Rationale and Motivation for the Study 4

1.3. Possible Therapeutic Applications of the Delivery System 7

1.4. Novelty of the Delivery System 7

1.5. Aim and Objectives 8

1.6. Overview of the Thesis 9

1.7 Concluding Remarks 10

1.8 References 11

CHAPTER 2 14

A REVIEW OF INJECTABLE POLYMERIC HYDROGEL SYSTEMS FOR APPLICATION IN BONE TISSUE ENGINEERING 14

2.1. Introduction 14

2.2. Approaches to the Synthetic Fabrication of Injectable Hydrogels for Application in Bone Tissue Engineering 18

2.2.1 Thermo-Induced Gelation: Classical Poly(NIPAAm) 18

2.2.2 Ionic-Mediated Gelation: The Stimulation of Alginate 21

2.2.3 Free Radical Polymerized Gelation: The Essential Vinyl Monomer 22

2.2.4 Self-Assembled Gelation: The Independent Amphiphiles 24
2.2.5 Chemically Crosslinked Gelation: The Sentimental Alkynes, Azides and Amines 25
2.3. Polymers Employed for the Synthesis of Stimuli-Responsive Hydrogel Systems 26
2.3.1 Natural Polymers 26
2.3.1.1 Hyaluronic acid 26
2.3.1.2 Chitosan-based hydrogels 27
2.3.1.3. Cellulose derived hydrogels 29
2.3.1.4 Other natural polymers 30
2.3.2 Synthetic Polymers 32
2.3.2.1. Polyacrylamide derived thermo-responsive hydrogels 32
2.3.2.2. Poly (oligo (ethylene glycol) methacrylate) derived thermo-sensitive hydrogels 33
2.3.2.3. Polyphosphazene derived thermo-sensitive hydrogels 34
2.3.2.4. Pluronic derived thermo-sensitive hydrogels 34
2.3.2.5 PEG-polyester derived thermo-sensitive hydrogels 35
2.4. Injectable/Implantable Research Technologies Employed in Bone Tissue Engineering Applications 39
2.4.1 Research Focused on Biomedical Applications 39
2.4.1.1. Bone repair 39
2.4.1.2. Regeneration of bone tissue 40
2.5. Nano-Enabled Thermo-Responsive Hydrogel Systems 41
2.6. Advancing the Efficacy of Hydrogels in Drug Delivery Applications 43
2.6.1. Drug-hydrogel interactions 43
2.6.1.1. Physical interactions 43
2.6.1.2 Covalent bonding 44
2.7. Analogous Cell and Biomaterial Characterization for *In Vitro* Success and *In Vivo* Translation 44
2.8. Current Research Approaches to Date 45
2.9. Concluding Remarks 47
2.10. References 48

CHAPTER 3 62

DEVELOPMENT OF AN INJECTABLE PSEUDO-BONE THERMO-GEL FOR APPLICATION IN SMALL BONE FRACTURES 62
3.1. Introduction 62

3.2. Materials and Methods 64
3.2.1 Materials 64
3.2.2 Synthesis of Poly (Propylene Fumarate) (PPF) 64
3.2.3 Copolymer Blend to Form the Pseudo-bone Thermo-gel....65
3.2.4 Chemical Evaluation Undertaken on the Pseudo-bone Thermo-gel....67
3.2.5 Determination of Thermal Characteristics of the Monomers, Polymers and the Pseudo-bone Thermo-gel....67
3.2.6 Determination of Viscoelastic Properties of the Pseudo-bone Thermo-gel 68
3.2.7 Surface and Structural Morphological Evaluation of the Pseudo-bone Thermo-gel....68
3.2.8 In Vitro Drug Release of the Pseudo-bone Thermo-gel 68
3.2.9 Inducing a Butterfly Bone Fracture and Evaluating Fractal Dimensions on Human Clavicle Bones....69
3.3. Results and Discussion 70
3.3.1 Chemical Evaluation Undertaken on Monomers, Polymers and the Pseudo-bone Thermo-gel....70
3.3.2 Thermal Evaluation of the Monomers, Polymers and the Pseudo-bone Thermo-gel....75
3.3.3 Determination of Storage and Loss Modulus of the Pseudo-bone Thermo-gel 77
3.3.4 Surface and Structural Morphological Evaluation of the Pseudo-bone Thermo-gel....78
3.3.5 *Ex-vivo* Evaluation of the Pseudo-bone Thermo-gel Using Ultrasound and X-ray Evaluation for Determination of Matrix Hardness and Matrix Resilience on Human Clavicle Bones....80
3.3.6 *In Vitro* Analysis of the Pseudo-bone Thermo-gel....82
3.4. Concluding Remarks 84
3.5 References....85

CHAPTER 4 90

3D BIOPRINTED PSEUDO-BONE DRUG DELIVERY SCAFFOLD FOR BONE FRACTURE IMPLANTATION....90
4.1. Introduction 90
4.2. Materials and methods 91
4.2.1 Materials 91
4.2.2 Synthesis of the bioink formulation 92
4.2.3 Artificial neural network design and optimization of the 3D bioprinted scaffold 92
4.2.4 3D design of the bioprinted pseudo-bone drug delivery scaffold....96

4.2.5 Chemical and thermal evaluation of the 3D bioprinted pseudo-bone scaffold 98
4.2.6 Morphological analysis of the 3D bioprinted pseudo-bone scaffold 98
4.2.7 In vitro drug release evaluation on the designed 3D bioprinted pseudo-bone drug delivery scaffolds 99
4.2.8 Textural analysis of the human clavicle bone and 3D bioprinted pseudo-bone scaffold 99
4.3. Results and Discussion 100
4.3.1 Design and optimization of the 3D bioprinted pseudo-bone drug delivery scaffold employing artificial neural networks 100
4.3.2 Chemical and Thermo-gravimetric analysis of the optimized 3D bioprinted pseudo-bone scaffold 103
4.3.3 Morphological analysis undertaken on the 3D bioprinted pseudo-bone scaffold 106
4.3.4 *In vitro* analysis of the designed 3D bioprinted drug delivery scaffolds 108
4.3.5 Matrix analysis of the 3D bioprinted scaffold in fracture-induced human clavicle bones 110
4.4. Concluding Remarks 111
4.5 References 112

CHAPTER 5 115

TAILOR DESIGNING OF THE 3D BIOPRINTED SCAFFOLD FOR BIOCOMPATIBILITY AND *IN VIVO* APPLICATION EMPLOYING A NEW ZEALAND WHITE RABBIT MODEL 115
5.1. Introduction 115
5.2. Materials and Methods 116
5.2.1 Materials 116
5.2.2 Tailor Designed 3D Bioprinted Pseudo-bone Drug Delivery Scaffold 117
5.2.3. Biomaterial Testing Undertaken on the Tailor Designed 3D bioprinted Scaffold 119
5.2.4 *In Vitro* Cell Culture Studies Undertaken on the Tailor Designed 3D Bioprinted Drug Delivery Scaffold and *In Vitro* Biodegradation Analysis 119
5.2.5. In Vivo Evaluation of the Tailor Designed 3D Bioprinted Drug Delivery Scaffold Employing a New Zealand White Rabbit Model 120
5.2.6. Immunohistochemistry Evaluation of the Induced Nasal Bone Fracture Samples, Following *In Vivo* Evaluation 121
5.3. Results and Discussion 122
5.3.1 Physicomechanical Analysis Undertaken on the Tailor Designed 3D Bioprinted Scaffold 122

5.3.2 *In Vitro* Cell Culture Studies Undertaken on the Tailor Designed 3D Bioprinted Drug Delivery Scaffold and *In Vitro* Biodegradation Analysis 124
5.3.3 *In Vivo* Evaluation of the Tailor Designed 3D Bioprinted Drug Delivery Scaffold Employing a New Zealand White Rabbit Model 128
5.4. Concluding Remarks 134
5.5. References 134

CHAPTER 6 137

CONCLUSION AND FUTURE RECOMMENDATIONS 137
6.1 Conclusion 137
6.2 Future Outlook and Recommendations 138
7. APPENDICES 141
7.1. Animal Ethics Clearance Certificate 141
7.2 International Published Review Paper 142
7.3 International Published Research Paper 1 143
7.4 5th Nano Today Conference, Waikoloa Beach Marriott, Hawaii, USA, December 6th-10th, 2017. Poster presentation. 144
7.5 7th International Conference on Mechanics of Biomaterials and Tissues, Waikoloa Hawaii, USA, 10-14th December 2017. Oral presentation 145

LIST OF FIGURES

Figure 1.1: Schematic representing the 3D printed scaffold drug delivery system for bone tissue engineering at the site of a fractured bone.

Figure 2.1: Schematic representing the outlined procedure undertaken for tissue engineering and drug delivery (Adapted with permission from Khan et al, 2015).

Figure 2.2: Physical gelation system derived from increased temperature due to interaction of hydrophilic and hydrophobic blocks for promoting an amphiphilic polymer.

Figure 2.3: Free radical polymerization steps involved in copolymerization techniques.

Figure 2.4: Chemical structures of selected most commonly used thermo-responsive polymers discussed in application for drug and tissue engineering (adapted with permission from Matanovic et al., 2014).

Figure 2.5: Schematic representation of tissue engineering application, delivering drug-loaded thermo-sensitive polymers with bioactive signals.

Figure 3.1: Schematic representation of the synthesis for PPF, using a 2-step method involving bis(hydroxypropyl) fumarate as an intermediate.

Figure 3.2: Schematic representation strategy undertaken for the preparation of the copolymer blend

Figure 3.3: H^1 NMR evaluation for monomers, polymers and the pseudo-bone thermo-gel; **(a)** PEG_{4000}, **(b)** PEG-PCL-PEG, **(c)** PPF and **(d)** Pseudo-bone thermo-gel.

Figure 3.4: ATR-FTIR analysis undertaken on; **(a)** PEG_{4000}, **(b)** PEG-PCL-PEG **(c)** PPF and **(d)** Pseudo-bone thermo-gel.

Figure 3.5: XRD analysis undertaken on **(a)** PEG_{4000}, **(b)** PEG-PCL-PEG **(c)** PPF and **(d)** Pseudo-bone thermo-gel.

Figure 3.6: DSC undertaken on monomer, polymers and the pseudo-bone thermo-gel; **(a)** PEG_{4000}, **(b)** PCL, **(c)** PEG-PCL-PEG, **(d)** PF127, **(e)** PPF and **(f)** Pseudo-bone thermo-gel.

Figure 3.7: Rheological evaluation of the pseudo-bone thermo-gel in relation to change in temperature.

Figure 3.8: Morphological evaluation undertaken, reflecting; **(a)** SEM analysis on the pseudo-bone thermo-gel, **(b)** TEM analysis on the pseudo-bone thermo-gel; and **(c)** comparative SEM imaging of human bone under high magnification.

Figure 3.9: X-ray and ultra sound images undertaken on a human clavicle osteoporotic female bone; **(a)** X-ray image before inducing a fracture on the human clavicle specimen, **(b)** Ultra-sound image before inducing a fracture on the human clavicle specimen, **(c)** X-ray image after inducing a fracture on the human clavicle specimen, **(d)** Ultra-sound image after inducing a fracture on the human clavicle specimen, **(e)** X-ray image after treatment with the pseudo-bone thermo-gel at the site of the fracture induced human clavicle specimen, **(f)** Ultra-sound image after treatment with the pseudo-bone thermo-gel at the site of the fracture induced human clavicle specimen.

Figure 3.10: *In vitro* analysis of the pseudo-bone thermo-gel with variation in concentrations of % PPF and temperature conditions over 24 hours. F1 and F3 were blended as 8%$^{w}/_{v}$ PPF, and F2 and F4 as 20%$^{w}/_{v}$ PPF. F1 and F2 were evaluated at room temperature (±25°C), F3 and F4 at body temperature (±37.5°C).

Figure 3.11: *In vitro* analysis of the pseudo-bone thermo-gel with variation in concentrations of % PPF and temperature conditions over 14 days. F1 and F3 were blended as 8%$^{w}/_{v}$ PPF, and F2 and F4 as 20%$^{w}/_{v}$ PPF. F1 and F2 were evaluated at room temperature (±25°C), F3 and F4 at body temperature (±37.5°C).

Figure 4.1: CAD specification design of the optimised 3D bioprinted scaffold.

Figure 4.2: 3D representation of the ANN design formulations, reflecting the percentage of PPF and PF127, with the optimization factor for each formulation.

Figure 4.3: 3D representation of the designed bioink formulations using a cubic function surface plot, with the highest point on the surface plot representing the optimum polymer concentrations.

Figure 4.4: Gelation temperature of the 39 bioink design formulations prior to 3D printing.

Figure 4.5: NMR analysis of the 3D bioprinted pseudo-bone scaffold, reflecting chemical shifts and copolymeric composition.

Figure 4.6: TGA analysis undertaken in the region of 30°C to 900°C for **(a)** PEG-PCL-PEG, **(b)** PF127, **(c)** PPF and **(d)** 3D bioprinted scaffold.

Figure 4.7: SEM analysis of the 3D bioprinted scaffold at 3500 times magnification, demonstrating the micro-architecture and inner porous nature of the 7 layers of the designed 3D scaffold matrix.

Figure 4.8: *In vitro* simvastatin release analysis of the designed 3D bioprinted drug delivery scaffolds.

Figure 4.9: Correlation of *in vitro* simvastatin release analysis of the optimized 3D bioprinted scaffold with predicted release kinetics using ANN modelling.

Figure 4.10: X-ray images of the human clavicle bone **(a)** before fracture, **(b)** after fracture and **(c)** after treatment with the 3D bioprinted scaffold respectively. **(d)** Light microscope image at 24 times magnification of the 3D bioprinted scaffold immersed in phosphate buffer solution, **(e)** human clavicle bone induced with a fracture, representing missing bone fragments, **(f)** human clavicle bone tested after incubation at 37.5°C for 2 hours, demonstrating sealing of the induced fracture site, with properties of matrix hardness and resilience comparable to original bone properties.

Figure 5.1: CAD specification design of the tailor designed 3D bioprinted scaffold for implantation in a nasal bone fracture induced rabbit model.

Figure 5.2: Diagram illustrating the superior view of rabbit skull, with induced surgical bone defects. a) represents a rabbit skull diagram of the induced surgical procedure undertaken on the

rabbit nasal bone; b) representing the actual surgical procedure undertaken on the rabbit model, reflecting the implantation of the scaffold on the right of the nasal bone defect and left reflecting the control.

Figure 5.3: Biomaterial testing analysis undertaken on the 3D printed scaffold, illustrating a) tracking and x-y forces experienced on the scaffold, and b) illustrating young's modulus, indicating the stress and strain experienced on the scaffold.

Figure 5.4: Representation of a) cell viability analysis using MG63 cells, seeded on the 3D bioprinted scaffold, evaluated over 30 days; b) biodegradation analysis of the scaffold undertaken over a 30-day period.

Figure 5.5: SEM (3350-3500X magnification) and light microscope (10X magnification) images reflecting cell seeding on the 3D bioprinted scaffold, captured on respective days; a) day-0, b) day-10, c) day-20 and d) day-30. As seen in the figure, the cell proliferation within the scaffold clearly increasing over day-0 to day-30, with exponential cell growth over time.

Figure 5.6: X-ray images reflecting nasal bone defects by surgical inducement. It was observed that the statin-loaded 3D bioprinted scaffold displayed greater bone regenerative properties after 4 weeks of the study than the non-statin loaded 3D bioprinted scaffold. However, significant bone regeneration and healing was observed in the non-statin loaded 3D bioprinted scaffold in comparison to the control, attributed to the copolymeric nature of the 3D printed scaffold.

Figure 5.7: Histological evaluation of the nasal bone induced fracture after treatment with; a) 3D scaffold loaded with simvastatin after 4-week evaluation illustrating prominent osteoblastic activity; b) 3D scaffold loaded with simvastatin after 2-week evaluation with mild periosteal reactions and peripheral new bone formation; c) 3D scaffold loaded with no simvastatin after 4-week evaluation with new bone formation noted on the periphery with osteoblastic activity, d) 3D scaffold loaded with no simvastatin after 2-week evaluation reflecting osteoblastic activity and surrounding granulation tissue.

LIST OF TABLES

Table 2.1: Summary of injectable hydrogels for tissue engineering.

Table 4.1: Design specifications of the 3D bioprinted scaffold formulations using MATLAB Simulink®.

Table 4.2: Specification design dimensions of the 3D bioprinted scaffold using Autodesk Inventor®

Table 4.3: 3D bioprinting parameters of the drug delivery scaffold employing the 3D Bioplotter®

Table 4.4: Thermal evaluation of the 3D bioprinted pseudo-bone scaffold using a TGA 4000 thermogravimetric analyser.

Table 4.5: Parameters of textural analysis of the human clavicle bone and 3D bioprinted scaffold for determination of MH and MR.

Table 4.6: Training functions undertaken for optimisation of the design formulations.

Table 5.1: Design dimensions of the 3D bioprinted pseudo-bone scaffold using Autodesk Inventor® of the polymer based material.

Table 5.2: 3D printing parameters of the tailor designed pseudo-bone drug delivery scaffold employing the 3D Bioplotter®.

LIST OF ABBREVIATIONS

ALP- Alkaline Phosphatase

ANN- Artificial Neural Networks

API- active pharmaceutical ingredient

ATR-FTIR- Attenuated Total Reflectance-Fourier Transform Infrared

BCP- Biphasic Calcium Phosphate

BCS- Biopharmaceutics Classification System

Bfgf- Fibroblast Growth Factor

BMP -2- Bone Morphogenic Proteins -2

BMPs- Bone Morphogenic Proteins

CA- Cellulose Acetate

CAD- Computer-Aided Design

CaP- Calcium Phosphate

CAS- Central Animal Services

ChS-F- Furfurylamine Grafted Chondroitin Sulfate

CMC- Carboxymethyl Cellulose

DCl_3- Deuterated Chloroform

DCM- Dichloromethane

DTPH–HA- Dithiodipropionate Hydrazide-Modified HA

DX- P-dioxanone

EBM-2- Endothelial Cell Growth Basal Medium-2

ECM- extra cellular matrix

EMEM- Eagle's Minimal Essential Medium

GP- Glycerophosphate

HA- Hyaluronic Acid

HAP- Hydroxyapatite

HCl- Hydrochloric Acid

HE- Hematoxylin and Eosin

HEMA- Hydroxyethyl Methacrylate

HPA- Hydroxyphenylpropionic Acid

HPMC- Hydroxypropyl Methyl Cellulose

HRP- Horseradish Peroxidase

HTCC- N-(2- hydroxyl) Propyl-3-Trimethylammonium Chitosan Chloride

HTEC- N-(2-hydroxyl) Propyl-3-Triethyl Ammonium Chitosan Chloride

IleOEt- L-isoleucine Ethyl Ester

IPN- Interpenetrating Network

LCST- Lower Critical Solution Temperature

LEV–PEG–LEV- Polyethylene Glycol Dilevulinate

MBAAm- Methylenebisacrylamide

MEO_2MA- 2-(2-methoxyethoxy) ethyl methacrylate

MH- Matrix Hardness

Mpeg-PCL- Methoxy-terminated PEG-PCL

MR- Matrix Resilience

MTT- Methyl Thiazoly Tetrazolium

Mw- Molecular Weight

NHPDCS- N-(2-hydroxyl-phenyl)- N,N-dimethyl Chitosan

NHS- N- hydroxysuccinimide

NIPAAm- N-isopropylacrylamide

NMR- Nuclear Magnetic Resonance

OC- Osteocalcin

OEGMA- Oligo (ethylene glycol) Methacrylate

OligoLA-HEMA- oligolactide-(2- hydroxymethyl methacrylate)

P- Pullulan

PBS- Phosphate-Buffered Saline

PCL- Polycaprolactone

PCLLA- Poly (caprolactone-co-lactide)

PDO- Polydioxanone

PEG- Poly(ethylene glycol)

PEG2K–AMI- Maleimido-terminated Poly (ethylene glycol)

PEGMA- Poly(ethylene glycol) Methacrylate

PEO- Poly (ethylene oxide)

PEO-PPO-PEO- poly (ethylene oxide)-b-poly (propylene oxide)-b-poly (ethylene oxide)

PF-127- Pluronic 127

PGA- Polyglycolide

PHEMA- Poly(2-hydroxyethyl methacrylate)

PL- Platelet Lysate

PLA- Polylactide

PLG- Poly (lactide-co-glycolide)

PLGA- Poly(lactide-co-glycolide)

PNIPAAm- Poly(N-isopropylacrylamide

POEGMA- Poly (oligo (ethylene glycol) methacrylate)

PPF- Poly (propylene fumarate)

PPF- Poly-propylene Fumarate

PVCL- Polyvinyl chloride

PVP- Poly (N-vinyl pyrrolidone

RBF- Round Bottom Flask

SBF- Simulated Body Fluid

SEM- Scanning Electon Microscopy

SMO- Sulfamethazine Oligomer

$Sn(Oct)_2$- Stannous Octoate

SNP- Silicon Nanoparticles

STL- Stereolithography

STMP- Trisodium Trimetaphosphate

TEM- Transition Electron Microscopy

TG- Transglutaminase

TGA- Thermogravimetric Analysis

TGS- Thermally-induced Gelation Systems

TMC- Trimethyl Chitosan

US- United States

VPTT- Volume Phase Transition Temperature

XRD- X-ray Diffraction

Zn-TPP- Zinc Tetraphenylporphyrin

$ZnCl_2$- Zinc chloride

CHAPTER 1
INTRODUCTION

1.1 Background into Bone Tissue Engineering

Skeletal fractures are predominantly common in adults following trauma due to the absence of the thicker adipose tissue, which is found in children (Zimmermann, et al., 2005). Nonetheless, research shows that one child in a population of 500 000 people requires treatment for bone fractures each day (Gassner, et al., 2004). In cases of multiple traumas, children with injuries respond better than their adult counterparts due to greater active bone proliferation factors and adipose tissue supporting collision events (Mayer, et al., 1980). However, it should be noted that there are various challenges in the management of skeletal fractures in children, example, mandibular fractures resulting in translocation of metal plates and screws, which are often used for managing such conditions, risking potential growth and teeth disturbances, as well as secondary removal depending on the degree of damage (Eppley, et al., 2005). For patients with poor prognosis, early surgery might be beneficial; however, age is a very important determinant of the prognosis index, with older patients having a lesser probability of complete recovery (Robinson, et al., 2005). Certain pathological conditions such as hypovolemia, hypothyroidism, diabetes mellitus and peripheral vascular disease, which impede bone formation, complicate the problem even further.

Malunion of bones following a fracture can present with symptoms such as pain, loss of strength, rapid fatigue, numbness of the arm and hand, problems sleeping on the back as well as cosmetic inconvenience (Hillen, et al., 2010). Kitsis and co-workers revealed that the average time of symptom resolution following surgery can take up to 7 months, with the average time to return to work being 8 months. There is much controversy with regard to patients requiring surgery following a bone fracture. Surgical intervention following a clavicle fracture is indicated in cases where skin tenting, open fractures, presence of neurovascular damage results in multiple trauma complications (Kitsis, et al., 2003, Paladini, et al., 2012). In addition to this, surgery increases the risk of infection in these complicated conditions, worsening the effects of pain and internal tissue damage to a significant degree (Coleman, et al., 1997).

For treating these conditions of bone injuries, biodegradable, stimuli-responsive polymers are essential platforms for application of bone tissue engineering. Various thermo-responsive hydrogels display water based homogenous properties to encapsulate, manipulate and transfer its contents to the surrounding tissue, in the least invasive manner. A hydrogel is a network of polymer chains that are water-insoluble, which is sometimes found as a colloidal gel, in which water is the dispersion medium. A thermo-gel is a hydrogel, which has thermo-responsive properties, behaving as a solution at room temperature, and changing its physical properties at body temperature, thereby forming a semi-solid elastic material and releasing its loaded content.

The success of bioengineered injectable tissue modified delivery systems, are significantly dependent on chemical, physical and biological properties. Irrespective of shape and defect geometry, injectable therapy has an unparalleled advantage in which intricate sites of therapy can be effortlessly targeted with minimally invasive procedures. Stimuli-responsive hydrogel systems enhance cellular responses and cell distribution at any site prior to the transitional phase leading to gelation. The substantially hydrated nature allows significant simulation of the extra cellular matrix (ECM), due to its similar structural properties. Significant current research strategies have been identified and reported to date by various institutions, with particular attention to thermo-responsive hydrogel delivery systems, and their pertinent focus to bone tissue engineering.

Prior to technology of current times, peptides which inhibit bone resorption have been developed for parenteral administration as well as systemic application (Aoki, et al., 2012). Following the use of statins, these anabolic agents have shown significant results in bone repair at doses similar to the lipid-lowering doses used in humans (Mundy, et al., 1999). Simvastatin has been proved to successfully promote bone growth and healing, with substantial positive results explained. Simvastatin has low oral bioavailability and poor aqueous solubility, categorised as a Biopharmaceutics Classification System (BCS) class II drug. Its oral dosage also reacts to various side effects, and absorption of the drug varies, hence the need for injectable technology to deliver site specific therapeutic advancement (Tiwari, et al., 2011). Thermo-responsive injectable hydrogels have gained much popularity as carrier systems because of their ability to remain in solution at lower temperatures and maintain a semi-gel matrix at body temperature (Qiao, et al., 2013). Bone Morphogenic Proteins (BMPs) have been shown to increase the formation of new bone development in animal studies, however, there are some undesirable effects associated with the use of BMPs, namely, high costs, unwanted ectopic bone formation, and local inflammatory reactions (McGovern, et al., 2010). Results have shown that simvastatin gel

implantation in mice yielded 159 -172% increases in bone thickness and 144 -180% increase in bone area, significantly providing a supportive mechanism for bone reformation (Calixto, et al., 2011). The mechanism through which simvastatin enhances bone formation is through induction of bone metabolism agents namely, Bone Morphogenic Proteins -2 (BMP -2), Alkaline Phosphatase (ALP) induction as well as type I collagen (Maeda, et al., 2001). Results obtained from Chen and co-workers further emphasised that expression of BMP-2 and ALP mRNA was significantly greater in simvastatin treated mice than in the control groups for both agents (Chen, et al., 2010).

Nanotechnology is a valuable advancement for specific drug delivery due to significant bioavailability and enhanced absorption of various drugs and biological compounds. This technique uses materials of nanometer scale, often in the form of polymeric nanoparticles to interact with biological systems at a molecular level (Modi, et al., 2009). The use of fibrin glue in bone formation has proven to be effective, however, bone glue has the disadvantage of limiting diffusion of Bone Morphogenic Proteins (BMPs) and thereby limiting bone formation (Patel, et al., 2006). The release rate of the transported biological factors are determined by diffusion rate, ionic interaction, degradation of the polymer, swelling of the polymer and site specific dissolution for absorption (Mehta, et al., 2012). The use of hydrogels as a vehicle for therapeutics promotes wound healing as well as cartilage/ bone regeneration through sustained release of the bioactive materials (Bae, et al., 2014).

The properties of a thermo-gel refer to a system by which a substance undergoing change must in all instances be in thermodynamic equilibrium with its surroundings. The pressure and temperature of the substance should differ minimally from its surroundings at a stage of slow cycle operation. Frictional forces must be minimum, with least loss of energy due to conduction, convection or radiation during the cycle process (Egner, et al., 2016, Lucia, et al., 2016, Santapuri, et al., 2016). The transition from sol to gel, correspond to a change in temperature conditions. However, once substantial energy is dissipated from the system and thermodynamic equilibrium is lost, the system will lose its gelation nature. In an injectable thermo-gel system, due to minimum interferences from its environment *in situ*, properties of its responsive nature will be preserved in a substance/material at a given temperature range. Properties such as stability, biocompatibility and biodegradability are conserved when physiological conditions are maintained (Deng, et al., 2014, Nguyen, et al., 2015, Jung, et al., 2017).

This research thus focused on the formulation of a novel 3D printed scaffold which was optimized using a bioink formulation. The formulation was loaded with a suitable active pharmaceutical ingredient (API), and evaluated for its chemical, physical and rheological properties. A successful design and evaluation of a novel bioink formulation was accomplished. This bioink formulation was composed of unique copolymers, synthesized using ring opening free radical polymerization chemistry, strategically modifying hydrophilic and hydrophobic block polymers. The mechanism of this technology behaved in a thermo-responsive manner.

Thereafter, the bioink formulation was used to optimize a bone tissue engineered drug delivery scaffold that was implanted *in situ*, using 3D bio-plotting technology and stimuli-responsive copolymers for greater bone fracture repair and healing properties. This bone tissue engineered drug delivery scaffold also delivered encapsulated MG-63 cells, providing a fitting environment for osteoblastic differentiation *in situ*. This technology will thus substantially reduce the risk of fatal surgical complications derived from bone fracture surgical treatment, thereby reducing the invasive procedures and improve the quality of life of people affected with such fracture related injuries.

1.2. Rationale and Motivation for the Study

Skeletal fractures following various accidental incidents often result in several debilitating symptoms such as pain, bruising, swelling as well as malunion of bones. Management of these fractures can occur by providing support for bone healing, surgery and holding the fracture in position by means of pins. Complications may arise during these procedures, such as malunion of pins used to support the bones or infections arising from certain surgery procedures. In some instances, where fractures occur in positions where casts and pins cannot assist in the repair of the fracture; such as clavicles, wrists, phalanges, nasal septum's and many other small bone areas; this technology proposed will have significant benefits and direct healing *in situ*. Certain disease states such as diabetes and autoimmune conditions, further delay the wound healing process, in which case, direct delivery at the site of injury would be the most efficient and effective form of therapy. The loaded statin drug also promotes significant bone healing in patients taking long term corticosteroid therapies, assisting with bone strengthening at sites of weaken loading bearing areas such as hips and shoulders, with particular importance in post-menopausal women on chronic corticosteroid therapy. Patients with bone fractures usually heal within 3 months of

their injury, however, direct treatment into the bone results in enhanced bioactive activity, with a much shorter duration of recovery.

To date, 3D printed scaffolds for application in tissue engineering in the field of orthopedic sciences has produced many benefits over previous application methods. 3D printed scaffolds are appealing for use in bony defects because they have a unique advantage in which difficult sites of injury can be easily targeted with least invasive procedures, forming a composite, irrespective of shape and defect geometry. 3D Scaffold drug delivery systems can be used to fill critical-size bone defects and injuries in non-load bearing sites, even though they do not have the mechanical strength that is needed to provide support for load-bearing functions. Furthermore, this form of delivery can enhance physico-mechanical properties of injured/pathological bone, delivering a variety of bio-actives, drug molecules, as well as growth factors for therapeutic application.

After successfully designing and evaluating the novel bioink formulation, a 3D bioprinted scaffold was optimized. The 3D bone tissue engineered scaffold behaved in a thermo-responsive manner, swelling to a desired ratio, releasing its encapsulated cells and drug *in situ*. The scaffold possessed considerable matrix hardening properties, sufficient elastic resilience and stimuli-responsive characteristics. Detailed flow simulations and artificial neural network designs were undertaken for evaluating the 3D scaffold technology. *In vivo* studies (at the Central Animal Services, (CAS) at the University of the Witwatersrand) using a rabbit model was undertaken once sufficient *in vitro* and *ex vivo* evaluation was completed. Human bone specimens were also used for *ex vivo* evaluation of the 3D scaffold technology, with ethical permissions and waivers granted from the Faculty of Anatomical Sciences at the University of the Witwatersrand. Figure 1.1 depicts schematic representation of the 3D scaffold technology.

The mechanism through which the 3D scaffold drug delivery system reacted *in situ*, followed a temperature responsive release approach, forming a matrix hardness and resilience similar to bone tissue. This bioengineered 3D scaffold was implanted at the site of the fracture, with a controlled release kinetics over 20 days of sustained delivery. The biomatrix 3D scaffold significantly enhanced bone tissue formation through enhanced differentiation and proliferation of osteoblasts.

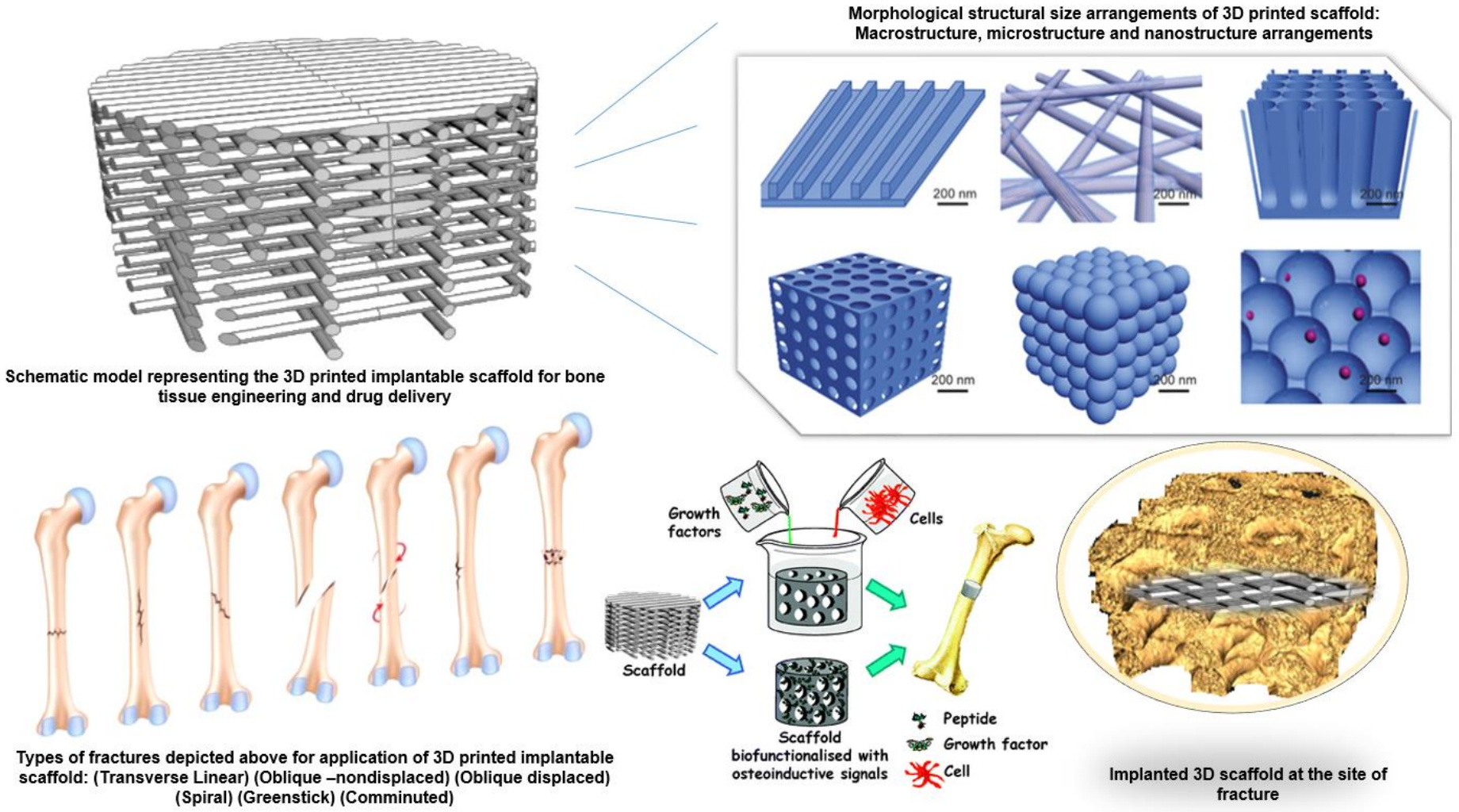


Figure 1.1: Schematic representing the 3D printed scaffold drug delivery system for bone tissue engineering at the site of bone fracture.

1.3. Possible Therapeutic Applications of the Delivery System

Developing a 3D scaffold drug delivery system for bone tissue engineering has been an area of significant concern in current times, taking into consideration the need for time dependent controlled kinetic properties, aiming at achieving maximum bone growth and repair, in the least time duration (Khoshroo, et al., 2017). This unique implantable copolymeric 3D scaffold drug delivery system was analysed loading simvastatin, which further promoted bone growth and repair. The following possible therapeutic applications included, but were not excusive to:

- Clavicle/ rib/ cranial/ facial fractures following trauma, either through a fall onto the shoulder or motor vehicle collision.
- Clavicle/ rib/ cranial/ facial fractures where applying a cast or traction is impractical.
- Large bone fractures, where direct adhesive bone support is required
- Skeletal fractures in menopausal women.
- Age related skeletal fractures.

The bioink formulation demonstrated significant *in vitro* and *ex vivo* outcomes. The next stage of the study was directed at further promoting a controlled kinetic technology, which modified the surface area and particle dimensions and resulted in an optimum bioengineered bone tissue scaffold. The degree of success in the 3D engineered drug delivery scaffold was evaluated using in depth cell tissue *ex vivo* evaluation, using real time analysis for obtaining high resolution cell encapsulation of the loaded drug. *In vivo* studies were undertaken in a rabbit model which demonstrated significant bone regeneration and repair. In addition, ANN and analytical optimization was undertaken on the implantable technology, which determined the efficacy, efficiency and bioavailability of the 3D bioengineered delivery system. Further flow dynamic modelling was undertaken to obtain rheological mechanistic flow properties, which evaluated integrated dynamic mechanisms of particle charge, as well as dose enhancing coefficient loading and release kinetics.

1.4. Novelty of the Delivery System

The following advanced attributes ascribed to the novelty of the research.
A novel 3D printed scaffold drug delivery system comprising of poly-propylene fumarate (PPF), a triblock polymer of polyethylene glycol and polycaprolactone (PEG-PCL-PEG), pluronic 127 (PF-127) and loaded with simvastatin drug, was designed using CAD software. Its thermo-responsive

nature and swelling kinetics were also evaluated. Physiochemical and physiomechanical studies were undertaken on the developed 3D scaffold drug delivery system. The bioink formulation and 3D technology were evaluated *in vitro* and *ex vivo,* as well as *in vivo* evaluation of the 3D printed scaffold. All *in vitro* drug release studies were undertaken using dialysis tubing, for precise evaluation of drug release analysis. Further toxicology studies were employed on the 3D printed scaffold to prove non-toxicity of the system, and determine other effects the delivery system will have on specific organs/tissues. Inducement of a small bone fracture in the nasal septum of a rabbit was undertaken for precise determination of bone growth and repair. The bioink formulation and the 3D printed scaffold were evaluated for its thermo-sensitive properties, determining the efficacy of the copolymeric system, as well as its pH responsive nature, thereby proving complete stability of the technologies *in situ*. A slow release delivery system, lasting a minimum of 20 days was a major characteristic of the 3D scaffold drug delivery system, thereby promoting less patient frequent treatment, promoting patient compliance.

In silico statistical modeling was undertaken on the 3D printed scaffold to attain maximum viable results for proving the concept of a sustained release thermo-reversible implantable bone tissue engineered drug delivery system. NMR, TEM, SEM, FTIR, XRD, DCS, TGA as well rheological evaluation were undertaken on all formulations, to determine its essential characteristic behaviour and classification. Monte Carlo simulation and analytical optimization will be undertaken on both injectable and implantable technologies. Further flow dynamic modelling was undertaken to obtain rheological mechanistic flow properties, evaluating integrated dynamic mechanisms of particle charge, as well as dose enhancing coefficient loading and bioavailable dose concentrations. MG-63 cell culture studies were undertaken for incorporation in the 3D scaffold drug delivery system, and further cell toxicity studies were undertaken, proving the biocompatible nature delivery system.

1.5. Aim and Objectives

The aim of the study was to design a 3D scaffold bone tissue engineered drug delivery system, for the treatment of bone fractures. This system was loaded with a statin drug and evaluated for its *in vitro*, *ex vivo*, *in silico* and *in vivo* properties. The 3D scaffold bone tissue engineered drug delivery system was stimuli responsive, providing maximum efficient pharmacokinetic responses, for significant bone repair and healing.

The following objectives were defined for the study:

1. Development of a copolymeric system, loaded with simvastatin, taking into account aqueous solubility of the polymers chosen as well as properties of the drug for ease of incorporation.
2. Preparation of a thermosensitive bioink formulation in the form of a thermo-gel system, such that there will be drug release at 37˚C and remain in liquid form at room temperature, enabling injection into bone.
3. The bioink thermo-gel system was evaluated on a physicochemical and physiomechanical basis, for determination of the stability of the formulations and their characteristic profiles. Texture Analysis, Scanning Electon Microscopy (SEM), Transition Electron Microscopy (TEM), Attenuated Total Reflectance-Fourier Transform Infrared (ATR-FTIR), Thermogravimetric Analysis (TGA), Nuclear Magnetic Resonance (NMR), rheology and in vitro drug release were some of the many characterization studies undertaken.
4. X-ray and ultrasound evaluation of the bioink thermo-gel was undertaken on a human clavicle bone, after inducing a hair-line fracture and to determine the effect the thermo-gel has on the fracture induced bone.
5. Development of a controlled release novel 3D scaffold bone tissue engineered drug delivery system, implanted *in situ* at the site of bone fracture.
6. *In vivo* analysis was undertaken on the 3D scaffold bone tissue engineered drug delivery system (loaded with simvastatin) using a rabbit model.
7. Evaluation of the physicochemical and physicomechanical properties of the 3D scaffold drug delivery system using NMR and XRD, as well as determination of the stability of the formulation.
8. *In vitro* cell culture studies, using the MG-63 cell line, were performed on the 3D scaffold for determination of cell viability.

1.6. Overview of the Thesis

This thesis covers all aspects of the research from pre-formulation design studies to *in vitro* and *in vivo* critical evaluation of the drug delivery system.

Chapter 1 entails an inclusive overview of the rational and motivation for undertaking this research, thereby describing the mechanism of action of the delivery system, as well as research previously undertaken in the field of bone tissue engineering. The aims and objectives of the study are clearly explained, ensuring clarity and analytical sequence throughout the study.

Chapter 2 discusses in detail the different biodegradable, stimuli-responsive polymers and biomaterials used in the field of bone tissue engineering. This chapter covers natural and synthetic

polymers employed in bone tissue engineering, as well as approaches to the synthetic fabrication of injectable hydrogels and scaffold technologies. Injectable and implantable research technologies currently employed in bone tissue engineering applications, with specific focus on bone repair and regeneration is also discussed.

Chapter 3 entails the synthesis and evaluation of the bioink thermo-gel for its physicochemical, physicomechanical and rheological properties, with its application to treat small bone fractures. A strategic copolymeric blend of Polypropylene fumerate (PPF), Pluronic F127 and PEG-PCL-PEG is discussed, obtaining a thermo-responsive delivery system, to mimic the mechanical properties of bone with sufficient matrix hardness and resilience. A Biopharmaceutics Classification System (BCS) class II drug, simvastatin, was loaded in the thermo-gel for its bone healing properties. *In vitro drug* release studies as well as *ex vivo* studies employing human clavicle bones were also studied for its *ex vivo* fracture adhesive properties.

Chapter 4 expounds the design and optimization of a 3D bioprinted pseudo-bone drug delivery scaffold using Computer Aided Design (CAD) software, MATLAB® software and artificial neural networks (ANN). Chemical, morphological, mechanical and *in vitro* release properties, for evaluation of its behavior for application as an implantable scaffold at the site of fracture is also discussed.

Chapter 5 critically discusses *in vivo* studies conducted on 12 New Zealand White (NZW) rabbits. Histological evaluation of nasal bone samples following treatment with the 3D bioprinted scaffold is explored. *In vivo* responses determining bone regeneration and repair from the induced nasal bone fractures in the rabbit model was exclusively evaluated. *In vitro* cell culture studies employing MG-63 cells are also discussed, determining the percentage of cell viability over a period of 30 days. The capability of the 3-D bioprinted scaffold to withstand deformation under an applied tensile load is also examined for biaxial determination of the stiffness of the material.

Chapter 6 summarizes the entire study as a concludry chapter and considers recommendations for future studies.

1.7 Concluding Remarks

This chapter introduces the purpose of the novel research undertaken and the significance of conducting this research. This thesis is the foundation into a revolutionary platform of bone tissue engineering, looking at the most convenient, least invasive route of administration, thus providing patients with a simple hope of maintaining a healthy lifestyle. This technology will provide a novel

unique system, for effortless implantation at the site of fracture, resulting in an enormous impact to scientific research of revolutionary standards for treating bone fractures.

1.8 References

Aoki, K.; Alles, N.; Soysa, N.; Ohya, K. 2012. Peptide- based delivery to bone. *Advanced Drug Delivery Reviews* 2012, *64*, 1220- 1238.

Bae, M.; Ohe, J.; Lee, J.; Heo, D.; Byun, W.; Bae, H.; Kwon, Y.; Kwon, I. Photo-Cured Hyaluronic Acid-Based Hydrogels Containing Growth And Differentiation Factor 5 (GDF-5) For Bone Tissue Regeneration. *Bone* 2014, *59*, 189-198.

Calixto, J.; Villaboim de Castro Lima, C.; Frederico, L.; Pio dos Santos de Castro Lima, R.; Anbinder, A. The Influence Of Local Administration Of Simvastatin In Calvarial Bone Healing In Rats. *Journal of Cranio-Maxillofacial Surgery* 2011, *39*, 215-220.

Chen, P.; Sun, J.; Tsuang, Y.; Chen, M.; Weng, P.; Lin, F. Simvastatin Promotes Osteoblast Viability And Differentiation Via Ras/Smad/Erk/BMP-2 Signaling Pathway. *Nutrition Research* 2010, *30*, 191-199.

Coleman, R. Skeletal Complications Of Malignancy. *Cancer* 1997, *80*, 1588-1594.

Deng, C.; Wu, J.; Cheng, R.; Meng, F.; Klok, H.; Zhong, Z. Functional Polypeptide And Hybrid Materials: Precision Synthesis Via A-Amino Acid N-Carboxyanhydride Polymerization And Emerging Biomedical Applications. *Progress in Polymer Science* 2014, *39*, 330-364.

Egner, W.; Egner, H. Thermo-Mechanical Coupling In Constitutive Modeling Of Dissipative Materials. *International Journal of Solids and Structures* 2016, *91*, 78-88.

Eppley, B. Use Of Resorbable Plates And Screws In Pediatric Facial Fractures. *Journal of Oral and Maxillofacial Surgery* 2005, *63*, 385-391.

Gassner, R.; Tuli, T.; Hächl, O.; Moreira, R.; Ulmer, H. Craniomaxillofacial Trauma In Children: A Review Of 3,385 Cases With 6,060 Injuries In 10 Years. *Journal of Oral and Maxillofacial Surgery* 2004, *62*, 399-407.

Hillen, R.; Burger, B.; Pöll, R.; Gast, A.; Robinson, C. Malunion After Midshaft Clavicle Fractures In Adults. *Acta Orthopaedica* 2010, *81*, 273-279.

Jung, Y.; Park, W.; Park, H.; Lee, D.; Na, K. Thermo-Sensitive Injectable Hydrogel Based On The Physical Mixing Of Hyaluronic Acid And Pluronic F-127 For Sustained NSAID Delivery. *Carbohydrate Polymers* 2017, *156*, 403-408.

Khoshroo, K.; Jafarzadeh Kashi, T.; Moztarzadeh, F.; Tahriri, M.; Jazayeri, H.; Tayebi, L. Development Of 3D PCL Microsphere/Tio 2 Nanotube Composite Scaffolds For Bone Tissue Engineering. *Materials Science and Engineering: C* 2017, *70*, 586-598.

Kitsis, C.; Marino, A.; Krikler, S.; Birch, R. Late Complications Following Clavicular Fractures And Their Operative Management. *Injury* 2003, *34*, 69-74.

Lucia, U. Econophysics And Bio-Chemical Engineering Thermodynamics: The Exergetic Analysis Of A Municipality. *Physica A: Statistical Mechanics and its Applications* 2016, *462*, 421-430.

Maeda, T.; Matsunuma, A.; Kawane, T.; Horiuchi, N. Simvastatin Promotes Osteoblast Differentiation And Mineralization In MC3T3-E1 Cells. *Biochemical and Biophysical Research Communications* 2001, *280*, 874-877.

Mayer, T.; Matlak, M.; Johnson, D.; Walker, M. The Modified Injury Severity Scale In Pediatric Multiple Trauma Patients. *Journal of Pediatric Surgery* 1980, *15*, 719-726.

McGovern, S.; Fong, W.; Wang, J. Can Bone Morphogenetic Protein Binding Peptide Increase Efficiency Of Bone Formation?. *Spine* 2010, *35*, 1655-1659.

Mehta, M.; Schmidt-Bleek, K.; Duda, G.; Mooney, D. Biomaterial Delivery Of Morphogens To Mimic The Natural Healing Cascade In Bone. *Advanced Drug Delivery Reviews* 2012, *64*, 1257-1276.

Modi, C.; Wicks, L.; Srinivasan, K. Reconstruction Of Humeral Head Defect For Locked Posterior Shoulder Dislocation. *Orthopedics* 2009, *32*, 691-693.

Mundy, G. Stimulation Of Bone Formation In Vitro And In Rodents By Statins. *Science* 1999, *286*, 1946-1949.

Nguyen, Q.; Huynh, D.; Park, J.; Lee, D. Injectable Polymeric Hydrogels For The Delivery Of Therapeutic Agents: A Review. *European Polymer Journal* 2015, *72*, 602-619.

Paladini, P.; Pellegrini, A.; Merolla, G.; Campi, F.; Porcellini, G. Treatment of clavicle fractures. *Translational Medicine* 2012, 2(6), 47 – 58.

Patel, V.; Zhao, L.; Wong, P.; Pradhan, B.; Bae, H.; Kanim, L.; Delamarter, R. An In Vitro And In Vivo Analysis Of Fibrin Glue Use To Control Bone Morphogenetic Protein Diffusion And Bone Morphogenetic Protein–Stimulated Bone Growth. *The Spine Journal* 2006, *6*, 397-403.

Qiao, Y.; Qin, G.; Yu, L. The Triblock Copolymers Hydrogel Through Intracameral Injection May Be A New Potential Ophthalmic Drug Delivery With Antiscaring Drugs After Glaucoma Filtration Surgery. *Medical Hypotheses* 2013, *80*, 23-25.

Robinson, C.; Court-Brown, C.; Mcqueen, M.; Wakefield, A. Estimating The Risk Of Nonunion Following Nonoperative Treatment Of A Clavicular Fracture. *The Journal of Bone and Joint Surgery-American Volume* 2004, *86*, 1359-1365.

Santapuri, S. Thermodynamic Restrictions On Linear Reversible And Irreversible Thermo-Electro-Magneto-Mechanical Processes. *Heliyon* 2016, *2*, e00164.

Tiwari, R.; Pathak, K. Nanostructured Lipid Carrier Versus Solid Lipid Nanoparticles Of Simvastatin: Comparative Analysis Of Characteristics, Pharmacokinetics And Tissue Uptake. *International Journal of Pharmaceutics* 2011, *415*, 232-243.

Zimmermann, C.; Troulis, M.; Kaban, L. Pediatric Facial Fractures: Recent Advances In Prevention, Diagnosis And Management. *International Journal of Oral and Maxillofacial Surgery* 2005, *34*, 823-833.

CHAPTER 2
A REVIEW OF INJECTABLE POLYMERIC HYDROGEL SYSTEMS FOR APPLICATION IN BONE TISSUE ENGINEERING

2.1. Introduction

Injury, age related bone defects, as well as pathological conditions are some of the most common impairments related to bone fractures. This usually results in a prolonged healing time, and in some instances, relapse occur due to the treatment not reaching the specific site of action (Stolzing, et al., 2008). Current forms of treatment for these defects usually include bone grafts or metallic prosthetic implants. Allografts, xenografts, and autografts are categorized based on their natural tissue source. The most common form of bone implantation therapy is autografts, sampled from the patient's own body, thereby reducing the risk of tissue rejection. However, this form of therapy is restricted in many cases due to donor site morbidity, long recovery times, as well as substantial tissue damage resulting from surgery (Kofron, et al., 2006, Arrington, et al., 1996). Consequently, principles of developing autografts and allograft bone substitutes, using biomaterial of a degradable and biocompatible nature, are increasing owing to the varying biological, structural and physico-mechanical properties that this engineering provides (Healy, et al., 2007). Research published in 2011 estimates over one million surgical procedures done involving bone defects in the United States (US) per year. This is as a result of trauma, along with non-union healing fractures requiring the implementation of bone grafts. This also affects older patients, thereby incurring greater strain on the healthcare industry, totaling greater than 5 billion dollars annually (Tran, et al., 2011, Ngiam, et al., 2009). Hence, a significant alternative in the treatment of bone injuries is most certainly required, filling in the gaps of bone grafts, which cannot be undertaken in many instances, due to the limitations of current therapeutic procedures. Bone tissue engineering has shown promising results in this regard. Various scaffold materials are utilized in bone tissue engineering applications, and hydrogels form a major group of these materials (Ramesh, et al., 2013). Hydrogels have a hydrophilic nature and therefore have the capacity to absorb several fold of their dry weight in water. This allows the cells to adhere and differentiate onto the hydrogels (Luis, et al., 2016). This form of bone tissue engineering is a multifaceted specialization, involving chemical, biological and material science (Langer, et al., 1993). The basic element of tissue engineering relies on cells, signals, scaffolds and bioreactors.

These cells are three-dimensionally seeded onto a scaffold, cultured *in vitro* which are supplemented by proper signals, and thereafter implanted as a prosthesis *in vivo* as outlined in Figure 2.1 (Khan, et al., 2015). These cells can be autologous, xenogenic or allogenic, tissue specific stem cells or progenitor cells, which are isolated and cultured *in vitro*. An extracellular matrix for cell growth, synthetic or natural in composition, is formulated as a scaffold, delivered as a hydrogel. For proliferation and cell differentiation, signals are constructed into the system, enhancing cell adhesion. Bioreactors are also implemented into the system, simulating kinetic responses in the body, which further improve mechanical stimuli and mass transport to emerging tissue (Rabkin, et al., 2002, Vacanti, et al., 1999).

To date, injectable hydrogels for application in tissue engineering in the field of orthopedic sciences has produced many benefits over previous application methods. Injectable hydrogel systems are appealing for use in bony defects because they can be formed *in situ* and have a unique advantage in which difficult sites of injury can be easily targeted with least invasive procedures, forming a composite, irrespective of shape and defect geometry. Hydrogels can be used to fill critical-size bone defects and injuries in non-load bearing sites, even though they do not have the mechanical strength that is needed to provide support for load-bearing functions (Hunt, et al., 2010). Furthermore, this form of delivery can enhance physico-mechanical properties of injured/pathological bone, delivering a variety of bio-actives, drug molecules, as well as growth factors for therapeutic application (Kretlow, et al., 2007, Ifkovits, et al., 2007). Injectable hydrogels display a remarkable platform for bone tissue engineering due to its state of composition, which have water based homogeneous properties, to encapsulate, manipulate and transfer its contents to the surrounding tissue, in the least invasive manner (Drury, et al., 2003). The injected hydrogel, loaded with drug, growth factors and/or cultured cells, reach its site of action efficiently, further reacting to a stimulus, changes its chemical and physical properties, behaving as a transitional gel-solution system (Nuttelman, et al., 2008). The properties of the hydrogel promote cellular responses and cell distribution at any site prior to the transitional phase leading to gelation. The substantially hydrated nature allows significant simulation of the extra cellular matrix (ECM), due to its similar structural properties.

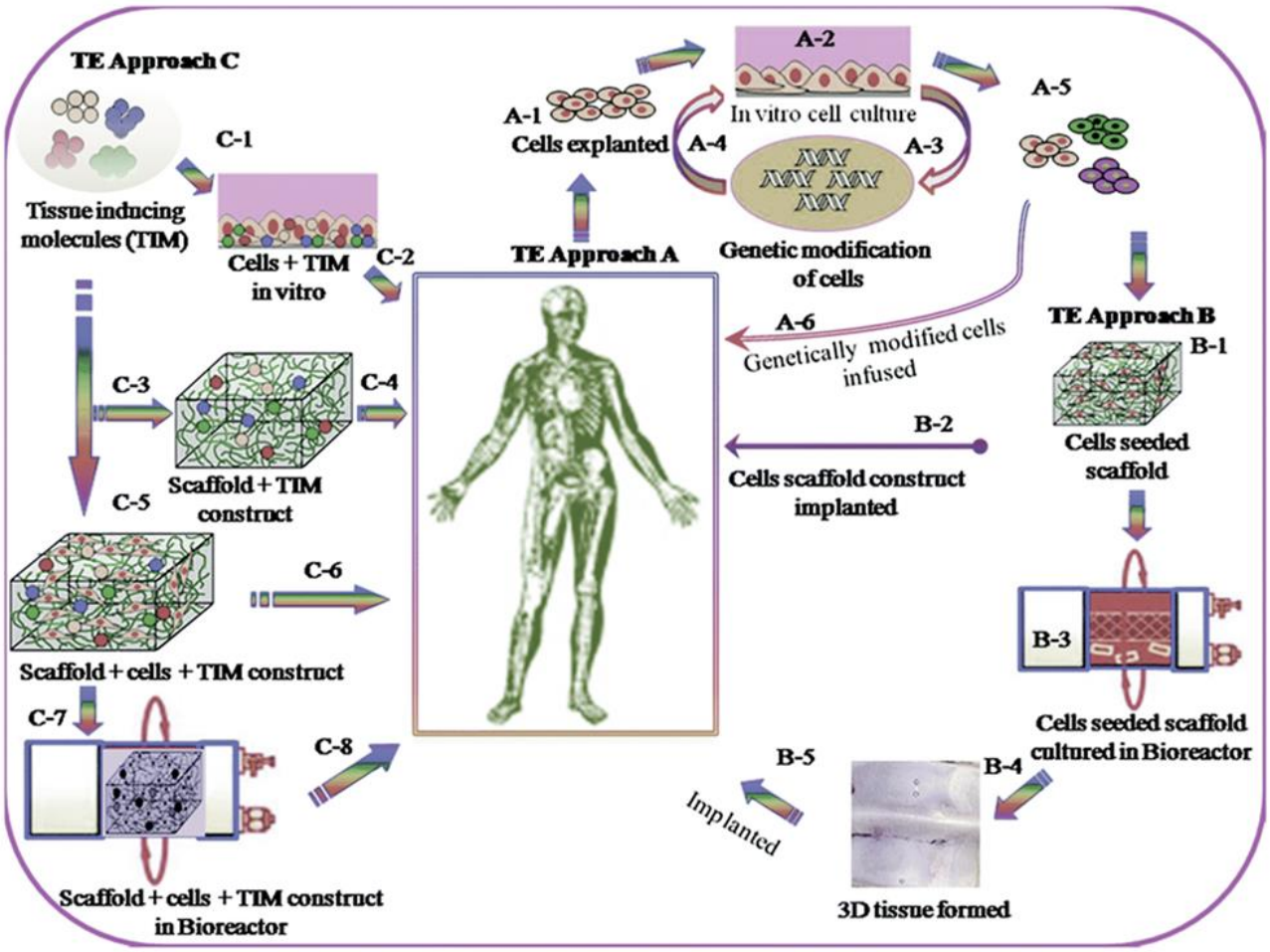


Figure 2.1. Schematic representing the outlined procedure undertaken for tissue engineering and drug delivery (Adapted with permission from Khan et al, 2015).

This provides an ideal environment for cellular regeneration and proliferation, thus allowing cells encapsulated in the hydrogel to grow and secrete new ECM for restoration of damaged tissue (Nicodemus, et al., 2008). Conventional methods for bone tissue regeneration, such as pre-formed hydrogels or scaffolds, face the issue of surgical implantation. The risk of infections and improper adaptation to the injury site using these conventional procedures increases significantly, with the possibility of leading to scaffold failure (Sivashanmugam, et al., 2015). Injectable hydrogels in the field of bone tissue engineering is gaining substantial importance by overcoming these challenges, as they can reach the target site with minimum invasiveness, and thus provide a much greater degree of bone repair and regeneration (Yu, et al., 2014).

Thus far, many polymers have been exclusively evaluated for its use as a thermo-responsive hydrogel, as an injectable delivery system, for application in bone tissue engineering, due to its

biocompatible and biodegradable nature, having specific stimuli responsive behavior, which is composed of either natural or synthetic material, designed to effectively deliver its encapsulated contents (Ramesh, et al., 2016). Natural polymers possess greater biocompatible properties compared to synthetically derived polymers, which usually have to be modified for a biologically structural response (Brandl, et al., 2007). Injectable hydrogel synthesis can be categorized as either physical or chemical gels, in accordance to its gel formulated structure. Physical association crosslinking between polymeric chains or particles in the hydrogel network is regarded as a physical gel system, whereas a chemical gel is covalently bonded between polymeric chains in the network system (Yu, et al., 2008). However, various limitations exist, which include unstable functional groups, the use of cytotoxic reagents, and low coupling efficiency. Thus, an application of more simple, efficient and specific methods of reaction synthesis is required, preserving the biological nature of the bioactive materials, and possessing substantial biocompatible and biodegradable properties. It is of great consideration when delivering a hydrogel for bone tissue engineering that the bio-kinetics and biodegradable nature of the hydrogel sustain and improve cellular growth as well as conditions simulated for ECM complementation. To attain these ideal properties, a chemical modification must be undertaken in the structure and density of the crosslinked moieties. Many bio-actives can be attached to the backbone of the polymeric system, thereby improving the function and regulation of cells in the hydrogel system. This chapter therefore outlines various techniques of formulating injectable stimuli-responsive hydrogel systems using different natural and synthetic polymers, and its application in bone tissue engineering.

Many approaches exist for the development of an ideal injectable hydrogel for use in bone tissue engineering, capable of increasing healing, adding support, and being biocompatible. This chapter provides the most current and significant advances in the field of bone tissue engineering, with particular focus on thermo-responsive polymer applications, with various chemical modifications, reporting novel bioengineered delivery systems, currently under evaluation. An area of discussion comprises the various limitations of these delivery systems as well, while the main focus considerably aligns to formulating a system that has exceptional physical, chemical, structural as well as biological advantages, with a unique thermo-responsive nature, enabling the bioengineered system to deliver its loaded content most effectively.

2.2. Approaches to the Synthetic Fabrication of Injectable Hydrogels for Application in Bone Tissue Engineering

Research in the field of chemical crosslinking and physical gelation strategies forms an integral part of the behavioral properties of the hydrogel system for utilization in bone tissue engineering. Physical gelation occurs when 2 or more polymeric chains form a link due to physical interaction, such as hydrophobicity, ionic or self-assembly due to environmental stimuli of temperature, pH or polymer precipitation. Chemical crosslinking, on the other hand, provides greater sustained release kinetics, due to high crosslinking densities to the polymeric network, providing complimentary mechanical properties for scaffold based delivery. A drawback of this, however, is the nature of the crosslinking agents used in the reactions, which often possess toxic chemical profiles, affecting bioactive materials and cells which are incorporated into the hydrogel. Physical gelation may prevent the use of crosslinking agents, though demonstrating less physical effective properties. The various mechanisms of solidification of injectable hydrogels for application in bone tissue engineering will be discussed in this section in response to the diverse environmental stimuli.

2.2.1 Thermo-Induced Gelation: Classical Poly(NIPAAm)

Thermally induced gelation systems (TGS) are uniquely composed of an interpenetrating network of polymeric chains that are able to undergo phase transitions to the gel-sol state, due to the manipulation of temperature. The polymeric chains are amphiphilic in nature, being composed of an interaction between hydrophobic and intermolecular forces, in which the molecular weights of these segments are responsible. In both chemical and physical polymeric systems, drugs are loaded at room temperature. Once the formulation is injected, the gel shrinks, entrapping the loaded contents, modulating its release. One of the proposed mechanisms for thermal transition include the shrinkage of the outer shell, forming a barrier, reducing the pore size of the gel, thereby reducing the diffusion rate of the water molecules. One of the oldest polymers for biomedical administration is Poly(N-isopropylacrylamide) (PNIPAAm). This is due to its lower critical solution temperature (LCST) being very close to body temperature. Crosslinking of this polymer causes a coil to globule transition, thereby decreasing the volume of gel, releasing the entrapped drug, following a linear controlled release rate (Jones, et al., 2008). It was also reported that hydrophobic drugs strengthen the structure of the hydrogel system, and by varying the crosslinker concentration, the release rate of the drug from PNIPAAm gels could be altered (Coughlan, et al.,

2008). This polymer also demonstrated a considerable change in LCST due to the salt concentration in the polymeric network, lowering the LCST of the polymer, due to the Hofmeister effect on the water molecules (Jhon, et al., 2006).

Research undertaken, demonstrated that co-networks of PNIPAAm and hydroxyethyl methacrylate (HEMA) resulted in an LCST of 34°C, resulting in favourable *in vivo* administration for drug release (Jones, et al., 2008). A similar study was undertaken by crosslinking zinc tetraphenylporphyrin (Zn-TPP) into PNIPAAm- co-PHEMA. Results revealed that above the LCST, Zn-TPP release was significantly decreased, thereby controlling the degree kinetics, due to polymer concentration and manipulation of the LCST (Jones, et al., 2007). Studies have been undertaken by crosslinking PNIPAAm with polyamino acids, resulting in thermo-responsive hydrogels (Yoshida, et al., 2003). Further research in this field reported the synthesis of elastin based thermo-responsive polymers, existing in the solvated state bellow its transition temperature, and above its LCST of 30°C, the polymeric chains change their conformation to form nanoparticles, entrapping molecules to deliver its active, such as a loaded-drug, protein or cell cultured system. They are also nontoxic and does not mount an immunogenic response once delivered, forming an amphiphilic copolymeric chain (Bessa, et al., 2010, Rincon, et al., 2006). Figure 2.2 further demonstrates the gelation mechanism brought about from the change in temperature, creating an amphiphilic copolymeric chain loaded with cells and drug molecules as desired for specific injectable technologies.

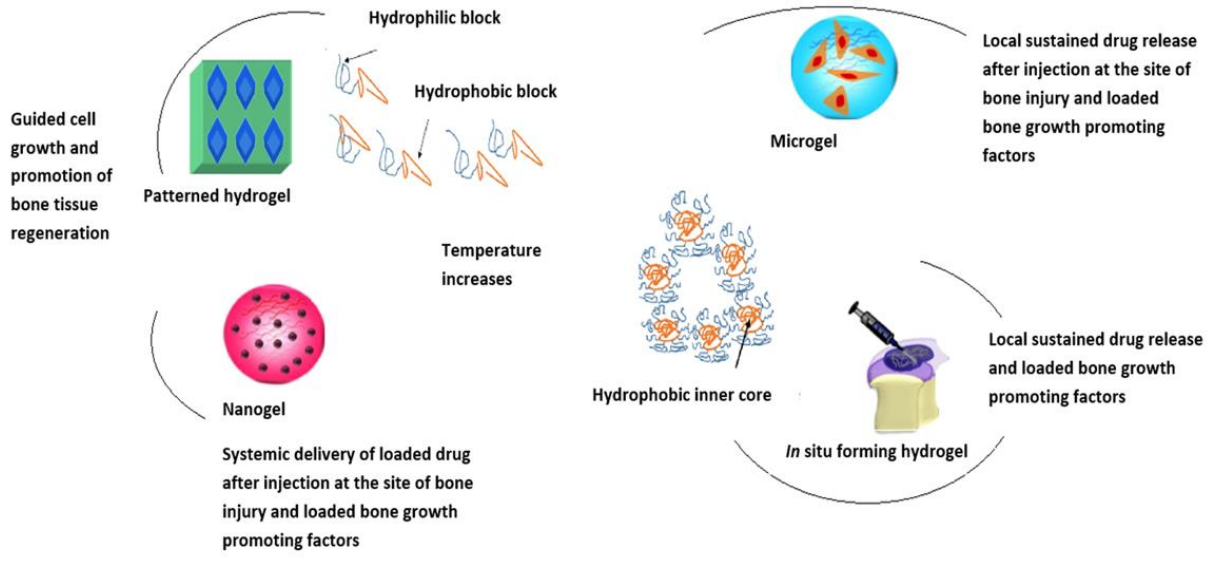


Figure 2.2. Physical gelation system derived from increased temperature due to interaction of hydrophilic and hydrophobic blocks for promoting an amphiphilic polymer.

Bessa and co-workers also reported that morphogenetic proteins could be delivered at a controlled rate for fourteen days, consequently enhancing bone formation (Bessa, et al., 2010). Another study undertaken by grafting PNIPAAm and PVCL-HEMA on a dextran chain, produced a thermos-responsive biodegradable hydrogel with sustained drug release for numerous days, with no immunological responses (Wu, et al., 2009). Hydrogels incorporating PEGMA and iron oxide displayed a positive thermo-responsive drug delivery application by de-swelling once the temperature was increased. It also displayed magnetic properties by heating upon application upon an alternating magnetic field, leading to de-swelling of the hydrogel (Meenach, et al., 2010). Similarly, another study reported hydrogels possessing super-paramagnetic properties, incorporating magnetite nanoparticles through polymerization, demonstrating tunable super-paramagnetic properties proportional to the concentration of magnetite by increasing the stimuli of temperature (Papaphilippou, et al, 2011). Research undertaken by Ma et al, synthesized a hydrogel of PNIPAAm (constituting 80% and greater polymer concentration), PHEMA, incorporating a monomer of lactic acid, which then demonstrated LCSTs in the range of 10-20°C, possessing significant tensile strength, degrading over several months when used for bone tissue engineering application (Ma, et al., 2010).

Among other polymers, methylcellulose has been studied for decades, demonstrating its thermo-responsive properties. A study demonstrated that conjugation of methylcellulose with Laminin protein produced a sustainable hydrogel for neural defective tissue, increasing cell adhesion by the addition of a protein conjugate (Stabenfeldt, et al., 2006). A series of PEGylated polymers were also studied for tissue engineering. Further research evaluation demonstrated that by implementing PEG-alt-Thiol conjugates, this biodegradable polymeric system showed *in vivo* biocompatible cell matrices (Wang, et al., 2008). Conjugation of Pluronics with peptides increases cell adhesion and growth responses in scaffold formulations (Garty, et al., 2010). Kan et al delivered a zero order drug delivery thermo-responsive polymer PEG-b-PLGA-b-PEG, forming an oil in water emulsion. The hydrophilic phase displayed a gel at 20-30°C, above the polymer LCST, preventing the drug from erupting, and encapsulating the oil droplets with a controlled drug release (Kan, et al., 2005).

The most significant factor in all of the above polymeric systems is the level of solubility that is attained above the LCST, due to the entanglement and collapse of the polymeric network chains. Factors such as polymer concentration, chemical structure and molecular weight affects the gelation process. Other examples of polymers implemented as thermo-sensitive hydrogels

include poly (propylene oxide), poly (ethylene oxide), poloxamers or pluronics, chitosan, gelatin as well as cellulose derivatives which have been identified in great extents in the field of drug delivery and bone tissue engineering.

Research undertaken at the University of California, Berkeley, reported the osteogenic differentiation via soft bioinspired hydrogels (Jha, et al., 2014). Many physical and biochemical factors guide the osteogenic differentiation of human mesenchymal stem cells. Modulus (rigidity) of the ECM is one factor which has gained much attention as a physical osteoinductive signal that can contribute to endochondral ossification of a cartilaginous skeletal template. To understand the function of the matrix interactions in this process, osteogenic differentiation of human mesenchymal stem cells cultured on low moduli (102 Pa) poly(NIPAAm) based semi-interpenetrating networks, modified with the integrin engaging peptide bsp-RGD (105 μM), was analyzed. It was concluded that within the low moduli poly(NIPAAm) substrate, a very high affinity adhesive ligand serves as a substitute for a rigid matrix to promote osteogenic differentiation. Among this research, various other studies using this polymer was evaluated for it application in bone tissue engineering, with similar positive results derived. Thus it can be deduced that poly(NIPAAm) demonstrates promising results in the field of bone tissue engineering.

2.2.2 Ionic-Mediated Gelation: The Stimulation of Alginate

This system is mediated by the formation of ionic chain connections with di or trivalent cations of the polymeric networks. Alginate is the most studied polymer, with its ability to crosslink with calcium and zinc cations at different positions of the alginate chain, due to its polysaccharide structure, composed of homopolymeric blocks of 1,4-linked b-D-mannuronic acid and a-L-guluronic acid (Leea, et al., 2012). The polyguluronic acid block makes this polymer more selective for binding to calcium ions. Zinc cations are less selective for crosslinking, resulting in greater zinc alginate crosslinked hydrogel systems (Place, et al., 2011). The rate of crosslinking has been reported to be inversely proportional to the concentration of alginate used and the rate of crosslinking influenced by the concentration of multivalent cations and polyguluronic acid segments present (Russo, et al., 2007).

A remarkable study undertaken by Roman et al., evaluated a core–shell fibrous collagen-alginate hydrogel cell delivery system for bone tissue engineering (Perez, et al., 2014). In this study, a novel stem cell delivery system constituting alginate and collagen as the core and shell was designed. Mesenchymal stem cells were loaded into the collagen solution. This was then placed

immediately into a fibrous structure while concurrently sheathing with alginate by use of a newly designed core-shell nozzle. The continuous fibrous structure of the inner cell-collagen part was successfully maintained, as the alginate encapsulation was attained by the crosslinking within an adjusted calcium-containing solution. A continuous fiber with a diameter of ~700–1000 μm for the core and 200–500 μm for the shell area was displayed by the constructed hydrogel carriers. This was greatly dependent on the alginate concentration (2%–5%) and the injection rate (20–80 Ml/h). The mesenchymal stem cells which were encapsulated within the collagen exhibited exceptional viability. It also displayed remarkable cellular proliferation for up to 21 days with levels comparable to pure collagen gel matrix which was used as a control. The cells which were allowed to differentiate under osteogenic conditions displayed favorable levels of bone-related genes, comprising of osteocalcin, osteopontin and bone sialoprotein. Bone healing was considerably enhanced when the core-shell fibrous carriers were implanted in a rat calvarium defect, more so after an osteogenic induction of the mesenchymal stem cells before implantation. Based on the results of this experiment, the newly fabricated core–shell collagen-alginate fibrous carrier is regarded favorable to permit the encapsulation of tissue cells and their delivery into damaged tissues, including bone with defect-turnability for bone tissue engineering.

2.2.3 Free Radical Polymerized Gelation: The Essential Vinyl Monomer

Free radical polymerization techniques are commonly generated by radical generating initiators such as gamma, ultraviolet light as well as redox initiators. This technique involves a radical generating initiator system and a radical-liable oligomer or monomer (Bulmus, et al., 2011). This fundamental process proceeds only by the presence of free-radical initiation. Vinyl groups commonly generate free radicals upon physiological stimuli, containing radical-liable moieties, which further undergo propagation steps in the polymerization network formation. After completing the initiation phase, radical initiators homolytically cleave the radical-liable moieties, inducing the propagation phase, as seen in Figure 2.3. The final step takes place as a termination step by which 2 radicals in the propagation polymer bond covalently, thereby completing the crosslinking process (Bulmus, et al., 2011). The efficiency of the hydrogel can be evaluated by its mechanical properties, crosslinking density as well as its biodegradable profiles, which are dependent on the radical-liable moieties, nature of the solvents used and the concentration of the initiator. Redox initiated systems are preferred in areas of limited light rays where crosslinking of the polymeric networks are homogenous, and photo-initiated systems are preferred where spatial and temporal control are essential to develop structured patterned complexes (Davis, et al.,

2003).

These free radical polymerization reactions are essential methods in synthesizing various thermo-responsive copolymers. Using a crosslinker and an initiator in the reactions, successful copolymerization can occur in favorable conditions. Application of these reactions for polymeric scaffold design using 3D bio-plotting are currently a huge focus for incorporation of cell cultured systems, delivering a host of growth factors and drugs for the treatment of bone related injuries. These thermo-responsive scaffolds swell at body temperature, with great biocompatibility properties, introducing tissue cells and growth factors at the site of injectable delivery. At body temperatures, these free radical copolymerized polymers begin to change from the solution to gel state, further providing mechanical support and significant matrix resilience at the site of bone injury (Bulmus, et al., 2011, Davis, et al., 2003).

A recent study described thermoplastic starch/ethylene vinyl alcohol/forsterite nanocomposite as a candidate material for bone tissue engineering (Mahdieh, et al., 2016). The aim of the study was to synthesize nanocomposite biomaterial which was composed of a blend of thermoplastic starch and ethylene vinyl alcohol as the polymer matrix. Nano-structured forsterite was used as the ceramic reinforcing phase for bone tissue engineering. It was found that blending thermoplastic starch and ethylene vinyl alcohol modified the degradation rate and water resorption of thermoplastic starch. The nanoforsterite improved the mechanical and biological traits and decreased the weight loss of the thermoplastic starch and ethylene vinyl alcohol blend in simulated body fluid. Furthermore, this modified the pH in the methyl thiazoly tetrazolium (MTT) assay and prompted cell proliferation. A favorable interaction between cells and the biomaterial was demonstrated by cell adhesion assays. It was concluded that the proposed nanocomposite displays pertinent biocompatibility and mechanical properties and can be used in bone tissue engineering.

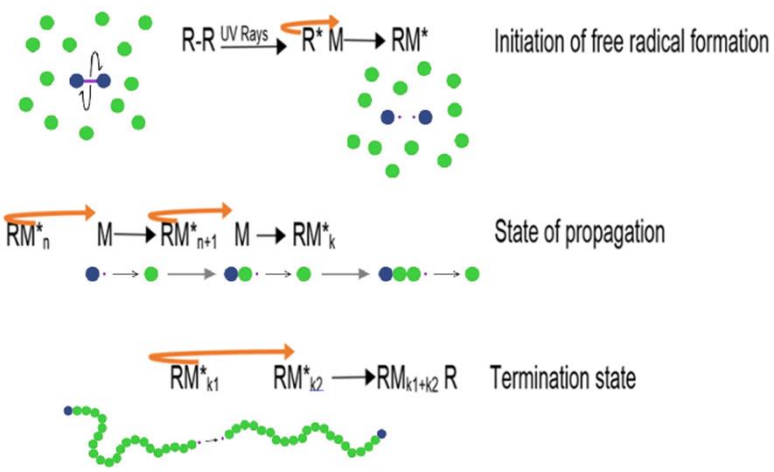


Figure 2.3. Free radical polymerization steps involved in copolymerization techniques.

2.2.4 Self-Assembled Gelation: The Independent Amphiphiles

Many amphiphilic polymers have displayed properties of gelation due to their complexation as a result of de-solvation, collapse and intermolecular association of nonpolar segments of the monomers. Further stability is displayed when these amphiphiles are charged, possessing electrostatic and van de waals forces (Tu, et al., 2004). Various peptide bio-actives display amphiphilic properties in injectable tissue engineering, with the hydrogel displaying low viscous properties at lower temperature, and changing its conformation to a gel form once injected *in vivo* (Wong, et al., 2009). Hydrophobic polymers also display self-assembly via phase segregation, in which water soluble solvents have been injected with these biodegradable polymers (Hosseinkhani, et al., 2007). A precipitation reaction occurs when water diffuses into the polymer matrix and solvent diffuses into the tissue space, resulting in a hydrophobic polymeric complex at the site of injury into the injected cavity. Factors affecting the rate of precipitation include the molecular weight of the polymer, concentration of polymer in solvent, addition of a surfactant and the type of solvent used (Hosseinkhani, et al., 2006). Many biologicals have been encapsulated and delivered, such as bone morphogenetic protein-2 (BMP-2) and fibroblast growth factor (Bfgf), formulating a suspension of these bio-actives in aqueous solution of amphiphilic peptide, forming a self-assembly hydrogel system. Some examples of solvents used in this approach are N-methyl-2-pyrrolidone, propylene glycol, dimethyl sulfoxide, acetone, 2-pyrrolidone and tetrahydrofuran (Royals, et al., 1999). This system is indeed useful in incorporating biological actives and peptide based therapeutics, increasing its stability and mechanical structural properties by using a good selection of amphiphilic polymers with the correct type of solvents.

2.2.5 Chemically Crosslinked Gelation: The Sentimental Alkynes, Azides and Amines

Polymers containing high affinity for each other and displaying significant solubility in its injectable medium can be modified to form a covalently linked network at the site of delivery (Strehin, et al., 2010). Most frequently reported molecules having this relationship include, alkyne to azides, N-hydroxysuccinimide (-NHS) to amines (-NH_2) and an a,b-unsaturated carbonyl compound in the presence of a 1,4-addition carbon nucleophile. The degree of network formation, stability, and kinetics of the system are proportional to the affinity of molecules. Much research has been conducted on amine-based polymers in the field of bone tissue engineering. Researchers investigated the *in vitro* and *in vivo* osteogenic activity of the novel vancomycin-loaded bone-like hydroxyapatite/poly (amino acid) scaffold (Cao, et al., 2016).

Bone-like hydroxyapatite/poly(amino acid) scaffolds have been shown to display some osteogenic and osteo-conductive properties. It also exhibit controllable biodegradability, and nontoxicity. A homogenous method which utilized a diffusion control system was used to successfully produce a vancomycin-loaded bone-like hydroxyapatite/poly(amino acid). *In vitro* tests included incubating MG63 cells with the vancomycin-loaded scaffold. This was done to observe its effect on the activation of osteoblast cells. The *in vivo* tests were conducted on a rabbit model. The scaffolds were implanted into the rabbit model which possessed chronic osteomyelitis. The MG63 cells displayed good proliferative activity and increased calcium and phosphatase synthesis. *In vivo* test results showed an increase in bone growth in infectious bone defects as compared to the control group, regardless of the type of staphylococcus aureus. It was thus concluded that due to ability to deliver antibiotics and promote bone regeneration, vancomycin-loaded bone-like hydroxyapatite/poly (amino acid) has great potential for the repair of infectious bone defects.

Polymers can also be crosslinked by enzymatic reactions, by which the phenol group undergo self-crosslinking in the presence of hydrogen peroxide (H_2O_2) and horseradish peroxidase (HRP). When proteins react with H_2O_2 and peroxidase, oxidation of phenol groups of tyrosine occurs, forming a crosslinked protein conjugate of dityrosine and tertyrosine (Sakai, et al., 2009). Polymers such as chitosan, dextran, hyaluronic acid and gelatin can introduce a phenol group on its structure by reacting their carboxylic or amine groups in the presence of 3,4-hydroxyphenylpropionic acid (HPA) or tyramine (Jin, et al., 2007). Poly (lysine-co-phenylalanine) and transglutaminase (TG) mediated glutaminamide- functionalized poly (ethylene glycol) (PEG)

have also been reported to display chemical crosslinking properties in place of HRP, employing calcium ions as cofactors (Sperinde, et al., 1997). The rate of crosslinking of the system can be attributed to the phenol functionality and the concentration of HRP and H_2O_2, however an excess of H_2O_2 can deactivate the crosslinking reaction by oxidising HRP (Goa, et al., 1994). This network formation therefore has great potential in tissue engineered hydrogel systems when incorporating protein derived bio-actives, forming stable networks of chemically crosslinked polymers.

2.3. Polymers Employed for the Synthesis of Stimuli-Responsive Hydrogel Systems

Various biocompatibility techniques for the delivery of natural and synthetic polymers can be explored by their structural activity relationship, forming stimuli responsive hydrogel systems. Polymers such as hyaluronic acid, chitosan, matrigel, collagen and agarose are natural polymers that can be modified for specialised application. Synthetic polymers such as poly (ethylene glycol) (PEG) and PNIPAAm are examples of modified release block polymers which can be crosslinked to naturally derived polymers to serve as hydrogel responsive carrier systems for biologicals and drug delivery.

2.3.1 Natural Polymers

2.3.1.1 *Hyaluronic acid*

This glycosaminoglycan found in extracellular matrix is often used as a key component in hydrogel systems. This is due to its biodegradable and biocompatible nature, forming a gel with substantial water content, used as a delivery carrier for drugs and protein molecules (Goa, et al., 1994). Hyaluronic acid (HA) can be enzymatically degraded, and therefore does not result in an immune responsive cascade, thus being effectively delivered as an injectable delivery system. HA is not thermo-responsive in nature, however, it is most often conjugated with thermo-responsive polymers to provide a modified hydrogel, being biodegradable, biocompatible and thermo-responsive (Ohya, et al., 2001). Many publications have demonstrated the conjugation of PNIPAAm with HA, displaying admirable properties as a thermo-sensitive hydrogel (Mayol, et al., 2008). The thermal transition temperature of the conjugated HA-PNIPAAm was independent of the molecular mass of HA, PNIPAAm grafting ratio and its chain length, maintaining the poor reactivity in cell adhesion, being highly applicable in tissue grafting technology (Tiffany, et al.,

2015). To improve the cell adhesive properties of HA, researchers have conjugated HA with stimuli responsive polymers such as PNIPAAm, Pluronic and gelatin (Zhang, et al., 2007). Pluronic has significant properties in response to temperature, which can be chemically or physically modified to HA. Its copolymeric structure has chains of poly (ethylene oxide)-b-poly (propylene oxide)-b-poly (ethylene oxide) (PEO-PPO-PEO). HA-Pluronic copolymeric hydrogels displayed admirable drug release studies, delivering chemotherapeutic drugs, following a Fickian diffusive mechanism (Hsu, et al., 2009). It can therefore be affirmed that the properties of HA have substantial advantages in the delivery of bioactive formulations, further conjugated to stimuli responsive polymers to yield biocompatible and biodegradable injectable technologies.

The development of an injectable calcium phosphate/hyaluronic acid microparticles system for platelet lysate sustained delivery aiming bone regeneration was designed and evaluated (Babo, et al., 2016). The incorporation of calcium phosphate (CaP) cement in conjunction with HA microparticles loaded with platelet lysate (PL) to enhance the degradability and biological performance of the proposed cements was investigated. Cement formulations were developed, which consisted of increasing weight ratios of either HA microparticles or microparticles loaded with PL (10 and 20 wt %). Formulations with cements directly incorporating PL were also fabricated. Homogeneous particles distribution as well as increased interconnectivity between the HA microparticles were exhibited by morphological analysis. A sustained release of 8 days was observed with the cements incorporating PL proteins. This sustained release of PL modulates the expression markers in seeded human adipose tissue derived stem cells. This therefore suggests the stimulatory role of this combination system toward osteogenic commitment as well as bone regeneration and repair applications.

2.3.1.2 *Chitosan-based hydrogels*

The polysaccharide, chitin, derived from the exoskeleton of crustaceans and insects, is one of the most abundant naturally available polymers. Chitosan is derived from chitin by deactylation reactions of N-acetyl-D-glucosamine (Bhattarai, et al., 2010). Chitosan is not a thermo-sensitive polymer, however the addition of glycerophosphate (GP) in solution of chitosan, provides a thermo-sensitive hydrogel, by which the pH of the solution must be less than 6 for the solubility of the chitosan polymer. GP reacts with chitosan to form hydrogen bonds when the temperature is increased, thereby leading to a gel formation. The different drug loading and release properties of chitosan was studied with various gelation time and drug release kinetics for various chitosan

conjugated systems. Chitosan-GP copolymer was studied *in vivo* in a rodent model, delivering bone morphogenetic protein (BMP) for cartilage repair. The bioactive loaded hydrogel system was injected subcutaneously and was observed to show a gelling time of 10 min. This application demonstrated a low degree of success, due to the extensive time of gelation for delivering the loaded bioactive (Chenite, et al., 2000).

To enhance the duration of gelation, an approach of obtaining chitosan chloride with GP was investigated, displaying greater solubility than chitosan, with a gelation time of 1 min. This system was investigated to deliver insulin, retaining the protein efficiency, displaying success as an injectable hydrogel delivery system for diabetes (Shi, et al., 2011). This however has a disadvantage of the rapid release rate of drugs and protein molecules. The study showed that within a few hours, all of the drug was released with no sustained kinetic profiles, proving inefficiency to deliver long term controlled formulations. Another strategy of interest was to encapsulate a low molecular weight molecule using liposomes in the chitosan-GP hydrogel system. The drug carboxyfluorescein was used to determine the release behaviour of the hydrogel, displaying a sustained kinetic profile of 2 weeks (Ruel-Gariepy, et al., 2002). It was noted that the liposome addition did not change the gel transition temperature, however, the size of the liposomes affected the release rate of the drug. Another manipulation strategy to delay the release rates of the loaded bioactive was investigated, by which silicon nanoparticles (SNP) was used to encapsulate ovalbumin from a chicken, suspended in a chitosan-GP hydrogel system. Results obtained demonstrated a 40% release rate at day 14, in comparison to a 100% release without encapsulation of SNP. It can be explained that the SNP hindered the release, due to possible temperature and nanoparticle interaction with the protein, preventing substantial release from taking place at once (Gordon, et al., 2010).

A disadvantage of the above-mentioned study was further reported, by which toxicology of chitosan-GP hydrogels were described. Foreign body immune modulated responses were detected when the hydrogel formulation was administered. Different ratios of chitosan-GP concentrations, as well as adding anti-inflammatory agents did not hinder the immune response, hence allowing detection of foreign materials *in vivo* (Molinaro, et al., 2002). It can therefore be deduced that chitosan has significant potential for delivery of bioactive molecules by conjugating to various stimuli responsive polymers, or using various carrier strategies to effectively manipulate the release kinetics, providing a variety of mechanisms for successful injectable delivery.

The modification of chitosan side chains can provide a diversity of derivatives for bone tissue engineering applications (LogithKumar, et al., 2016). Chitosan was modified into N,N,N- trimethyl chitosan (TMC) by reaction with methyl iodide and in another example, N-(2- hydroxyl) propyl-3-trimethylammonium chitosan chloride (HTCC) was prepared by dissolving chitosan in NaOH/CHPTAC aqueous solution by a pressure-equalizing dropping funnel (Fan, et al., 2015). Other modifications of chitosan include N-(2-hydroxyl) propyl-3-triethyl ammonium chitosan chloride (HTEC) and N-(2-hydroxyl-phenyl)- N,N-dimethyl chitosan (NHPDCS) (Yang, et al., 2015). Disrupting the negatively charged outer membrane of microbes is how chitosan exerts its antimicrobial activity. This is one of the many important characteristics that is needed in bone tissue engineering, and is currently still being evaluated in various bone tissue engineered delivery hydrogel systems, due to substantial biocompatible, tissue regenerative properties.

2.3.1.3. *Cellulose derived hydrogels*

Cellulose is composed of repeating units of b-(1,4)-D-glucose, an elementary component of plant cell walls, being the most abundant natural polymer available (Teeri, et al., 2007). This polymer does not possess thermo-sensitive properties, however modification of hydrophobic groups on cellulose makes the polymer thermo-sensitive. It is widely used in skin tissue and wound healing engineering. The incorporation of alkyl groups on cellulose provides significant thermo-sensitivity, proportional to the gelation rate of the hydrogel (Lee, et al., 2005). Blending was also investigated with cellulose using other natural and synthetic polymers to provide thermo-sensitivity. Alginate salts and chitosan displayed thermo-responsive properties blended to cellulose, however, incorporating chitosan- carboxymethyl cellulose (CMC) hydrogel displayed both thermo-sensitive and pH responsive behavior (Chen, et al., 2008). An alginate/hydroxypropyl methyl cellulose (HPMC) copolymeric hydrogel was also investigated, displaying a controlled release rate of 400 hours, using a prototype drug of heparin (Karewicz, et al., 2010). Similar studies were carried out using synthetic polymers of CMC blended with poly (N-vinyl pyrrolidone) (PVP), which also displayed pH and thermo-sensitive properties. The gelation was found to occur between 24 to 29 °C, although the release of the loaded bovine serum albumin from the hydrogel was greater as the pH transitioned from acid to basic (Lu, et al., 2010). Cellulose can certainly be a great potential for injectable delivery of bio-actives, since its amphiphilic properties, through conjugation with other polymers, results in highly responsive characteristics, allowing controlled release rates and maximum delivery of its loaded bioactive molecules.

A study conducted by Deniz and co-workers, looked at crosslinked pullulan/cellulose acetate fibrous scaffolds for bone tissue engineering (Atila, et al., 2016). Pullulan (P) and cellulose acetate (CA) were electrospun at different P/CA ratios (P80/CA20, P50/CA50, and P20/CA80%) to fabricate a 3D fibrous network. To enhance the mechanical properties, the scaffolds were thereafter crosslinked with trisodium trimetaphosphate (STMP). This also delayed rapid weight loss. Groups that were crosslinked with P/STMP 2/1 for 10 min displayed the lowest weight loss. Fiber morphologies were more uniform with the P50/CA50 group, without phase separation. This group was also crosslinked more effectively than the other groups. Crosslinked P50/CA50 scaffolds, among all groups, had more uniform pores. This group was thus used for bio-activity and cell culture studies. After incubation, apatite-like structures were noticed on the fibers. Human osteogenic sarcoma cell line seeded onto the crosslinked adhered and proliferated P50/CA50 scaffolds. ALP activity of the cells was used to measure the functionality of the cells. The results demonstrated their osteoblastic differentiation. It was concluded that the crosslinked P50/CA50 scaffolds were the best candidate cell carrier for bone tissue engineering in this study, with similar correlations reported by many researchers to date.

2.3.1.4 *Other natural polymers*

Other naturally available polymers are gelatin, collagen, agarose and matrigel, which also possess thermo-sensitive properties. Gelatin, collagen and agarose, however, possess negative thermo-sensitive properties, forming a gel at lower temperature and having liquid state properties at higher temperature conditions. Matrigel on the other hand, has positive thermo-sensitivity, solidifying at higher temperature states. This polymer is a mixture of components of basement membrane compounds, derived from chondrosarcoma, which has also been shown to display negative carcinogenic effects *in vivo*, due to its tumor based origin (Kleinman, et al., 2005, Tai, et al., 2003). Matrigel is the trade name by the company Becton Dickinson, which was shown to have significant cytocompatibility, allowing cells such as endothelial and chondrocytes to turn into a functional phenotype on the matrigel. It has been used as a cellular simulated environment for evaluating immune responses to drugs and other bioactive molecules. Anticancer loaded drugs in matrigel have been shown to inhibit the progression of tumours, thereby displaying a liquid characteristic at 4°C, forming a gel like substance at body temperature swelling to release its loaded bioactive molecules (Le, et al., 2008, Compte, et al., 2010). It can be considered that these natural polymers have characteristics that are essential in simulating biocompatible matrices, however their limitations allow for using synthetic polymers in combination to deliver refined,

highly specific stimuli responsive bioactive loaded copolymeric system.

The main component of connective tissue in mammals is collagen. Collagen type 1 exists in the form of elongated fibrils in bone (Velasco, et al., 2015). It is the abundant in nature and is reviewed for various bone tissue engineering applications as it has low antigenicity and excellent biocompatibility. Another reason why collagen is considered in many bone tissue engineering applications is that it has good crosslinking abilities, thus mechanical and degradation properties can be modified.

Enzymatically crosslinked carboxymethyl–chitosan/gelatin/nano-hydroxyapatite injectable gels for *in situ* bone tissue engineering application was studied by Mishra et al (Mishra, et al., 2011). The results of this study revealed that at physiological temperature, a combination of p-cresol (2 Mm) and tyrosinase (60U), as crosslinkers, yield rigid gels when applied to carboxymethyl–chitosan /gelatin within 35 minutes in the presence of nano-hydroxyapatite. An increase in carboxymethyl–chitosan concentration in the gel was observed by FTIR and rheological analysis. This leads to increased strength as well as a greater degree of crosslinking. SEM analysis revealed that the pore sizes of the injectable gels increased with higher concentrations of gelatin.

In vivo application of the injectable gels in mice showed that the degree of crosslinking and carboxymethyl–chitosan concentration determined the stability of the *in situ* formed gels. The study concluded that the carboxymethyl–chitosan/gelatin/nano-hydroxyapatite injectable gels could be used for bone cell delivery as well as in the treatment of irregular small bone defects with very little clinical invasion. A study conducted by Puértolas et al., researched compression behavior of biphasic calcium phosphate and biphasic calcium phosphate–agarose scaffolds for bone regeneration (Puértolas, et al., 2011). In order to study the potential applications of biphasic calcium phosphate (BCP) bioceramics and BCP-agarose systems for bone tissue engineering, static and dynamic compression tests have been assessed. A brittle behavior was experienced by the dense and designed porous design scaffolds in the BCP systems. Agarose displayed toughness, ductility as well as a rubbery consistency up to 60% in bioceramic BCP-agarose systems. This resulted in maximum strength, without losing its initial cylindrical structure, of 10–50 Mpa. A greater mechanical resistance was displayed by dried and rehydrated BCP-agarose systems, which is substantially higher than standard hydrogel systems. The BCP-agarose system is very promising for bone tissue engineering because it has excellent mechanical properties, as well as exceptional biocompatibility, biodegradability and affinity for proteins and cells.

2.3.2 Synthetic Polymers

Due to the lack in versatility and responsiveness in natural polymers as thermo-sensitive hydrogel carriers, synthetically derived polymers have been used as the basis for modification and conjugation with natural polymers, allowing chemical alteration in the design and responsiveness of the hydrogel system. Due to the complexity of specific carrier systems, natural polymers may not have the capacity to deliver the loaded bioactive efficiently. Synthetic thermo-sensitive polymers can be designed with flexibility for reactivity, release kinetics, gelation temperature, as well as biodegradation properties. This section will discuss the various synthetic based derivatives as thermo-sensitive hydrogel systems.

2.3.2.1. *Polyacrylamide derived thermo-responsive hydrogels*

Acrylamide based polymers have been studied for decades, being applicable to deliver thermo-responsive bioactive molecules, manipulating the lower critical solution temperature (LCST), forming a homogenous injectable delivery system (Vihola, et al., 2005, Akimoto, et al., 2009). N-substituted polyacrylamides such as poly (N, N-dimethylacrylamide), poly (N-(2-hydroxypropyl) methacrylamide lactate, poly (N-vinyl caprolactam) and PNIPAAm have significant potential as injectable hydrogel delivery systems, where molecules exist in the hydrated form due to N-substituted hydrophobic functional groups (Alzari, et al., 2009, Censi, et al., 2010). When the temperature is above LCST, interaction between N-substituted hydrophobic groups' increase above hydration energy, leading to crosslinking of the polymeric chains, forming a hydrogel dispersed network of particles. Swelling of the hydrogel system occur bellow the volume phase transition temperature (VPTT) and breaks down above VPTT (Misra, et al., 2009). The most widely used polyacrylamide is PNIPAAm, having significant properties in response to the physiological environment, forming a hydrogel at 32 °C, being able to deliver a variety of bioactive molecules as an injectable delivery system (Zhang, et al., 2010).

This section will explore the various research techniques undertaken for advancing the reactivity, LCST, swelling properties and biodegradable nature of PNIPAAm and its crosslinked copolymers. One of the drawbacks of using pure PNIPAAm hydrogels, is the instability in hydrophilic environments, dissolving rapidly, thereby releasing its loaded bioactive molecules at a rate faster than desired. Polymers such as N,N-methylenebisacrylamide (MBAAm) and 2-hydroxyethyl methacrylate (HEMA), which have 2 double bonds, are usually crosslinked to provide a greater

stability ratio for a controlled release delivery system (Kabanov, et al., 2002, Hsiue, et al., 2003). Interpenetrating network (IPN) formation is another technique for prolonging the release of PNIPAAm based polymers. Silk fibroin/PNIPAAm and NIPAAm/MBAAm IPN polymerization solution displayed greater stability than non IPN formulations (Kim, et al., 2006). Another technique was copolymerization of N-isopropylacrylamide (NIPAAm) with monomers such as oligolactide-(2- hydroxymethyl methacrylate) (oligoLA-HEMA), which successfully delivered insulin to the retina, displaying high encapsulation and sustained release rates over a 7-day period (Jiemiao, et al., 2016). A significant limitation to this versatile polymer is the inability to degrade under physiological conditions, above 32°C. Cho et al used strategies to copolymerize biodegradable polymers to PNIPAAm by altering the LCST of the hydrogel using PLA and L-lysine (Cho, et al., 2010). A similar approach was undertaken by Zhao et al incorporating poly(NIPAAm-co-HEMA) and biodegradable poly (L-glutamic acid), which possessed biodegradable properties as well as pH and thermo-sensitive characteristics (Zhao, et al., 2009). In conjunction with the success of deriving a biodegradable system, the limitation of toxic degradation products of low-molecular mass PNIPAAm displayed cytotoxicity in reproductive cells (Ankareddi, et al., 2008). In an attempt to combat these toxicological profiles, research was conducted using PNIPAAm biodegradable copolymers, having various LCSTs before and after degradation due to its biodegradable hydrophobic side chains, which have gelation temperatures below 37°C before degrading, forming hydrogels in the body. After degradation of the side chains, the gelation temperature increased above 37°C, dissolving the degraded products in the body fluid, thereby being removed from the body, and remaining in higher molecular mass due to unchanging of the backbone of the conjugated copolymer (Guan, et al., 2008). It is thus believed that these copolymeric hydrogels have great potential in injectable delivery systems, due to its ability to significantly manipulate the gelation temperatures of the copolymer and its by-products derived under physiological conditions.

2.3.2.2. *Poly (oligo (ethylene glycol) methacrylate) derived thermo-sensitive hydrogels*

Poly (oligo (ethylene glycol) methacrylate) (POEGMA) derived hydrogels have thermo-sensitive and biocompatible properties. This hydrogel system has been reported to deliver a variety of chemotherapeutic drugs (Zhou, et al., 2010). This system can be modified for drug release and variation in thermal response. It was reported that protein loaded in this polymer showed nonspecific protein adsorption, being applicable for non-protein loaded delivery systems. Oligo (ethylene glycol) methacrylate (OEGMA) and 2-(2-methoxyethoxy) ethyl methacrylate (MEO_2MA)

copolymerization demonstrated gelation temperature between 26 to 90°C, having a vast degree of application in biomedical and chemically derived injectable delivery systems. The alteration in the concentration of OEGMA contributes to the LCST of the hydrogel (Ahn, et al., 2009, Al-Abd, et al., 2010). This system is however not applicable to injectable cell delivery, but highly beneficial for drug delivery of non-protein systems.

2.3.2.3. *Polyphosphazene derived thermo-sensitive hydrogels*

Polyphosphazenes are desirable polymers for thermo-sensitive delivery systems, having immense potential for chemical modification due to its alternating single and double bonds of nitrogen and phosphorus functionalities. This makes them targets for conjugation with other polymers, attributing to their biocompatible nature (Kumbar, et al., 2006, Teasdale, et al., 2013). The side chains can be modified to obtain poly (organo phosphazene)s with a-amino-w-methoxypoly(ethylene glycol) which is hydrophilic in nature and hydrophobic L-isoleucine ethyl ester (IleOEt), which can be altered to have thermo-sensitive and pH responsive properties with various gelation temperatures (Allcock, et al., 2012). The degradation of polyphosphazenes are non-toxic, which results in alcohol, ammonia and phosphate by-products, therefore being readily biocompatible *in vivo,* which is especially seen in chemotherapeutics (Muhammad, et al., 2016). It can therefore be inferred that this hydrogel system has good loading, release and gelation properties, providing a versatile system for the delivery of many bio-actives and drug delivery systems (Choi, et al., 2010).

2.3.2.4. Pluronic derived thermo-sensitive hydrogels

Thermo-sensitive copolymer PEO-PPO-PEO, commonly referred to as pluronic, has various applications as adjustable block lengths, having a liquid state at lower temperatures due to the interaction with PEO and forming a gel at higher temperatures due to hydrophobic interaction (Gil, et al., 2004). Pluronic hydrogels are unstable in physiologically simulated environment, having a rapid dissolution, as a result, making the hydrogel limited for application in control release systems (Niu, et al., 2009). To decrease the release from the delivery system, chemical crosslinking can be undertaken, incorporating thiol and acrylate groups at either side of the chemical chain, increasing the drug retention time and the stability of the hydrogel (Clapper, et al., 2007). It was also found that by crosslinking these groups to pluronic, the loading capacity of the drug substantially increased (Yang, et al., 2008). Chemical modification can easily be obtained due to

the end hydroxyl functionalities on the chain. Studies undertaken on chemotherapeutic drugs displayed increased retention times, and greater sensitivity to tumours, by conjugating with linoleic acid, once injected at the site of the tumor (Guo, et al., 2009). Studies carried out on antithrombotic drugs showed similar results, having a high encapsulation and a sustained zero order delivery rate, with higher bioactivity (Liu, et al., 2007). The area of concern for this polymer is its biodegradability in which polyether chains cannot degrade under physiological conditions, making their application limited to many injectable hydrogel delivery systems. Their application has been noted in protein therapeutics of drug delivery (Kondiah, et al., 2013), however, there is much to be considered when the polymer is not biodegradable for *in vivo* application, when applied to injectable drug delivery.

Tissue-engineered bone formation using periosteal-derived cells and polydioxanone/pluronic F127 scaffold (PDO/Pluronic F127), with pre-seeded adipose tissue-derived CD146 positive endothelial-like cells were studied by Lee et al., from the Department of Advanced Materials, Hannam University, South Korea (Lee, et al., 2011). CD146 positive adipose tissue-derived cells were sorted to purify more endothelial cells in characterization, considering the hematopoietic and mesenchymal phenotypes of adipose tissue-derived cells cultured in EBM-2 medium. These cells were indicated as adipose tissue-derived CD146 positive endothelial-like cells. A great source of osteogenic cells for tissue engineered bone formation is periosteum. In a PDO/Pluronic F127 scaffold, Periosteal-derived cells were established to possess great osteogenic capacity. This could provide a fitting environment for osteoblastic differentiation of these cells. These cells could be investigated in EBM-2 with osteogenic induction factors through the study of capillary-like tube formation on matrigel and the cellular proliferation of adipose tissue-derived CD146 positive endothelial-like cells cultured in various media conditions. It was also observed that in the early period of culture, the osteogenic activity of periosteal-derived cells is satisfactory in EBM-2 with osteogenic induction factors. *In vivo* studies in a pig model revealed that tissue-engineered bone formation can be utilized to restore the bony defects of the maxillofacial region using periosteal-derived cells and PDO/Pluronic F127 scaffold with pre-seeded adipose tissue-derived CD146 positive endothelial-like cells.

2.3.2.5 ***PEG-polyester derived thermo-sensitive hydrogels***

Thermo-sensitive PEG-polyester based hydrogels include polyglycolide (PGA), polylactide (PLA), poly(d-valerolactone), polycaprolactone (PCL) and poly(lactide-co-glycolide) (PLGA), which are

prepared by linking ends of polyester chains at PEG ends (Buwalda, et al., 2010). The advantage of this polymer is the great biodegradable nature, providing a stimuli responsive and biocompatible platform. Polyester- PEG-polyester structures have been shown to display significant thermo-sensitivity, such as PEG-PLA copolymer, inserting a p-dioxanone(DX), resulting in physiological enhanced thermo-responsiveness. According to Kato et al, BMP loaded PEG-polyester hydrogel was delivered *in vivo*, using similar polymerisation techniques. Results showed a dual responsive pH and thermo-sensitivity, delivering the bioactive with high loading capacity in the hydrogel, displaying significant regeneration of bone at the site of delivery (Kato, et al., 2006). According to Shim et al, sulfamethazine oligomer (SMO) was copolymerized with PEG polyester copolymers, reacting to pH and temperature of physiological conditions (pH 7.4 at 37°C), nonetheless, displaying decreased degradation due to the buffering effects of SMO (Shim, et al., 2006). Exploring the degree of gelation temperature ranges, it was found that 2 polyester blocks between PEG based polymer, displays a wider range of gelation, increasing the mechanical, loading capacity and drug release profiles of the hydrogel system (Changjiang, et al., 2015). It was also shown that polyester copolymers such as poly (caprolactone-co-glycolide), poly (lactide-coglycolide) as well as diblock copolymers such as methoxy-terminatedPEG-b-poly (caprolactone-co-lactide) (PCLLA) and methoxy-terminated PEG-PCL (Mpeg-PCL) display significant thermos-sensitivity, varying their gelation temperatures to substantial ranges. A drawback of PEG-polyester copolymers are the by-products being acidic in nature, providing an immune responsive mechanism once injected at the site of delivery (Jiang, et al., 2007). However, these polymers are one of the most frequently used hydrogels for thermo-responsive application, delivering a diverse range of drugs, proteins and various bioactive molecules, with admirable loading capacity, release rate and biodegradation properties. Figure 2.4 illustrates the chemical structures of the most commonly used polymers for thermo-responsive tissue and drug engineered applications. **Table 2.1** represents a summary of the various polymers mentioned in tissue engineered applications, as well as their mechanism of gelation, delivering its bio-actives in response to a specific stimulus.

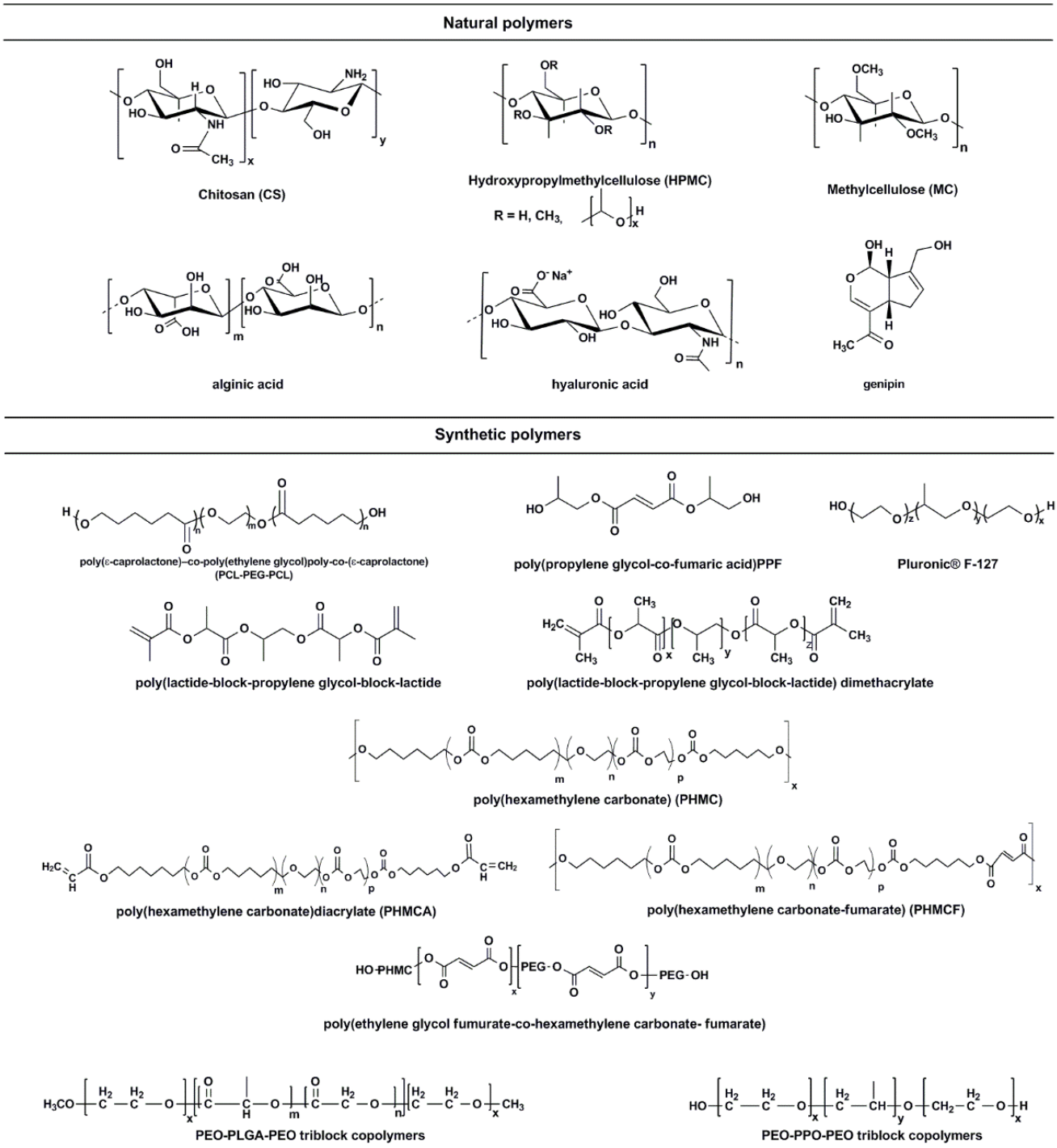


Figure 2.4. Chemical structures of selected most commonly used thermo-responsive polymers discussed in application for drug and tissue engineering (adapted with permission from Matanovic et al., 2014).

Table 2.1: Summary of injectable hydrogels for tissue engineering.

Hydrogel Source	Polymer/s Used	Gelation Mechanism	References
Natural	Hyaluronic acid, chitosan	Thermal/chemical/free radical crosslinking	[59], [65], [66], [68]
	Cellulose, Agarose, Matrigel	Thermal crosslinking	[75], [76], [78]
	Gelatin, Collagen	Thermal/chemical crosslinking	[80], [81], [82], [83]
Synthetic	PDMA, PHPMA, PNVCL PNIPAAm, Fibroin, PLA NIPAAm/MBAAm		
	Oligolactide-(2-HEMA) OligoLA-HEMA, L-Lysine PNIPAAm-Co-HEMA) P(L-glutamic acid)	Thermal crosslinking	[87], [88], [91], [92], [97], [98]
	POEGMA, OEGMA, MEO2MA	ATRP crosslinking	[101], [102], [103]
	Poly(organophosphazene) a-amino-w-methoxypoly(ethylene glycol), lleoEt	Chemical crosslinking	[104], [106], [108]
	PEO-PPO-PEO, Mpeg-PCL PEG, PGA, PLA, PCL, PLGA PVL, DX, SMO, PCLLA	Thermal crosslinking	[111], [112], [114], [117]

2.4. Injectable/Implantable Research Technologies Employed in Bone Tissue Engineering Applications

2.4.1 Research Focused on Biomedical Applications

Research in the field of bone tissue engineering has gained significant recognition in the last 7 years, with particular attention to polymeric technologies, injected as hydrogels or implanted as scaffolds; 3D printed as well, due to the specificity of the condition encountered by the researcher (Klouda, et al., 2015). Much research has focused on bone repair and healing, whilst other areas of research has focused on the regeneration of bone material. In cases of bone injuries and tumor-related defects, these biomedical technologies mimic the mechanical and ideal material composition of bone, delivering a variety of growth factors, biocompatible polymers, proteins, as well as controlled delivery of active pharmaceutical ingredients (Petit, et al, 2014, Sandker , et al., 2013, Zhang , et al., 2010, Karam, et al., 2014).

2.4.1.1. *Bone repair*

Research in the area of bone repair has demonstrated a vast interest in a variety of strategies to promote osteogenic and angiogenic responses. Of significant interest is the application of collegen-bioglass derived materials. Various bioglass®45S5, 58S, S53P4 as well as Biosilicate® has gained much popularity in bone repair (Xu, et al., 2011). Research has also been conducted using collagen-bioactive glass scaffolds, which demonstrated enhanced mineralization compared to pure collagen based scaffolds. In addition, researchers further evaluated cell cultured MC3T3-E1 cells in both scaffold variations, demonstrating greater metabolic and alkaline phosphatase (ALP) activity in both scaffolds, with lower swelling in situ when combined with bioglass (Marelli, et al., 2011). Another study reported cobalt-loaded 3D printed macroporous scaffolds of collagen and bioglass, demonstrating a compressive strength in the range of trabecular bone, with significant stability of the scaffold (Quinlan, et al., 2015). Studies using chitosan crosslinked with collagen and reinforced with bioactiveglass, as a nanoparticulate thermo-responsive injectable system, demonstrated significant gelation at body temperature, with promising potential as an injectable bone tissue engineered system (Moreira, et al., 2016). One of the benefits of injectable treatments compared to implantable technologies is that, invasive surgery is kept to a minimum, however implantable scaffolds demonstrated greater immediate weight-bearing, due to the strength and stiffness which is obtained nearly instantaneously from a scaffold implantation

(Kuttappan, et al., 2016).

2.4.1.2. *Regeneration of bone tissue*

In the field of research involving regenerative bone tissue material, various studies have been undertaken, evaluating the differentiation of osteoblasts, various growth factors and re-mineralization in bone tissue. Many studies demonstrated the application of chitosan, crosslinked with various salts and phosphate materials, indicating significant bone regenerative effects. One of the studies using this strategy was conducted by Niranjan and coworkers. They developed a thermo-sensitive hydrogel scaffold of zinc doped chitosan/beta-glycerophosphate, which exhibited geometrically defined pore networks, with significant crystalline and swelling properties. The polymeric system was proved to demonstrate antibacterial, biocompatible and substantial osteoblast differentiation (Niranjan, et al., 2013).

In other research studies, stimuli-responsive polymeric bone regenerative systems involving the use of cyclodextrins, adamantine and crosslinking of PNIPAM was found to be particularly beneficial in bone regeneration applications. A thermo-sensitive hydrogel, crosslinked with the above chemical entities, enabled gelation after injectable delivery *in vivo*, and was further proved to demonstrate biocompatible and biodegradable properties. Furfurylamine grafted chondroitin sulfate (ChS-F) and maleimido-terminated poly (ethylene glycol) (PEG2K–AMI), significantly increased the mechanical strength of the system, further substantiating that the hydrogel considerably induced bone regeneration when tested in a male Kunming mice model (Bai, et al., 2016).

Figure 2.5 outlines the general approach undertaken when formulating a stimuli-responsive bone tissue engineered delivery system, incorporated with biological growth factors and signals, specific cell cultures biocompatible with the copolymeric material, as well as active pharmaceutical ingredients, able to promote bone repair and regeneration. Another study explaining this concept, as seen in Figure 2.5, successfully proved mineralization, new bone formation and tissue responses to PNiPAAm based hydrogels, evaluated in a rat cranial defected model. The implanted scaffold demonstrated substantial bone regeneration within 12 weeks of implantation. It was reported that the hydrogel promoted matrix hydrophobicity-dependent mineralization, demonstrating significant strategies for stem cell and growth factor biocompatibility within the hydrogel system for effective bone regenerative application (Vo, et al., 2015).

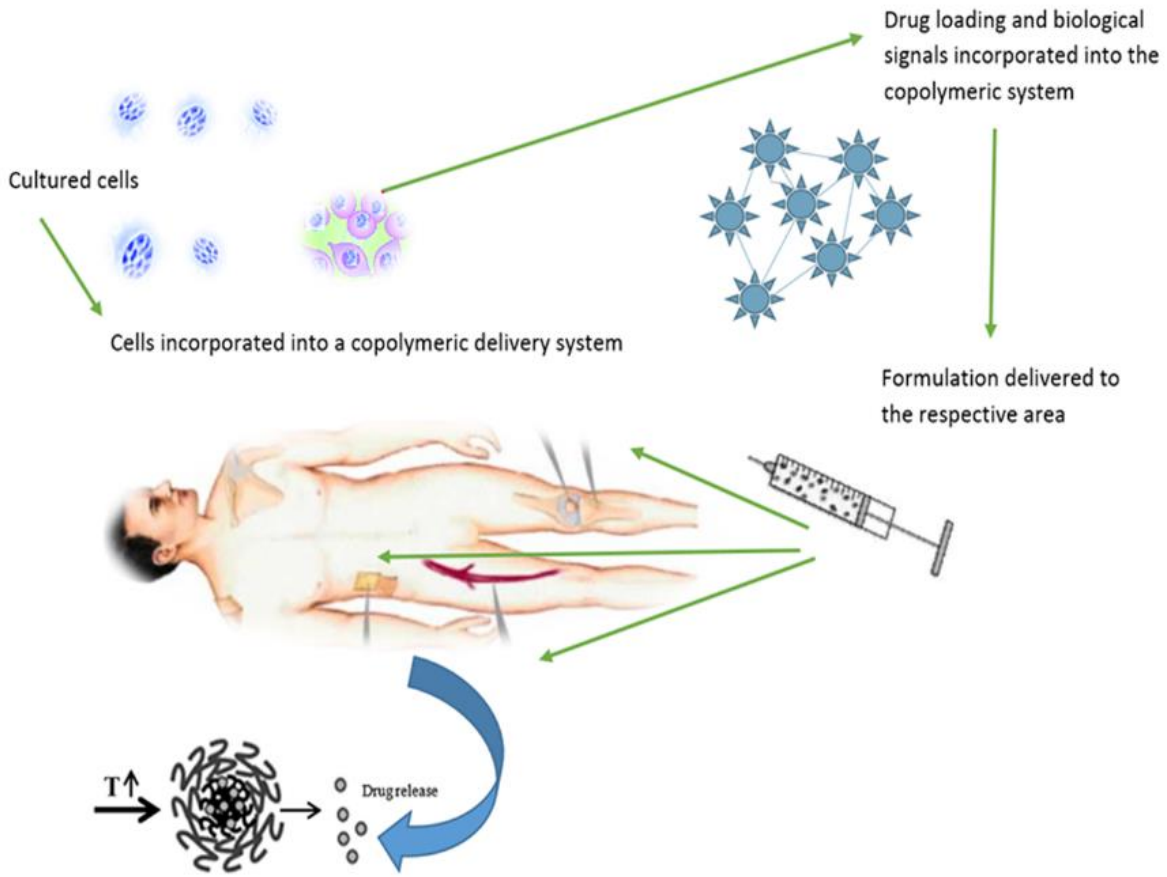


Figure 2.5. Schematic representation of tissue engineering application, delivering drug-loaded thermo-sensitive polymers with bioactive signals.

2.5. Nano-Enabled Thermo-Responsive Hydrogel Systems

The integration of stimuli-responsive hydrogels with numerous nano-carriers is a promising technique for extended delivery of growth factors, proteins, polymeric network of molecules as well as loading of bone repairing and regenerative active pharmaceutical agents. Surface decoration of nanoparticles is also one of the uses of thermo-responsive polymers. The combination of *in situ* forming gelling systems with nano-sized drug delivery, for example diverse liposomes or nanoparticles, have become a growing interest to date, with the strategy of achieving a controlled kinetic system by increasing the surface area to volume ratio of the copolymeric delivery system (Grabnar, et al., 2011). The utilization of poloxamer gels and polylactic-co-glycolic acid (PLGA) nanoparticles were investigated *in vitro* and *in vivo*. Their combined polymeric properties for subcutaneous delivery of peptides and proteins with short half-lives were also analyzed (Barichello, et al., 1999). Results demonstrated that formulations containing protein-

loaded PLGA nanoparticles, possessed greater long-term therapeutic effects, in comparison to non-nano systems evaluated. The incorporation of poly (3- hydroxybutyrate-co-3-hydroxyhexanoate), further exemplified the controlled mechanism of release in the hydrogel, promoting a sustained injectable delivery system, suitable for chronic osteoporosis conditions (Peng, et al., 2013).

With regards to poorly soluble drugs, biodegradable thermo-responsive nano-particulate hydrogels can be useful for local injectable delivery, especially applicable in small bone fractures, where the use of pins and casts are not practically incorporated. To operate as a platform for the slow release of hydrophobic drugs, such as simvastatin, used to promote bone strengthening, thermo-responsive Pluronic F127 hydrogels with poly (e-caprolactone)-poly (ethylene glycol)-poly (e-caprolactone) nanoparticles serve as a prototype formulation, among many other crosslinked combinations, having hydrophobic and hydrophilic units, able to load a variety of drugs and BMPs for bone repair and strengthening, releasing them in a controlled mechanistic approach. It was established that the LCST of this system can be improved with a larger mass of the incorporated nanoparticles (Gou, et al., 2008).

Thermo-responsive polymers may also be useful in the biomedical field in the form of nano-carriers (Licciardi, et al., 2012). The emergence of several types of nano-carriers with magnetic targeting capability, by coating them with thermo-responsive polymers, have been revealed in numerous articles (Lien, et al., 2013, Lien, et al., 2008, Lien, et al., 2011). Due to their inimitable properties, these magnetic, redox responsive and thermo-sensitive nanoparticles have demonstrated immense potential in controlled drug delivery and greater therapeutic efficacy *in vivo*. To establish a targeted drug delivery system in response to higher temperature conditions, novel thermo-responsive nanoparticles formulated by the self- assembly of poly(N,N-diethylacrylamide-co-acrylamide)- block-poly(g-benzyl)L-glutamate were designed and evaluated (Li. et al., 2009). It was therefore capable of adjusting the LCST of nanoparticles to a value between body temperature and the temperature in local hyperthermia (~43℃). This system has significant potential for bone related injuries, especially reacting to the stimulus of inflammatory markers, where greater temperature dependent stimuli-responsive properties in the hydrogel are essential.

2.6. Advancing the Efficacy of Hydrogels in Drug Delivery Applications

Prompt drug release from the gel matrix results in the large water content of nearly all hydrogels, especially in the instance of hydrophobic drugs for which the deliverance of hydrogels is predominantly employed. This release profile is more concise than that which is achieved by macroscopic or microscopic mechanisms. These processes are based on more hydrophobic polymeric systems. Therefore, many different ideas have been investigated to lower the rate of release of drugs within a hydrogel system.

2.6.1. Drug-hydrogel interactions

To improve the binding between a loaded drug and the hydrogel matrix, chemical and physical strategies can be utilized to prolong the duration of drug release.

2.6.1.1. *Physical interactions*

To amplify the strength of the interactions between the gel and a target drug, charge interactions between ionic polymers and charged drugs have commonly been utilized to cause the release of the drug to be delayed. Phosphate-functionalized polymers have become useful in this regard. This is particularly due to their multivalent anionic charge. Phosphate-containing soft contact lenses can bind a cationic drug such as naphazoline in amounts which are directly proportional to the phosphate content (Sato, et al., 2005). Amino functional groups can be used to bring about a delayed release of anionic drugs. Anionic and cationic properties of functional groups can have an influence in extending the release of a drug which is of opposite charge. This is generally found in carbohydrate-based polymers (Rodriguez, et al., 2003). Hyaluronic acid has been used as a delivery vehicle for local anesthetics due to its charge interactions, biocompatibility and viscosity (Hassan, et al., 1988, Doherty, et al., 1995, Johansson, et al., 1985). Monomers or polymers with particular nonionic affinities to a specific drug can be copolymerized into hydrogels, as alternatives, to postpone or augment the release of the drug. Amphotericin B, an antifungal drug, has significant interaction with photocross-linked dextran-based hydrogels, which therefore allows contact eradication of fungi for 2 months (Zumbuehl, et al., 2007). The precise binding mechanism is vague as Amphotericin B did not bind to PEG-derived hydrogels of equal chain density. The precise mechanism of molecular binding remains uncertain.

2.6.1.2 *Covalent bonding*

To ensure that the release of the drug is essentially controlled by the rate of chemical or enzymatic cleavage of the polymer-drug bond, the drug can be covalently conjugated to the hydrogel matrix. For example, to facilitate osteogenic differentiation of human mesenchymal stem cells, dexamethasone has been conjugated to a photo-reactive mono-acrylated PEG through a degradable lactide bond (Nuttelman, et al., 2006). On the other hand, hydrolysis of the polymer backbone can also regulate drug release, perhaps stimulating the release of a relatively altered drug analogue. For instance, methacrylic functionalized non-steroidal anti-inflammatory drugs, by means of UV radiation, have been conjugated to methacrylic functionalized dextrans; a chemically modified drug analogue is released as the dextran hydrogel degrades (Feeney, et al., 2007, Schoenmakers, et al., 2004).

2.7. Analogous Cell and Biomaterial Characterization for *In Vitro* Success and *In Vivo* Translation

The efficacy of tissue development should be characterized in vitro and in vivo, after selecting or designing the appropriate biomaterial and cell source for an injectable tissue engineering system. There have been several cell types and polymer systems that have been useful to bone tissue engineering in injectable systems in vivo and in vitro, with regards to cartilage. Paige *et al* encapsulated chondrocytes in alginate and thereafter subcutaneously implanted it in mice. This was one of the first examples of injectable cartilage tissue. Matrix production of cartilage-relevant molecules was revealed by histological analysis. In a similar manner, Sims applied chondrocytes to PEG, a synthetic polymer (Sims, et al., 1996). Cartilage production observed with PEG and alginate was similar. Collagen, PEG encapsulated with poly-lactic or –glycolic groups and polyvinyl alcohol, are other examples of biological and synthetic polymers that have been combined with chondrocytes (Bryant, et al., 1999, Bryant, et al., 2003). A clinically used tissue glue, fibrin, could also be combined with chondrocytes to yield high-quality cartilage (as determined through biochemical analysis, as well as histologically) (Ronga, et al., 2004, Silverman, et al., 1999, Ting, et al., 1998, Isogai, et al., 2000). However, fibrin glue has weak mechanical properties which unfortunately limit its application in cartilage tissue engineering in vivo.

For bone tissue engineering, chondrocytes can be isolated from various cartilages such as costal

(rib) (Ting, et al., 1998, Thirion, et al., 2004), articular, nasal septum (Kafienah, et al., 2002, Chia, et al., 2004) as well as auricular (Saadeh, et al., 1999, Fussenegger, et al., 2003). Chondrocytes from these sources, in addition to variable ease in clinical access for biopsy, have unpredictable tissue formation and proliferation characteristics. Using chondrocytes isolated from different regions embedded in fibrin glue, cartilage development in an injectable tissue engineering system was evaluated (Xu, et al., 2004). Considerable differences were observed in mass and biochemical properties of tissue engineered from articular, auricular and costal cartilage, with the greatest size and mechanical properties being generated by auricular-based tissue. Articular chondrocytes were found to have inferior tissue production. This is perhaps due to their requirement for mechanical stimulation which was absent in the subcutaneous environment where the constructs were implanted.

The majority of the injectable cartilage tissue engineering scaffolds rely on hydrogel materials as a scaffold. Mercier et al., in a recent study, obtained a technique to produce an injectable cartilage repair system using a solid polymer, poly (lactide-co-glycolide) (PLG) (Mercier, et al., 2004). PLG was used to create an injectable system by forming microspheres of polymers that were injected with a suspension of chondrocytes.

2.8. Current Research Approaches to Date

Brenden et al., from the Department of Bioengineering of Rice University, Houston, investigated biodegradable, phosphate-containing, dual-gelling macromers for cellular delivery in bone tissue engineering (Watson, et al., 2015). When elevated to physiological temperature, the injectable, biodegradable, dual-gelling macromers were utilized to encapsulate mesenchymal stem cells within stable hydrogels. To improve the biointergration and to facilitate hydrogel degradation, pedant phosphate groups were incorporated within the N-isopropyl acrylamide-based macromers. The live cells remained within the hydrogel for 28 days *in vitro*. Acellular and cell-laden hydrogels were then implanted into a critical-size rat cranial defect for 4 and 12 weeks, and were thereafter shown to degrade *in vivo* as well as help to facilitate bone growth at the site of defect. Improved bone bridging of the defect was observed, as well as direct bone-to-hydrogel contact was noticed in the majority of the implants. Thus it was concluded that this class of marcomers is a promising material for craniofacial bone tissue engineering.

PEG-silk hydrogel combined with polymeric particles was also investigated for delivering rhBMP-

2 for bone regeneration (Ma, et al., 2016). A composite hydrogel was developed which consisted of PLA/PLGA polymeric particles which was used as a BMP-2 delivery vehicle. The initiation of PLA into PEG-silk gels resulted in the hydrogel having new hydrophobicity properties. This inhibited the burst release of BMP-2 as well as improved the gel's structural ability. Furthermore, these composite gels could stabilize entrapped proteins and conserve their bioactivity *in vitro*. *In vivo*, the bio-degradability experiment indicated that this system was biocompatible. The new hydrophobicity properties remarkably decreased the degradation rate. In a rat critical-sized cranial fracture model, the gel containing PLA promoted the most bone formation. The results of this research indicated that the employment of PLA changed the physicochemical properties of gels more appropriate as a BMP-2 carrier and this induced bone regeneration significantly in large bone fractures.

Biomineralization of calcium phosphate crystals on chitin nanofiber hydrogel for bone regeneration material was investigated by Mari and co-workers (Kawataa, et al., 2016). A calcium phosphate/chitan nanofibre hydrogel was prepared for bone tissue engineering. Calcium phosphate was mineralized on the hydrogel. This was done by incubation in a solution of diammonium hydrogen phosphate followed by calcium nitrate tetrahydrate. The formation of calcium phosphate crystals was revealed by Fourier transform infrared spectroscopy (FTIR) and X-ray diffractometry (XDR). The morphology of the calcium phosphate crystals was contingent on the calcification time. The reinforcement effect of the calcium phosphate crystal lead to the improvement of the mechanical properties of the hydrogel after mineralization. Calcium phosphate/chitin nanofibre hydrogel increased mineralization in subcutaneous tissues in an animal model. Morphological osteoblasts were also noticed.

Studies using Hyaluronic acid (HA) based hydrogel scaffolds with a triple degradation behavior for bone tissue engineering was also strategically investigated (Cui, et al., 2015). HA hydrogels which have a triple degradation behavior were synthesized to better mimic the nature of bone extracellular matrix. These hydrogels were synthesized from 3,3′-dithiodipropionate hydrazide-modified HA (DTPH–HA) and polyethylene glycol dilevulinate (LEV–PEG–LEV) through the reaction of ketone carbonyl groups of LEV–PEG–LEV with the hydrazide groups of DTPH–HA. Results from the study revealed that the HA hydrogels displayed a very porous morphology and had pore diameters which ranged from 20-200μm. Hyaluronidase and reducing substances or acidic pH values could be used to degrade the HA hydrogels. Osteoblast-like MC3T3-E1 cells by live/dead staining and MTT assays were used to analyze the biocompatibility of the HA hydrogels.

The results indicated that these hydrogels had very good compatibility and could also support the attachment and proliferation of MC3T3-E1 cell. All the results of this experiment revealed that the HA hydrogels synthesized by hydrazone bond crosslinking have substantial potential to be used in bone tissue engineering.

It can thus be concluded that all the above mentioned studies are promising research avenues in the field of bone tissue engineering. Many of these studies have been done by more than one research platforms, confirming similar positive correlation results. These responsive polymers are significantly capable of promoting new cell growth and increasing the rate of tissue repair. Furthermore, these studies have been evaluated *in vivo*, producing significant responses to the bioengineered system, having a defined positive potential advancement for promoting bone regeneration and repair.

2.9. Concluding Remarks

Injectable stimuli responsive hydrogels exhibit a significant platform for bone tissue engineering with the benefit that cells as well as drugs can be infused into the gelling matrix. The success of injectable tissue constructs is greatly dependent on chemical, physical and biological properties. Hydrogels display water based homogenous properties to encapsulate, manipulate and transfer its contents to the surrounding tissue, in the least invasive manner. Numerous attempts have been made to augment injectable hydrogels, and accordingly, assist the enhancement of natural and functional tissues. Thus far, injectable tissue engineering in the field of orthopedic sciences has produced countless benefits over previous application methods. Irrespective of shape and defect geometry, injectable therapy has an unparalleled advantage in which intricate sites of therapy can be effortlessly targeted with minimum invasive procedures. The field of thermo-responsive hydrogels is of great interest to biomedical researchers and engineers. Excellent progress has been made by studying the different natural and synthetic polymers that can be utilized in this field of bone tissue engineering and thus novel materials have been proposed. Key factors such hydrophilic/hydrophobic balance in the molecular composition have been modified in order to produce hydrogels with desired features. Biodegradability, physiological range, as well as augmentation of mechanical properties have been an important research focus, producing exciting potential for employing thermo-responsive hydrogels in bone tissue engineering applications. The global bone graft substitutes market is growing rapidly due to patient need and health care improvement. The design and production of biodegradable hydrogels for bone tissue

engineering applications has thus become a major research and development interest, with significant bone tissue technologies currently being investigated to date, thus expecting major advancements in the near future for bone tissue engineered delivery systems.

2.10. References

Ahn, S.; Monge, EC.; Song, SC. Ion and Ph effect on the lower critical solution temperature phase behavior in neutral and acidic poly(organophosphazene) counterparts. *Langmuir*. 2009, *25, 2407-18.*

Akimoto, J.; Nakayama, M.; Sakai, K.; et al. Temperature-induced intracellular uptake of thermoresponsive polymeric micelles. B*iomacromolecules*. 2009, *10, 1331-6.*

Al-Abd, A.M.; Hong, K.Y.; Song, S.C.; et al. Pharmacokinetics of doxorubicin after intratumoral injection using a thermosensitive hydrogel in tumor-bearing mice. *J Control Release*. 2010, *142, 101-7.*

Allcock, H.R.; Morozowich, N.L. Investigation of Apatite Mineralization on Antioxidant Polyphosphazenes for Bone Tissue Engineering. *Polym. Chem*. 2012, *3, 578–590.*

Alzari, V.; Monticelli, O.; Nuvoli, D.; et al. Stimuli responsive hydrogels prepared by frontal polymerization. *Biomacromolecules.* 2009, *10, 2672-7.*

Ankareddi, I.; Bailey, M.M.; Brazel, C.S.; et al. Developmental toxicity assessment of thermoresponsive poly(Nisopropylacrylamide-co-acrylamide) oligomers in CD-1 mice. *Birth Defects Res B Dev Reprod Toxicol.* 2008, *83, 112-16.*

Arrington, E.; Smith, W.; Chambers, H.; Bucknell, A.; Davino, N, Clin. Iliac wing fracture following graft harvesting from the anterior iliac crest: Literature review based on a case report. *Orthopaedics Rel. Res.* 1996, *329,* 300.

Atila, D.; Keskin, D.; Tezcaner, A. Crosslinked pullulan/cellulose acetate fibrous scaffolds for bone tissue engineering. *Materials Science and Engineering*. 2016, 69, 1103-1115.

Babo, P.S.; Santo, V.E.; Gomes, M.E.; Reis, R.L. Development of an Injectable Calcium Phosphate/Hyaluronic Acid Microparticles System for Platelet Lysate Sustained Delivery Aiming Bone Regeneration. *Macromol Biosci*. 2016, 10, 1002.

Bai, X., Lü, S., Cao, Z., Gao, C., Duan, H., Xu, X., Sun, L., Gao, N., Feng, C., Liu, M. Self-reinforcing injectable hydrogel with both high water content and mechanical strength for bone repair. Chemical Engineering Journal. 2016, 288, 546–556.

Barichello, J.M.; Morishita, M.; Takayama, K.; Nagai, T. Absorption of insulin from Pluronic F-127 gels following subcutaneous administration in rats. *Int. J. Pharm*. 1999, *184, 189–198.*

Bessa, P.C.; Machado, R.; Nurnberger, S.; Dopler, D.; Banerjee, A.; Cunha, A.M.; Rodriguez-Cabello, J.C.; Redl, H.; van Griensven, M.; Reis, R.L.; et al. Thermoresponsive self-assembled elastin-based nanoparticles for delivery of bmps. *J. Control. Release*. 2010, *142, 312-318.*

Bhattarai, N.; Gunn, J.; Zhang, M. Chitosan-based hydrogels for controlled, localized drug delivery. *Adv Drug Deliv Rev.* 2010, *62, 83-99.*

Brandl, F.; Sommer, F.; Goepferich, A. Rational design of hydrogels for tissue engineering: Impact of physical factors on cell behaviour. *Biomaterials.* 2007, *28,* 134–146.

Bryant, S.J.; Anseth, K.S. Controlling the spatial distribution of ECM components in degradable PEG hydrogels for tissue engineering cartilage. *J. Biomed. Mater. Res.* 2003, *64(1), 70-79*.

Bryant, S.J.; Nuttelman, C.R.; Anseth, K.S. The effects of crosslinking density on cartilage formation in photocrosslinkable hydrogels. *Biomed. Sci. Instrum*. 1999, *35, 309-314*.

Bulmus, V. RAFT polymerization mediated bioconjugation strategies, *Polym. Chem*. 2011, *2, 1463–1472.*

Buwalda, S.J.; Dijkstra, P.J.; Calucci, L.; et al. Influence of amide versus ester linkages on the properties of eight-armed PEGPLA star block copolymer hydrogels. *Biomacromolecules*. 2010, *11, 224-32.*

Cao, Z.; Jiang, D.; Yan, L.; Wu, J. In vitro and in vivo osteogenic activity of the novel vancomycin-loaded bone-like hydroxyapatite/poly(amino acid) scaffold. *Journal of Biomaterials Applications.* 2016, *30, 1566-77*.

Censi, R.; Vermonden, T.; Deschout, H.; et al. Photopolymerized thermosensitive poly(HPMAlactate)-PEG-based hydrogels: effect of network design on mechanical properties, degradation, and release behavior. *Biomacromolecules*. 2010, *11, 2143-51.*

Changjiang, F.; Dong-An, W. A biodegradable PEG-based micro-cavitary hydrogel as scaffold for cartilage tissue engineering. *European Polymer Journal*. 2015, 72, 651–660.

Chen, H.; Fan, M. Novel thermally sensitive Ph-dependent chitosan/ carboxymethyl cellulose hydrogels. *J Bioact Compat Polym.* 2008, *23, 38-48.*

Chenite, A.; Chaput, C.; Wang, D.; et al. Novel injectable neutral solutions of chitosan form biodegradable gels in situ. *Biomaterials*. 2000, *21, 2155-61.*

Chia, S.H.; Schumacher, B.L.; Klein, T.J.; et al. Tissue-engineered human nasal septal cartilage using the alginate-recovered-chondrocyte method. *Laryngoscope*. 2004, *114(1), 38-45.*

Cho, E.C.; Kim, J.W.; Hyun, D.C.; et al. Regulating volume transitions of highly responsive hydrogel scaffolds by adjusting the network properties of microgel building block colloids. *Langmuir.* 2010, *26, 3854-9.*

Choi, W.I.; Yoon, K.C.; Im, S.K.; et al. Remarkably enhanced stability and function of core/shell nanoparticles composed of a lecithin core and a pluronic shell layer by photo-crosslinking the shell layer: in vitro and in vivo study. *Acta Biomater.* 2010, *6, 2666-73.*

Clapper, J.; Skeie, J.; Mullins, R.; et al. Development and characterization of photopolymerizable biodegradable materials from PEG–PLA–PEG block macromonomers. *Polymer (Guildf).* 2007, *48, 6554-64.*

Compte, M.; Alonso-Camino, V.; Santos-Valle, P.; et al. Factory neovessels: engineered human blood vessels secreting therapeutic proteins as a new drug delivery system. *Gene Ther.* 2010, *17, 745-51.*

Coughlan, D.C.; Corrigan, O.I. Release kinetics of benzoic acid and its sodium salt from a series of poly (N-isopropylacrylamide) matrices with various percentage crosslinking. *J. Pharm. Sci.* 2008, *97,* 318-330.

Davis, K.A.; Burdick, J.A.; Anseth, K.S. Photoinitiated crosslinked degradable copolymer networks for tissue engineering applications. *Biomaterials*, 2003, *24, 2485.*

Doherty, M.M.; Hughes, P.J.; Korszniak, N.V.; Charman, W.N. Prolongation of Lidocaine-Induced Epidural Anesthesia by Medium Molecular Weight Hyaluronic Acid Formulations: Pharmacodynamic and Pharmacokinetic Studies in the Rabbit. *Anesthesia and Analgesia*. 1995, *80(4), 740e6.*

Drury, J.L.; Mooney, D.J. Hydrogels for tissue engineering: Scaffold design variables and applications. *Biomaterials.* 2003*, 24,* 4337–4351

Fan, L.; Yang, J.; Wu, H.; Hu, Z.; Yi, J.; Tong, J.; *et al*., Preparation and characterization of quaternary ammonium chitosan hydrogel with significant antibacterial activity. *International Journal of Biological Macromolecules*. 2015, 79, 830–836.

Feeney, M.; Giannuzzo, M.; Paolicelli, P.; Casadei, M.A. Hydrogels of Dextran Containing Nonsteroidal Anti-Inflammatory Drugs as Pendant Agents. *Drug Delivery.* 2007, *14(2), 87e93.*

Fussenegger, M.; Meinhart, J.; Hobling, W.; Kullich, W.; Funk, S.; Bernatzky, G. Stabilized autologous fibrin-chondrocyte constructs for cartilage repair in vivo. *Ann. Plast. Surg*. 2003, *51(5), 493-498.*

Garty, S.; Kimelman-Bleich, N.; Hayouka, Z.; Cohn, D.; Friedler, A.; Pelled, G.; Gazit, D. Peptide-modified “smart” hydrogels and genetically engineered stem cells for skeletal tissue engineering. *Biomacromolecules*. 2010, *11, 1516-1526.*

Gil, E.; Hudson, S. Stimuli-reponsive polymers and their bioconjugates. *Polyme*r. 2004, *29, 1173-222.*

Goa, K.L.; Benfield, P. Hyaluronic acid. A review of its pharmacology and use as a surgical aid in ophthalmology, and its therapeutic potential in joint disease and wound healing. *Drugs,* 1994, *47, 536-66.*

Gordon, S.; Teichmann, E.; Young, K.; et al. In vitro and in vivo investigation of thermosensitive chitosan hydrogels containing silica nanoparticles for vaccine delivery. *Eur J Pharm Sci*. 2010, *41, 360-8.*

Gou, M.; Li, X.; Dai, M.; Gong, C.; Wang, X.; Xie, Y.; Deng, H.; Chen, L.; Zhao, X.; Qian, Z.; Wei, Y. A novel injectable local hydrophobic drug delivery system: biodegradable nanoparticles in thermo-sensitive hydrogel. *Int. J. Pharm*. 2008. *359, 228–233*.

Grabnar, A.; P.; Kristl, J. The manufacturing techniques of drug-loaded polymeric nanoparticles from preformed polymers. *J. Microencapsulation*. 2011, *28, 323–335.*

Guan, J.; Hong, Y.; Ma, Z.; et al. Protein-reactive, thermoresponsive copolymers with high flexibility and biodegradability. *Biomacromolecules*. 2008, *9, 1283-92.*

Guo, D.D.; Xu, C.X.; Quan, J.S.; et al. Synergistic anti-tumor activity of paclitaxel-incorporated conjugated linoleic acid-coupled poloxamer thermosensitive hydrogel in vitro and in vivo. *Biomaterials*. 2009, *30, 4777-85.*

Hassan, H.G.; Akerman, B.; Renck, H.; Lindberg, B. Effects of macromolecular adjuvants on the duration of prilocaine. *Acta Anaesthesiologica Scandinavica*. 1988, *29(4), 384e8.*

Healy, K.E.; Guldberg, R.E. Bone tissue engineering. *J Musculoskelet Neuronal Interact.* 2007, *7(4):*328-330

Hosseinkhani, H.; Hosseinkhani, M.; A. Khademhosseini, A.; Kobayashi, H.; Tabata, Y. Enhanced angiogenesis through controlled release of basic fibroblast growth factor from peptide amphiphile for tissue regeneration. *Biomaterials*. 2006, *27, 5836*.

Hosseinkhani, H.; Hosseinkhani, M.; Khademhosseini, A.; Kobayashi, H. J. Bone regeneration through controlled release of bone morphogenetic protein-2 from 3-D tissue engineered nano-scaffold. *Control Release*. 2007, *117, 380.*

Hsiue, G.H.; Chang, R.W.; Wang, C.H.; Lee, S.H Development of in situ thermosensitive drug vehicles for glaucoma therapy. *Biomaterials.* 2003, *24, 2423-30.*

Hsu, S.H.; Leu, Y.L.; Hu, J.W.; et al. Physicochemical characterization and drug release of thermosensitive hydrogels composed of a hyaluronic acid/pluronic f127 graft. *Chem Pharm Bull (Tokyo).* 2009, *57, 453-8.*

Hunt, N.C.; Grover, L.M. Cell encapsulation using biopolymer gels for regenerative medicine. *Biotechnol. Lett*. 2010, 32, 733e742.

Ifkovits, J.L.; Burdick, J.A. Photopolymerizable and Degradable Biomaterials for Tissue Engineering Applications. *Tissue Eng*. 2007, *13,* 2369.

Isogai, N.; Landis, W.J.; Mori, R.; et al. Experimental use of fibrin glue to induce site-directed osteogenesis from cultured periosteal cells. *Plast. Reconstr. Surg*. 2000, *105(3), 953-963.*

Jha, A.K.; Jackson, W.M.; Healy, K.E. Controlling Osteogenic Stem Cell Differentiation via Soft Bioinspired Hydrogels. *PloS One*. 2014, 9(6), 98640.

Jhon, Y.K.; Bhat, R.R.; Jeong, C.; Rojas, O.J.; Szleifer, I.; Genzer, J. Salt-induced depression of lower critical solution temperature in a surface-grafted neutral thermoresponsive polymer. *Macromol. Rapid Commun*. 2006, *27,* 697-701.

Jiang, W.W.; Su, S.H.; Eberhart, R.C.; et al. Phagocyte responses to degradable polymers. *J Biomed Mater Res A.* 2007, *82, 492-7.*

Jiemiao, Y.; Liangrong, Yang.; Xiangfeng, L.; Tingting, D.; Hongnan, Q.; Meng, R.; Huizhou, L. Aptamer and PNIPAAm co-conjugated nanoparticles regulate activity of enzyme with different temperature. *Talanta*. 2016, 159, 47–54.

Jin, R.; Hiemstra, C.; Zhong, Z.; Feijen, J. Enzyme-mediated fast in situ formation of hydrogels from dextran–tyramine conjugates. *Biomaterials*. 2007, *28, 2791.*

Johansson, A.; Hassan, H.; Renck, H. Effects of Adjuvants to Local Anaesthetics on Their Duration. *Acta Anaesthesiologica Scandinavica.* 1985, *29(7), 736e8*.

Jones, D.S.; Lorimer, C.J.; Andrews, G.P.; McCoy, C.P.; Gorman, S.P. An examination of the thermorheological and drug release properties of zinc tetraphenylporphyrin-containing thermoresponsive hydrogels, designed as light activated antimicrobial implants. *Chem. Eng. Sci*. 2007, *62,* 990-999.

Jones, D.S.; Lorimer, C.P.; McCoy, C.P.; Gorman, S.P. Characterization of the physicochemical, antimicrobial, and drug release properties of thermoresponsive hydrogel copolymers designed for medical device applications. *J. Biomed. Mater. Res.* 2008, *85B,* 417-426.

Jones, D.S.; Lorimer, C.P.; McCoy, C.P.; Gorman, S.P. Characterization of the physicochemical, antimicrobial, and drug release properties of thermoresponsive hydrogel copolymers designed for medical device applications. *J. Biomed. Mater. Res. Part B.* 2008, *85B,* 417-426.

Kabanov, A.V.; Batrakova, E.V.; Alakhov, V.Y. Pluronic block copolymers as novel polymer therapeutics for drug and gene delivery. *J Control Release.* 2002, *82, 189-212.*

Kafienah, W.; Jakob, M.; Demarteau, O.; et al. Three-dimensional tissue engineering of hyaline cartilage: Comparison of adult nasal and articular chondrocytes. *Tissue Eng*. 2002, *8(5), 817-826*.

Kan, P.; Lin, X.Z.; Hsieh, M.F.; Chang, K.Y. Thermogelling emulsions for vascular embolization and sustained release of drugs. *J. Biomed. Mater. Res. Part B.* 2005, *75B, 185-192.*

Karam, J.P., Muscari, C., Sindji, L., Bastiat, G., Bonafe, F., Venier-Julienne, M.C., Montero-Menei, N.C. Pharmacologically active microcarriers associated with thermosensitive hydrogel as a growth factor releasing biomimetic 3D scaffold for cardiac tissue-engineering. J. Control. Release. 2014, 192, 82–94.

Karewicz, A.; Zasada, K.; Szczubiałka, K.; et al. 'Smart' alginate-hydroxypropylcellulose microbeads for controlled release of heparin. *Int J Pharm.* 2010, *385, 163-9.*

Kato, M.; Toyoda, H.; Namikawa, T.; et al. Optimized use of a biodegradable polymer as a carrier material for the local delivery of recombinant human bone morphogenetic protein-2 (rhBMP-2). *Biomaterials.* 2006, *27, 2035-41.*

Kawataa, M.; Azumab, K.; Izawaa, H.; Morimotoa, M.; Saimotoa, H.; Ifukua, S. Biomineralization of calcium phosphate crystals on chitin nanofiber hydrogel for bone regeneration material. *Carbohydrate Polymers*. 2016, 136, 964–969. Cui, N.; Qian, J.; Liu, T.; Zhao, N.; Wang, H. Hyaluronic acid hydrogel scaffolds with a triple degradation behavior for bone tissue engineering. *Carbohydrate Polymers*, 2015, 126, 192–198.

Khan, F.; Tanaka, M.; Ahmad, S.R. Fabrication of polymeric biomaterials: a strategy for tissue engineering and medical devices. *J. Mater. Chem. B*. 2015, 3, 8224-8249.

Kim, Y.S.; Gil, E.S.; Lowe, T.L. Synthesis and characterization of thermoresponsiveco – biodegradable linear-dendritic copolymers. *Macromolecules.* 2006, *39, 7805-11.*

Kleinman, H.K.; Martin, G.R. Matrigel: basement membrane matrix with biological activity. *Semin Cancer Biol.* 2005, *15, 378-86.*

Klouda, L. Thermoresponsive hydrogels in biomedical applications. A seven-year update. European Journal of Pharmaceutics and Biopharmaceutics. 2015, 97, 338–349.

Kofron, M.; Laurencin, C. Bone tissue engineering by gene delivery. *Advanced Drug Delivery. Rev*. 2006, *58,* 555-576

Kondiah, P.P.D.; Choonara, Y.E.; Tomar, L.K.; Tyagi, C.; du Toit, L.S.; Kumar, P.; Modi, G,; Pillay, V. Novel pH sensitive oral Interferon-β delivery system for application in Multiple Sclerosis. *IJP*. 2013, *456, 459-472.*

Kretlow, J.; Klouda, L.; Mikos, A. Injectable matrices and scaffolds for drug delivery in tissue engineering. *Adv. Drug Deliv. Rev*. 2007, *59,* 263.

Kumbar, S.G.; Bhattacharyya, S.; Nukavarapu, S.P.; et al. In vitro and in vivo characterization of biodegradable poly(organophosphazenes) for biomedical applications. *J Inorg Organomet P.* 2006, *16, 365-85.*

Kuttappan, S., et al. Biomimetic composite scaffolds containing bioceramics and collagen/gelatin for bone tissue engineering- A mini review Int. J. Biol. Macromol. 2016., http://dx.doi.org/10.1016/j.ijbiomac.2016.06.043.

Langer, R.; Vacanti. Tissue engineering: the design and fabrication of living replacement devices for surgical reconstruction and transplantation. *J. Science*. 1993, 260, 920

Le, U.M.; Shaker, D.S.; Sloat, B.R.; et al. A thermo-sensitive polymeric gel containing a gadolinium (Gd) compound encapsulated into liposomes significantly extended the retention of the Gd in tumors. *Drug Dev Ind Pharm.* 2008, *34, 413-18.*

Lee, J.; Kim, J.; Oh, S.; Kim, S.; Hah, Y.; Park, B.; Deok Ryong Kim, D.; Gyu-Jin Rho, G.; Maeng, G.; Jeon, G.; Lee, H.; Kim, J.; Kim, G.; Kim, U.; Byun, J. Tissue-engineered bone formation using periosteal-derived cells and polydioxanone/pluronic F127 scaffold with pre-seeded adipose tissue-derived CD146 positive endothelial-like cells. *Biomaterials*. 2011, 32, 5033-5045.

Lee, S.C. Control of thermogelation properties of hydrophobically-modified methylcellulose. *J Bioact Compat Polym.* 2005, *20, 5-13.*

Leea, K.Y.; Mooneya, D.J. Alginate: Properties and biomedical applications. *Progress in Polymer Science.* 2012, *37, 106–126.*

Li, Y.; Pan, S.; Zhang, W.; Du, Z. 2009. Novel thermo-sensitive core-shell nanoparticles for targeted paclitaxel delivery. *Nanotechnology*. 2009, *20, 0957–4484*.

Licciardi, M.; Amatoa, G.; Cappellic, A.; Paolinoc, M.; Giulianic, G.; Belmonted, B.; Guarnottad, C.; Pitarresi, G.; Giammona, G. Evaluation of thermoresponsive properties and biocompatibility of polybenzofulvene aggregates for leuprolide delivery. *Int. J. Pharm*. 2012, *438, 279–286*.

Lien, Y.H.; Wu, J.H.; Liao, J.W.; Wu, T.M. In vitro evaluation of the thermosensitive and magnetic nanoparticles for the controlled drug delivery of vitamin D3. *Macromol. Res*. 2013, *21, 511–518.*

Lien, Y.H.; Wu, T.M. Preparation and characterization of thermosensitive polymers grafted onto silica-coated iron oxide nanoparticles. *J. Colloid Interf. Sci*. 2008, *326, 517–521*.

Lien, Y.H.; Wu, T.M.; Wu, J.H.; Liao, J.W. Cytotoxicity and drug release behaviour of PNIPAM grafted on silica-coated iron oxide nanoparticles. *J. Nanopart. Res*. 2011, *13, 5065–5075.*

Liu, Y.; Lu, W.L.; Wang, J.C.; et al. Controlled delivery of recombinant hirudin based on 54hermos-sensitive Pluronic F127 hydrogel for subcutaneous administration: in vitro and in vivo characterization. J Control Release 2007;117:387-95

LogithKumar, R.; KeshavNarayan, A.; Dhivya, S.; Chawla, A.; Saravanan, S.; Selvamurugan, N. A review of chitosan and its derivatives in bone tissue engineering. *Carbohydrate Polymers*, 2016, 151, 172–188.

Lu, S.; Liu, M.; Ni, B.; et al. A novel pH- and thermo-sensitive PVP/CMC semi-IPN hydrogel: swelling, phase behavior, and drug release study. *J Polym Sci B Polym Phys.* 2010, *48, 1749-56.*

Luis, A.C.D.; Mohamed, E.; Alberto, S.; Julie, E.G.; Aline, F.M. Osteogenic differentiation of human mesenchymal stem cells promotes mineralization within a biodegradable peptide hydrogel. *Journal of Tissue Engineering*. 2016, 7, 1–15.

Ma, D.; An, G.; Liang, M.; Liu, Y.; Zhang, B.; Wang, Y. A composited PEG-silk hydrogel combining with polymeric particles delivering rhBMP-2 for bone regeneration. *Materials Science and Engineering*. 2016, 65, 221–231.

Ma, Z.W.; Nelson, D.M.; Hong, Y.; Wagner, W.R. Thermally responsive injectable hydrogel incorporating methacrylate-polylactide for hydrolytic lability. *Biomacromolecules.* 2010, *11, 1873-1881.*

Mahdieh, Z.;, Bagheri, R.; Eslami, M.; Mohammad Amiri , M.; Shokrgozar, M.A.; Mehrjoo, M. Thermoplastic starch/ethylene vinyl alcohol/forsterite nanocomposite as a candidate material for bone tissue engineering. *Materials Science and Engineering.* 2016, *C 69, 301–310.*

Marelli, B., Ghezzi, C.E., Mohn, D., Stark, W.J., Barralet, J.E., Boccaccini, A.R., Nazhat, S.N. Accelerated mineralization of dense collagen-nano bioactive glass hybrid gels increase scaffold stiffness and regulates osteoblastic function. Biomat. 2011, 32, 34, 8915–8926.

Mayol, L.; Quaglia, F.; Borzacchiello, A.; et al. A novel poloxamers/hyaluronic acid in situ forming hydrogel for drug delivery: rheological, mucoadhesive and in vitro release properties. *Eur J Pharm Biopharm.* 2008, *70, 199-206.*

Meenach, S.A.; Anderson, K.W.; Hilt, J.Z. Synthesis and characterization of thermoresponsive poly(ethylene glycol)-based hydrogels and their magnetic nanocomposites. *J. Polym. Sci. Part A.* 2010, *48, 3229-3235.*

Mercier, N.R.; Costantino, H.R.; Tracy, M.A.; Bonassar, LJ. A novel injectable approach for cartilage formation in vivo using PLG microspheres. *Ann. Biomed. Eng*. 2004, *32(3), 418-429.*

Mishra, D.; Bhunia, B.; Banerjee, I.; Datta, P.; Dhara, S.; Maiti, T.K. Enzymatically crosslinked carboxymethyl–chitosan/gelatin/nano-hydroxyapatite injectable gels for in situ bone tissue engineering application. *Materials Science and Engineering*. 2011, 31, 1295–1304.

Misra, G.P.; Singh, R.S.J.; Aleman, T.S.; et al. Subconjunctivally implantable hydrogels with degradable and thermoresponsive properties for sustained release of insulin to the retina. *Biomaterials.* 2009, *30, 6541-7.*

Molinaro, G.; Leroux, JC.; Damas, J.; et al. Biocompatibility of thermosensitive chitosan-based hydrogels: an in vivo experimental approach to injectable biomaterials. *Biomaterials.* 2002, *23, 2717-22.*

Moreira, C.D., Carvalho, S.M., Mansur, H.S., Pereira, M.M. Thermogelling chitosan–collagen–bioactive glass nanoparticle hybrids as potential injectable systems for tissue engineering, Mater. Sci. Eng. 2016, 58, 1207–1216.

Muhammad, A.; Haojie, Y.; Li, W.; Hamad, K.; Nasir, M. A.; Zain-ul-Abdin.; Yongsheng, C.; Fujie, Ren.; Muhammad, S. Sustained release of hydrophilic drug from polyphosphazenes/poly(methyl methacrylate) based microspheres and their degradation study. *Materials Science and Engineering*. 2016, 58, 169–179.

Ngiam, M.; Liao, S.; Patil, A.J.; Cheng, J.; Chan, C.K.; Ramakrishna. The fabrication of nano-hydroxyapatite on PLGA and PLGA/collagen nanofibrous composite scaffolds and their effects in osteoblastic behavior for bone tissue engineering. *S. Bone*. 2009, 45,4

Nicodemus, G.D.; Bryant, S.J. Cell encapsulation in biodegradable hydrogels for tissue Engineering applications. *Tissue Eng*. 2008, *14,* 149–165.

Niranjan, R., Koushik, C., Saravanan, S., Moorthi, A., Vairamani, M., Selvamurugan, N. A novel injectable temperature-sensitive zinc doped chitosan/beta –glycerophosphate hydrogel for bone tissue engineering. Int. J. Biol. Macromol. 2013, 54, 24– 29.

Niu, G.; Du, F.; Song, L.; et al. Synthesis and characterization of reactive poloxamer 407s for biomedical applications. *J Control Release.* 2009, *138, 49-56.*

Nuttelman, C.R.; Rice, M.A.; Rydholm, A.E.; Salinas, C.N.; Shah, D.N.; Anseth, K.S. Macromolecular monomers for the synthesis of hydrogel niches and their application in cell encapsulation and tissue engineering. *Prog. Polym*. *Sci*. 2008, *33,* 167–179

Nuttelman, C.R.; Tripodi, M.C.; Anseth, K.S. Dexamethasone-functionalized gels induce osteogenic differentiation of encapsulated hMSCs. *Journal of Biomedical Materials Research Part A.* 2006, *76(1), 183e95*.

Ohya, S.; Nakayama, Y.; Matsuda, T. Thermoresponsive artificial extracellular matrix for tissue engineering: hyaluronic acid bioconjugated with poly(N-isopropylacrylamide) grafts. *Biomacromolecules.* 2001, *2, 856-63.*

Papaphilippou, P.C.; Pourgouris, A.; Marinica, O.; Taculescu, A.; Athanasopoulos, G.I.; Vekas, L.; Krasia-Christoforou, T. Fabrication and characterization of superparamagnetic and thermoresponsive hydrogels based on oleic-acid-coated Fe3O4 nanoparticles, hexa(ethylene glycol) methyl ether methacrylate and 2-(acetoacetoxy)ethyl methacrylate. *J. Magn. Magn. Mater*. 2011, *323, 557-563.*

Peng, Q.; Sun, X.; Gong, T.; Wu, C.Y.; Zhang, T.; Tan, J.; Zhang, Z.R. Injectable and biodegradable thermosensitive hydrogels loaded with PHBHHx nanoparticles for the sustained and controlled release of insulin. *Acta Biomater*. 2013, *9, 5063–5069*.

Perez, R.A.; Kim, M.; Kim, T.; Kim, J.; Lee, L.H.; Park, J.; Jonathan, C.; Kim, K.H. Utilizing Core–Shell Fibrous Collagen-Alginate Hydrogel Cell Delivery System for Bone Tissue Engineering. *Tissue Eng Part A*. 2014, 1, 20(1-2), 103–114.

Petit, A., Sandker, M., Muller,B.,Meyboom, R., van Midwoud, P., Bruin, P., Redout, E.M., Versluijs-Helder, M., van der Lest, C.H., Buwalda, S.J., de Leede, L.G., Vermonden, T., Kok, R.J., Weinans, H., Hennink, W.E. Release behavior and intraarticular biocompatibility of celecoxib-loaded acetyl-capped PCLA-PEG-PCLA thermogels. Biomat. 2014, 35, 7919–7928.

Place, E.S.; Rojo, L.; Gentleman, E.; Sardinha, J.P.; Stevens, M.M. Strontium- and Zinc-Alginate Hydrogels for Bone Tissue Engineering. *Tissue Engineering Part A*. 2011, *17(21-22): 2713-2722*.

Puértolas, J.A.; Vadillo, J.L.; Sánchez-Salcedo, S.; Nieto, A.; Gómez-Barrena, E.; Vallet-Regí, M. Compression behavior of biphasic calcium phosphate and biphasic calcium phosphate–agarose scaffolds for bone regeneration. *Acta Biomaterialia*. 2011, 7, 841–847.

Quinlan, E., Partap, S., Azevedo, M.M., Jell, G., Stevens, M.M., O'Brien, F.J. Hypoxia-mimicking bioactive glass/collagen glycosaminoglycan composite scaffolds to enhance angiogenesis and bone repair. Biomat. 2015, 52, 358–366.

Rabkin, E.; Schoen, E.F. Integration of concepts: Cardiac extracellular matrix remodeling after myocardial infarction. *Cardiovasc. Pathol*. 2002, *11,* 305.

Ramesh, N.; Alka, A.M. Biodegradable and biocompatible temperature sensitive triblock copolymer hydrogels as draw agents for forward osmosis. *Separation and Purification Technology.* 2016, 168, 83–92.

Ramesh, N.; Chandru, K.; Sekaran, S.; Ambigapathi, M.; Mariappanadar, V.; Nagarajan, S. A novel injectable temperature-sensitive zinc doped chitosan/□-glycerophosphate hydrogel for bone tissue engineering. *International Journal of Biological Macromolecules*. 2013, 54, 24–29.

Rincon, A.C.; Molina-Martinez, I.T.; de Las Heras, B.; Alonso, M.; Bailez, C.; Rodriguez-Cabello, J.C.; Herrero-Vanrell, R. Biocompatibility of elastin-like polymer poly(vpavg) microparticles: In vitro and in vivo studies. *J. Biomed. Mater. Res. Part A.* 2006, *78A, 343-351.*

Rodriguez, R.; Alvarez-Lorenzo, C.; Concheiro, A. Interactions of ibuprofen with cationic polysaccharides in aqueous dispersions and hydrogels: Rheological and diffusional implications. *European Journal of Pharmaceutical Sciences*. 2003, *20(4e5), 429e38*.

Ronga, M.; Grassi, F.A.; Bulgheroni, P. Arthroscopic autologous chondrocyte implantation for the treatment of a chondral defect in the tibial plateau of the knee. *Arthroscopy.* 2004, *20(1), 79-84.*

Royals, M.A.; Fujita, S.M.; Yewey, G.L.; Rodriguez, J.; Schultheiss, P.C.; Dunn, R.L. Biocompatibility of a biodegradable *in situ* forming implant system in rhesus monkeys, *J. Biomed. Mater. Res.* 1999, *45, 231*.

Ruel-Gariepy, E.; Leclair, G.; Hildgen, P.; et al. Thermosensitive chitosan-based hydrogel containing liposomes for the delivery of hydrophilic molecules. *J Control Release.* 2002, *82, 373-83.*

Russo, R.; Malinconico, M.; Santagata, G. Effect of Cross-Linking with Calcium Ions on the Physical Properties of Alginate Films. *Biomacromolecules*. 2007, 8 *(10), pp 3193–319.*

Saadeh, P.B.; Brent, B.; Mehrara, B.J.; et al. Human cartilage engineering: chondrocyte extraction, proliferation, and characterization for construct development. *Ann. Plast. Surg*. 1999, *42(5), 509-513*.

Sakai, S; Hirose, K.; Taguchi, K.; Ogushi, Y.; Kawakami, K. An injectable, *in situ* enzymatically gellable, gelatin derivative for drug delivery and tissue engineering. *Biomaterials*. 2009, *30, 3371*.

Sandker, M.J., Petit, A., Redout, E.M., Siebelt, M., Muller, B., Bruin, P., Meyboom,R., Vermonden, T., Hennink, W.E., Weinans, H. In situ forming acyl-capped PCLA-PEG- PCLA triblock copolymer based hydrogels. Biomat. 2013, 34, 8002– 8011.

Sato, T.; Uchida, R.; Tanigawa, H.; Uno, K.; Murakami, A. Application of polymer gels containing side-chain phosphate groups to drug-delivery contact lenses. *Journal of Applied Polymer Science*. 2005, *98(2), 731e5.*

Schoenmakers, R.G.; van de Wetering, P.; Elbert, D.L.; Hubbell, J.A. The effect of the linker on the hydrolysis rate of drug-linked ester bonds. *Journal of Controlled Release.* 2004, *95(2), 291e300.*

Shi, W.; Ji, Y.; Zhang X.; et al. Characterization of pH- and thermosensitive hydrogel as a vehicle for controlled protein delivery. *J Pharm Sci.* 2011, *100, 886-95.*

Shim, W.S.; Kim, J.H.; Park, H.; et al. Biodegradability and biocompatibility of a pH- and thermosensitive hydrogel formed from a sulfonamide-modified poly(epsilon-caprolactone-co-lactide)-poly (ethylene glycol)-poly(epsiloncaprolactone-co-lactide) block copolymer. *Biomaterials*. 2006, *27, 5178-85.*

Silverman, R.; Passaretti, D.; Haung, W.; Randolph, M.A.; Yaremchuk, M.J. Injectable tissue-engineered cartilage using a fibrin glue polymer. *Plast. Reconstr. Surg*. 1999, *103, 1809-1818.*

Sims, D.; Butler, P.E.; Casanova, R.; et al. Injectable cartilage using polyethylene oxide polymer substrates. *Plast. Reconstr. Surg*. 1996, *98, 843-850*.

Sivashanmugam, A.; Arun Kumar, R.; Vishnu Priya, M.; Nair, S.V.; Jayakumar, R. An overview of injectable polymeric hydrogels for tissue engineering. *European Polymer Journal*. 2015, 72, 543–565.

Sperinde, J.; Griffith, L. Synthesis and Characterization of Enzymatically-Cross-Linked Poly(ethylene glycol) Hydrogels. *Macromolecules*. 1997, *30, 5255*.

Stabenfeldt, S.E.; Garcia, A.J.; LaPlaca, M.C. Thermoreversible laminin-functionalized hydrogel for neural tissue engineering. *J. Biomed. Mater. Res. Part A.* 2006, *77A, 718-725*.

Stolzing, A.; Jones, E.; McGonagle, D.; Scutt, A. Age-related changes in human bone marrow-derived mesenchymal stem cells: Consequences for cell therapies Mechanisms of Ageing and Development. *Cytotherapy.* 2008, *129, 3,* 163-173

Strehin, I.; Nahas, Z.; Arora, K.; Nguyen, T.; Elisseeff, J. A versatile Ph sensitive chondroitin sulfate–PEG tissue adhesive and hydrogel. *Biomaterials*. 2010, *31, 2788.*

Tai, K.F.; Chen, P.J.; Chen, D.S.; et al. Concurrent delivery of GM-CSF and endostatin genes by a single adenoviral vector provides a synergistic effect on the treatment of orthotopic liver tumors. *J Gene Med.* 2003, *5, 386-98.*

Teasdale, I.; Brüggemann, O. Polyphosphazenes: Multifunctional, Biodegradable Vehicles for Drug and Gene Delivery*. Polymers*. 2013, *5, 161–187.*

Teeri, T.T.; Brumer, H.; Daniel, G.; et al. Biomimetic engineering of cellulose-based materials. *Trends Biotechnol.* 2007, *25, 299-306.*

Thirion, S.; Berenbaum, F. Culture and phenotyping of chondrocytes in primary culture. *Methods Mol. Med*. 2004, *100, 1-14.*

Tiffany, N. Vo.; Adam, K.E.; Patrick, P.S.; Brendan, M.; Stephanie, N.T.; Terrence, T.R.; Antonios, G.M. In vitro and in vivo evaluation of self-mineralization and biocompatibility of injectable, dual-gelling hydrogels for bone tissue engineering. *Journal of Controlled Release*. 2015, 205 25–34.

Ting, V.; Sims, C.D.; Brecht, L.E.; et al. In vitro prefabrication of human cartilage shapes using fibrin glue and human chondrocytes. *Ann. Plast. Surg*. 1998, *40(4), 413-420.*

Tran, R.T.; Gyawali, D, Nair, P.; Yang, J. Synthesis, Degradation and Applications. Biodegradable Injectable Systems for Bone Tissue Engineering. *International Journal of Polymer Science.* 2011, 14, 97-100

Tu, R.S.; Tirrell, M. Cytotoxicity of nanoparticle-loaded polymer capsules. *Adv. Drug Deliv. Rev*. 2004, *56, 1537.*

Vacanti, J.P.; Langer, R. Lancet. Tissue engineering: the design and fabrication of living replacement devices for surgical reconstruction and transplantation. *The lancet.* 1999, *354,* 32.

Velasco*, M.A.; Narváez-Tovar, C.A.; Garzón-Alvarado, D.A. Design, Materials, and Mechanobiology of Biodegradable Scaffolds for Bone Tissue Engineering. BioMed Research International. 2015, 10.1155.*

Vihola, H.; Laukkanen, A.; Valtola, L.; et al. Cytotoxicity of thermosensitive polymers poly(N-isopropylacrylamide), poly(Nvinylcaprolactam) and amphiphilically modified poly(N-vinylcaprolactam). *Biomaterials*. 2005, *26, 3055-64.*

Vo, T.N., Ekenseair, A.K., Spicer, P.P., Watson, B.M., Tzouanas, S.N., Roh, T.T., Mikos, A.G. In vitro and in vivo evaluation of self-mineralization and biocompatibility of injectable, dual-gelling hydrogels for bone tissue engineering, J Controlled Release. 2015, 205, 25–34

Wang, N.; Dong, A.; Radosz, M.; Shen, Y.Q. Thermoresponsive degradable poly(ethylene glycol) analogues. *J. Biomed. Mater. Res. Part A.* 2008, *84A, 148-157.*

Watson, B.M.; Vo, T.N.; Tatara, A.M.; Shah, S.R.; Scott, D.W.; Engel, P.S.; Mikos, A.G. Biodegradable, phosphate-containing, dual-gelling macromers for cellular delivery in bone tissue engineering. *Biomaterials*. 2015, 67, 286-296.

Wong Po Foo, C.T.; Lee, J.S.; Mulyasasmita, W.; Parisi-Amon, A.; Heilshorn. A modular approach to the design of protein-based smart gels. S.C. *Proc. Natl. Acad. Sci. U S A.* 2009, *106, 22067.*

Wu, D.Q.; Qiu, F.; Wang, T.; Jiang, X.J.; Zhang, X.Z.; Zhuo, R.X. Toward the development of partially biodegradable and injectable thermoresponsive hydrogels for potential biomedical applications. *ACS Appl. Mater. Interfaces.* 2009, *1, 319-327.*

Xu, C., Su, P., Chen, X., Meng, Y., Yu, W., Xiang, A.P., Wang, Y. Biocompatibility and osteogenesis of biomimetic bioglass-collagen-phosphatidylserine composite scaffolds for bone tissue engineering. Biomat. 2011, 32, 4, 1051–1058.

Xu, J.W.; Zaporojan, V.; Peretti, G.M.; et al. Injectable tissue-engineered cartilage with different chondrocyte sources. *Plast. Reconstr. Surg*. 2004, *113(5) 1361-1371.*

Yang, X.; Zhang, C.; Qiao, C.; Mu, X.; Li, T.; Xu, J.; *et al.,* A simple and convenient method to synthesize N-[(2-hydroxyl)-propyl-3-trimethylammonium] chitosan chloride in an ionic liquid. *Carbohydrate Polymers*. 2015, 130, 325–332.

Yang, Z.; Ding, J. A thermosensitive and biodegradable physical gel with chemically crosslinked nanogels as the building block. *Macromol Rapid Commun.* 2008, *29, 751-6.*

Yoshida, T.; Aoyagi, T.; Kokufuta, E.; Okano, T. Newly designed hydrogel with both sensitive thermoresponse and biodegradability. *J. Polym. Sci. Part A.* 2003, *41, 779-787*.

Yu, F.; Cao, X.; Li, Y.; Zeng, L.; Yuan, B.; Chen, X. An injectable hyaluronic acid/PEG hydrogel for cartilage tissue engineering formed by integrating enzymatic crosslinking and Diels–Alder ‘‘click chemistry’’. *Polym. Chem*. 2014, 5, 1082–1090.

Yu, L.; Ding, J. Injectable hydrogels as unique biomedical materials. *Chem. Soc. Rev.* 2008, *37,* 1473–1481.

Zhang, J.T.; Keller, T.F.; Bhat, R.; et al. A novel two-level microstructured poly (N-isopropylacrylamide) hydrogel for controlled release. *Acta Biomater.* 2010*, 6, 3890-8.*

Zhang, T.; Yan, Y.; Wang, X.; et al. Three-dimensional Gelatin and Gelatin/ Hyaluronan Hydrogel Structures for Traumatic Brain Injury. *J Bioact Compat Polym.* 2007, *22, 19-29.*

Zhang, Z., Lai, Y., Yu, L., Ding, J. Effects of immobilizing sites of RGD peptides in amphiphilic block copolymers on efficacy of cell adhesion. Biomat. 2010, 31, 7873–7882.

Zhao, C.; Zhuang, X.; He, P.; et al. Synthesis of biodegradable thermo- and pH-responsive hydrogels for controlled drug release. *Polymer (Guildf).* 2009, *50, 4308-16.*

Zhou, T.; Wu, W.; Zhou, S. Engineering oligo(ethylene glycol)-based thermosensitive microgels for drug delivery applications. *Polymer (Guildf).* 2010, *51, 3926-33*.

Zumbuehl, A.; Ferreira, L.; Kuhn, D.; Astashkina, A.; Long, L.; Yeo, Y.; et al. Antifungal hydrogels. *Proceedings of the National Academy of Sciences of the United States of America*. 2007,*104(32), 12994e8.*

CHAPTER 3
DEVELOPMENT OF AN INJECTABLE PSEUDO-BONE THERMO-GEL FOR APPLICATION IN SMALL BONE FRACTURES

3.1. Introduction

Approximately 2.2 million bone graft surgeries are conducted globally each year. As a result, surgeons are faced with multiple clinical challenges in bone reconstruction. Some of these challenges are defect sizes, anatomic sites, mechanical stresses and available soft tissue cover (Tang, et al., 2016). The gold standard for repairing skeletal defects is autologous bone grafting, however, this method has many disadvantages which include bone graft loss, problems relating to the surgical site, short-term instability in massive defects and autograft failure rates which is greater than 50% in complicated healing environments (Bosco, et al., 2016). Due to these shortcomings, the utilization of synthetic implants is becoming increasingly popular. Nevertheless, present day biomaterials were initially fabricated for other engineering approaches, as a result, there may be many limitations such as a foreign-body reaction, infection, as well as extrusion of the implanted biomaterial (Iwase, et al., 2016).

Recently, the development of injectable polymeric hydrogels and thermo-gels for the treatment of bone defects are gaining much research popularity. These systems are composed of various polymers that have specific properties that will heal the defected bone and support bone regeneration (Zhao, et al., 2016, LogithKumar, et al., 2016). To date, injectable thermo-gels in the field of bone tissue engineering has provided numerous advantages over former approaches. Injectable therapy has an unparalleled benefit in which complex defected areas can be effortlessly targeted without invasive methods. It can also increase the physico-mechanical properties of the damaged bone by delivering many drug molecules as well as growth factors to the site of injury (Farokhi, et al., 2016).

Due to the thermo-gel possessing water based homogenous properties, it displays a remarkable platform for bone tissue engineering. It has the ability to encapsulate, manipulate and transfer its constituents to the surrounding tissue. Polymeric thermo-gels, loaded with a statin drug, has been known to increase bone repair. The polymeric gel further provides mechanical support at the site of bone injury (Nayef, et al., 2016). A thermo-responsive injectable system behaves as a transitional sol-gel system. This occurs by reacting the injectable system to a stimulus, resulting

in a change of physical and chemical properties (Ma, et al., 2016). Upon gelation of the injectable thermo-gel, cellular responses and cell distribution are promoted. Due to the significant hydrated nature of the thermo-gel, simulation of the extra cellular matrix (ECM) is an essential property responsible for bone healing and repair (Jeong, et al., 2016, Khoshroo, et al., 2017). To date, numerous polymers, due to their biocompatible and biodegradable properties, have been analysed for injectable delivery (Luo, et al., 2016). These polymers possess specific stimuli responsive properties, which efficiently deliver its encapsulated constituents at the site of injury (Hashimoto, et al., 2015, Tang, et al., 2016, Caetano, et al., 2016, Caramella, et al., 2016, Yunus, et al., 2015).

The properties of maintaining thermo-gelation refers to a system by which a substance undergoing change must in all instances be in thermodynamic equilibrium with its surroundings. The pressure and temperature of the substance should differ minimally from its surroundings at a stage of slow cycle operation. Frictional forces must be minimum, with least loss of energy due to conduction, convection or radiation during the cycle process (Santapuri, et al., 2016, Lucia, et al., 2016, Egner, et al., 2016). The transition from sol to gel, correspond to a change in temperature conditions. However, once substantial energy is dissipated from the system and thermodynamic equilibrium is lost, the system will lose its gelation nature. In an injectable thermo-gel system, due to minimum interferences from its environment *in situ*, properties of its responsive nature will be preserved in a substance/material at a given temperature range. Properties such as stability, biocompatibility and biodegradability are conserved when physiological conditions are maintained (Jung, et al., 2017, Nguyen, et al., 2015, Deng, et al., 2014).

This chapter focuses on the formulation of an injectable pseudo-bone thermo-gel drug delivery system, possessing considerable fluid dynamic properties as a sol-gel formulation. The formulation, loaded with a suitable active pharmaceutical ingredient (API), was evaluated for its chemical, physical and rheological properties. This chapter discusses the remarkable characteristics of the pseudo-bone thermo-gel, substantially proving its potential for application in bone fracture repair, and the restoration of bone matrix hardness and resilience.

3.2. Materials and Methods

3.2.1 Materials

Diethyl fumarate, 98%; diethyl ether (anhydrous); hydrochloric acid,1.85% $^{v}/_{v}$; hydroquinone, 99% purity; methylene chloride; propylene glycol (1,2-propandiol); sodium sulphate and zinc chloride were purchased from Merck (Pty) Ltd. PEG (Mw 4000), epsilon-caprolactone, 99%; stannous octoate, 92.5%; petroleum ether, 90%; pluronic F-127; poly(ethylene glycol) diacrylate and simvastatin (molecular weight: 418.57), 97% purity, were procured from Sigma-Aldrich (St. Louis, MO, USA). All other reagents were of analytical grade and were employed as received. All synthetic reactions were carried out under inert conditions.

3.2.2 Synthesis of Poly (Propylene Fumarate) (PPF)

Poly (propylene fumarate) (PPF) was prepared by a two-step procedure involving bis(hydroxypropyl) fumarate as an intermediate owing to the relative lower by-product formation associated with this synthetic procedure, as seen in Figure 3.1. Initially diethyl fumarate (30.52g, 180 mmol) and propylene glycol (40.75g, 540 mmol) were reacted in an oven-dried 500 ml round bottom flask (RBF), under inert conditions, at a temperature of 90°C. To this stirred solution, the crosslinking inhibitor hydroquinone (0.0303 g, 0.266 mmol), and the Lewis acid catalyst $ZnCl_2$ (0.2 g, 1.53 mmol) was added. Thereafter, the temperature of the system was increased to 110 °C. Following this step, the temperature was gradually increased from 110 °C in increments of 10 °C every 30 minutes to 130 °C. This reaction step yielded the intermediate bis(hydroxypropyl) fumarate and ethanol (distillate), and the reaction was ceased when 90% of the theoretical ethanol was collected in the receiving flask.

In the second step, the bis(hydroxypropyl) fumarate was transesterified to afford PPF and ethanol as the primary by-product. This reaction was carried out under vacuum (<1 mmHg) while the temperature was slowly increased from 100 to 130°C (increment of 10 °C every 30) until the required molecular weight of PPF was obtained. The crude polymer product was thereafter dissolved in dichloromethane (DCM) and the reaction mixture was washed twice with a 1.85 % $^{v}/_{v}$ solution of HCl to remove the catalyst. Thereafter the purification step was repeated with doubled-distilled water and portions of brine solution respectively. The organic phase was dried over anhydrous sodium sulphate, filtered and DCM was removed by rotary evaporation. The resulting

polymer solution was poured into a previously chilled diethyl ether solution for removal off excess hydroquinone by precipitation of the purified PPF. Subsequently, the precipitate was isolated and re-suspended in DCM which was also removed under vacuum to yield the pure PPF polymer (average yield obtained as 70%) (Shung, et al., 2002, Kasper, et al., 2009, Timmer, et al., 2003).

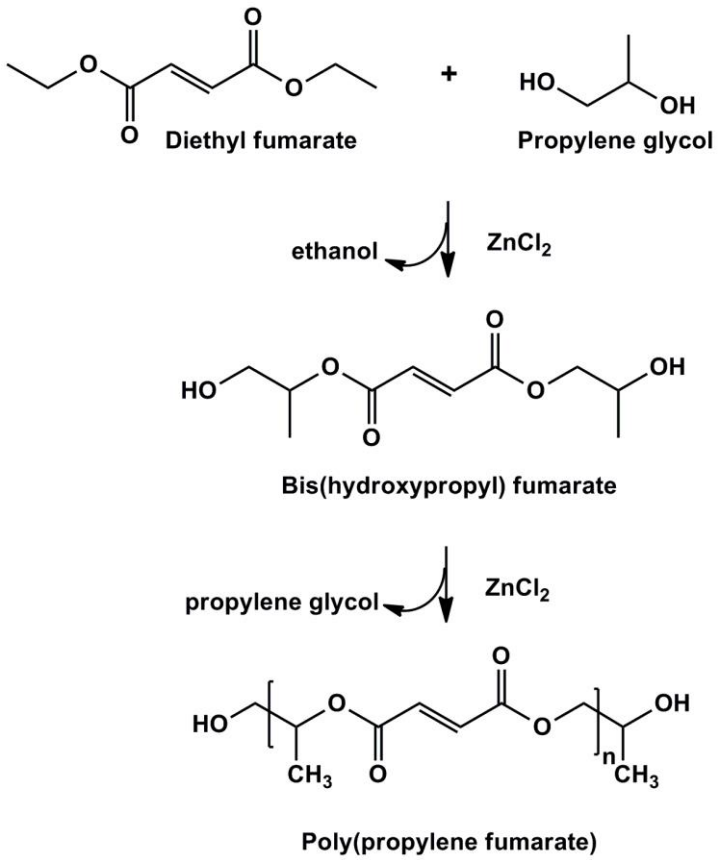


Figure 3.1: Schematic representation of the synthesis for PPF, using a 2-step method involving bis(hydroxypropyl) fumarate as an intermediate.

3.2.3 Copolymer Blend to Form the Pseudo-bone Thermo-gel

a) Preparation of Copolymer Blend by Free Radical Polymerization

The copolymer blend was synthesized by free radical polymerization of ε-caprolactone using PEG (Mw 4000) as the macro initiator and stannous octoate, $Sn(Oct)_2$ as a catalyst. An oven dried 3-neck round-bottomed flask (RBF) equipped with a stir bar was charged with 0.007M of PEG 4000 and 0.098M of ε-caprolactone, capped with a rubber septum and flushed with nitrogen for several minutes. To the flask was added $Sn(Oct)_2$ (100μL). A reaction temperature of 125 °C was

maintained for 6 hours under constant purge of nitrogen gas. Subsequently, synthesised PPF was added to formulate 4 reaction mixtures (F1-F4) in triplicate. F1 and F3 were blended as 8%$^{w}/_{v}$ PPF and F2 and F4 as 20% $^{w}/_{v}$ PPF. 16% $^{w}/_{v}$ Pluronic F-127 was then added in all formulations. These percentages were obtained during pre-formulation studies, as limits between formulation ranges. The ratios of PEG-PCL-PEG: PPF:PF127 was carried out as 4:1:1. Thereafter, the reaction temperature was increased to 140°C and was maintained for 6 hours. This can be seen in Figure 3.2.

The reaction mixture was then allowed to cool to room temperature and the copolymer blend was dissolved in DCM and precipitated with chilled petroleum ether. The resulting precipitate was washed and filtered under vacuum, thereafter dried at room temperature for 24 hours. The resulting copolymer blend was evaluated using NMR, FTIR-ATR and XRD, evaluating its chemical characteristics as well as its crystalline and amorphous phases.

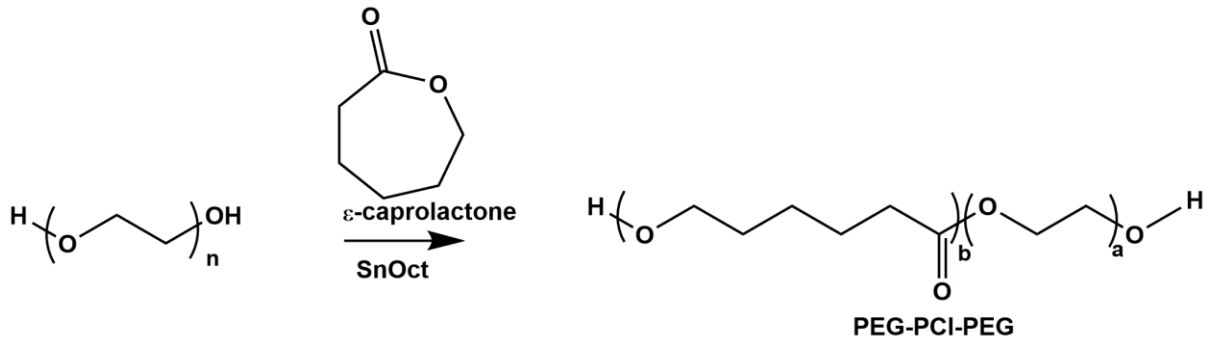


Figure 3.2: Schematic representation strategy undertaken for the preparation of the copolymer blend

b) Preparation of Pseudo-bone Thermo-gel Copolymer Blend

Distilled water was added to the copolymer blend, (copolymer blend: water ratio; 6.5:3.5), for its application of drug loading and *in vitro* studies. Drug was loaded in the thermo-gel at a temperature of 10°C for 6 hours. Thereafter, the loaded thermo-gel was incubated at 25°C for 2 hours, to ensure maximum drug loading occurred during the gelling phase.

3.2.4 Chemical Evaluation Undertaken on the Pseudo-bone Thermo-gel

Fourier transform infrared (FTIR) spectra was performed on PEG 4000, PEG-PCL-PEG, PPF and the pseudo-bone thermo-gel. FTIR spectroscopy (PerkinElmer Spectrum 2000) was used to evaluate the vibrational changes in the chemical structures of these compounds by using a single-reflection diamond MIRTGS detector (PerkinElmer Spectrum 100, Llantrisant, Wales, UK). Samples were placed on a single bounce diamond crystal and analysed by universal ATR polarization accessory for the FTIR spectrum series. This was done at a resolution of 4 cm^{-1}, with the spectrum ranging from 4000-6000cm^{-1}, at a constant pressure of 120psi.

The Bruker AVANCE II 500 MHz (Bruker Avance Biospin, Germany) instrument was used to evaluate the nuclear magnetic resonance (NMR) spectra of the monomer, polymers and the pseudo-bone thermo-gel. Chemical shifts were evaluated in deuterated chloroform (DCl_3) as the solvent for analysing the samples at a temperature of 25°C.

X-ray diffraction (XRD) of the monomer, polymers and pseudo-bone thermo-gel was investigated using a Rigaku MiniFlex 600 Benchtop X-ray Diffractometer (Rigaku Corporation, Tokyo, Japan). The Rigaku MiniFlex guidance software (version 1.2.0) was used to evaluate the samples and the Rigaku PDXL basis software was utilized for analysis and determination of the degree of crystallinity of the samples. Samples were scanned at 0-100°/min. An angle diffraction range of 3°-60° 2θ was used.

3.2.5 Determination of Thermal Characteristics of the Monomers, Polymers and the Pseudo-bone Thermo-gel

Thermal properties of PEG 4000, PEG-PCL-PEG, PPF, PF-127 and the pseudo-bone thermo-gel were assessed using the Mettler Toledo DSC-1 STAR^e system (Mettler Toledo, DSC1, STAR^e System, Swchwerzenback, Switzerland). Samples of 10mg were weighed and sealed in a 40μL aluminium crucible pan, with a 0.2mm puncture on the lid of the pan. Inert atmospheric conditions were maintained, with a flow rate of 50Ml/min of N_2 gas, for the entire duration of assessment. Samples were analysed from 0°C to 200°C, at a temperature ramping of 10°C/min, determining the thermal properties of the monomers, polymers and the pseudo-bone thermo-gel.

3.2.6 Determination of Viscoelastic Properties of the Pseudo-bone Thermo-gel

The viscoelastic behaviour of the pseudo-bone thermo-gel was evaluated using a Modular Advanced Rheometer (ThermoHaake MARS Modular Advanced Rheometer, Thermo Electron, Karlsruhe, Germany), which comprises of a C35/1° Ti sensor. Rheological measurements were evaluated from 10- 40°C, using a cone and plate inertia of 1.721 $X10^{-6}kg.m^2$. 0.5Ml of the sample was examined over a range of 0-1.0 Hz, falling within the shear independent plateau of the strain amplitude sweep stress (Gioffredi, et al., 2016). The effects of elastic energy (storage modulus or G'), viscous energy (loss modulus or G") or a resultant of both can be observed after subjecting the sample to sinusoidal oscillation (Schramm, et al., 2004).

3.2.7 Surface and Structural Morphological Evaluation of the Pseudo-bone Thermo-gel

The surface morphology of the pseudo-bone thermo-gel was analysed using scanning electron microscopy (SEM). The sample was sputter coated on an aluminium spud, by an EPI sputter coater (SPI Module TM sputter-coater and control unit, West Chester, PA, USA), using gold compound. The FEI ESEM Quanta 400F (FEI^{TM}, Hillsboro, OR, USA) electron microscope, using an electron acceleration charge of 20 Kv, was used to produce high resolution images of the particles.

The structural morphology was carried out using transmission electron microscopy (TEM) (Jeol 1200 EX, Japan). The copolymeric blend was suspended in double distilled water (0.5 mg/Ml). A drop was placed on a 200 mesh thick formvar copper grid (TABB Laboratories Equipment, Berks, UK), using a pipette. The thermo-gel was left to be adsorbed onto the surface of the copper grid. A drop of 2% $^{v}/_{w}$ uranyl acetate in double distilled water was thereafter added to the adsorbed copolymeric system. This was left to dry at room temperature for an hour before evaluation.

3.2.8 *In Vitro* Drug Release of the Pseudo-bone Thermo-gel

Distilled water was added to the copolymer blend, (copolymer blend: water ratio; 6.5:3.5), for its application of drug loading and release analysis. 10mg drug was loaded in the thermo-gel at a temperature of 10°C for 6 hours. Thereafter, the loaded thermo-gel was incubated at 25°C for 2 hours, to ensure maximum drug loading occurred during the gelling phase.

In vitro drug release was undertaken on 4 formulations, with a therapeutic dose of 10mg simvastatin loaded in all formulations (n=3). The formulations were evaluated, using 8%$^{w}/_{v}$ and 20%$^{w}/_{v}$ concentrations of PPF, varying the temperature evaluation conditions at 25°C and 37.5°C. F1 and F3 were blended as 8%$^{w}/_{v}$ PPF, and F2 and F4 as 20%$^{w}/_{v}$ PPF. F1 and F2 were evaluated at room temperature (25°C) and F3 and F4 at body temperature (37.5°C).
As seen in rheological evaluation, at room temperature (±25°C), the sample begins to gel. Therefore, release of simvastatin at room temperature in comparison to body temperature was undertaken, evaluating the controlled mechanism of release at body temperature, in relation to normal room temperature behaviour.

In vitro drug release analysis was carried out employing dialysis membranes (MWCO: 1.2 kDa) in a buffer solution (PBS pH 6.8). An orbit shaker incubator (LM-530-2, MRC Laboratory Instruments Ltd, Hahistadrut, Holon, Israel) at 37 ± 0.5 °C, with 50 rpm, was used to incubate all samples during the entire duration of the release studies. 1 mL of sample was withdrawn at each time point for analysis and replaced with the same volume of fresh buffer. This was done to maintain sink physiological conditions throughout the entire duration of the release studies. For evaluation at room temperature, samples were magnetically stirred at 50rpm, maintaining sink conditions as mentioned above. Samples were analysed using UV spectrophotometer, at wavelength 238 nm (IMPLEN Nanophotometer^{TM}, Implen GmbH, München Germany), using a 10 times dilution factor of path-length 0.1 mm (Zhang, et al., 2011).

3.2.9 Inducing a Butterfly Bone Fracture and Evaluating Fractal Dimensions on Human Clavicle Bones

The relationship between bone fractal properties are significantly dependant on macro and microscopic density, mass and volume of porous nature, with significant correlation to pore size properties. The state of bone in normal and osteoporotic bone is drastically different in its gross composition. Therefore, patients with this bone condition run the risk of various bone injuries and complications. It is for this situation of osteoporosis and bone related injuries that a pseudo-bone thermo-gel was formulated and evaluated. In this instance, we looked at the physical dimensions of a human clavicle bone, determining its fractal magnitude.

In this study, we evaluated osteoporotic female human dried clavicle bones and induced 4mm diameter fractures in the region between the cervical fascia and the area bellow the conoid

tubercle (Sanchez-Molina, et al., 2013). The clavicle bones were acquired from the Department of Anatomical Sciences, University of the Witwatersrand, South Africa with ethical waiver clearance. The bones were evaluated using X-ray and ultrasound imaging. Real-time ultrasound imaging of the human clavicle bones was visualized using a high-frequency ultrasound scanner (Vevo® 2100, Visualsonics, Toronto, Ontario, Canada) with an MS-250 transducer. The bones were evaluated with X-ray and ultrasound before and after inducing a 4mm diameter butterfly-fracture.

The butterfly fracture was induced using a 4mm punch and dye apparatus, using a hydraulic pressure of 0.6 Mpa. The bones were evaluated with X-ray and ultrasound once again after injecting the bones at the site of fracture with the pseudo-bone thermo-gel, and incubating the bones for 15min in an orbital shaker bath, immersed in phosphate buffer solution (PBS). A well calibrated textual analyzer (TA.Xt*plus*, Stable Microsystems, Surrey, UK), under standard conditions (temperature of 25 °C and pressure of 1atm), was used to evaluate the matrix hardness (MH) and matrix resilience (MR) on the bones before inducing the fracture and after treatment with the injected pseudo-bone thermo-gel on the fractured bones respectively. A steel flat tip probe of 2mm diameter was used to determine MH and a steel cylindrical probe of 50mm diameter for determination of MR.

3.3. Results and Discussion

3.3.1 Chemical Evaluation Undertaken on Monomers, Polymers and the Pseudo-bone Thermo-gel

^{1}HNMR evaluation, ATR-FTIR and XRD analysis was carried out on individual monomers, polymers, as well as the pseudo-bone thermo-gel. PEG_{4000} (a), PEG-PCL-PEG (b), PPF (c) and the pseudo-bone thermo-gel (d) was evaluated for all the above mentioned chemical characteristic analysis. ^{1} HNMR is seen in Figure 3.3, with a peak commonly observed in all spectras at 7.25ppm being deuterated chloroform as the selected solvent for analysis.

As seen in Figure 3.3a, significant $–CH_2-$ and $–CH_2CHO-$ groups are displayed at 3.5ppm and 3.65ppm respectively. Figure 3.3b displays characteristic functional groups of PEG-PCL-PEG, with peaks in the regions of 3.35, 1.6, 2.2 and 3.92ppm attributed to methylene protons of $–(CH_2)_3$, $-OCCH_2-$, and $–CH_2OOC-$ in the PCL block unit. The peak reflected at 3.65ppm in PEG-PCL-PEG

can be clearly attributed to the PEG unit, signalling $–CH_2CHO-$ functionalities. As reflected by the synthesis of this copolymer, it was further confirmed that the ratio of PEG:PCL was 3.5:1. This was significant due to the desire for a high capacity of hydrophilicity of the copolymer, with further implementation for its precursor synthesis reaction for the thermo-gel.

Figure 3.3c reflects the successful synthesis of PPF. Major peaks are seen in the regions of 6.75, 5.29, 4.25, 4.24 and 1.2ppm, designated to the olefinic (O=C-CH=CH-C=O), methine, methylene and methyl protons repated respectively. A range of minor peaks are also evident in the spectrum, ranging from 4.9, 4.22, 4.09, 3.7, 1.28 and 1.22ppm. These groups are signified as the end groups of the PPF polymeric chain unit. Integrating these major and minor peaks, the average molecular weight (M_n) of PPF polymer was established as ~1000Da, falling in the reported range of 500-4000Da [24].

Figure 3.3d reflects the spectrum of the thermo-gel copolymer blend, with various shifts occuring in the backbone of PPF. In the regions of 3.5 and 3.65ppm, broad signal $–(CH_2)-$ PEG functionalities are retained, further accompaning peaks in the regions of 1.6 and 2.2ppm, due to the PCL block unit present in the thermo-gel copolymer blend, with functional groups of $–OCCH_2-$, and $–CH_2OOC-$ reflected respectively. In the region of 1.1ppm, $-CH_3-$ groups of PF127 are evident. In the region of 6.75ppm, -HC=CH- of PPF was noticably unaffected due to the non-participation of these functionalities.

Further evaluation of the spectrum reflected no chemical shifts for $–CH_3-$ protons in the backbone of PEG-PCL, however peaks observed in the region 1-1.3ppm are most likely due to $–CH_3-$ groups found in PPF and PF127, appearing as chemical shifts from the parent compounds respectively. PF127 peaks were also observed at 3.4ppm, attributed to the hydrogen atoms of individual functional groups. Further elimination of the minor peaks of PPF in the thermo-gel suggests successful copolymeric blending in the thermo-gel, with the end groups of the PPF polymeric chain unit eliminated (Jo, et al., 2000, Behravesh, et al., 2002, Zhou, et al., 2011).

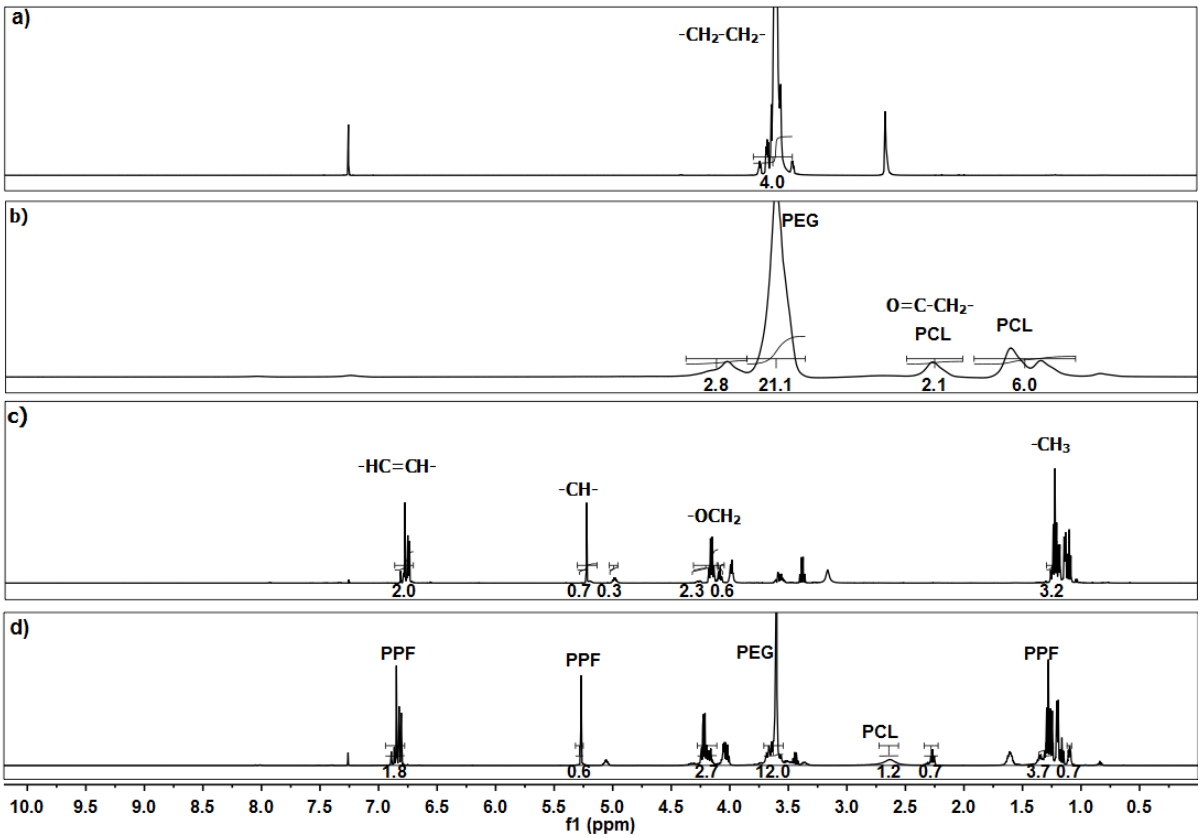


Figure 3.3: H^1 NMR evaluation for monomers, polymers and the pseudo-bone thermo-gel; a) PEG_{4000}, b) PEG-PCL-PEG, c) PPF and d) Pseudo-bone thermo-gel.

ATR-FTIR spectra analysis as seen in Figure 3.4 further supports results obtained in ^{1}HNMR analysis. As denoted in Figure 3.4a for PEG_{4000}, significant functional groups are marked, showing –O-H-, -C-H- and –C-O-H- stretching in the regions of 2950cm^{-1}, 2780cm^{-1}, and 1350cm^{-1} respectively. In the copolymer of PEG-PCL-PEG (Figure 3.4b), the characteristic peaks at 3500cm^{-1}, 2900cm^{-1}-2800cm^{-1}, 1733cm^{-1} and 1152cm^{-1}-1100cm^{-1}, are signals of –OH, -CH_2, C=O, C-O-C, and –COO- bands respectively. For PPF (Figure 3.4c), characteristic peaks at 1713cm^{-1}, 1645cm^{-1}, 1250cm^{-1} and 1149cm^{-1} are indicative of C=O stretching, C=C stretching, asymmetric C-O-C stretching and symmetric C-O-C stretching bands respectively.

The peak observed at 1645cm^{-1} in PPF (Figure 3.4c) and the pseudo-bone thermo-gel (Figure 3.4d), further substantiates that the C=C double bond was not affected in the copolymeric chain unites, after blending occurred to form the thermo-gel. Further peaks in the regions 1570cm^{-1}, 1378cm^{-1} and 1166cm^{-1} in the 72hermos-gel (Figure 3.4d), are attributed to the asymmetric and symmetric CO_2- bands of stretching respectively, thereby further indicating successful formulation of the pseudo-bone thermo-gel. An overlap of strong C=O stretching in the region of 1730cm^{-1}

was observed for PEG-PCL-PEG, PPF and PF127. These strong ester bonds can be seen in the thermo-gel due to the blending of PPF and PF127 with PEG-PCL-PEG copolymer.

The stretching vibrations of C-H of the PEO unit in PF127 are shifted slightly and evident in the thermo-gel (Figure 3.4d) in the regions of 2975cm^{-1} and 2880cm^{-1}. The intensity of the signal at 1118cm^{-1} is clearly indicative of C-O-C stretching vibration of PF127 in the thermo-gel. The resulting functional peaks thus implies successful blending of the polymers to form the pseudo-bone thermo-gel system.

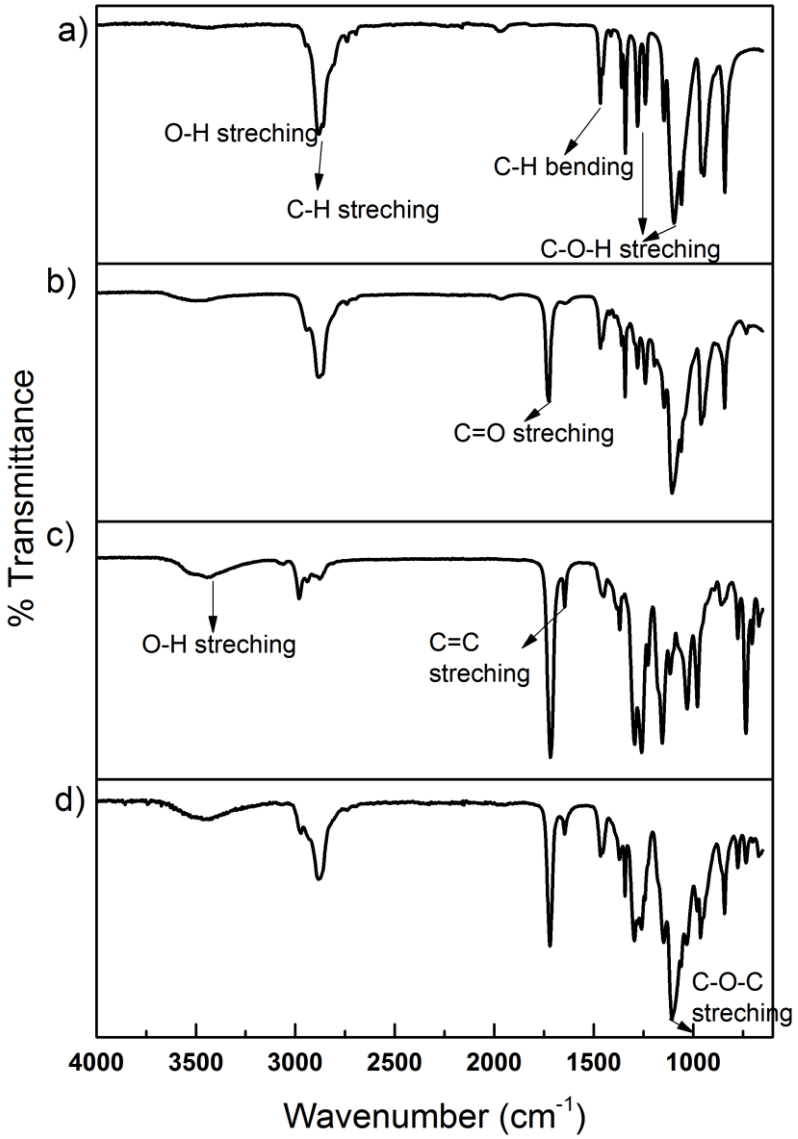


Figure 3.4: ATR-FTIR analysis undertaken on; a) PEG_{4000}, b) PEG-PCL-PEG c) PPF and d) Pseudo-bone thermo-gel.

Using XRD analysis, the pseudo-bone thermo-gel displayed greater crystallinity than PPF and PEG-PCL-PEG, possibly accounting for the greater chemical equivalence signals due to fewer structural conformations of chemical inequivalence, therefore producing more signals. PEG_{4000} (Figure 3.5a) displayed distinctive sharp peaks at 2 theta =20.2° and 22.7° due to a high molecular weight of PEG used. In PEG-PCL-PEG (Figure 3.5b), these peaks are no longer sharp and narrow due to the segments of the copolymer becoming amorphous with the incorporation of PCL.

PEG-PCL-PEG copolymer also reflected peaks at 2 theta =21.6° and 23.5°, correlating to the lattice planes of orthorhombic PCL unites (Yin, et al., 2015). As seen in PPF (Figure 3.5c), a substantial amorphous arrangement of the polymer is reflected. Figure 3.5d illustrates the thermo-gel, showing a semi-crystalline nature of the copolymer blend. This can be attributed to the high crystallinity of the PEG unit, further reflecting these peaks of PEG in the thermo-gel. The thermo-gel also demonstrated higher crystalline nature than PEG-PCL-PEG and PPF, further reasoning the advantage of blending these polymers to obtain a higher crystalline copolymer blend which is confirmed at 2 theta =19.4 and 23.9°.

This semi-crystalline nature also substantiates the slow-release *in vitro* kinetics of the pseudo-bone thermo-gel, which is discussed in detail in the later sections of the chapter. This property allows a uniform sustained release of the loaded drug in the thermo-gel, thereby reacting to the thermal stimulus, releasing its loaded drug over a prolonged duration of time. The semi-crystalline nature of the pseudo-bone thermo-gel further enhances the amphiphilic drug release properties, promoting greater drug loading capacity due to a substantial hydrophobic affinity for the statin-loaded thermo-gel copolymer blend. It can therefore be confirmed that the thermo-gel has a greater order of molecules in its crystal lattice. This can be attributed to many factors such as chain lengths, inter-chain interactions and chain branching interactions.

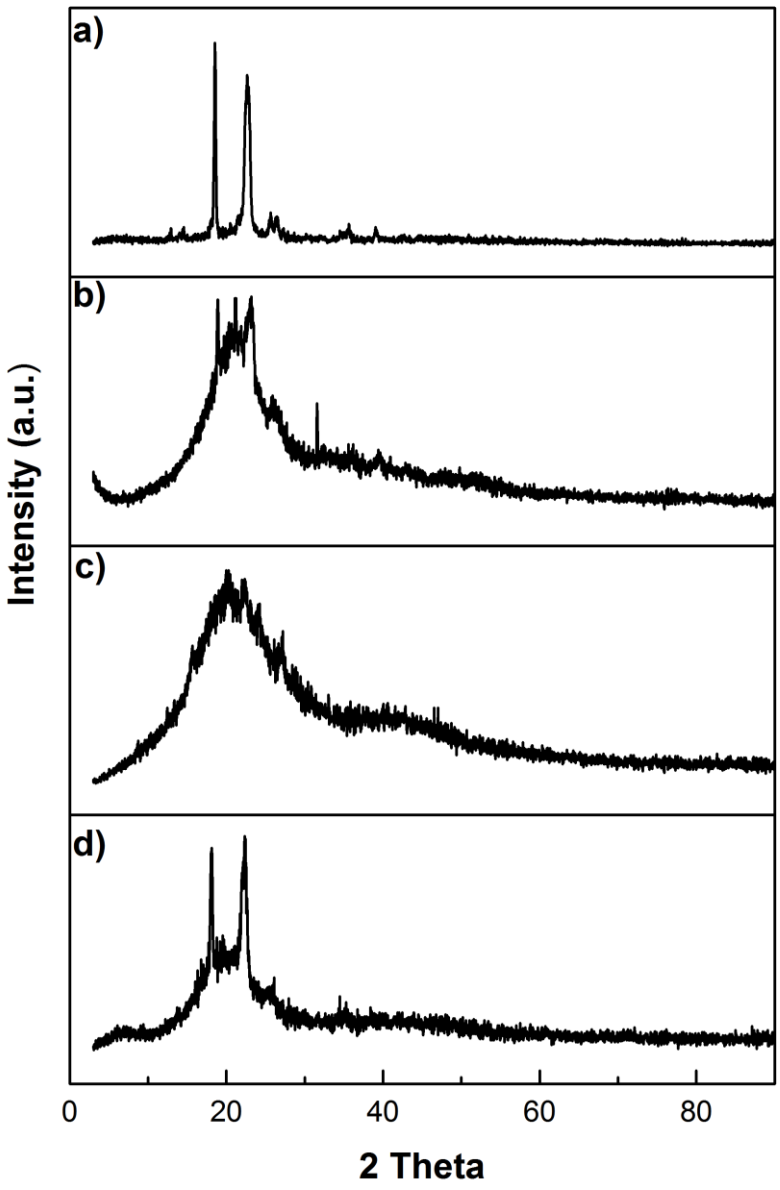


Figure 3.5: XRD analysis undertaken on a) PEG_{4000}, b) PEG-PCL-PEG c) PPF and d) Pseudo-bone thermo-gel.

3.3.2 Thermal Evaluation of the Monomers, Polymers and the Pseudo-bone Thermo-gel

DSC was undertaken on PEG_{4000}, PCL, PEG-PCL-PEG, PF127, PPF and the pseudo-bone thermo-gel. The DSC thermogram of PEG-4000 exhibited two split melting endotherm peaks at 57.13°C and 61.71°C respectively (Figure 3.6a). This observation is significantly due to the existence of both folded and extended chains in the PEG matrix (Ginés, et al., 1996). The endotherm peak at 61.93°C in the thermogram of PCL (Figure 3.6b) was indicative of melting, and shifted to 51.90°C in the thermogram of PEG-PCL-PEG (Figure 3.6c). The endotherm at

44.48°C in Figure 3.6c can be attributed to melting of the PEG crystal domains through the heating period (Zhou, et al., 2003). As seen in PF127 (Figure 3.6d), the melting of crystalline phases was observed at 55.18°C, with polymer chain exothermic reactivity of PF127, observed in the region of 160 °C. In Figure 3.6e, it was observed that PPF displayed a slight transition in its amorphous polymer state in the region of 4.05°C [36]. The Pseudo-bone thermo-gel (Figure 3.6f) displayed a broad endotherm in the region of 20.7°C-38.18°C, attributed to the aliphatic flexible chains coupled in PEG-PCL-PEG and PF127. Characteristic peaks of PPF could not be significantly observed in the thermo-gel, due to the diminishing free chain ends after copolymeric blending (Lee, et al., 2006).

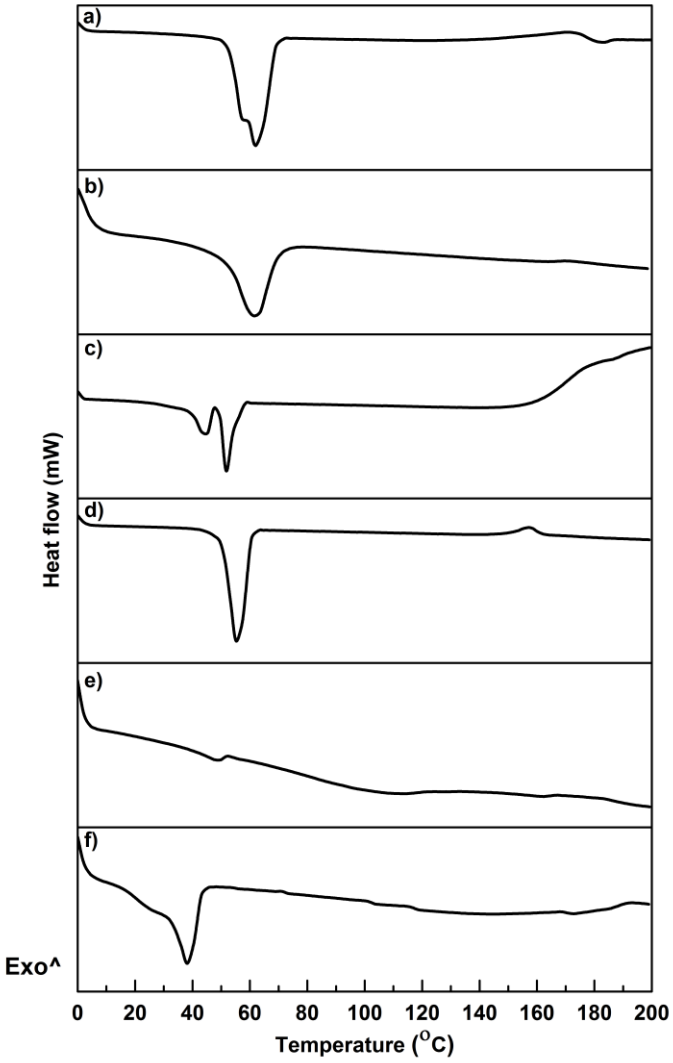


Figure 3.6: DSC undertaken on monomer, polymers and the pseudo-bone thermo-gel; a) PEG_{4000}, b) PCL, c) PEG-PCL-PEG, d) PF127, e) PPF and f) Pseudo-bone thermo-gel.

3.3.3 Determination of Storage and Loss Modulus of the Pseudo-bone Thermo-gel

The pseudo-bone thermo-gel was evaluated with respect to change in temperature, at a constant applied force, evaluating the characteristic response of the thermo-gel due to change in temperature, as seen in Figure 3.7. G' is described as the measure of deformation energy within the pseudo-bone thermo-gel, referring to the elastic, solid properties of the thermo-gel. In contrast, G'' is the measure of the viscous and deformation energy used and lost in the thermo-gel over a given temperature range. As seen in Figure 3.7, G' begins at 23 °C, starting to form a semi-solid gelling property, and thereafter at 32°C, completely switches to the elastic phase property, remaining above G'' throughout the evaluation of the sample. It was observed that the viscosity of the sample gradually increases above room temperature, ±25°C, maintaining a higher elastic phase property (gel) than the liquid state (sol) at body temperature conditions.

The thermo-gel will be injected at the site of the small bone fracture. At this stage, the body temperature will allow the thermo-gel to increase its visco-elastic properties, forming a semi-solid material at the site of bone injury. Since all materials employed in the copolymer blend are approved biodegradable and biocompatible, the gel will degrade and release its loaded drug over a prolonged duration of time, in a controlled release mechanism. The thermo-gel system at body temperature does not become brittle and cracked, instead as seen in the rheological evaluation, maintains a high elastic property, and acts like a 'glue-like' substance, filling the gaps between the fracture site and further allowing significant adhesion of the bone to promote substantial healing. The loaded drug in the pseudo-bone thermo-gel is further released and absorbed at the site of injury, promoting exponential repair of the bone in a shortened time period, behaving as a controlled release system (Zhang, et al., 2011, Vandenhaute, et al., 2014).

We can therefore conclude that the pseudo-bone thermo-gel has substantial thermo-responsive properties, with a significant change in modulus due to temperature variations. At controlled storage temperature 10-20°C (ideal and safe storage would be refrigeration at 10°C), only viscous modulus is present in the range of 0.1- 0.3Pa. When physiological temperature is reached, the thermo-gel increases strength by 45 000 times (from 0.1Pa to 4500Pa). As body temperature is reached by the thermo-gel, the gel forms a solid, semi-elastic substance, thereby gradually releasing drug in a controlled, sustainable manner.

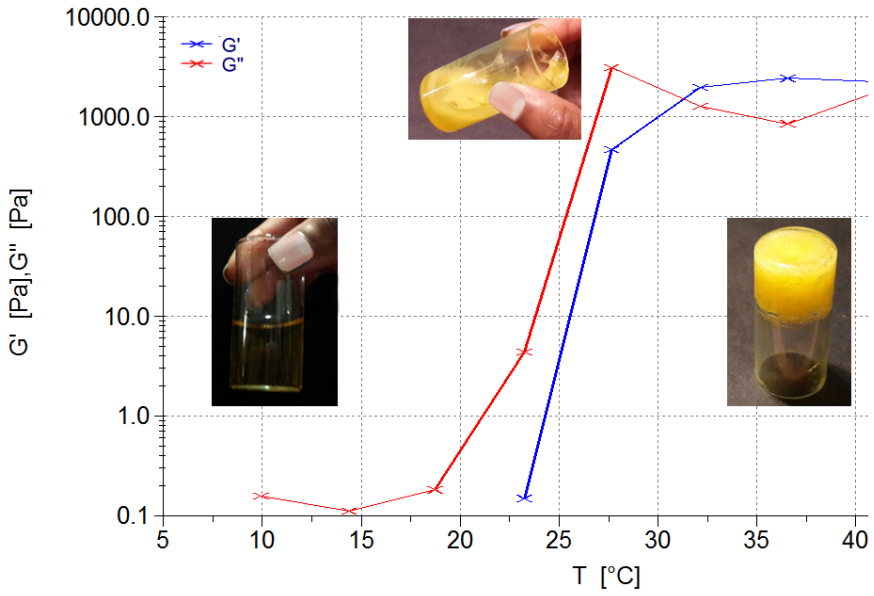


Figure 3.7: Rheological evaluation of the pseudo-bone thermo-gel in relation to change in temperature.

3.3.4 Surface and Structural Morphological Evaluation of the Pseudo-bone Thermo-gel

SEM and TEM analysis was undertaken on the pseudo-bone thermo-gel to determine the morphological properties of the thermo-gel system. As seen in Figure 3.8a, SEM reflects the copolymer blend network of the thermo-gel, with distinctive intertwined patterns, forming a uniformed regular arrangement. This can be correlated to results obtained in XRD analysis, complementing the semi-crystalline nature of the pseudo-bone thermo-gel. The ordered arrangement of the pseudo-bone thermo-gel demonstrates substantial potential for high drug entrapment and release properties. Drug release properties from the pseudo-bone thermo-gel highly correlates with the structural arrangement of the micrograph, evidently due to the highly ordered arrangement of the particles in the pseudo-bone thermo-gel.

TEM analysis was then sought for viewing individual copolymeric blend particles as seen in Figure 3.8b. Particles appeared ovoid in nature with an average diameter of 80nm, further confirmed using particle size analysis. The TEM image can be viewed as 3 particles overlapped on one another (each particle on the side, with another particle in the centre of each), with a clear representation of the distinctive outline of each particle. Due to substantial dilutions of preparing the sample for evaluation, a final distinctive image was obtained viewing a single particle out of

the highly inter-penetrating network of particles in the pseudo-bone thermo-gel system. Samples were evaluated at room temperature, making it easier to view a 'less clumped' state of particles with less water absorbed in this conformation (Gong, et al., 2009, Rainer, et al., 2011). The particle uniformity is essential for volume and surface area advantages, thereby having a greater capacity to predict the desirable behaviour of the pseudo-bone thermo-gel *in vivo* due to reliable kinetics based on the morphological characteristics of the uniform copolymer blend particles (Pandit, et al., 1996, Volkmer, et al., 2013, Niu, et al., 2009). An SEM of bone tissue under high magnification was also compared to the pseudo-bone thermo-gel (Singh, et al., 2016) (Figure 3.8c). As seen in these images, a comparable conformational network is observed in bone tissue and the pseudo-bone thermo-gel. This array of interpenetrating networks with various pores can be seen in bone tissue and the pseudo-bone thermo-gel. Due to these morphological similarities, the corresponding mechanical nature of the pseudo-bone thermo-gel can be understood. Using these strategically blended copolymers, the resulting thermo-gel not only resembles morphological similarities to bone, but also matrix hardness and resilience properties *in situ*, when exposed to physiological parameters, as discussed in section 3.3.5. The pseudo-bone thermo-gel's thermo-responsive nature allows a defined tightly packed network of particles to resemble bone tissue surface conformation, evidently supporting its structure by a continuous alignment of interconnected copolymeric network particles.

We can thus affirm that the pseudo-bone thermo-gel has substantial potential for application as an injectable delivery system, supported morphologically by SEM and TEM analysis.

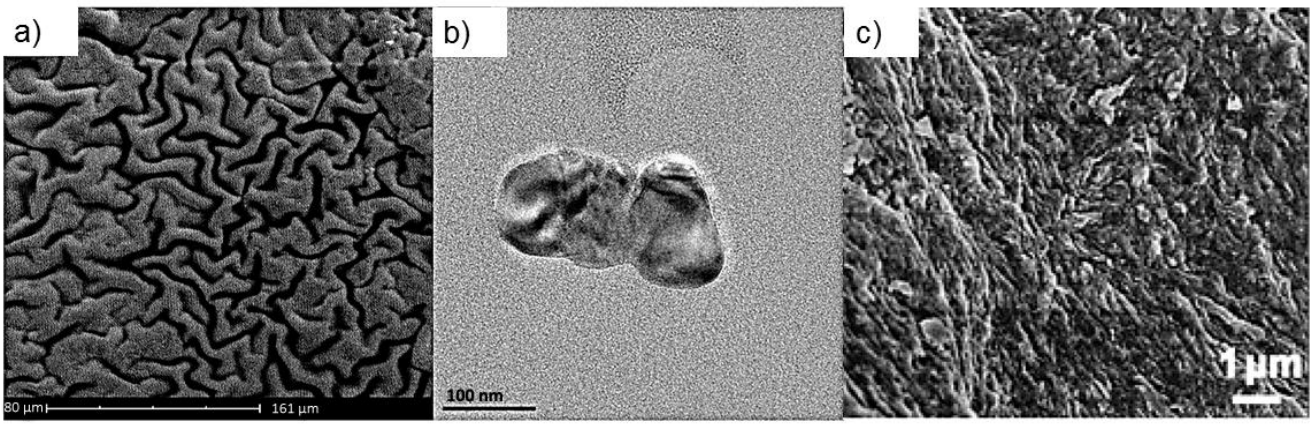


Figure 3.8: Morphological evaluation undertaken, reflecting; a) SEM analysis on the pseudo-bone thermo-gel, b) TEM analysis on the pseudo-bone thermo-gel; and c) comparative SEM imaging of human bone under high magnification.

3.3.5 *Ex-vivo* Evaluation of the Pseudo-bone Thermo-gel Using Ultrasound and X-ray Evaluation for Determination of Matrix Hardness and Matrix Resilience on Human Clavicle Bones

Human clavicle bones were evaluated using X-ray, ultrasound, as well as textural analysis to determine the matrix hardness (MH) and matrix resilience (MR) of the bones before fracture, after fracture and after injecting the bones with the pseudo-bone thermo-gel at the site of the induced 4mm diameter butterfly fracture. Clavicular fractures are categorized by the site of injury. As seen in Figure 3.9a and 3.9b, an X-ray image and ultrasound image was captured before inducing a fracture respectively. Thereafter, another X-ray (Figure 3.9c) and ultrasound (Figure 3.9d) image was captured on the resulting fracture site. At this instance, the resulting bone appeared normal with a 4mm diameter fracture at 2 positions (noted as darker portions in the X-ray (Figure 3.9c) and white portions in the ultrasound image (Figure 3.9d). These portions of the bones were then injected with the pseudo-bone thermo-gel and evaluated once more for acquiring X-ray (Figure 3.9e) and ultrasound (Figure 3.9f) images. After several imagining of various bones, the most defined images were selected for representation.

It can be clearly seen in the above mentioned images the distinct differences with the structural texture of the bone during the 3 stage procedure. The bones were then covered with a dialysis membrane, as to roughly mimic the periosteum layer of the bones. Thereafter the bone covered with the membrane was incubated in a shaker bath at a temperature of 37°C, with 50rpm for 2 hours in PBS. The pseudo-bone thermo-gel was then injected at the site of the fracture, and left back to incubate in the same condition for 15min. Following this stage, the membrane was then removed and the bones evaluated once more using X-ray (Figure 3.9e) and ultrasound imaging (Figure 3.9f). It can be clearly seen that the pseudo-bone thermo-gel penetrated deep into the sites of fracture, allowing adhesion and sealing of the fracture sites of the bone. As noted in the images, the X-rays appear much ‘less dark’ in Figure 3.9e in comparison to Figure 3.9c. Similarly, ultrasound images show sealing of the fracture site in Figure 3.9f in comparison to the fracture line seen in Figure 3.9d. This clearly demonstrates the highly temperature responsive nature of the pseudo-bone thermo-gel, providing a firm sealing of the fracture once injected.

The MH and MR of the bones were also evaluated. MR is the capacity of a given material to deform elastically, but revert to its usual state, once the force is removed. The average MH was calculated as 18.61 N/mm with a 9.48% MR before fracture. After inducing the fracture and

injecting the bone with the thermo-gel system (MH and MR evaluation was undertaken 30min after injecting and incubating the bone at 37°C with the thermo-gel system), 18.3 N/mm MH and 9.28% MR was observed at the site of fracture, which was visibly lacking substantial bone material at the site when fractured. MR was calculated using a force-time profile, evaluating the ratio of the area under the curve (AUC), from peak to base, after eliminating the force initiated (AUC_{2-3}), over the baseline to peak, before removing the force (AUC_{1-2}), resulting in a % MR value. The gradient represents the flexibility and elastic property of the bone, whilst the AUC is the amount of deformation energy observed in the bone (Ellison, et al., 2008).

It can thus be concluded that; even after inducing a fracture on the bone, following injection of the pseudo-bone thermo-gel, the fractured bone area displayed almost equivalent MH and MR to the original bone samples. We can therefore conclude that the pseudo-bone thermo-gel sealed the voids within the cracks of the fractured bone, allowing the bone the capacity to maintain significant mechanical integrity after treatment with the pseudo-bone thermo-gel.

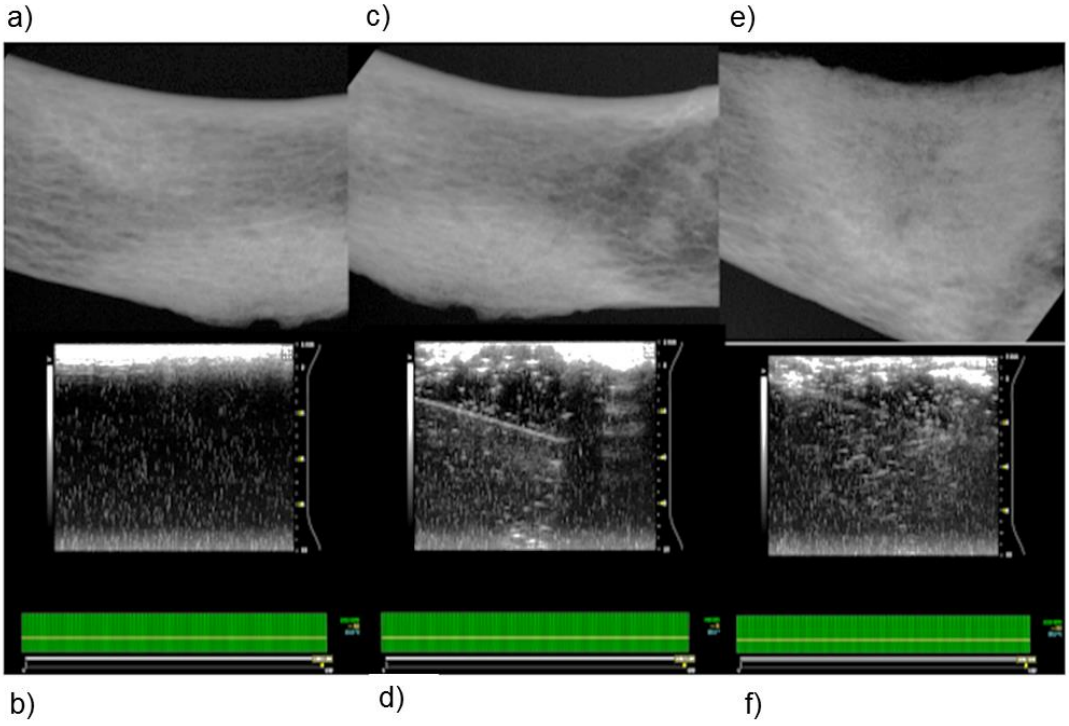


Figure 3.9: X-ray and ultra sound images undertaken on a human clavicle osteoporotic female bone; a) X-ray image before inducing a fracture on the human clavicle specimen, b) Ultra-sound image before inducing a fracture on the human clavicle specimen, c) X-ray image after inducing a fracture on the human clavicle specimen, d) Ultra-sound image after inducing a fracture on the human clavicle specimen, e) X-ray image after treatment with the pseudo-bone thermo-gel at the site of the fracture induced human clavicle specimen, f) Ultra-sound image after treatment with the pseudo-bone thermo-gel at the site of the fracture induced human clavicle specimen.

3.3.6 *In Vitro* Analysis of the Pseudo-bone Thermo-gel

Drug release studies were undertaken in different temperature conditions, to prove the thermo-responsive properties of the copolymer thermo-gel, thereby behaving as a controlled drug release formulation at body temperature, in comparison to a shorter duration of release at room temperature conditions. The range of PPF concentration used in the thermo-gel, was calculated determining the desirable strength required from the thermo-gel when exposed to physiological temperature condition.

As seen in Figure 3.10, all formulations displayed a gradual increase in drug release from 0 to 6 hours at both 25°C and 37.5°C. Thereafter, formulations at body temperature conditions increased greater from 6 hours to 24 hours, compared to room temperature samples. Formulations F1 and F2 displayed an average release of up to 10 days. At this stage, the formulation displayed a semi-gelling composition, in comparison to an elastic-solid gel which is formed at body temperature (F3 and F4). As seen in Figure 3.11, F3 and F4 released over 14 days, confirming the controlled release behaviour achieved with exposure to physiological temperature condition. This ideal gradual release of drug is an essential characteristic for obtaining desirable pharmacokinetic profiles, preventing spikes of drug release with unpredictable behaviour. We can thus conclude that the pseudo-bone thermo-gel has significant potential for injectable drug delivery, forming an elastic solid-gel composition at body temperature, releasing a desirable uniformed drug concentration over a significant duration of patient therapeutic recovery time.

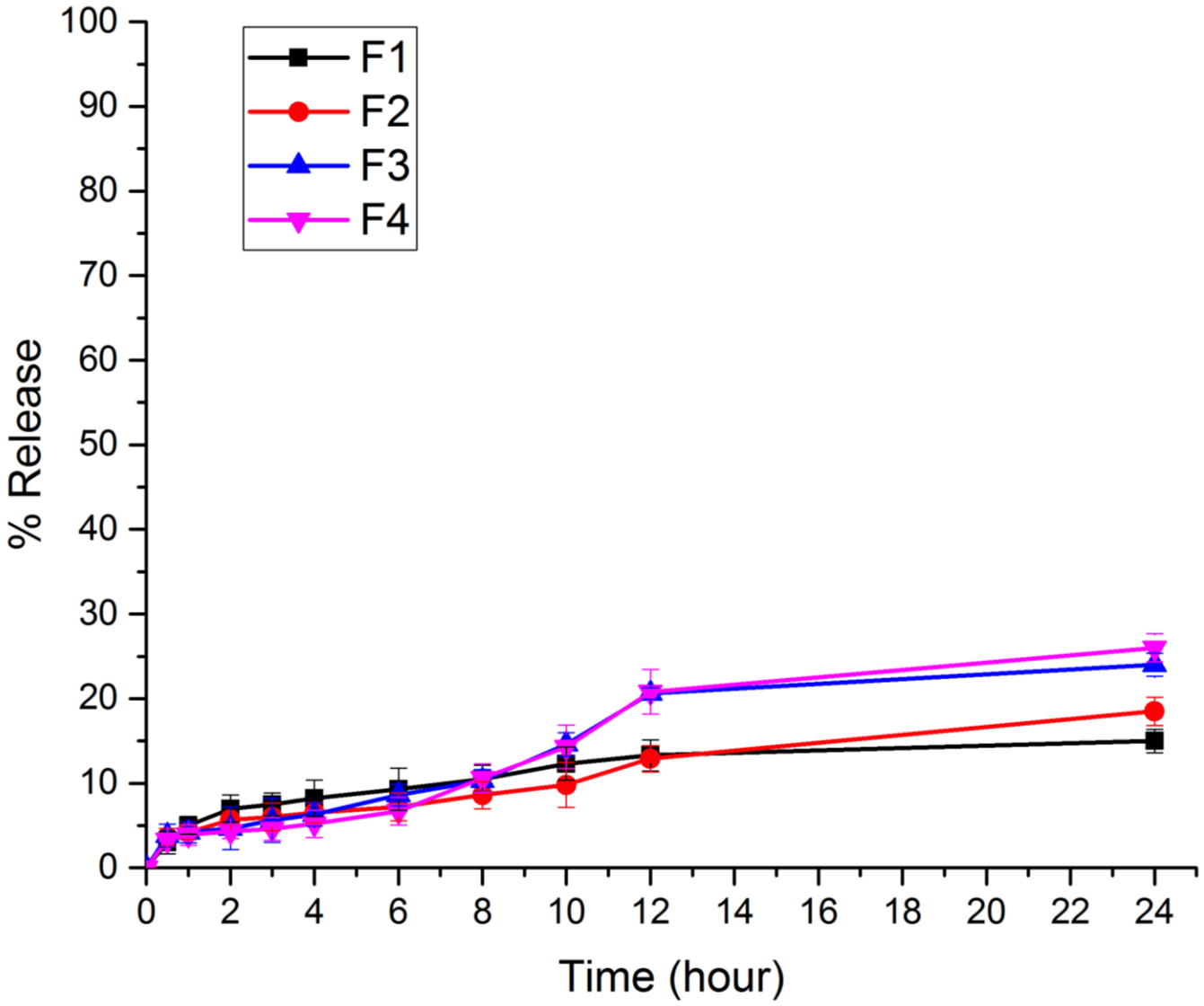


Figure 3.10: *In vitro* analysis of the pseudo-bone thermo-gel with variation in concentrations of % PPF and temperature conditions over 24 hours. F1 and F3 were blended as 8%$^{w}/_{v}$ PPF, and F2 and F4 as 20% $^{w}/_{v}$ PPF. F1 and F2 were evaluated at room temperature (±25°C), F3 and F4 at body temperature (±37.5°C).

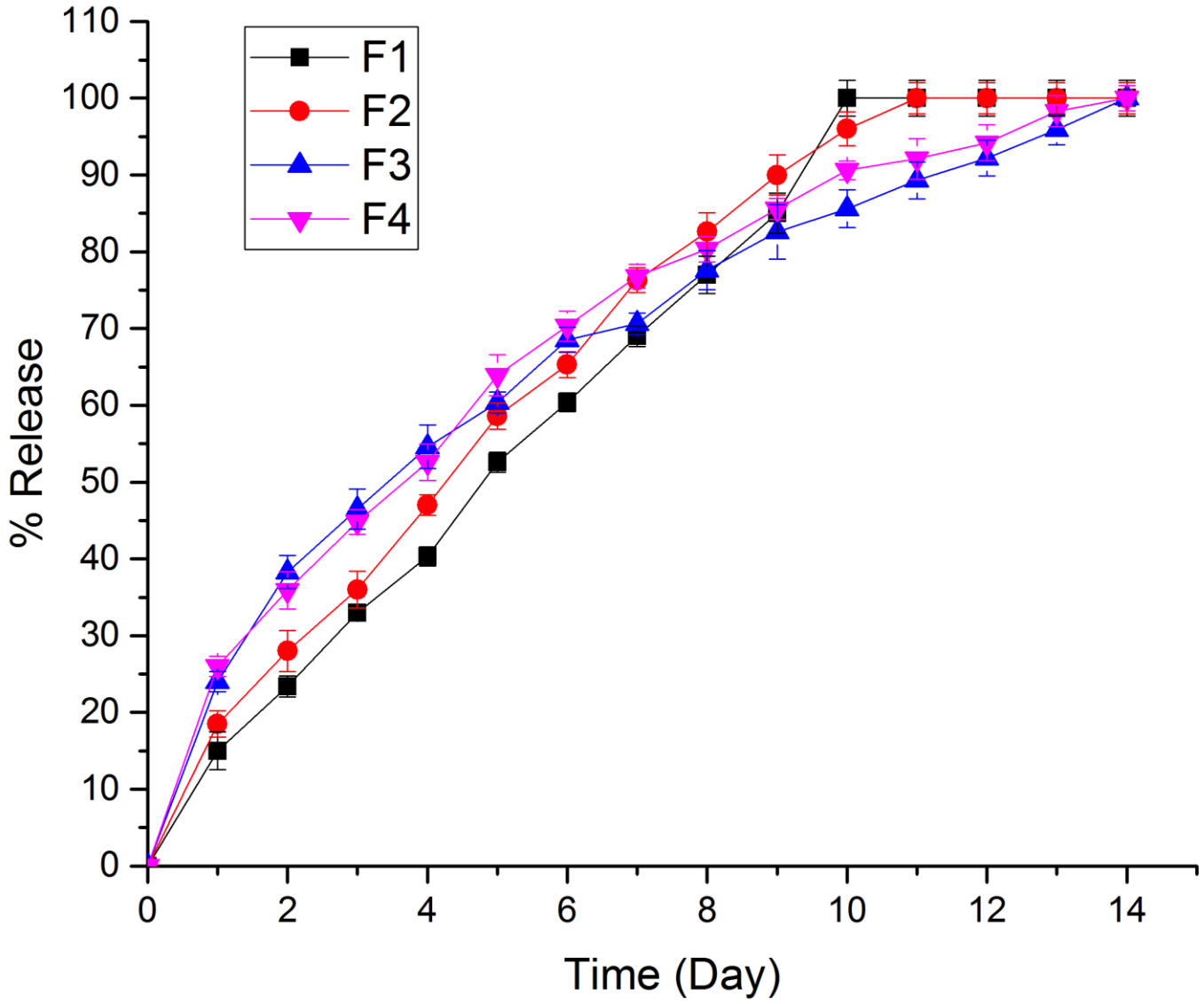


Figure 3.11: *In vitro* analysis of the pseudo-bone thermo-gel with variation in concentrations of % PPF and temperature conditions over 14 days. F1 and F3 were blended as 8%$^{w}/_{v}$ PPF, and F2 and F4 as 20% $^{w}/_{v}$ PPF. F1 and F2 were evaluated at room temperature (±25°C), F3 and F4 at body temperature (±37.5°C).

3.4. Concluding Remarks

A pseudo-bone thermo-gel was synthesised and evaluated for its physico-chemical and mechanical properties. ^{1}HNMR, ATR-FTIR and XRD studies confirmed successful copolymeric blending, using PEG-PCL-PEG, PPF and Pluronic F127®. The pseudo-bone thermo-gel demonstrated significant thermo-responsive properties, which was further affirmed using rheological and *in vitro* evaluation at varrying temperature conditions. A BCS class 2 drug, simvastatin was loaded in the thermo-gel, demonstrating significant drug release characteristics

at body temperature over 14 days, compared to non-physiological temperature conditions, which displayed drug release for 10 days. *Ex vivo* analysis was undertaken using induced 4mm diameter butterfly fractured human clavicle bones. These bones were analysed using X-ray, ultrasound and textural analysis, undertaken on the induced fractured bone before and after treatment of the thermo-gel. Results displayed significant bone filling, matrix hardening and matrix resilience properties, similar to the original density of the bone. It can thus be concluded that the developed pseudo-bone thermo-gel has significant potential for *in vivo* evaluation, with promising therapeutic benefits for treating small bone fractures.

3.5 References

Behravesh, E.; Shung, A.; Jo, S.; Mikos, A. Synthesis And Characterization Of Triblock Copolymers Of Methoxy Poly(Ethylene Glycol) And Poly(Propylene Fumarate). *Biomacromolecules* 2002, *3*, 153-158.

Bosco, A.; Faleiros, P.; Carmona, L.; Garcia, V.; Theodoro, L.; de Araujo, N.; Nagata, M.; de Almeida, J. Effects Of Low-Level Laser Therapy On Bone Healing Of Critical-Size Defects Treated With Bovine Bone Graft. *Journal of Photochemistry and Photobiology B: Biology* 2016, *163*, 303-310.

Caetano, G.; Violante, R.; Sant´Ana, A.; Murashima, A.; Domingos, M.; Gibson, A.; Bártolo, P.; Frade, M. Cellularized Versus Decellularized Scaffolds For Bone Regeneration. *Materials Letters* 2016, *182*, 318-322.

Caramella, C.; Conti, B.; Modena, T.; Ferrari, F.; Bonferoni, M.; Genta, I.; Rossi, S.; Torre, M.; Sandri, G.; Sorrenti, M. et al. Controlled Delivery Systems For Tissue Repair And Regeneration. *Journal of Drug Delivery Science and Technology* 2016, *32*, 206-228.

Deng, C.; Wu, J.; Cheng, R.; Meng, F.; Klok, H.; Zhong, Z. Functional Polypeptide And Hybrid Materials: Precision Synthesis Via A-Amino Acid N-Carboxyanhydride Polymerization And Emerging Biomedical Applications. *Progress in Polymer Science* 2014, *39*, 330-364.

Egner, W.; Egner, H. Thermo-Mechanical Coupling In Constitutive Modeling Of Dissipative Materials. *International Journal of Solids and Structures* 2016, *91*, 78-88.

Ellison, C.; Ennis, B.; Hamad, M.; Lyon, R. Measuring The Distribution Of Density And Tabletting Force In Pharmaceutical Tablets By Chemical Imaging. *Journal of Pharmaceutical and Biomedical Analysis* 2008, *48*, 1-7.

Farokhi, M.; Mottaghitalab, F.; Shokrgozar, M.; Ou, K.; Mao, C.; Hosseinkhani, H. Importance Of Dual Delivery Systems For Bone Tissue Engineering. *Journal of Controlled Release* 2016, *225*, 152-169.

Ginés, J.; Arias, M.; Rabasco, A.; Novák, C.; Ruiz-Conde, A.; Sánchez-Soto, P. Thermal Characterization Of Polyethylene Glycols Applied In The Pharmaceutical Technology Using Differential Scanning Calorimetry And Hot Stage Microscopy. *Journal of Thermal Analysis* 1996, *46*, 291-304.

Gioffredi, E.; Boffito, M.; Calzone, S.; Giannitelli, S.; Rainer, A.; Trombetta, M.; Mozetic, P.; Chiono, V. Pluronic F127 Hydrogel Characterization And Biofabrication In Cellularized Constructs For Tissue Engineering Applications. *Procedia CIRP* 2016, *49*, 125-132.

Gong, C.; Shi, S.; Dong, P.; Zheng, X.; Fu, S.; Guo, G.; Yang, J.; Wei, Y.; Qian, Z. In Vitro Drug Release Behavior From A Novel Thermosensitive Composite Hydrogel Based On Pluronic F127 And Poly(Ethylene Glycol)-Poly(Epsilon-Caprolactone)-Poly(Ethylene Glycol) Copolymer. *BMC Biotechnology* 2009, *9*, 8.

Hashimoto, Y.; Mukai, S.; Sawada, S.; Sasaki, Y.; Akiyoshi, K. Nanogel Tectonic Porous Gel Loading Biologics, Nanocarriers, And Cells For Advanced Scaffold. *Biomaterials* 2015, *37*, 107-115.

Iwase, T.; Morita, D.; Ito, T.; Takemoto, G.; Makida, K. Favorable Results Of Primary Total Hip Arthroplasty With Acetabular Impaction Bone Grafting For Large Segmental Bone Defects In Dysplastic Hips. *The Journal of Arthroplasty* 2016, *31*, 2221-2226.

Jeong, N.; Park, J.; Yoo, K.; Kim, W.; Kim, D.; Yoon, S. Preparation, Characterization, And In-Vitro Performance Of Novel Injectable Silanized-Hydroxypropyl Methylcellulose/Phase-Transformed Calcium Phosphate Composite Bone Cements. *Current Applied Physics* 2016, *16*, 1523-1532.

Jo, S.; Engel, P.; Mikos, A. Synthesis Of Poly(Ethylene Glycol)-Tethered Poly(Propylene Fumarate) And Its Modification With GRGD Peptide. *Polymer* 2000, *41*, 7595-7604.

Jung, Y.; Park, W.; Park, H.; Lee, D.; Na, K. Thermo-Sensitive Injectable Hydrogel Based On The Physical Mixing Of Hyaluronic Acid And Pluronic F-127 For Sustained NSAID Delivery. *Carbohydrate Polymers* 2017, *156*, 403-408.

Kasper, F.; Tanahashi, K.; Fisher, J.; Mikos, A. Synthesis Of Poly(Propylene Fumarate). *Nature Protocols* 2009, *4*, 518-525.

Khoshroo, K.; Jafarzadeh Kashi, T.; Moztarzadeh, F.; Tahriri, M.; Jazayeri, H.; Tayebi, L. Development Of 3D PCL Microsphere/Tio 2 Nanotube Composite Scaffolds For Bone Tissue Engineering. *Materials Science and Engineering: C* 2017, *70*, 586-598.

Lee, K.; Wang, S.; Lu, L.; Jabbari, E.; Currier, B.; Yaszemski, M. Fabrication And Characterization Of Poly(Propylene Fumarate) Scaffolds With Controlled Pore Structures Using 3-Dimensional Printing And Injection Molding. *Tissue Engineering* 2006, *12*, 2801-2811.

LogithKumar, R.; KeshavNarayan, A.; Dhivya, S.; Chawla, A.; Saravanan, S.; Selvamurugan, N. A Review Of Chitosan And Its Derivatives In Bone Tissue Engineering. *Carbohydrate Polymers* 2016, *151*, 172-188.

Lucia, U. Econophysics And Bio-Chemical Engineering Thermodynamics: The Exergetic Analysis Of A Municipality. *Physica A: Statistical Mechanics and its Applications* 2016, *462*, 421-430.

Luo, Z.; Yang, Y.; Deng, Y.; Sun, Y.; Yang, H.; Wei, S. Peptide-Incorporated 3D Porous Alginate Scaffolds With Enhanced Osteogenesis For Bone Tissue Engineering. *Colloids and Surfaces B: Biointerfaces* 2016, *143*, 243-251.

Ma, D.; An, G.; Liang, M.; Liu, Y.; Zhang, B.; Wang, Y. A Composited PEG-Silk Hydrogel Combining With Polymeric Particles Delivering Rhbmp-2 For Bone Regeneration. *Materials Science and Engineering: C* 2016, *65*, 221-231.

Nayef, L.; Mekhail, M.; Benameur, L.; Rendon, J.; Hamdy, R.; Tabrizian, M. A Combinatorial Approach Towards Achieving An Injectable, Self-Contained, Phosphate-Releasing Scaffold For Promoting Biomineralization In Critical Size Bone Defects. *Acta Biomaterialia* 2016, *29*, 389-397.

Nguyen, Q.; Huynh, D.; Park, J.; Lee, D. Injectable Polymeric Hydrogels For The Delivery Of Therapeutic Agents: A Review. *European Polymer Journal* 2015, *72*, 602-619.

Niu, G.; Du, F.; Song, L.; Zhang, H.; Yang, J.; Cao, H.; Zheng, Y.; Yang, Z.; Wang, G.; Yang, H. et al. Synthesis And Characterization Of Reactive Poloxamer 407S For Biomedical Applications. *Journal of Controlled Release* 2009, *138*, 49-56.

Pandit, N. Loss Of Gelation Ability Of Pluronic® F127 In The Presence Of Some Salts. *International Journal of Pharmaceutics* 1996, *1*, 129-136.

Rainer, A.; Giannitelli, S.; Accoto, D.; De Porcellinis, S.; Guglielmelli, E.; Trombetta, M. Load-Adaptive Scaffold Architecturing: A Bioinspired Approach To The Design Of Porous Additively Manufactured Scaffolds With Optimized Mechanical Properties. *Annals of Biomedical Engineering* 2011, *40*, 966-975.

Sanchez-Molina, D.; Velazquez-Ameijide, J.; Quintana, V.; Arregui-Dalmases, C.; Crandall, J.; Subit, D.; Kerrigan, J. Fractal Dimension And Mechanical Properties Of Human Cortical Bone. *Medical Engineering & Physics* 2013, *35*, 576-582.

Santapuri, S. Thermodynamic Restrictions On Linear Reversible And Irreversible Thermo-Electro-Magneto-Mechanical Processes. *Heliyon* 2016, *2*, e00164.

Schramm, G. A Practical Approach to Rheology and Rheometry. Thermo Electron (Karlsruhe), GmbH, *Federal Republic of Germany* 2004, Volume 2.

Shung, A.; Timmer, M.; Jo, S.; Engel, P.; Mikos, A. Kinetics Of Poly(Propylene Fumarate) Synthesis By Step Polymerization Of Diethyl Fumarate And Propylene Glycol Using Zinc Chloride As A Catalyst. *Journal of Biomaterials Science, Polymer Edition* 2002, *13*, 95-108.

Singh, A.; Gajiwala, A.; Rai, R.; Khan, M.; Singh, C.; Barbhuyan, T.; Vijayalakshmi, S.; Chattopadhyay, N.; Sinha, N.; Kumar, A. et al. Cross-Correlative 3D Micro-Structural Investigation Of Human Bone Processed Into Bone Allografts. *Materials Science and Engineering: C* 2016, *62*, 574-584.

Tang, D.; Tare, R.; Yang, L.; Williams, D.; Ou, K.; Oreffo, R. Biofabrication Of Bone Tissue: Approaches, Challenges And Translation For Bone Regeneration. *Biomaterials* 2016, *83*, 363-382.

Tang, Z.; He, C.; Tian, H.; Ding, J.; Hsiao, B.; Chu, B.; Chen, X. Polymeric Nanostructured Materials For Biomedical Applications. *Progress in Polymer Science* 2016, *60*, 86-128.

Timmer, M. In Vitro Degradation Of Polymeric Networks Of Poly(Propylene Fumarate) And The Crosslinking Macromer Poly(Propylene Fumarate)-Diacrylate. *Biomaterials* 2003, *24*, 571-577.

Vandenhaute, M.; Schelfhout, J.; Van Vlierberghe, S.; Mendes, E.; Dubruel, P. Cross-Linkable, Thermo-Responsive Pluronic® Building Blocks For Biomedical Applications: Synthesis And Physico-Chemical Evaluation. *European Polymer Journal* 2014, *53*, 126-138.

Volkmer, E.; Leicht, U.; Moritz, M.; Schwarz, C.; Wiese, H.; Milz, S.; Matthias, P.; Schloegl, W.; Friess, W.; Goettlinger, M. et al. Poloxamer-Based Hydrogels Hardening At Body Core Temperature As Carriers For Cell Based Therapies: In Vitro And In Vivo Analysis. *Journal of Materials Science: Materials in Medicine* 2013, *24*, 2223-2234.

Yin, G.; Chen, G.; Zhou, Z.; Li, Q. Modification Of PEG-B-PCL Block Copolymer With High Melting Temperature By The Enhancement Of POSS Crystal And Ordered Phase Structure. *RSC Advances* 2015, *5*, 33356-33363.

Yunus Basha, R.; T.S., S.; Doble, M. Design Of Biocomposite Materials For Bone Tissue Regeneration. *Materials Science and Engineering: C* 2015, *57*, 452-463.

Zhang, W.; Shi, Y.; Chen, Y.; Ye, J.; Sha, X.; Fang, X. Multifunctional Pluronic P123/F127 Mixed Polymeric Micelles Loaded With Paclitaxel For The Treatment Of Multidrug Resistant Tumors. *Biomaterials* 2011, *32*, 2894-2906.

Zhao, L.; Li, X.; Zhao, J.; Ma, S.; Ma, X.; Fan, D.; Zhu, C.; Liu, Y. A Novel Smart Injectable Hydrogel Prepared By Microbial Transglutaminase And Human-Like Collagen: Its Characterization And Biocompatibility. *Materials Science and Engineering: C* 2016, *68*, 317-326.

Zhou, Q.; Zhang, Z.; Chen, T.; Guo, X.; Zhou, S. Preparation And Characterization Of Thermosensitive Pluronic F127-B-Poly(Ɛ-Caprolactone) Mixed Micelles. *Colloids and Surfaces B: Biointerfaces* 2011, *86*, 45-57.

Zhou, S.; Deng, X.; Yang, H. Biodegradable Poly(E-Caprolactone)-Poly(Ethylene Glycol) Block Copolymers: Characterization And Their Use As Drug Carriers For A Controlled Delivery System. *Biomaterials* 2003, *24*, 3563-3570.

CHAPTER 4
3D BIOPRINTED PSEUDO-BONE DRUG DELIVERY SCAFFOLD FOR BONE FRACTURE IMPLANTATION

4.1. Introduction

3D bioprinting is currently the most explored field of research in tissue engineered systems (Huang, et al., 2012). The most common impairments employing 3D bioprinting research, significantly focuses on therapeutics designed to treat bone fractures as well as bone defects (Tang, et al., 2016). Consequently, bone-related costs and therapy are escalating (Caetano, et al., 2016). Typical treatment for these impairments include bone grafts or metal prosthetic implants. However, this form of therapy is restricted in many incidents due to significant tissue loss resulting from surgery, long recovery periods and donor site morbidity (Bosco, et al., 2016). Nonetheless, the limitations related to these forms of therapy have opened doors to the evolution of 3D bioprinting technology, employing cutting edge design and execution of drug delivery engineered platforms (Bose, et al., 2013). Bone tissue repair and regeneration employing non-invasive procedures have thus become a significant focus (Mironov , et al., 2009, Heintz , et al., 2016, Li , et al., 2015).

3D bioprinted scaffolds employed for bone tissue repair and healing, using computer-aided design (CAD) software, has numerous benefits such as; intensive care patient specific dose designs, customized geometrical site-specific drug delivery applications, as well as controlled drug release implantable platforms employing internal architecture modification designs (Lee, et al., 2014, Huang, et al., 2012). To date, 3D printing has gained superior recognition in the biotechnology market, ranging from medical devices, engineering components and pharmaceutical drug technologies (Günther , et al., 2014, Gioffredi , et al., 2016, Kang , et al., 2013, Wang , et al., 2014). This technology will not only provide a means of improving the cost effectiveness of products, due to minimum wastage and time efficiency, but will also produce highly accurate batches of therapeutic devices, as revolutionary technology designs (Arai, et al., 2011, Choonara, et al., 2016, Faulkner-Jones, et al., 2015, Shim, et al., 2011).

In this chapter, a pseudo-bone drug delivery scaffold was synthesized, possessing properties of comparable matrix hardness and resilience to healthy bone tissue, following incorporation *in situ*.

This 3D bioprinted pseudo-bone scaffold is a trajectory from previous pre-formulation studies undertaken (Kondiah, et al., 2017), with further optimization employing 3D bioprinting. The 3D bioprinted pseudo-bone scaffold formulations were designed using polymer-variable concentration optimization, employing MATLAB® software and artificial neural (ANN) networks. The 3D bioprinted scaffold was designed using Inventor® auto CAD, fabricating a strategic cylindrical shaped drug delivery scaffold, with uniform bioprinted filaments and pore size geometrical configuration. The pseudo-bone 3D bioprinted scaffold was designed to mimic the morphology, matrix strength and matrix resilience of biomaterial (healthy human bone). This was evaluated using healthy human clavicles in which butterfly fractures were induced. Ethical clearance waiver was granted from the Department of Human Anatomy, University of the Witwatersrand, for undertaking this study.

The tissue engineered system was optimized as a controlled release platform incorporating the drug simvastatin, used to increase bone regeneration and repair. The bioink was designed to gradually degrade and releasing its loaded contents in a sustained manner, allowing contact adhesion between fractured/damaged bone and formation of a pseudo-bone matrix within these sites. Polymers employed for formulating the bioink of the pseudo-bone scaffold consisted of; polypropylene fumarate (PPF), free radical polymerized polyethylene glycol- polycaprolactone (PEG-PCL-PEG) and Pluronic (PF127). The 3D bioprinted scaffold was characterized for its chemical, morphological, mechanical, *in vitro* release properties and optimization design, using MATLAB® software and ANN.

4.2. Materials and methods

4.2.1 Materials

PEG (Mw 4000g/mol), stannous octoate, 92.5%; Pluronic F-127; poly(ethylene glycol) diacrylate; epsilon-caprolactone, 99%; petroleum ether, 90%; and simvastatin (MW: 418.57g/mol), 97% purity, were procured from Sigma-Aldrich (St. Louis, MO, USA). Methanol, 99%; diethyl fumarate, 98%; diethyl ether (anhydrous); hydroquinone, 99% purity; methylene chloride; propylene glycol (1,2-propandiol); HCL,1.85% $^{v}/_{v}$; Na_2SO_4 and $ZnCl_2$ were purchased from Merck (Pty) Ltd Westfield, Lethabong, South Africa. All other reagents were of analytical grade and were used as received. All reactions were undertaken under inert conditions.

4.2.2 Synthesis of the bioink Scaffold

A strategically designed copolymeric blend; polypropylene fumarate (PPF), PEG-PCL-PEG, and Pluronic PF 127, was optimized for 3D bioprinting and loaded with simvastatin. Free radical polymerization was undertaken for preparation of copolymer PEG-PCL-PEG, using PEG as the macro-initiator and catalyst stannous octoate ($Sn(Oct)_2$). Briefly, 0.007M of PEG 4000 and 0.098M of ε-caprolactone was reacted in a round bottom flask, purged with N_2, at 125°C, under constant magnetic stirring (3500rpm). The catalyst (100μL) was then added and left for 6 hours under N_2 purging. PPF (8%$^w/_v$ -20%$^w/_v$) and PF127 (14%$^w/_v$- 16%$^w/_v$) was then added to the reaction mixture, specifying the concentrations as obtained by the formulation designed template using MATLAB® software. The reaction temperature was then increased to 140°C, and left for 6 hours under constant magnetic stirring of 3000rpm. The reaction mixture was then allowed to cool to room temperature, with further addition of DCM, and washing three times with deionised water. The organic solvent was then removed using rotary evaporation, and stored at 10°C for further use. Details of the above synthesis has previously been reported by the authors (Kondiah, et al., 2017). Simvastatin was then loaded into the copolymer, with a therapeutic dose calculated at 10mg per scaffold. The loading dose was calculated according to the material required for bioprinting, dependant on parameters employed, according to the optimization of fabrication procedures on the bioprinted scaffold, as discussed in Section 4.4. The bioink paste was then fabricated by formulating a ratio of 6:3:1 of the copolymer: methanol: deionized water, respectively. The copolymer then underwent microwave-assisted heating using a specific laboratory designed MAS-II Plus Microwave Synthesis Workstation (Sineo, China) set at 50°C for 10min, and 600 watts, as optimized parameters.

4.2.3 Artificial neural network design and optimization of the 3D bioprinted scaffold

Artificial neural networks (ANN) can be used to determine linear and non-linear sophisticated relationships between dependant and independent variables in a study (Agami, et al., 2009). The fundamental benefit of using ANN, is the capacity for the neural network to learn directly from an informal dataset, that has not been associated directly to a mathematical equation. In this study, MATLAB Simulink® R2016a edition (The MathWorks, Inc.) was employed to undertake neural networking.

Formulations were derived using variables of 14%$^w/_v$ – 16%$^w/_v$ of PF127 and 8%$^w/_v$ – 20%$^w/_v$ of PPF. Formulations were obtained using MATLAB®, determining combination integer matrices, in

1%$^{w}/_{v}$ concentration increments, within the variable range of PPF and PF127. The concentrations of PEG-PCL-PEG polymer, and all other reagents were kept constant during the design of the study. A total of 39 formulations were derived and synthesised using ANN (Table 4.1). All formulations were evaluated for parameters of temperature of gelation before bioprinting and the duration of drug release after bioprinting. This was then analysed as a factor (Equation 4.1), with the highest factor representing the optimised formulation matrix.

$$Factor = \frac{tg}{bt} \times Rd \tag{4.1}$$

Where *tg* represents the thermo-gelation temperature of the synthesised copolymer, *bt* representing body temperature and *Rd* representing the drug release duration. Performance training of the neural network was evaluated by the mean square error and regression analysis (Agami, et al., 2009).

The ANN, used a Multilayer Feed Forward-Back Propagation, containing an input, output, as well as a variety of hidden layers, where the gradient was computed for the multilayer non-linear network. This back propagation relationship, thus uses large input and output datasets, to determine a network mapping, thereby not requiring a definite mathematical equation to undertake the modelling. This gradient descent algorithm using back propagation is classified as the Widrow-Hoff learning rule, using multiple-layer networks, with various degrees of optimization to the algorithm.

For the neural network to display training algorithms on the basis of lowest mean square error, and highest accuracy correlations, a training percentage value of 70% was selected in the network. A validation of 15% was undertaken, measuring the network generalization, thereby terminating training when generalization of the network stops improving. A testing percentage of 15% was selected, resulting in no effect on training parameters, providing an indication of independent measure of performance during and after training of the network. Thus, this complies to 100% evaluation split in 3 categories of network priority. The algorithm employed in a study, depends on the complexity of variables and desired strategic outcome of modelling. In this study, we used 3 types of algorithms, such as; Levenberg-Marquardt, Scaled Conjugate Gradient and Bayesion Regulization. The algorithm which obtained the best training results, was employed for the ANN study (Agami, et al., 2009).

In terms of expressing data in the form of equation variables, the input to hidden layer *U*, was expressed by:

$$(U)=(W)(I) \tag{4.2}$$

W, representing the weight, and *I* the input. Each term of the hidden layer matrix can be explained as follows:

$$Uj = \sum_{i=1}^{n} WiIi - \Theta \tag{4.3}$$

$\boldsymbol{\Theta}$, representing the associated bias. Optimization in the hidden layer using transfer functions was conducted. Non-linear functions {log-sigmoid (logsig), hyperbolic tangent sigmoid function (tansig)} and linear function (purelin), was undertaken to investigate the ability to achieve optimum results. Equations (4.4), (4.5) and (4.6) were employed to understand the sequencing of optimisation of the network:

$$f(U)=u \tag{4.4}$$

$$f(U)=\frac{1}{[1+e^{(-u)}]} \tag{4.5}$$

$$f(U)=\frac{2}{[1+e^{(-2u)}]-1} \tag{4.6}$$

As a means of determining the effectiveness of the models, the determination coefficient (R^2), and the mean square error (MSE), was employed as follows:

$$\text{MSE}=\frac{1}{n}=\sum_{i=1}^{n}(Y\ response\ predicted - Y\ response\ experimental)^2 \tag{4.7}$$

$$R^2 = 1 - \frac{\sum_{i=1}^{n}(Y\ response\ predicted - Y\ response\ experimental)^2}{\sum_{i=1}^{n}(Y\ response\ experimental - Y\ response\ mean)^2} \tag{4.8}$$

The adaptation learning function employed was the gradient descent, with momentum weight and bias learning function. Optimisation of the learning function also varied with the number of neurons, resulting in observational learning with greater percentage validity. Parameters of the number of epochs, minimum gradient and Mu employed were evaluated at 10^2, 1^{-10} and 0.01,

respectively. Thermo-gelation analysis on the 39 bioink design formulations, as seen in Table 4.1, were undertaken using a Modular Advanced Rheometer (ThermoHaake MARS Modular Advanced Rheometer, Thermo Electron, Karlsruhe, Germany), comprising a C35/1° Ti sensor.

Table 4.1: Design specifications of the 3D bioprinted scaffold formulations using MATLAB Simulink®

Formulation Number	PPF (%$^{w}/_{v}$)	PF-127 (%$^{w}/_{v}$)
1	8	14
2	9	14
3	10	14
4	11	14
5	12	14
6	13	14
7	14	14
8	15	14
9	16	14
10	17	14
11	18	14
12	19	14
13	20	14
14	8	15
15	9	15
16	10	15
17	11	15
18	12	15
19	13	15
20	14	15
21	15	15
22	16	15
23	17	15
24	18	15
25	19	15
26	20	15
27	8	16
28	9	16
29	10	16
30	11	16
31	12	16
32	13	16
33	14	16
34	15	16
35	16	16
36	17	16
37	18	16
38	19	16
39	20	16

A temperature range of 10°C- 40°C was conducted, using a cone and plate inertia of 1.721×10^{-6}kg m^2, analysing 5ml of sample. The sample was analysed in the range of 0–1.0 Hz, in the region of the shear independent plateau of the strain amplitude sweep stress. G', representing the effects of elastic energy (storage modulus), and G'', representing the effects of viscous energy (loss modulus) was evaluated. The point of thermo-gelation occurred when the fluid nature of the gel

(G'') transitioned to a semi-solid composition (G'), being subjected to an increase in temperature, over constant sinusoidal oscillation.

4.2.4 3D design of the bioprinted pseudo-bone drug delivery scaffold

The 3D bioprinted scaffold was designed using Autodesk Inventor®, 3D computer-aided design (CAD), for precise fabrication prototyping, of the polymer based biomaterial. The scaffold was designed as a cylindrical implant, with dimensions comprising 16mm radius and a height of 4.2mm. After generating a Stereolithography (STL) file on Inventor®, this file was imported to EnvisionTEC Visual Machines software, thereby converting to a Borland Package Library (BPL) file for bioprinting processing. Design of internal features and uniform slicing of the design was then undertaken on this software, printing a strand diameter of 500μm, and creating an inner structure pattern between layers at 30°. The scaffold was designed with a total number of 7 layers, with the height of each layer being 0.6mm (Table 4.2).

A 3D Bioplotter® (EnvisionTEC GmbH, Gladbeck, Germany) was employed, using a pressure and temperature regulated syringe, with parameters optimized at 1.0 bar of pressure, speed at 1mm/s and syringe temperature regulated at 20°C. The temperature of the printing platform was maintained at 40°C. The transfer height and needle offset was set at 5mm and 0.5mm respectively. Pre-flow delay, post-flow delay and time between layers were set as 0, 0 and 120sec respectively (Table 4.3). The low pressure and speed of printing, provided sufficient time for the structure to solidify, thereby promoting accuracy and scaffold platform building to occur. This technology allows development of any object to be printed, provided the appropriate uniform viscosity is maintained throughout. Figure 4.1 illustrates the CAD design of the 3D bioprinted scaffold model.

Table 4.2: Specification design dimensions of the 3D bioprinted scaffold using Autodesk Inventor®

Design Parameters	Dimensions
Radius	16mm
Height	4.2mm
Strand diameter	500μm
Inner structure pattern between layers	30°
Total number of layers	7
Height of each layer	0.6mm

Table 4.3: 3D bioprinting parameters of the drug delivery scaffold employing the 3D Bioplotter®

Printing Parameters	Dimensions
Printing pressure	1.0 bar
Printing speed	1mm/s
Syringe temperature	20°C
Temperature of printing platform	40°C
Transfer height	5mm
Needle offset	0.5mm
Pre-flow delay time between layers	0 sec
Post-flow delay time between layers	120 sec

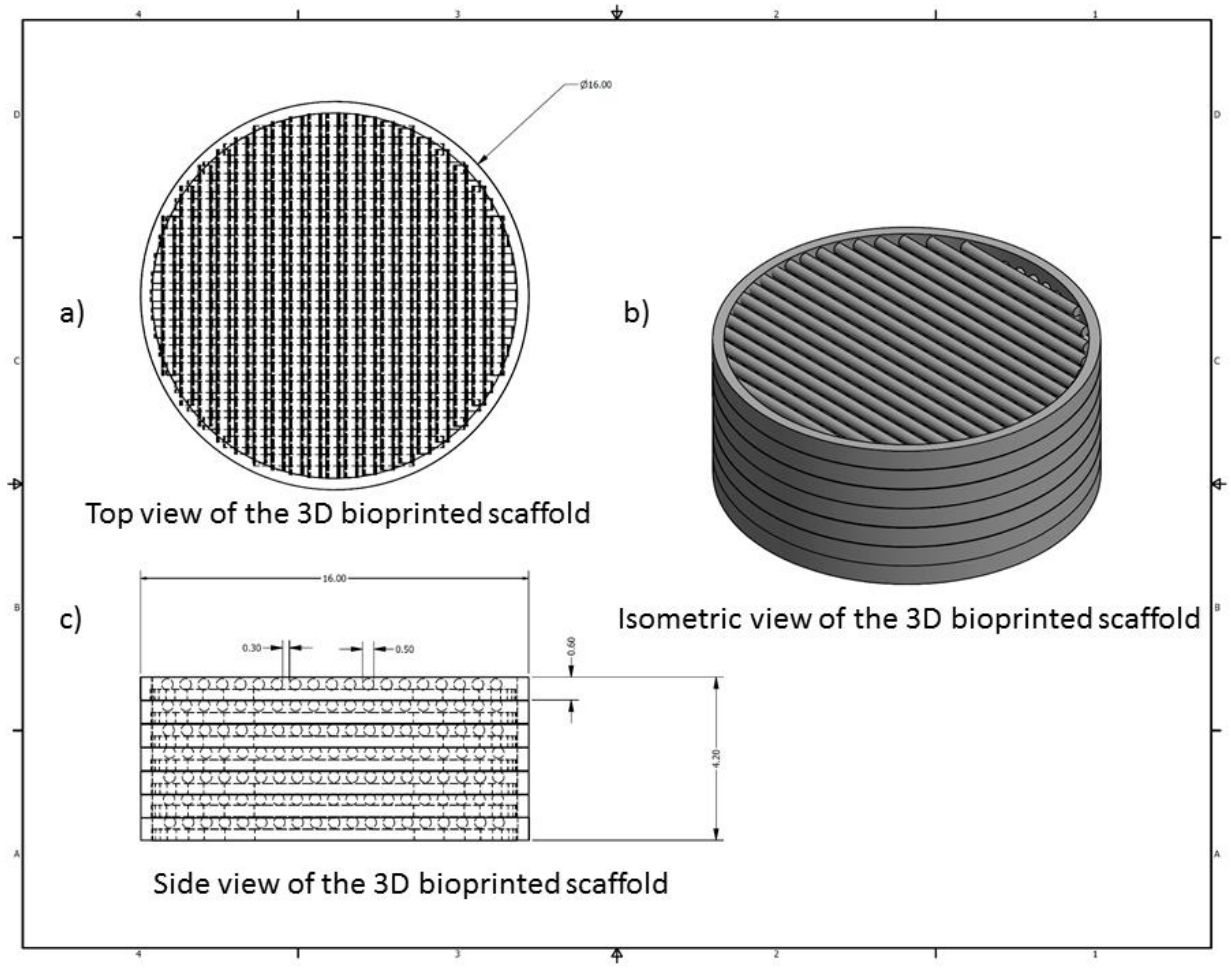


Figure 4.1: CAD specification design of the optimised 3D bioprinted scaffold.

4.2.5 Chemical and thermal evaluation of the 3D bioprinted pseudo-bone scaffold

Nuclear magnetic resonance (NMR) was undertaken on the 3D printed scaffold using a Bruker AVANCE II 500 MHz (Bruker Avance Biospin, Germany) instrument. Deuterated chloroform (DCl_3) was used to dissolve the scaffold, evaluating the sample at 25°C.

Thermogravimetric analysis was undertaken using a TGA 4000 thermogravimetric analyser (PerkinElmer Inc, Massachusetts, USA), over a temperature range of 30°C- 900°C. This was undertaken at a ramping rate of 10°C/min, under inert conditions, with a purge rate of 20ml/min of nitrogen (Table 4.4). A sample weight of 10mg was used, evaluating the percentage degradation of the 3D bioprinted scaffold. The 1st derivative was obtained after analysis of the thermogram, detecting the point of inflection for analysis. This peak indicates the point of greatest rate of change of the 3D bioprinted scaffold, with most significant weight loss observed.

Table 4.4: Thermal evaluation of the 3D bioprinted pseudo-bone scaffold using a TGA 4000 thermogravimetric analyser.

Thermogravimetric Parameters	Dimensions
Temperature evaluation range	30°C- 900°C
Ramping rate	10°C/min
Purge rate	20MI/min

4.2.6 Morphological analysis of the 3D bioprinted pseudo-bone scaffold

Scanning electron microscopy (SEM) analysis was undertaken to confirm the pore architecture of the 3D bioprinted scaffold, as well as to determine the accuracy of bioprinting parameters in relation to morphological characteristics between all 7 layers of the 3D scaffold. The 3D bioprinted scaffold sample was prepared by sputter coating on an aluminium spud, employing an EPI sputter coater (SPI Module TM sputter-coater and control unit, West Chester, PA, USA). The sample was then analysed using a FEI ESEM Quanta 400F (FEITM, Hillsboro, OR, USA) electron microscope, with an electron acceleration charge of 20Kv, producing high resolution images of the 3D bioprinted scaffold.

4.2.7 *In vitro* drug release evaluation on the designed 3D bioprinted pseudo-bone drug delivery scaffolds

All 39 bioprinted scaffolds (n=3) were evaluated, employing a dialysis membrane (MWCO: 1.2 kDa), immersed in phosphate buffer solution (PBS, pH 6.8). Samples were evaluated in an orbital shaker incubator (LM-530-2, MRC Laboratory Instruments Ltd, Hahistadrut, Holon, Israel) at 37.5°C, 50 rpm. 1 mL of sample was removed at each time point from the buffer (250 mL volume), and replaced equally with new buffer. Release samples were then analysed for simvastatin concentration using a UV spectrophotometer, at wavelength 238nm (IMPLEN Nanophotometer^{TM}, Implen GmbH, München Germany). This was undertaken using a 10 times dilution factor of path-length 0.1 mm (Zhang, et al., 2011).

4.2.8 Textural analysis of the human clavicle bone and 3D bioprinted pseudo-bone scaffold

Matrix hardness (MH) and matrix resilience (MR) analysis, employing a textual analyzer (TA.Xtplus, Stable Microsystems, Surrey, UK), under parameters of temperature at 37.5°C and pressure of 1 atm, was undertaken on a healthy human clavicle bone (obtained with ethical waiver clearance) and thereafter on the area of the bone which was fractured and treated with the 3D bioprinted scaffold. A steel flat tip probe of 2mm diameter was used for MH determination and a steel cylindrical probe of 50mm diameter was employed for MR evaluation. The clavicles were induced with a 4mm diameter fracture in the region between the cervical fascia and the area bellow the conoid tubercle (Sanchez-Molina, et al., 2013). This was undertaken using a 4mm punch and dye apparatus, with a hydraulic pressure of 0.6Mpa (Table 4.5). The fracture-induced human clavicle bone was then tested after incubation at 37.5°C for 2 hours, following hydration of the scaffold with 2Ml of PBS at the fracture site, with evaluation of the properties of matrix hardness and resilience on the bone thereafter.

Table 4.5: Parameters of textural analysis of the human clavicle bone and 3D bioprinted scaffold for determination of MH and MR.

Parameters of Textural Analyzer	Dimensions
Temperature	37.5°C
Pressure	1 atm
Diameter of steel flat tip probe	2mm
Diameter of steel cylindrical probe	50mm
Diameter of punch dye apparatus	4mm
Hydraulic pressure	0.6Mpa

4.3. Results and Discussion

4.3.1 Design and optimization of the 3D bioprinted pseudo-bone drug delivery scaffold employing artificial neural networks

The 3D bioprinted scaffolds, evaluated as 39 design formulations using MATLAB® software, comprised of variables of PPF ($8\%^{w}/_{v}$ - $20\%^{w}/_{v}$) and PF127 ($14\%^{w}/_{v}$ - $16\%^{w}/_{v}$), as presented in Table 4.1. These design scaffold formulations were studied in response to duration of release of simvastatin and the degree of thermo-gelation of the bioink formulation. Figure 4.2 reflects the formulation compositions and response factor from each design, using a 3D Simulink design graph. It was observed that with incremental increases in the concentration of PPF at constant PF127 levels, a comparatively greater concentration of simvastatin was released for the formulations. This can be attributed to the increasing incompatibility created by the hydrophobic chain regions of PPF encapsulating simvastatin, a biopharmaceutics classification system (BCS) class 2 drug, at higher concentrations. It was also observed that, as the PF127 variable increased, the scaffolds biodegraded over an extended duration due to stronger gelation of the scaffold with increased PF127 concentration, further controlling the release rate of the loaded drug. This slower sustained release effect of PF127 in the formulation is desirable for implantable systems (Raval, et al., 2017). Furthermore, the formulations also demonstrated a decrease in gelation temperature as the concentration of PF127 was increased, as observed in Figure 4.4.

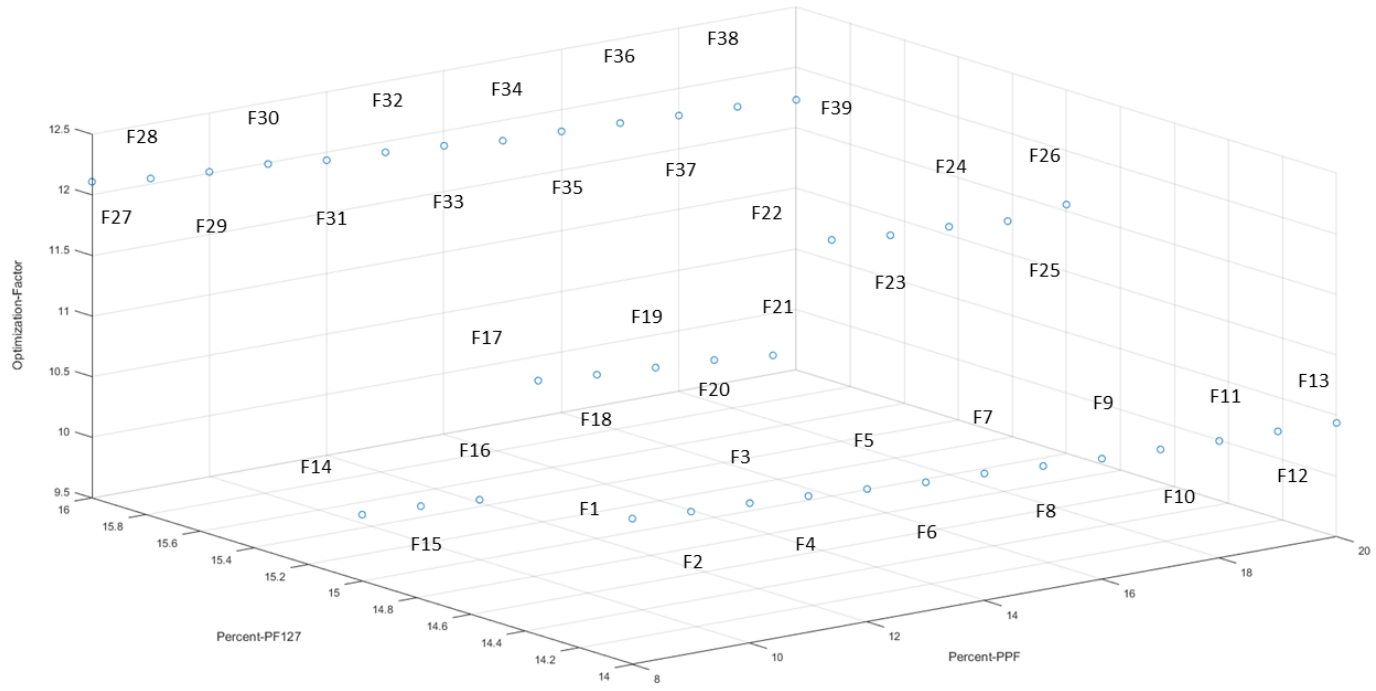


Figure 4.2: 3D representation of the ANN design formulations, reflecting the percentage of PPF and PF127, with the optimization factor for each formulation.

Providing these inputs in the software, Equation 4.1 was employed in determining the variable concentrations for the optimized formulation, thereafter training these inputs using ANN. The 546 number data set involved in the study was undertaken by varying the number of neurons in the hidden layer, using the sigmoid symmetric transfer function and using 3 different training functions for developing the model. The optimum network was derived using performance indicators of error function and R^2 values. A variation in the number of neurons in the hidden layer is an essential component in ANN. The network thus becomes under-performing or highly entangled to sort, when the number of neurons are too high or low. Thus, a region between 6-16 neurons was investigated, and considered an efficient model for optimum results. The optimum number of neurons after testing was found to be 10, thus producing the lowest mean square error and highest regression values for various training models.

For training of the network, the feed forward back propagation method was employed. Using the Levenberg-Marquardt, Bayesian Regularization and Scaled conjugate gradient training networks, the training network that resulted in the lowest error functions (Equation 4.7) and highest regression value (Equation 4.8) was evaluated. After much training and evaluation of input data,

the Levenberg-Marquardt training function was observed to be the most effective algorithm employed using the sigmoid (tansig) function. Table 4.6 reflects the results obtained from the training algorithm and parameter performance observed.

Table 4.6: Training functions undertaken for optimisation of the design formulations.

Training Algorithm	Mean Square Error (MSE)	Regression Function (R^2)
Levenberg- Marquardt	≤0.1	9.99
Bayesian Regularization	≤0.1	9.82
Scaled conjugate gradient	0.7	9.14

Figure 4.3 reflects a 3D cubic function of optimisation parameters using a surface computed plot. The optimized formulation with the greatest factor, representing an optimum ratio of release duration and bioink thermo-gelation was found to be 14%$^{w}/_{v}$ of PPF and 16%$^{w}/_{v}$ of PF127. This optimized formulation composition was thus selected as the superior formulation specification. Figure 4.4 represents the thermo-gelation temperature of the 39 bioink formulations, highlighting a decrease in gelation temperature as the concentration of PF127 was increased due to the characteristic nature of the polymer.

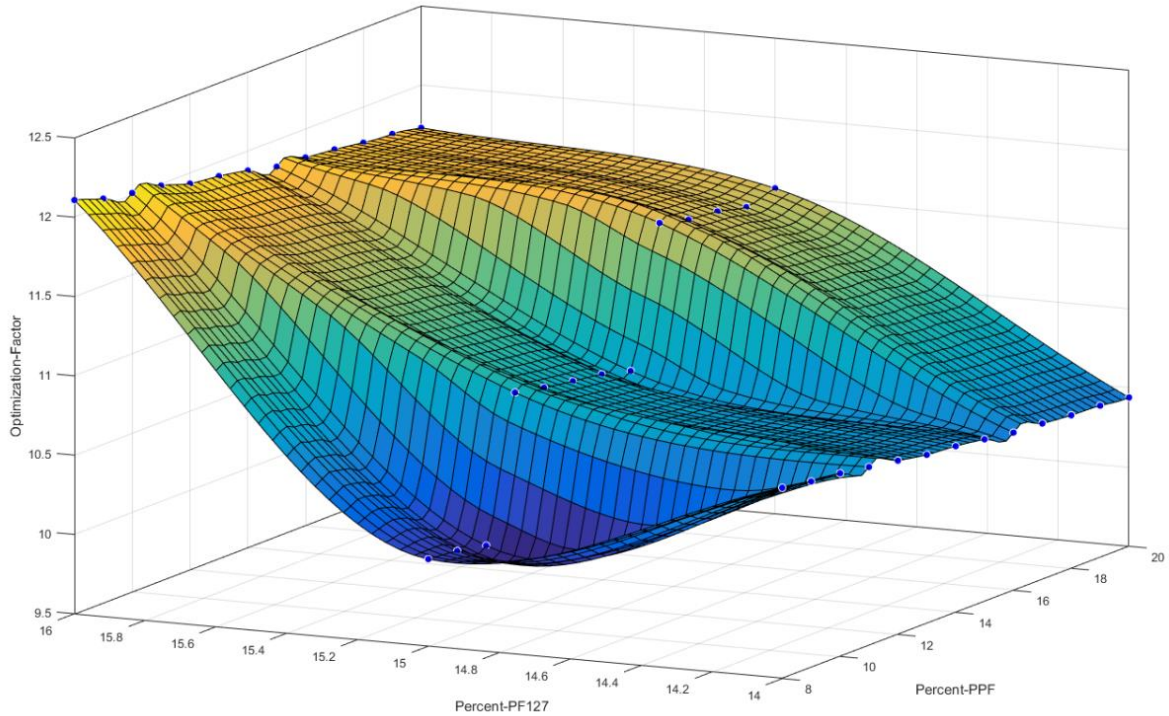


Figure 4.3: 3D representation of the designed bioink formulations using a cubic function surface plot, with the highest point on the surface plot representing the optimum polymer concentrations.

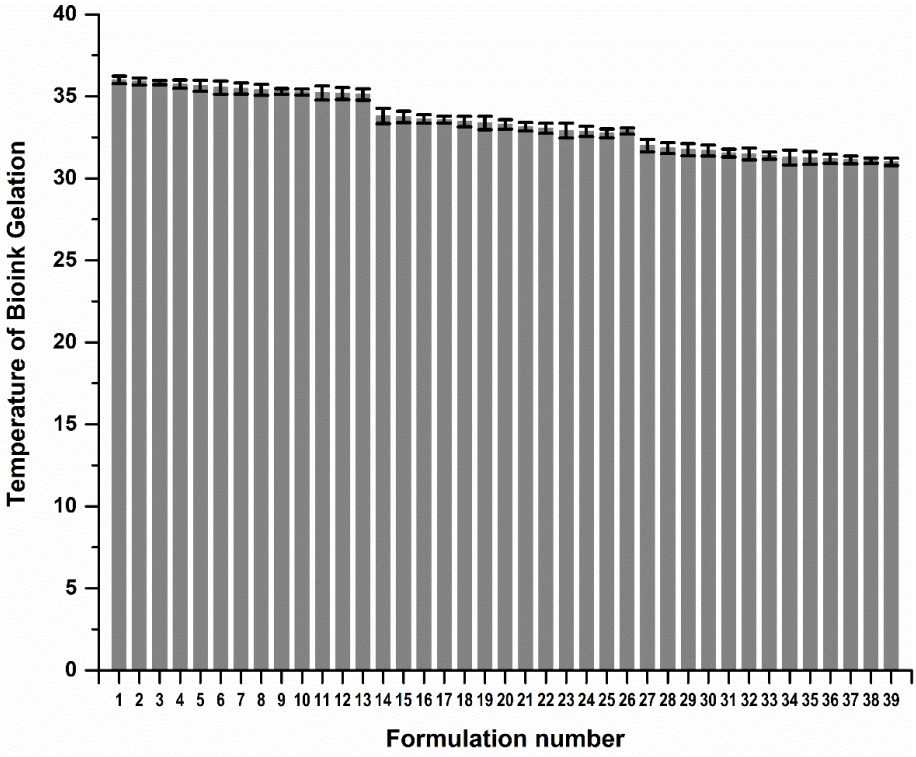


Figure 4.4: Gelation temperature of the 39 bioink design formulations prior to 3D printing.

4.3.2 Chemical and Thermo-gravimetric analysis of the optimized 3D bioprinted pseudo-bone scaffold

NMR analysis was undertaken on the 3D bioprinted scaffold, evaluating each chemical component in the formulation. As visualised in Figure 4.5, the broad signal peaks in the region of 3.5ppm and 3.65ppm represents the –(CH_2)- functional groups present in PEG, with PCL functionalities of –$OCCH_2$- and –CH_2OOC- in the regions of 1.6ppm and 2.2ppm, respectively. Evaluating peaks responsible for PPF, it was evident that the defining functionalities of –HC=CH- in the region of 6.75ppm remained intact in the PPF backbone structure. The –CH_3- functionality of PF127 was identified in the region of 1.1ppm, with further evaluation reflecting no chemical shifting of this functionality of protons in the backbone of PEG-PCL. The peaks observed in regions 1ppm-1.3ppm can thus be attributed to the –CH_3- groups present in PPF and PF127, respectively, responsible for chemical shifts from the parent compounds. Peaks for PF127 were also identified in the region of 3.4ppm, reflecting protons of individual functional groups. Minor peaks of PPF, not evident in the 3D bioprinted scaffold, was suggestive of successful copolymeric

blending interaction, with the end groups of the PPF polymeric chain implicated in the interaction (Zhou, et al., 2011, Behravesh, et al., 2002, Jo, et al., 2000).

Thermo-gravimetric analysis was undertaken to determine the temperature range, resulting in the greatest weight loss experienced in the 3D bioprinted scaffold, after being exposed to temperatures of 30°C – 900°C. Figure 4.6a represents polymer PEG-PCL-PEG, producing a double point of inflection, with the maximum degradation for PEG and PCL chains observed in the region of 387°C and 448°C respectively. An initial percentage of degradation below 100°C was attributed to the release of moisture in the sample, due to the hygroscopic nature of the polymer. PF127 demonstrated significant biodegradation in the range of 412°C, with PPF reflecting substantial weight loss at 379°C, as seen in Figure 4.6b and c, respectively. Figure 4.6d depicts the 3D bioprinted pseudo-bone scaffold. As observed, the higher point of inflection at 448°C indicated that the scaffold possessed greater thermal stability compared to individual polymers, possibly due to properties of increasing interfacial adhesion in the scaffold matrix.

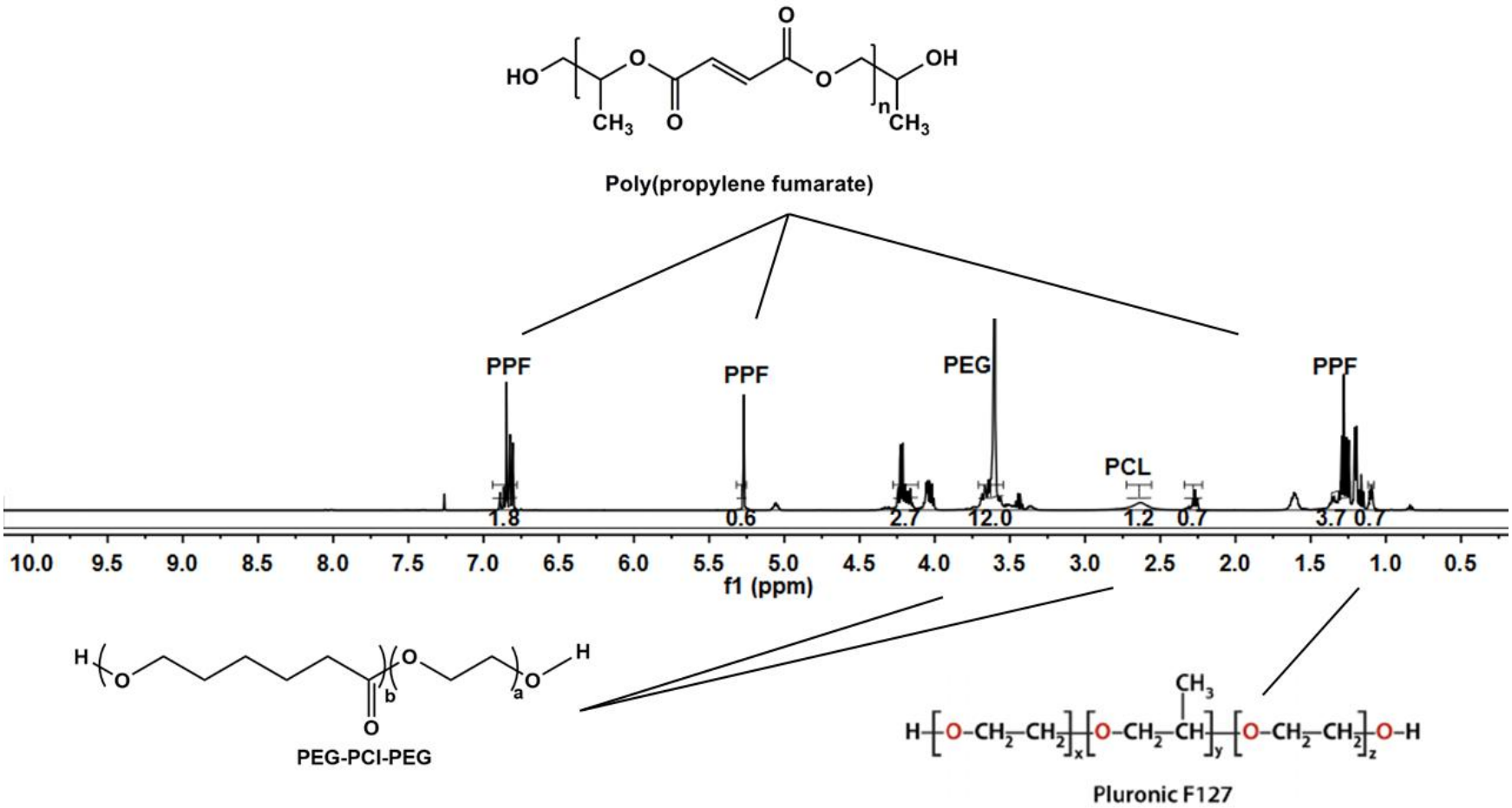


Figure 4.5: NMR analysis of the 3D bioprinted pseudo-bone scaffold, reflecting chemical shifts and copolymeric composition

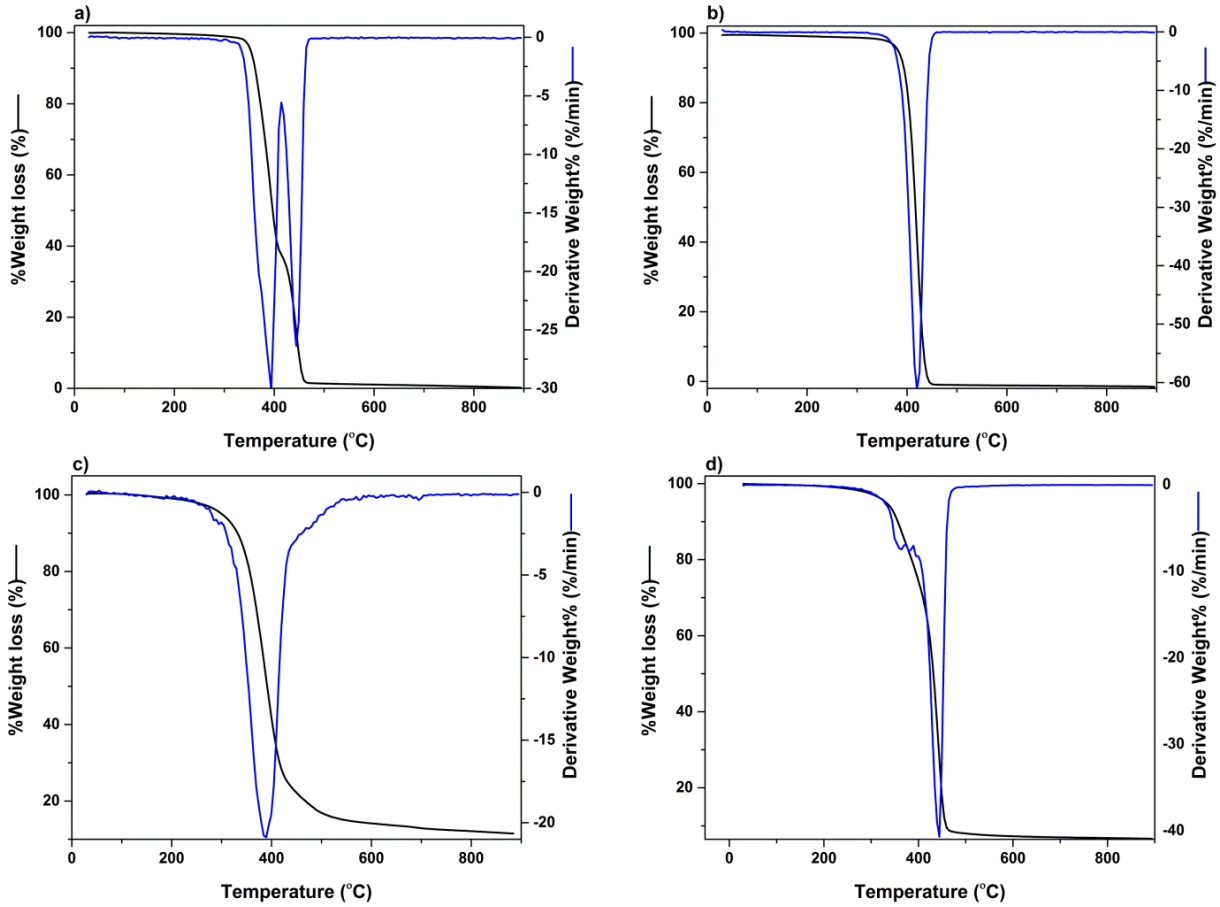


Figure 4.6: TGA analysis undertaken in the region of 30°C to 900°C for a) PEG-PCL-PEG, b) PF127, c) PPF and d) 3D bioprinted scaffold.

4.3.3 Morphological analysis undertaken on the 3D bioprinted pseudo-bone scaffold

Scanning electron microscopy was undertaken on the 3D bioprinted scaffold for determining the micro-architectural design according to the CAD bioprinting parameters. The morphology was investigated employing electron microscopy at an average of 3500 times magnification. As seen in Figure 4.7, each layer of the scaffold reflected a similar porosity configuration, with uniform intercalated threads of fibrous 3D printing, bioengineered for cell growth within the porous network. This configuration further allows easy diffusion of tissue medium through the scaffold matrix. Printing under low pressure and low speed parameters, thus allows for maximum consistency and uniformity in the micro-architectural design of the 3D scaffold. As observed in Figure 4.7, the intercalated “rope-like” nature with porous network architecture can be identified with multiple sites of scaffold printing, bonding between each designed layer.

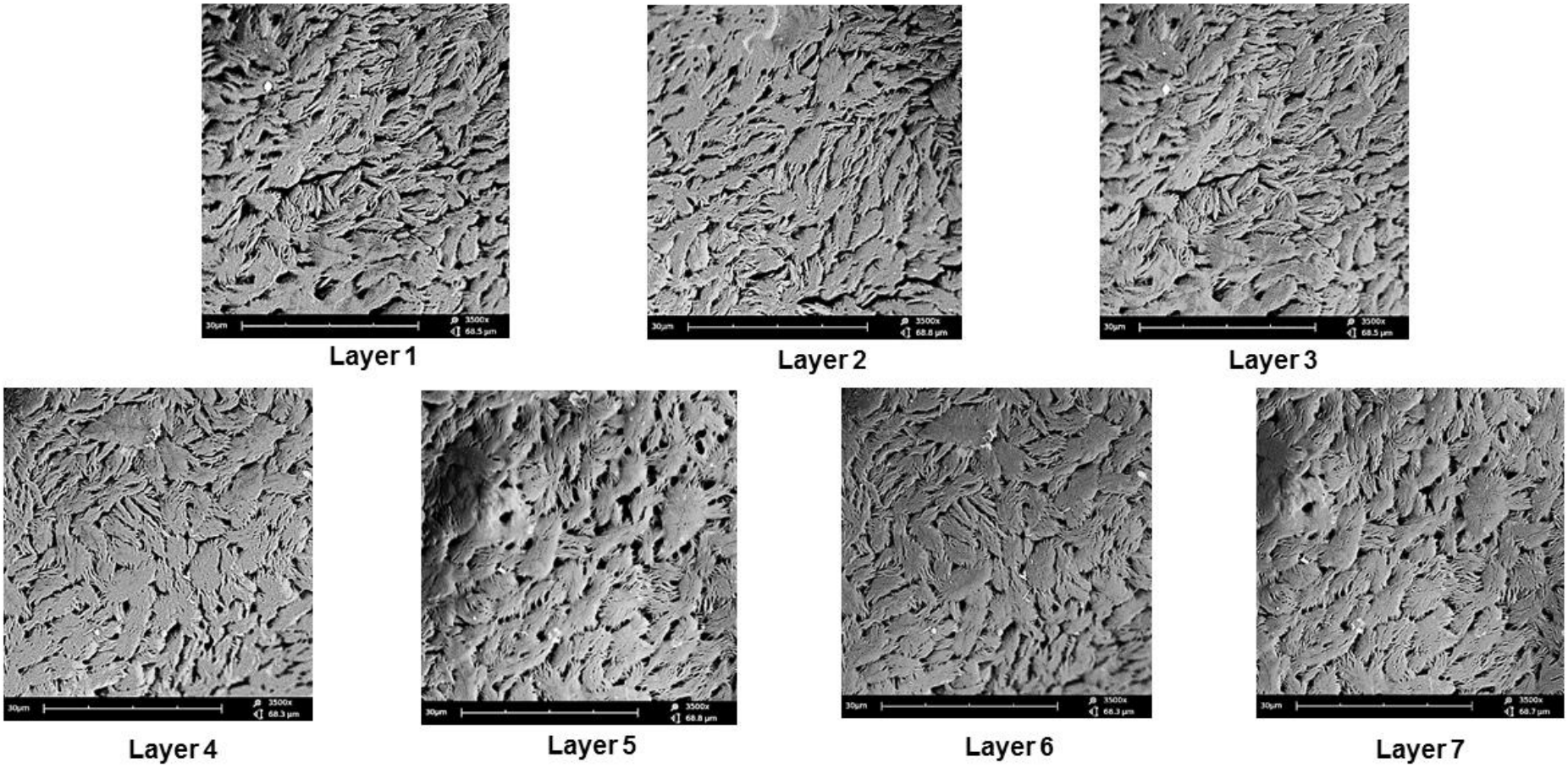


Figure 4.7: SEM analysis of the 3D bioprinted scaffold at 3500 times magnification, demonstrating the micro-architecture and inner porous nature of the 7 layers of the designed 3D scaffold matrix.

4.3.4 *In vitro* analysis of the designed 3D bioprinted drug delivery scaffolds

The 39 designed 3D scaffold formulations were analysed for their simvastatin release behaviour. It was observed that as PPF polymer ($8\%^{w}/_{v}$ – $20\%^{w}/_{v}$) was increased in percentage in the formulation, greater release of simvastatin from the scaffold over 24 hours was observed. This can be attributed to the ester linkage of PPF, accounting for hydrolysis of the polymer into biocompatible and excretable degradation products of fumaric acid and propylene glycol, with associated release of the drug from the matrix (Salarian, et al., 2014).

PF127 was incorporated at concentrations $14\%^{w}/_{v}$ to $16\%^{w}/_{v}$ in the formulations. It was observed that, as the concentration of PF127 was increased in the 3D scaffold, release of the loaded drug from the formulation was gradually slowed. This could possibly be explained in terms of increasing the amphiphilic nature of the 3D scaffold, resulting in an improved controlled release profile. The thermo-gelling capabilities of the system also contribute to the controlled release potential of the system by preventing particle aggregation, balancing hydrophilicity, surface roughness and surface charge (Raval, et al., 2017). As observed in Figure 4.8, formulations 1-16 released drug up to 13 days, formulations 17-26 up to 16 days, formulations 27-32 up to 19 days and formulation 33-39 up to 20 days. All formulations demonstrated near zero-order release kinetics. The optimised 3D bioprinted scaffold formulation, resulting in the highest factor of response (most sustained drug release), was thus synthesised incorporating $14\%^{w}/_{v}$ PPF and $16\%^{w}/_{v}$ PF127. The optimised 3D bioprinted scaffold displayed a controlled release of simvastatin over a 20-day duration, as seen in Figure 4.9, with significant correlation to the predicted release kinetics ascertained using ANN. It can be further emphasised that the morphological configuration in terms of the specialised shape and internal architecture, significantly influenced the release kinetics and biodegradation of the 3D bioprinted drug delivery scaffold. It can be concluded that the optimised 3D bioprinted scaffold possessing highly specific design features of micro-architectural pores and uniform bio-printed filaments of specific dimensional properties, has favourable controlled release kinetics *in vitro*, which demonstrated good correlation to the release predicted by the ANN model.

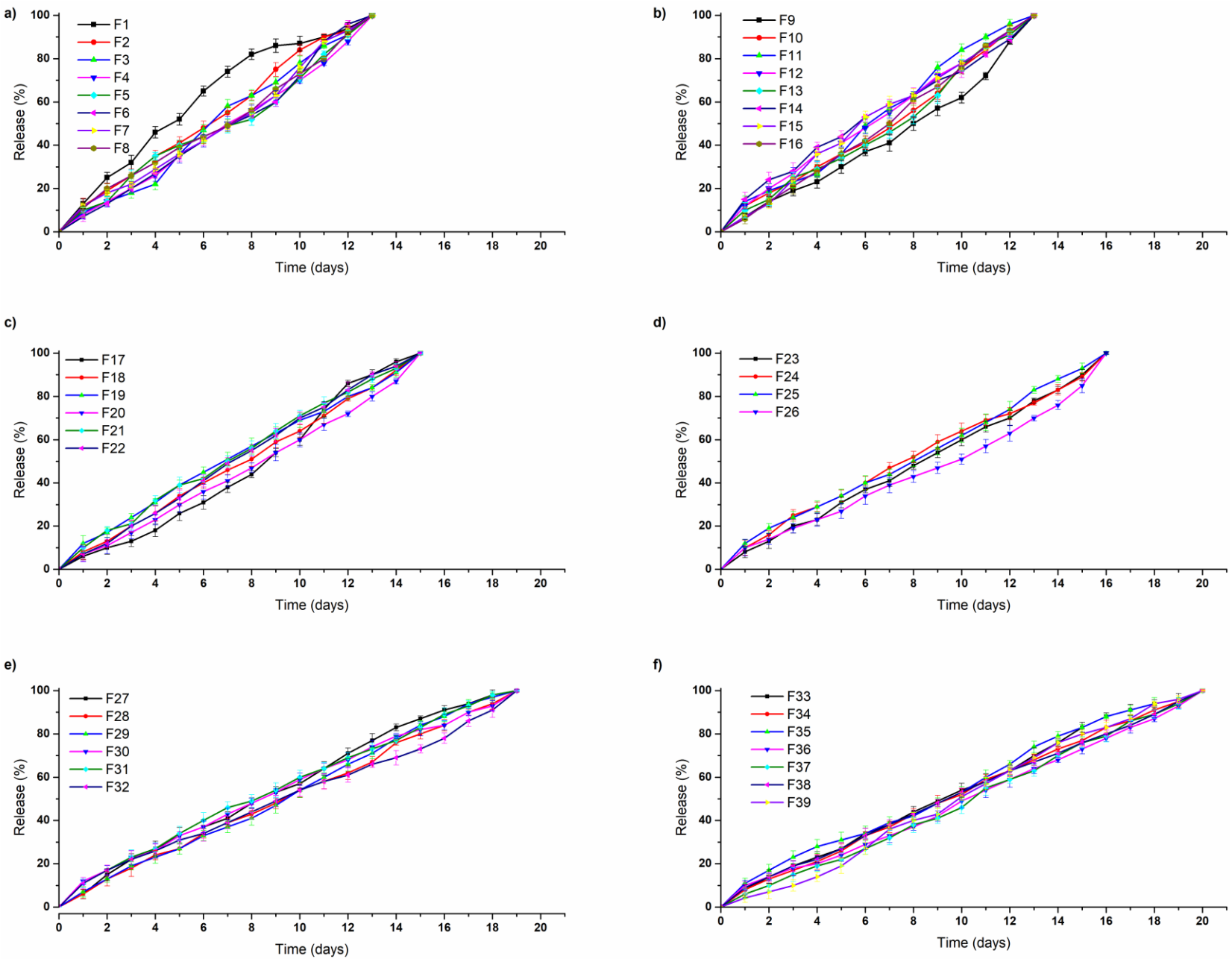


Figure 4.8: *In vitro* simvastatin release analysis of the designed 3D bioprinted drug delivery scaffolds.

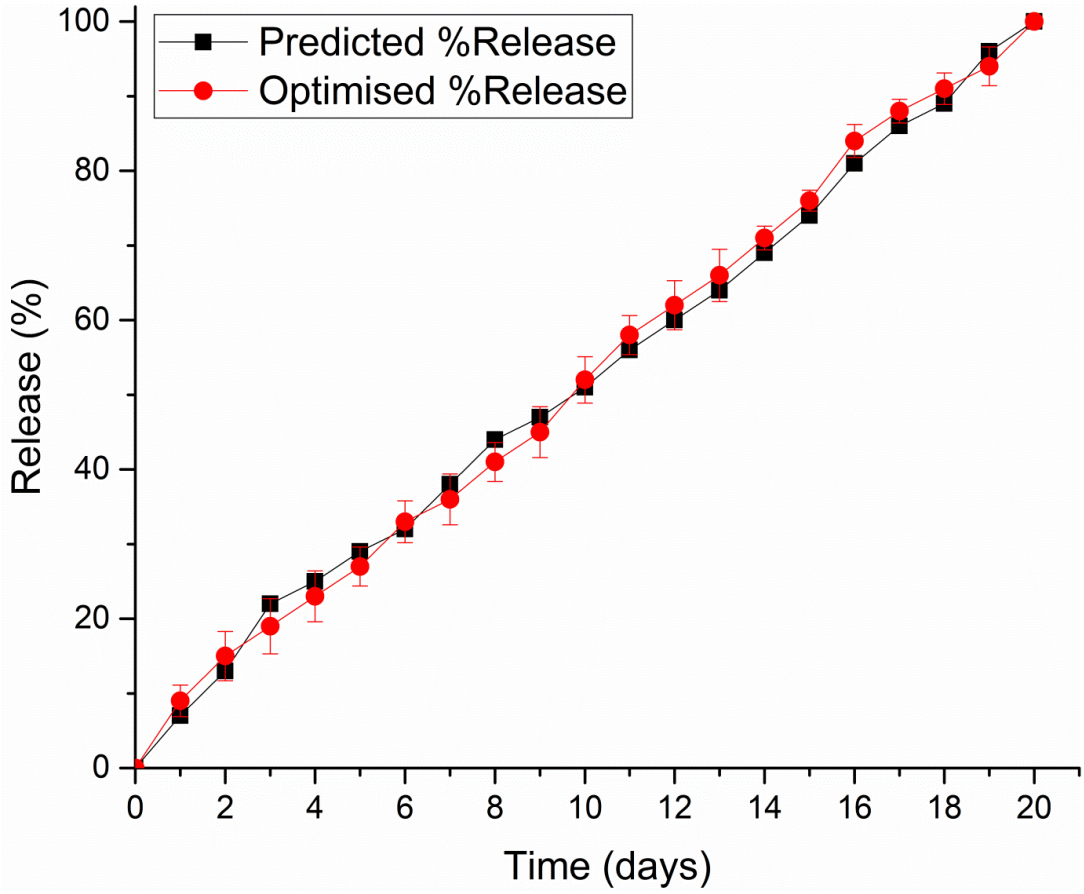


Figure 4.9: Correlation of *in vitro* simvastatin release analysis of the optimized 3D bioprinted scaffold with predicted release kinetics using ANN modelling.

4.3.5 Matrix analysis of the 3D bioprinted scaffold in fracture-induced human clavicle bones

Mechanical properties of 3D scaffolds are essential in relation to their site specific application (Hockaday, et al., 2012, Xu, et al., 2012). The MH and MR were evaluated employing a texture analyser resulting in values of 18.61N/mm and 9.48%, respectively, for the human clavicle before fracture. Figure 4.10 a, b, and c depicts an X-ray image of the human clavicle bone before fracture, after fracture, and after treatment with the 3D bioprinted scaffold, respectively (Xu, et al., 2012, Iannolo, et al., 2010). Following fracture, the missing bone mass was observed in the X-ray image (Figure 4.10b), as well as in Figure 4.10e, which is circled in red. After inducing the fracture, the 3D scaffold was applied at the site of defect, with immersion in PBS, and incubated at 37°C for 20 days. The bone was then evaluated for MH and MR. It was found that a MH of 18.45N/mm and MR of 9.33% was observed at the site of the fracture, thus possessing similar results to the non-fractured bone. Figure 4.10d represents a light microscope image at 24 times magnification

of the 3D bioprinted scaffold immersed in PBS. After incubation of the scaffold in PBS at 37.5°C for 2 hours at the fracture site, microscopic visualisation revealed significant filling of the fracture site, as observed in Figure 4.10f (depicting the architecture of the bone and the scaffold sealed sites). These values of MH and MR further exemplifies the unique properties of the 3D bioprinted pseudo-bone scaffold to fill in fracture sites in bones, thus promoting greater adhesion of bone, and restoration of damaged bone to its intended mechanical integrity.

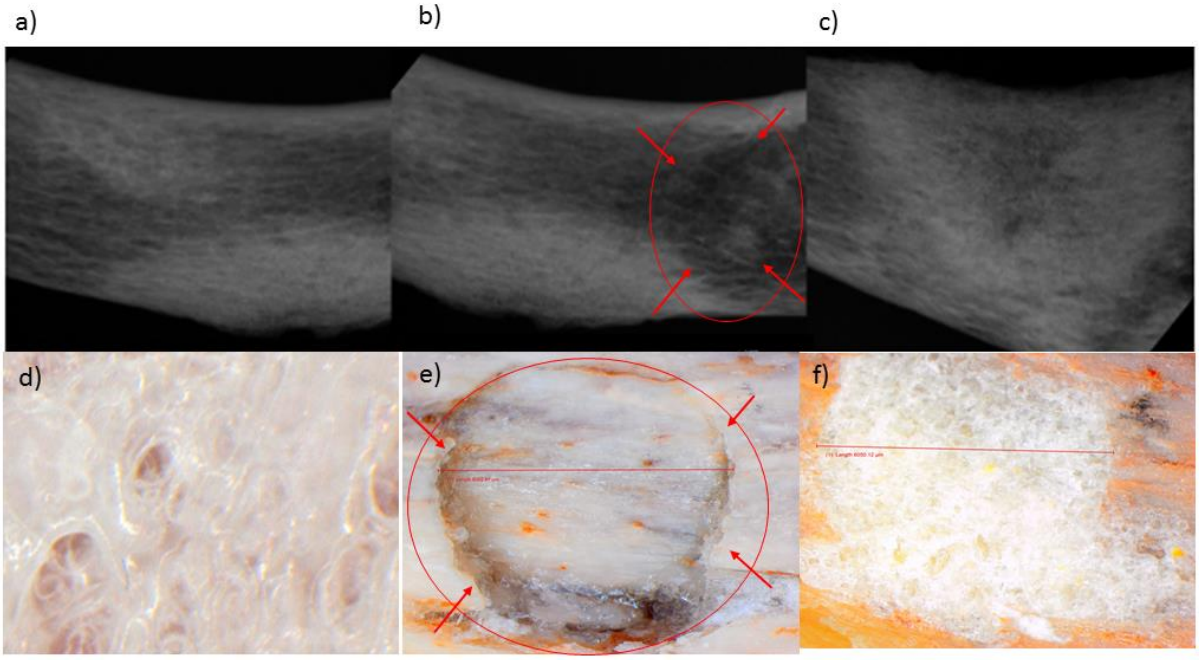


Figure 4.10: X-ray images of the human clavicle bone a) before fracture, b) after fracture and c) after treatment with the 3D bioprinted scaffold respectively. D) Light microscope image at 24 times magnification of the 3D bioprinted scaffold immersed in phosphate buffer solution, e) human clavicle bone induced with a fracture, representing missing bone fragments, f) human clavicle bone tested after incubation at 37.5°C for 2 hours, demonstrating sealing of the induced fracture site, with properties of matrix hardness and resilience comparable to original bone properties.

4.4. Concluding Remarks

A 3D bioprinted pseudo-bone drug delivery scaffold was designed to mimic the morphology, matrix strength and matrix resilience of healthy human bone. The 3D bioprinted scaffold was developed using computer aided design (CAD) software, with further optimisation of the design formulations employing MATLAB® software and ANN. Polymers employed for formulating the 3D bioprinted scaffold consisted of polypropylene fumarate (PPF), free radical polymerised polyethylene glycol- polycaprolactone (PEG-PCL-PEG) and pluronic (PF127). Simvastatin was incorporated into the 3D bioprinted scaffolds, to further promote bone healing and repair

properties. The 3D bioprinted scaffold was characterised for its chemical, morphological, mechanical and *in vitro* release properties, for evaluation of its behaviour for application as an implantable scaffold at the site of fracture. The ANN-optimised 3D bioprinted scaffold demonstrated favourable properties as a controlled release platform, displaying sustained drug release over 20 days. The 3D bioprinted scaffold thus promoted contact adhesion between fractured/damaged bone using a human clavicle bone model, promoting the formation of a pseudo-bone matrix within the fractured site.

4.5 References

Agami, N.; Atiya, A.; Saleh, M.; El-Shishiny, H. A Neural Network Based Dynamic Forecasting Model For Trend Impact Analysis. *Technological Forecasting and Social Change* 2009, *76*, 952-962.

Arai, K.; Iwanaga, S.; Toda, H.; Genci, C.; Nishiyama, Y.; Nakamura, M. Three-Dimensional Inkjet Biofabrication Based On Designed Images. *Biofabrication* 2011, *3*, 034113.

Behravesh, E.; Shung, A.; Jo, S.; Mikos, A. Synthesis And Characterization Of Triblock Copolymers Of Methoxy Poly(Ethylene Glycol) And Poly(Propylene Fumarate). *Biomacromolecules* 2002, *3*, 153-158.

Bosco, A.; Faleiros, P.; Carmona, L.; Garcia, V.; Theodoro, L.; de Araujo, N.; Nagata, M.; de Almeida, J. Effects Of Low-Level Laser Therapy On Bone Healing Of Critical-Size Defects Treated With Bovine Bone Graft. *Journal of Photochemistry and Photobiology B: Biology* 2016, *163*, 303-310.

Bose, S.; Vahabzadeh, S.; Bandyopadhyay, A. Bone Tissue Engineering Using 3D Printing. *Materials Today* 2013, *16*, 496-504.

Caetano, G.; Violante, R.; Sant´Ana, A.; Murashima, A.; Domingos, M.; Gibson, A.; Bártolo, P.; Frade, M. Cellularized Versus Decellularized Scaffolds For Bone Regeneration. *Materials Letters* 2016, *182*, 318-322.

Choonara, Y.; du Toit, L.; Kumar, P.; Kondiah, P.; Pillay, V. 3D-Printing And The Effect On Medical Costs: A New Era?. *Expert Review of Pharmacoeconomics & Outcomes Research* 2016, *16*, 23-32.

Faulkner-Jones, A.; Fyfe, C.; Cornelissen, D.; Gardner, J.; King, J.; Courtney, A.; Shu, W. Bioprinting Of Human Pluripotent Stem Cells And Their Directed Differentiation Into Hepatocyte-Like Cells For The Generation Of Mini-Livers In 3D. *Biofabrication* 2015, *7*, 044102.

Gioffredi, E.; Boffito, M.; Calzone, S.; Giannitelli, S.; Rainer, A.; Trombetta, M.; Mozetic, P.; Chiono, V. Pluronic F127 Hydrogel Characterization And Biofabrication In Cellularized Constructs For Tissue Engineering Applications. *Procedia CIRP* 2016, *49*, 125-132.

Günther, D.; Heymel, B.; Franz Günther, J.; Ederer, I. Continuous 3D-Printing For Additive Manufacturing. *Rapid Prototyping Journal* 2014, *20*, 320-327.

Heintz, K.; Bregenzer, M.; Mantle, J.; Lee, K.; West, J.; Slater, J. Biomimetic Microfluidic Networks: Fabrication Of 3D Biomimetic Microfluidic Networks In Hydrogels (Adv. Healthcare Mater. 17/2016). *Advanced Healthcare Materials* 2016, *5*, 2152-2152.

Hockaday, L.; Kang, K.; Colangelo, N.; Cheung, P.; Duan, B.; Malone, E.; Wu, J.; Girardi, L.; Bonassar, L.; Lipson, H. et al. Rapid 3D Printing Of Anatomically Accurate And Mechanically Heterogeneous Aortic Valve Hydrogel Scaffolds. *Biofabrication* 2012, *4*, 035005.

Huang, G.; Wang, L.; Wang, S.; Han, Y.; Wu, J.; Zhang, Q.; Xu, F.; Lu, T. Engineering Three-Dimensional Cell Mechanical Microenvironment With Hydrogels. *Biofabrication* 2012, *4*, 042001.

Huang, G.; Wang, L.; Wang, S.; Han, Y.; Wu, J.; Zhang, Q.; Xu, F.; Lu, T. Engineering Three-Dimensional Cell Mechanical Microenvironment With Hydrogels. *Biofabrication*2012, *4*, 042001.

Iannolo, M.; Werner, F.; Sutton, L.; Serell, S.; VanValkenburg, S. Forces Across The Middle Of The Intact Clavicle During Shoulder Motion. *Journal of Shoulder and Elbow Surgery*2010, *19*, 1013-1017.

Jo, S.; Engel, P.; Mikos, A. Synthesis Of Poly(Ethylene Glycol)-Tethered Poly(Propylene Fumarate) And Its Modification With GRGD Peptide. *Polymer* 2000, *41*, 7595-7604.

Kang, K.; Hockaday, L.; Butcher, J. Quantitative Optimization Of Solid Freeform Deposition Of Aqueous Hydrogels. *Biofabrication* 2013, *5*, 035001.

Kondiah, P.; Choonara, Y.; Kondiah, P.; Kumar, P.; Marimuthu, T.; du Toit, L.; Pillay, V. Development Of An Injectable Pseudo-Bone Thermo-Gel For Application In Small Bone Fractures. *International Journal of Pharmaceutics* 2017, *520*, 39-48.

Lee, J.; Hong, J.; Jung, J.; Shim, J.; Oh, J.; Cho, D. 3D Printing Of Composite Tissue With Complex Shape Applied To Ear Regeneration. *Biofabrication* 2014, *6*, 024103.

Li, J.; He, L.; Zhou, C.; Zhou, Y.; Bai, Y.; Lee, F.; Mao, J. 3D Printing For Regenerative Medicine: From Bench To Bedside. *MRS Bulletin* 2015, *40*, 145-154.

Mironov, V.; Trusk, T.; Kasyanov, V.; Little, S.; Swaja, R.; Markwald, R. Biofabrication: A 21St Century Manufacturing Paradigm. *Biofabrication* 2009, *1*, 022001.

Raval, A.; Pillai, S.; Bahadur, A.; Bahadur, P. Systematic Characterization Of Pluronic ® Micelles And Their Application For Solubilization And In Vitro Release Of Some Hydrophobic Anticancer Drugs. *Journal of Molecular Liquids* 2017, *230*, 473-481.

Salarian, M.; Xu, W.; Biesinger, M.; Charpentier, P. Synthesis And Characterization Of Novel Tio2-Poly(Propylene Fumarate) Nanocomposites For Bone Cementation. *J. Mater. Chem. B* 2014, *2*, 5145-5156.

Sanchez-Molina, D.; Velazquez-Ameijide, J.; Quintana, V.; Arregui-Dalmases, C.; Crandall, J.; Subit, D.; Kerrigan, J. Fractal Dimension And Mechanical Properties Of Human Cortical Bone. *Medical Engineering & Physics* 2013, *35*, 576-582.

Shim, J.; Kim, J.; Park, M.; Park, J.; Cho, D. Development Of A Hybrid Scaffold With Synthetic Biomaterials And Hydrogel Using Solid Freeform Fabrication Technology. *Biofabrication* 2011, *3*, 034102.

Tang, D.; Tare, R.; Yang, L.; Williams, D.; Ou, K.; Oreffo, R. Biofabrication Of Bone Tissue: Approaches, Challenges And Translation For Bone Regeneration. *Biomaterials* 2016, *83*, 363-382.

Wang, C.; Tang, Z.; Zhao, Y.; Yao, R.; Li, L.; Sun, W. Three-Dimensional In Vitro Cancer Models: A Short Review. *Biofabrication* 2014, *6*, 022001.

Xu, T.; Binder, K.; Albanna, M.; Dice, D.; Zhao, W.; Yoo, J.; Atala, A. Hybrid Printing Of Mechanically And Biologically Improved Constructs For Cartilage Tissue Engineering Applications. *Biofabrication* 2012, *5*, 015001.

Zhang, W.; Shi, Y.; Chen, Y.; Ye, J.; Sha, X.; Fang, X. Multifunctional Pluronic P123/F127 Mixed Polymeric Micelles Loaded With Paclitaxel For The Treatment Of Multidrug Resistant Tumors. *Biomaterials* 2011, *32*, 2894-2906.

Zhou, Q.; Zhang, Z.; Chen, T.; Guo, X.; Zhou, S. Preparation And Characterization Of Thermosensitive Pluronic F127-B-Poly(Ɛ-Caprolactone) Mixed Micelles. *Colloids and Surfaces B: Biointerfaces* 2011, *86*, 45-57.

CHAPTER 5
TAILOR DESIGNING OF THE 3D BIOPRINTED SCAFFOLD FOR BIOCOMPATIBILITY AND *IN VIVO* APPLICATION EMPLOYING A NEW ZEALAND WHITE RABBIT MODEL

5.1. Introduction

Since the times of Hippocrates and Galen, the potential for bone to regenerate itself has elicited intrigue and curiosity, thus prompting various studies in the medical field (Beger, et al., 2018, He, et al., 2018, Saletta, et al). Nevertheless, congenital and acquired pathologies encompassing infection, neoplasm, trauma and failed arthroplasty have the capability of leaving patients with bone defects exceeding a critical size which the body cannot repair. Therefore, such patients require routine invasive surgical procedures to facilitate healing of bone. This includes the use of bone substitute materials, bone grafts, free fibula vascularized grafts, growth factors as well as the placement of metalwork to enable stability, bone regeneration and repair (Turnbull, et al., 2018, Ashman, et al., 2013, Thaller, et al., 2014). Consequently, more than four million surgical procedures utilizing bone substitute materials and bone grafts occur annually, making bone the second most transplanted tissue globally (Brydone, et al., 2010, Wang, et al., 2017). Various bone graft methods exist, such as autografts, allografts and xenografts. Autografts are regarded as the gold standard therapy for bone regeneration since they contain osteogenic, osteoconductive and osteoinductive characteristics (Elsalanty, et al., 2009, Roseti, et al., 2017). However, there are many disadvantages that exist, such as pain, major vessel or visceral injuries during bone harvest and donor site morbidity. Alternative treatment for bone regeneration include allografts and xenografts, however these methods are very costly and have a high rate of infection, viral transmission immunogenicity as well as the risk of transmitting zoonotic diseases (Gruskin, et al., 2012, Curry, et al., 2016, Martin, et al., 2018).

To vanquish these disadvantages, 3D bioprinted scaffolds have been designed as an alternate strategy in the field of bone tissue engineering and regenerative medicine (Aljohani, et al., 2018). 3D bioprinted scaffolds comprising of polymers designed to promote bone growth and repair, can be fabricated with increased precision and accuracy, to encompass specific porosities, 3D filament diameter printing, and high mechanical strength (Li, et al., 2018, Luo, et al., 2018). These scaffolds, are designed to provide structural support, and to promote attachment, proliferation and differentiation of cells to ultimately promote bone repair. Bone regeneration and repair utilizing

non-invasive methods have become a remarkable focal point due to the implementation of 3D bioprinted technologies (Xie, et al., 2018, Xia, et al., 2018).

It has also become evident to date, that statins stimulate bone growth formation (Moraschini, et al., 2018). Statins are specific competitive inhibitors of 3-hydroxy-2-methyl-glutaryl coenzyme A (HMG-CoA) reductase. The proposition that statins increase bone formation has brought forth a thrilling new direction for research (Alam, et al., 2009). An approach to implant a statin loaded 3D printed scaffold was optimized extensively in the last Chapter, for means of investigating *in situ* bone healing properties.

In this Chapter, the optimized novel pseudo-bone 3D bioprinted scaffold comprising polypropylene fumarate (PPF), polyethylene glycol- polycaprolactone (PEG-PCL-PEG) and pluronic (PF127) was evaluated for its biocompatibility properties, employing MG63 cell seeding for cell viability analysis. After proving the 3D printed scaffold non-cytotoxic, the 3D scaffold was tailor designed for a nasal fracture induced rabbit model, with animal ethical clearance. Histological analysis was thus undertaken to prove the bone healing properties of the 3D bioprinted scaffold.

5.2. Materials and Methods

5.2.1 Materials

PEG (Mw 4000), stannous octoate, 92.5%; pluronic F-127; poly(ethylene glycol) diacrylate; epsilon-caprolactone, 99%; petroleum ether, 90%; simvastatin (molecular weight: 418.57), 97% purity, Eagle's minimal essential medium (EMEM), fetal bovine serum, amphotericin B, gentamicin, trypsin/EDTA, MTT assay kit and MG-63 cell line, were procured from Sigma-Aldrich (St. Louis, MO, USA). Methanol, 99%; diethyl fumarate, 98%; diethyl ether (anhydrous); hydroquinone, 99% purity; methylene chloride; propylene glycol (1,2-propandiol); hydrochloric acid,1.85% $^{v}/_{v}$; sodium sulphate and zinc chloride were purchased from Merck (Pty) Ltd. All other reagents were of analytical grade and were employed as received. All reactions were undertaken under inert conditions. 12 New Zealand white rabbits were provided by the Central Animal Service (CAS), University of the Witwatersrand, South Africa. The study protocol was evaluated and approved by the Research Animal Ethics Committee (AESC no. 2017/11/75D).

5.2.2 Tailor Designed 3D Bioprinted Pseudo-bone Drug Delivery Scaffold

The 3D bioprinted scaffold was designed using Autodesk Inventor®, 3D computer-aided design (CAD), for precise fabrication prototyping, of the polymer based biomaterial. The scaffold was designed as a cylindrical implant, with a diameter of 4.5mm and a height of 3.3mm, to accommodate the specific dimension of surgical defect (5mm in diameter, induced with a fissure bur surgical apparatus). After generating the Stereolithography (STL) file on Inventor®, this file was imported to EnvisionTEC Visual Machines software, thereby converting to a Borland Package Library (BPL) file for bioprinting processing. Design of internal features and uniform slicing of the scaffold model was then undertaken, bioprinting a strand diameter of 500µm, and creating an inner structure pattern between layers at 30°. The scaffold was designed with a total number of 11 layers, with the height of each layer being 0.3mm (Table 5.1). A 3D Bioplotter® (EnvisionTEC GmbH, Gladbeck, Germany) was employed, using a pressure and temperature regulated syringe, with parameters optimized at 1.0 bar of pressure, speed at 1mm/s and syringe temperature regulated at 20°C. The temperature of the printing platform was maintained at 40°C. Pre-flow delay, post flow delay and time between layers were set as 0, 0 and 120sec respectively (Table 5.2). The low pressure and speed of printing, provided sufficient time for the structure to solidify, thereby promoting accuracy and scaffold platform building to occur. This technology allows development of any object to be printed, provided the appropriate uniform viscosity is maintained throughout. Figure 5.1 illustrates the CAD design for the tailored 3D printed scaffold model.

Table 5.1: Design dimensions of the 3D bioprinted pseudo-bone scaffold using Autodesk Inventor® of the polymer based material.

Design Parameters	Dimensions
Diameter	4.5mm
Height	3.3mm
Strand diameter	500µm
Inner structure pattern between layers	30°
Total number of layers	11
Height of each layer	0.3mm

Table 5.2: 3D Printing parameters of the tailor designed pseudo-bone drug delivery scaffold employing the 3D Bioplotter®.

Printing Parameters	Dimensions
Printing pressure	1.0 bar
Printing speed	1mm/s
Syringe temperature	20°C
Temperature of printing platform	40°C
Transfer height	5mm
Pre-flow delay time between layers	0 sec
Post-flow delay time between layers	120 sec

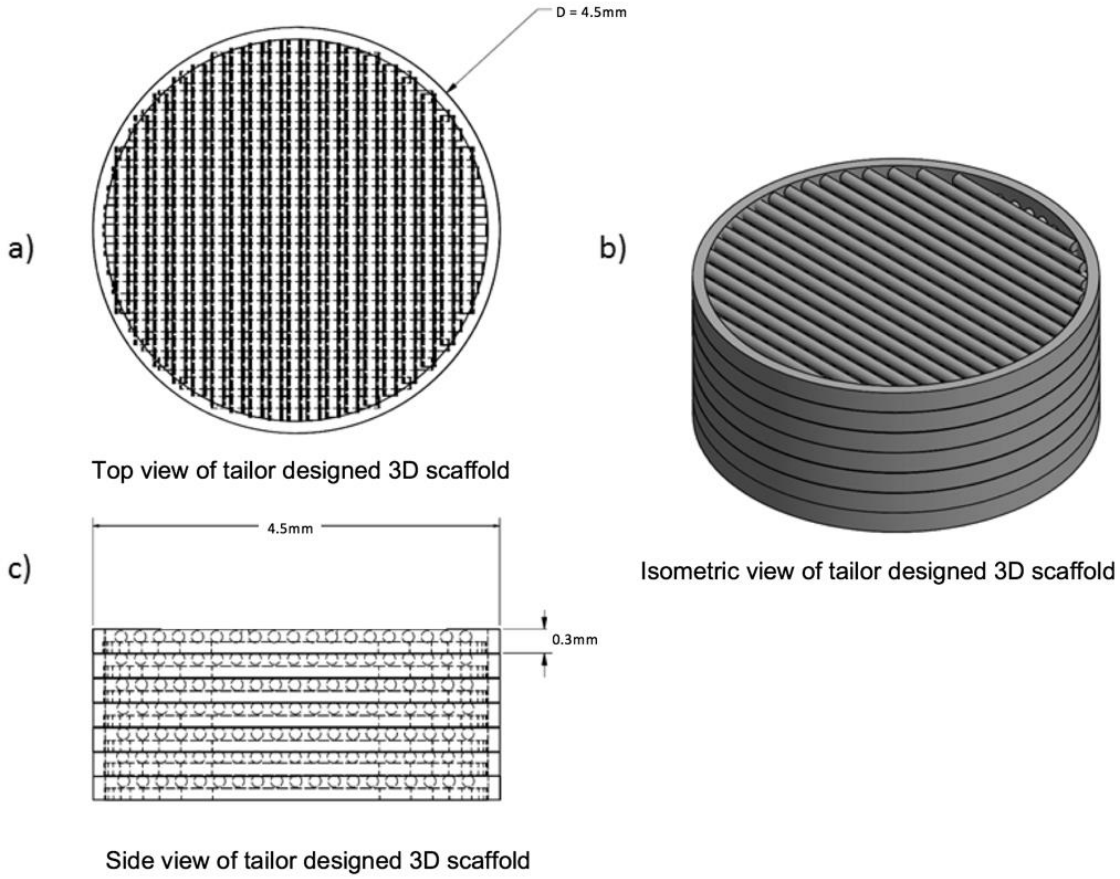


Figure 5.1: CAD specification design of the tailor 3D bioprinted scaffold, for implantation in an induced nasal bone fracture rabbit model.

5.2.3. Biomaterial Testing Undertaken on the Tailor Designed 3D bioprinted Scaffold

The tailor designed 3D bioprinted pseudo-bone scaffold was evaluated for its tensile modulus using a BioTester 5000 test system (CellScale Biomaterials Testing, Waterloo, Ontario), employing the BioRake tines of 1.7mm tine spacing, 305µm tine diameter and 1.9mm puncture depth. The strain properties of the 3D bioprinted scaffold was exposed to biaxial stretching, using the BioRakes on the Y-axis and 2500µm apart. A load cell of 10N was applied during the analysis, considering peak forces of abduction, internal rotation, peak torque, internal compressive forces, superior, posterior and peak 3D vector forces of internal rotation that could possibly be experienced by the implant *in situ*. Image tracking quantified in-plane motions as well as direct measure of resulting strains were analysed. Stress was evaluated as the force applied per unit area, and strain as the deformation experienced due to the stress (Kondiah, et al., 2017). The sample was analysed in simulated body fluid (SBF) at 37.5°C, with parameters used for the displacement test included, applying a stretch magnitude of 10% for 60 seconds, repeated for 3 cycles.

5.2.4 *In Vitro* Cell Culture Studies Undertaken on the Tailor Designed 3D Bioprinted Drug Delivery Scaffold and *In Vitro* Biodegradation Analysis

Human osteoblast-like cells (MG63) were used for cell culture studies. Although MG63 are osteosarcoma derived, they display typical characteristics of human osteoblast precursors or differentiated osteoblasts. In particular, MG63 produce type I collagen, osteocalcin (OC) and ALP, an enzyme crucial for bone matrix calcification (Su, et al., 2014). Cells were maintained in EMEM and supplemented with 10% fetal bovine serum, 200 µl/mL amphotericin B and 200 µl/mL gentamicin in an atmosphere of 5% CO_2 at 37 °C. Sub-cultivation was performed every 48 hours. The 3D bioprinted scaffold was weighed (W_0) after printing and immersed in 20 mL of 1 mg/mL lysozyme (hen egg white lysozyme) solution prepared in pH 7.4 phosphate buffer solution (PBS). This was incubated at body temperature conditions in an orbital shaker bath for 10, 20 and 30 days respectively. The 3D scaffolds were then removed from lysozyme-PBS at specified day intervals, freeze dried to completely remove moisture, and weighed accordingly (W_1). At regular intervals, the degradation solution was also changed, to depict *in situ* conditions. The percentage degradation of the 3D printed scaffold was calculated using the following equation. All experiments were undertaken in triplicate.

$$\text{Degradation weight } (\%) = \frac{W0-W1}{W0} \times 100 \quad \text{[Equation 5.1]}$$

5.2.4.1. *In Vitro* Cell Proliferation on the Tailor Designed 3D Bioprinted Drug Delivery Scaffold

The 3D bioprinted pseudo-bone scaffolds were sterilized with 70% ($^{v}/_{v}$) ethanol before cell seeding overnight at room temperature in a laminar flow cabinet. Thereafter, ethanol was removed and scaffolds were washed thrice with PBS. Scaffolds were then nourished with cell culture medium at 37 °C for 2 h. 50000 cell/well were seeded on scaffolds (1 × 1cm) with 20 µL inoculation volume and incubated for 4 h without medium to obtain cell attachment on scaffold surface. During proliferation studies, scaffolds were incubated at 37 °C/5% CO_2 with 500 µL medium in 3 different sets of 24 well plates, with a ratio of sample to control of 3: 4. The medium was changed twice a week. After 10, 20 and 30 days, methyl thiazolyl tetrazolium (MTT) assay was used for cytotoxic evaluation. Cell viability was calculated using equation 5.2:

$$\% \text{ Cell Viability} = \frac{Average\ absorbance\ value\ of\ sample}{Average\ absorbance\ value\ of\ control}\ X\ 100 \quad \text{[Equation 5.2]}$$

In addition, MG63 cells incubated on scaffolds were analysed by SEM using a FEI ESEM Quanta 400F (FEITM, Hillsboro, OR, USA) electron microscope, with an electron acceleration charge of 20kV, producing high resolution images of the cell seeded 3D bioprinted scaffold.

5.2.5. *In Vivo* Evaluation of the Tailor Designed 3D Bioprinted Drug Delivery Scaffold Employing a New Zealand White Rabbit Model

Twelve New Zealand white rabbits (2.5-3.0 kg) were used in this study consisting of 2 groups. Group 1 comprised of 6 rabbits, were treated with the tailor designed 3D bioprinted scaffold loaded with simvastatin drug. Group 2 also consisting of 6 rabbits, were treated with the tailor designed 3D bioprinted scaffold, with no simvastatin drug. Both groups were divided into 2 observation periods; 2 and 4 weeks post implantation, which were euthanized thereafter.

All surgical procedures were performed under sterile conditions. First, rabbits were anesthetized with ketamine hydrochloride (50 mg/kg) injected into the lateral ear vein. Thereafter, the nasal bone was shaved. 1.8 mL of 2% lidocaine containing 1:80 000 epinephrine was administered into

the operating site. Through a perpendicular incision, both the nasal bone and nasoincisal suture line were exposed. 2 nasal bone windows were outlined using a fissure bur. A surgical defect of 5 mm in diameter was made with a fissure bur using continuous saline irrigation. Caution was taken to avoid damage and to protect the nasal membrane (Alam, et al., 2009). Two bone defects, 1 experimental and 1 control, were created per rabbit as seen in Figure 5.2. The 3D bioprinted pseudo-bone scaffold was then implanted into right nasal bone defect of the rabbit and the left nasal bone defect was used as a control. No scaffold was implanted into the control. The bone defect described in this study is defined as a critical sized defect, with the size reported to prevent spontaneous repair of the bone.

5.2.6. Immunohistochemistry Evaluation of the Induced Nasal Bone Fracture Samples, Following *In Vivo* Evaluation

Rabbits were euthanized at weeks 2 and 4 post surgery. The nasal bone samples were fixed with 10% buffered formaldehyde at 4 °C for 24 hours. The samples were then demineralized with 14% EDTA for 4 weeks. Thereafter, the samples were dehydrated with ethanol, cleared in xylene, and placed in paraffin. 5 micrometer sections of the samples were sliced and mounted on gelatin-coated glass slides. The prepared sections were treated with hematoxylin and eosin (HE). Thereafter, for cell permeabilization, they were sequentially treated with 0.3% Tween 20 in phosphate-buffered saline (PBS) for 1 hour, and afterwards, to inhibit intrinsic peroxide activity, were treated with 0.3% hydrogen peroxide in methanol for 10 minutes. Following washing with PBS, the sites of the immunoreactions were envisioned by incubating the sections consecutively with biotinylated anti-rabbit IgG antibody at 1:200 dilutions for 1 hour, horseradish peroxidase–conjugated streptavidin at 1:300 dilutions for 1 hour, and 0.01% diaminobenzidine tetrahydrochloride in the presence of 0.02% hydrogen peroxide in 50 mmol/L Tris-HCL (pH 7.5) for 10 minutes. The sections counterstained with hematoxylin were detected under an Olympus BX 50 microscope (Olympus, Tokyo, Japan). The samples were then dehydrated in alcohol and mounted for light microscopy. This was undertaken to determine the number of active positively stained cells in the regeneration area. The evaluation site was preferred by the centre of the fracture site. In this area, the number of stained cells per 1000 cells was counted using high-magnification photomicrography (×100) (Alam, et al., 2009).

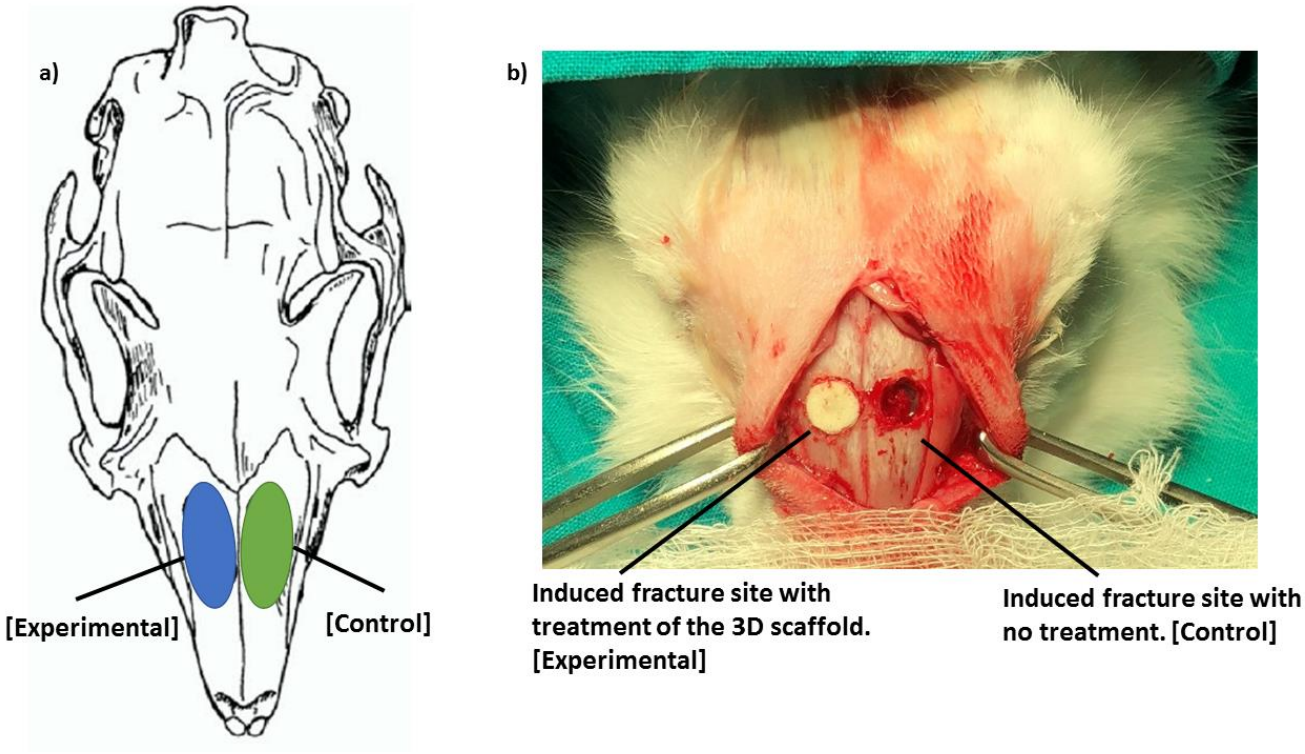


Figure 5.2: Diagram illustrating the superior view of rabbit skull, with induced surgical bone defects. a) represents a rabbit skull diagram of the induced surgical procedure undertaken on the rabbit nasal bone; b) representing the actual surgical procedure undertaken on the rabbit model, reflecting the implantation of the scaffold on the right of the nasal bone defect and left reflecting the control.

5.3. Results and Discussion

5.3.1 Physicomechanical Analysis Undertaken on the Tailor Designed 3D Bioprinted Scaffold

The 3D bioprinted scaffold was evaluated for its mechanical resistance using image tracking, calculating spatial variations of strains subjected to the bioprinted scaffold. Figure 5.3 illustrates a series of tracking images and x-y forces on the scaffold, representing the percentage strain experienced on the scaffold, while evaluating the sample at a force of 10N in SBF conditions. Due to the porous nature of the 3D bioprinted scaffold, the strain distribution experienced by the scaffold ranged up to 13.2% over 60sec. This response was due to the scaffold being tested by immersing in SBF. The structure still maintained its durable compact morphology, experiencing great elastic characteristics when exposed to SBF.

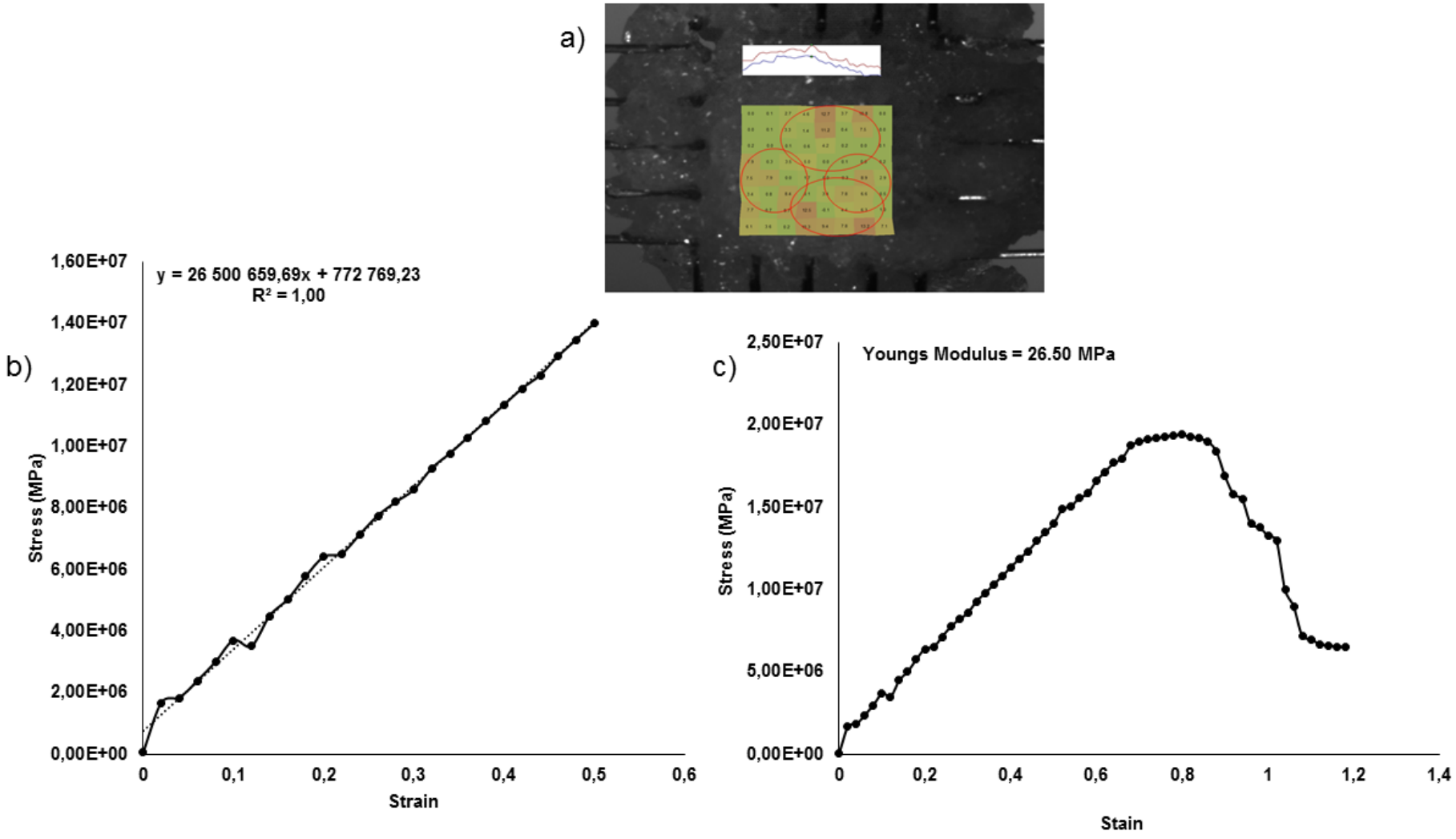


Figure 5.3: Physicomechanical testing analysis undertaken on the tailor designed 3D bioprinted scaffold, illustrating a) tracking and x-y forces experienced on the scaffold (red rings representing even force distribution experienced on the scaffold under tensile conditions); b) stress-strain graph depicting the linear regression of Young's modulus; c) illustrating complete region of evaluation of stress and strain experienced on the scaffold.

Matrix hardness is the force required to deform scaffold matrices in the presence of an external pressure, while deformation energy is the energy required to withstand the forces within the matrices. Analysis of the physicomechanical strength is employed to indicate the stability of the matrices and their ability to withstand applied pressure, which a bone scaffold would ultimately encounter *in vivo*. A harder and more resilient matrix, indicates a more compact substance which is likely to have higher Young's modulus. The hardness of the scaffold is also influenced by the inherent properties of the polymers employed in the formulation of the scaffold. The pseudo-bone copolymer was easily introduced into the body in a less invasive manner due to its physico-mechanical durability and biocompatible nature, consequently resulting in controlled drug release of simvastatin. The stress–strain curve highlighted the elastic behaviour of the scaffold. The Young's modulus (representative of material stiffness) of the bioprinted scaffold was calculated from the linear elastic portion (Figure 5.3b) of the stress–strain curve generated from the average forces and displacements in both x and y-directions, and was determined to be 26,5 MPa. The bioprinted scaffold exhibited the linear elastic behaviour recommended for bone tissue engineering, and the Young's modulus attained is within values reported for hybrid and nanobiocomposite bone tissue engineering systems (1–30 MPa), highlighting that the scaffold, in its current form, possesses the mechanical capabilities for certain bone tissue engineering applications (e.g., cancellous bone repair). Further resulted strengthening of the bioprinted scaffold was achieved by the presence of PPF, resulting in greater biomechanical and bone adhesion properties.

5.3.2 *In Vitro* Cell Culture Studies Undertaken on the Tailor Designed 3D Bioprinted Drug Delivery Scaffold and *In Vitro* Biodegradation Analysis

MTT assay for evaluating cell viability over 30 days, demonstrated a positive cell density after cell seeding occurred. Over the initial 10-day cell culture period, cells proliferated progressively, being attributed to the gradual degradation and fluid uptake nature of the 3D scaffold. The designed 3D porous architecture of the scaffold, further promoted cell adhesion and proliferation, which was clearly observed at day-20 of cell culture evaluation. During this period, it was detected that the 3D scaffold remained as a 47% mass formulation, allowing greater cell growth to occur as the scaffold gradually generated a further cell aided microenvironment for proliferation, as seen in Figure 5.4. Biodegradation analysis of the 3D bioprinted scaffolds reflected a gradual loss in polymer mass, with an initial 18% loss with 10 days of evaluation. It was also reflected that the

scaffold maintained its circular morphology throughout the degradation process, with at least over half of the mass degraded within 20 days. Thus at day-20, cells demonstrated substantial cell growth, allowing more nutrient media to come in contact with differentiating cells.

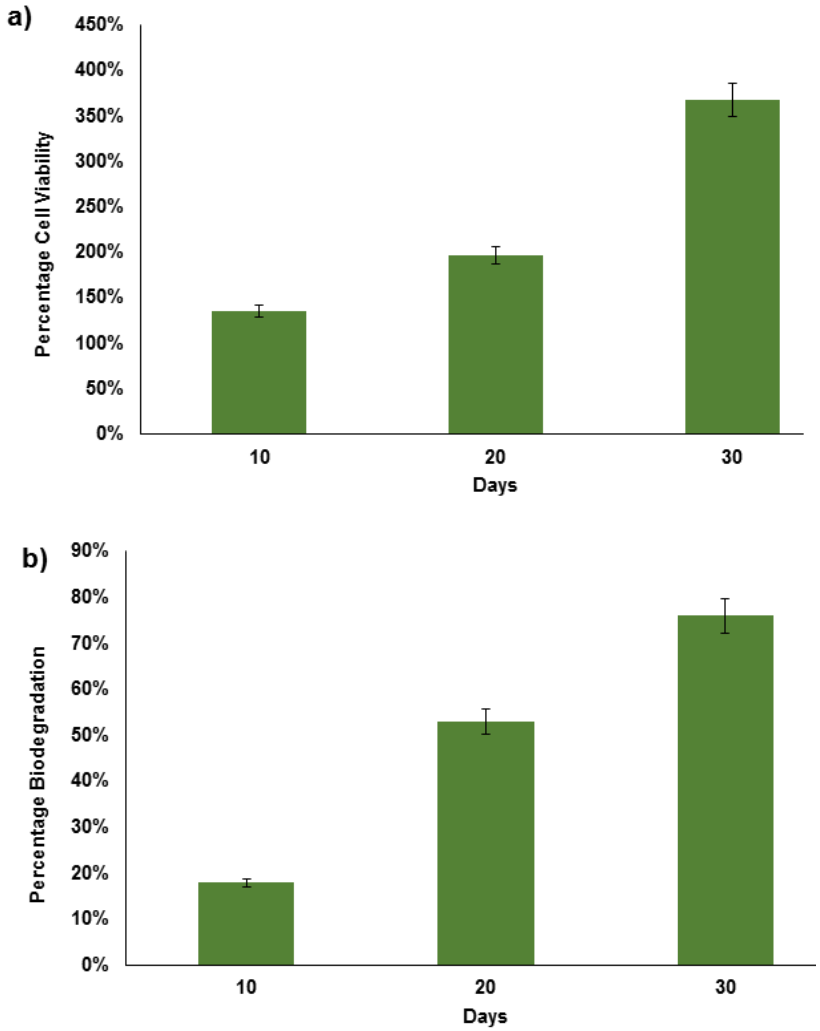


Figure 5.4: Representation of a) cell viability analysis using MG63 cells, seeded on the 3D bioprinted scaffold, evaluated over 30 days; b) biodegradation analysis of the scaffold undertaken over a 30-day period.

It was noted that as initial mass was lost, the scaffold increased in cell proliferation. This can be seen in SEM images captured on respective days (0, 10, 20 and 30). As seen in Figure 5.5, cell morphology seeded on the scaffold was evaluated at each time interval. At day 10, SEM confirmed cell growth attachment within micro pore spaces of the 3D printed filaments. This further confirmed a uniform distribution of cells throughout the 3D printed scaffold, demonstrating bioadhesion and cell proliferation. Over days 20 and 30 respectively, cells were clearly seen to

have spread with greater density of the 3D surface area, observing filopodias extending around the entire scaffold architecture and attached 3-dimensionally to the scaffold. At day-30, it was clearly observed that cells utilized the larger surface area of the scaffold, reaching confluence and covering almost the entire surface of the scaffold. Thus SEM analysis fully supported cell proliferation and viability analysis. By the end of day 30, almost 76% of the scaffold had been degraded (Figure 5.4b), further correlating to greater cell viability observed within the 3D scaffold matrix (Figure 5.4a). Thus the 3D printed scaffold demonstrated superior properties for cells to adhere and proliferate, confirming the non-cytotoxic nature of the 3D bioprinted scaffold.

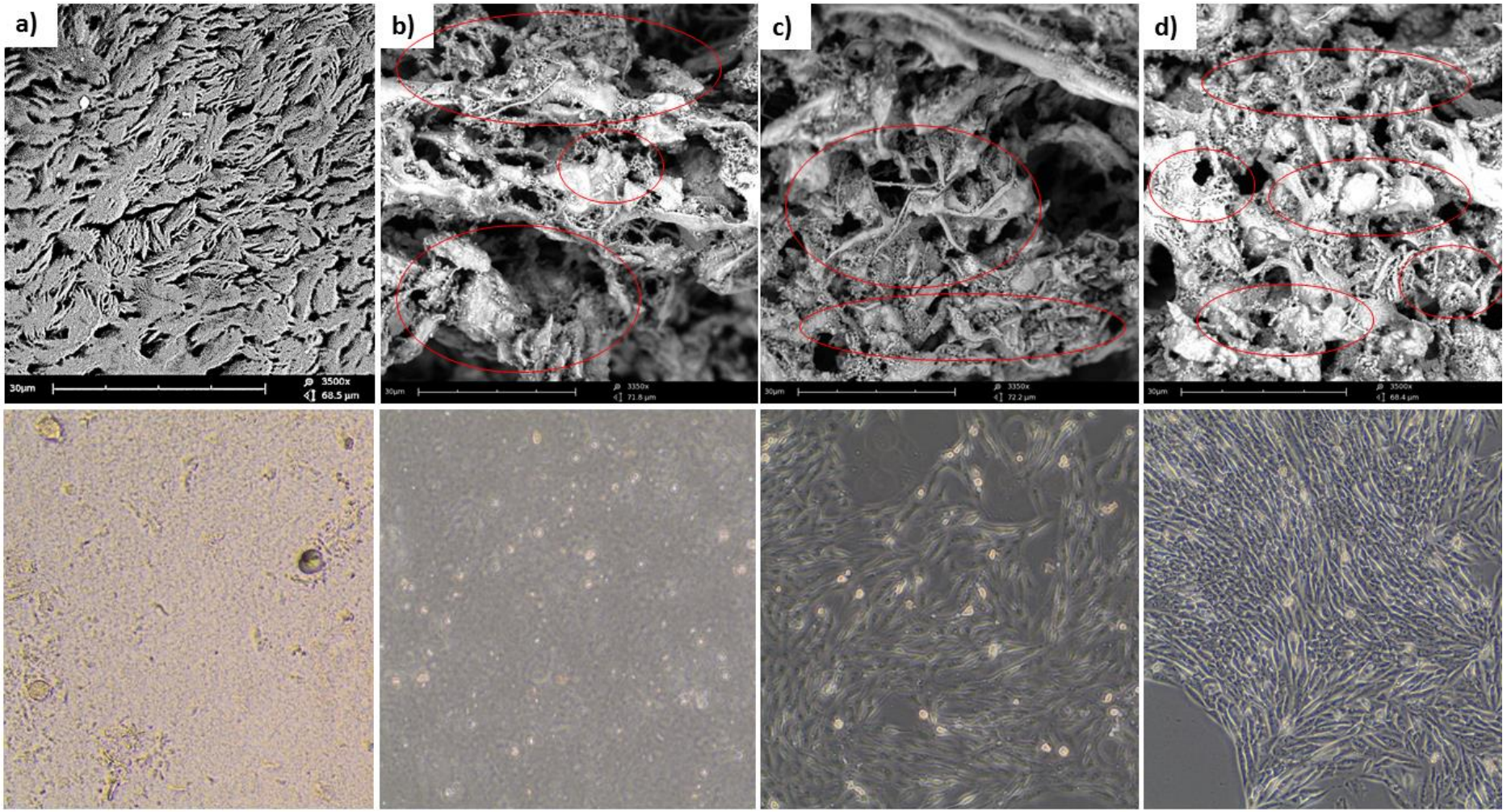


Figure 5.5: SEM (3350-3500X magnification) and light microscope (10X magnification) images reflecting cell seeding on the 3D bioprinted scaffold, captured on respective days; a) day-0, b) day-10, c) day-20 and d) day-30. As seen in the above figure, cell proliferation within the scaffold clearly increasing over day-0 to day-30, with exponential cell growth over time.

5.3.3 *In Vivo* Evaluation of the Tailor Designed 3D Bioprinted Drug Delivery Scaffold Employing a New Zealand White Rabbit Model

All rabbits in the study were evaluated histologically as well as using X-ray evaluation to determine the rate of bone healing and regeneration. All rabbits were X-rayed before and after fracture inducement, as well as after 2 and 4 weeks respectively, with treatment of the statin loaded and unloaded 3D bioprinted scaffold. All samples were evaluated at the site of nasal cortical bone defects. Each rabbit nasal defect in the study, simultaneously constituted a control and experimental segment, as seen in Figure 5.2. Figure 5.6 illustrates X-ray images of the rabbit model after nasal bone fracture, reflecting a faster rate of bone healing and regeneration using the statin-loaded 3D bioprinted scaffold. It was also eminent that noticeable bone healing and regeneration was observed by veterinary surgeons in the non-statin-loaded 3D bioprinted scaffold. This can be attributed to the bone regenerative properties of the copolymers employed. It was clearly identified after 2 weeks of nasal fracture inducement, that the fracture sites treated with the statin-loaded 3D bioprinted scaffold, demonstrated greater healing than the non-statin loaded 3D bioprinted scaffold.

In comparison to the control defect where no treatment was administered, it was clearly detected that a faster rate of bone healing and regeneration occurred by administration of the 3D bioprinted scaffold. This result was supported both by X-ray and histological analysis. Our studies further prove statins bone healing properties, as observed in X-ray images illustrated below.

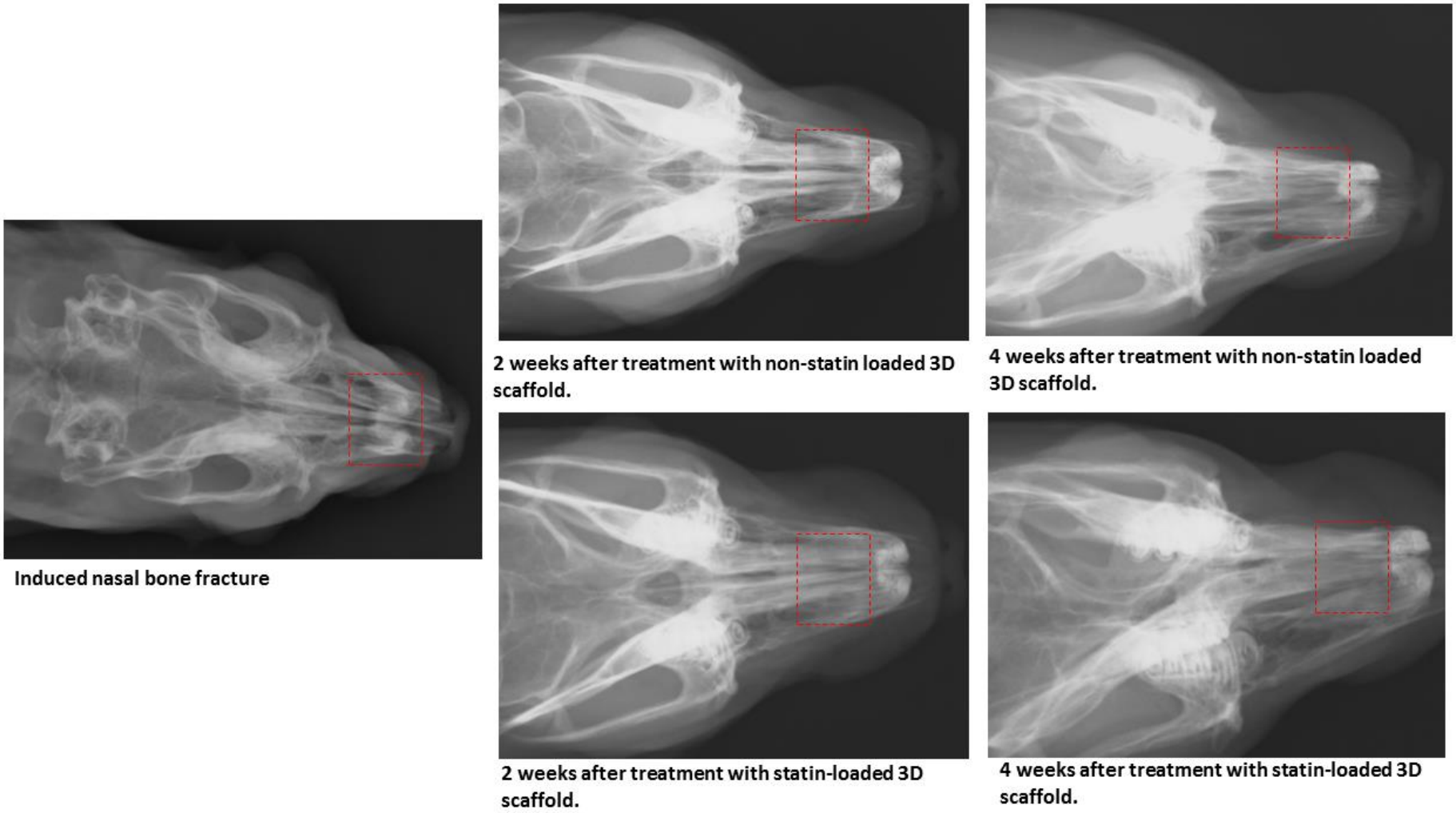


Figure 5.6: X-ray images reflecting nasal bone defects by surgical inducement. It was observed that the statin-loaded 3D bioprinted scaffold displayed greater bone regenerative properties after 4 weeks of the study than the non-statin loaded 3D bioprinted scaffold. However, significant bone regeneration and healing was observed in the non-statin loaded 3D bioprinted scaffold in comparison to the control, attributed to the copolymeric nature of the 3D printed scaffold.

Evaluation of the nasal bone induced fracture observed after treatment of the statin-loaded 3D bioprinted scaffold after 4 weeks, resulted in sample area of focal nasal bone regeneration, with mild periosteal reaction typical of new bone formation and prominent osteoblastic activity (arrows) (Figure 5.7a). Mild subcutaneous fibrosis was also noted, with no active inflammation. The nasal mucosa was evaluated to be healthy after treatment with the 3D bioprinted simvastatin-loaded scaffold. A few areas of the sample displayed specular brown material (3D bioprinted scaffold) with surrounding epithelioid macrophages, with scattered lymphocytes and plasma cells. The regenerated bone tissue was found to be regular with a mild focus of moderate pyogranulomatous inflammation in the adjacent subcutis with multinucleated giant cells. New bone formation was noted also around the periphery of the defect with prominent osteoblastic activity (arrows).

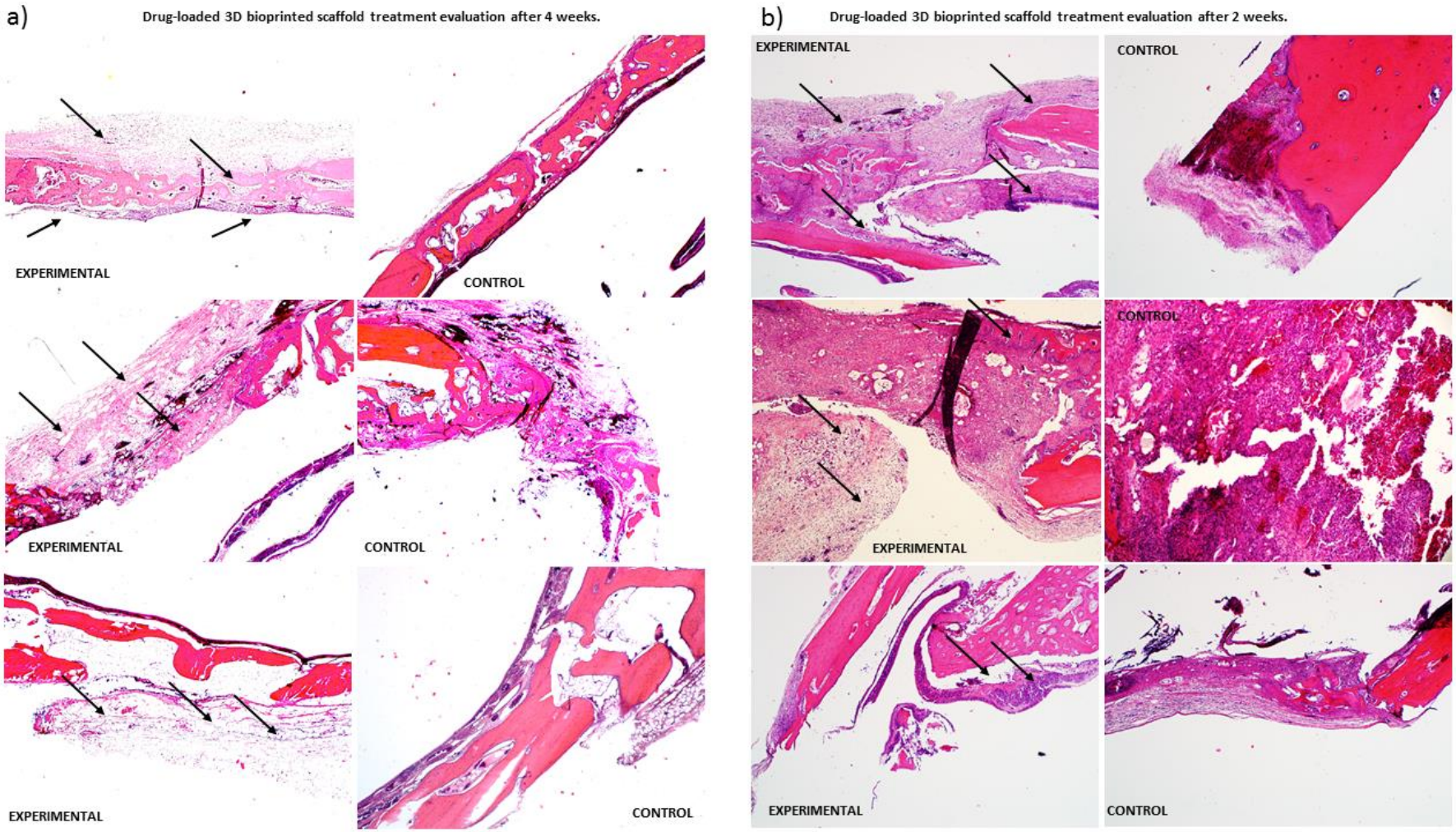
The control surface, induced with the defect and not treated with any delivery system, was found to display granulation tissue development and sever periosteal fibrosis. This was accompanied by mild to moderate inflammation with macrophages including multinucleated giant cells. The visible nasal mucosa was found to be normal with only mild submucosal lymphoplasmacytic infiltration noted. A focal area of mild subcutaneous fibrosis was also noted in the middle of the surface defect of the rabbit. Layers of adipose tissue build-up between layers of the bone surface was moderately observed.

Evaluation of the nasal bone induced fracture observed after treatment of the statin-loaded 3D bioprinted scaffold after 2 weeks resulted in sample areas of granulation tissue and accompanied by a mild periosteal reaction (Figure 5.7b). It was observed that multifocal areas with surrounding epithelioid macrophages and multinucleated giant cells were present in all tissue samples. Peripheral new bone formation was noted (arrows). There was also a moderate inflammatory reaction in the granulation tissue and overlying subcutis consisting of macrophages and occasional heterophils with clusters of perivascular lymphocytes and plasma cells. Histological samples also reflected newly formed bony trabeculae with prominent osteoblasts (arrows). Moderate periosteal reactions along with scattered multinucleated giant cells noted around small, necrotic bone fragments, with a few peripheral lymphocytes and plasma cells were observed. The control surface, induced with the defect and not treated with any delivery system was found to display a large focal defect in the nasal bone, present with granulation tissue and sever inflammation. A marked periosteal reaction was visible and there were multiple areas of epithelioid macrophages and multinucleated giant cells. Moderate infiltration by macrophages and heterophils was also noted in the defect, with moderate haemorrhage and few haemosiderin laden

macrophages. No significant new bone formation was noted. There were insignificant signs of bone proliferation observed in the control.

Evaluation of the nasal bone induced fracture observed after treatment of the non-statin-loaded 3D bioprinted scaffold after 4 weeks, reflected focal defects visible in the nasal bone, filled with granulation tissue (Figure 5.7c). There was also presence of necrotic bone with surrounding inflammation consisting of macrophages, including epithelioid macrophages and heterophils. Mild subcutaneous fibrosis and periosteal reactions were noted along with perivascular lymphocytes and plasma cells. New bone formation was noted on the periphery with osteoblastic activity (arrows). The control area displayed a focal defect, filled with granulation tissue. Necrotic bone fragments were noted in the nasal submucosa accompanied by scattered lymphocytes and plasma cells. Mild neovascularisation was noted and there was moderate congestion and neutrophilic leukostasis.

Evaluation of the nasal bone induced fracture observed after treatment of the non-statin-loaded 3D bioprinted scaffold after 2 weeks, reflected nasal bone tissue with marked periosteal fibrosis (Figure 5.7d). A large quantity of cartilage damage was visible in these samples. A focal area of prominent new bone formation (arrows) was noted with marked osteoblastic activity (arrows) and surrounding granulation tissue. Amorphous to spicular brown material (3D scaffold material) was noted and accompanied by surrounding macrophages and multinucleated giant cells. Necrotic bone fragments were noted with moderate surrounding lymphocytes, plasma cells and osteoblasts. The control reflected necrotic bone fragments and surrounding granulomatous inflammation in the adjacent subcutis with prominent multinucleated giant cells. Severe inflammatory reactions were noted in the control samples with central necrotic bone and surrounding multinucleated cells with macrophages as well as neutrophils.


a)
Drug-loaded 3D bioprinted scaffold treatment evaluation after 4 weeks.
EXPERIMENTAL
CONTROL
EXPERIMENTAL
CONTROL
EXPERIMENTAL
CONTROL
b)
Drug-loaded 3D bioprinted scaffold treatment evaluation after 2 weeks.
EXPERIMENTAL
CONTROL
EXPERIMENTAL
CONTROL
EXPERIMENTAL
CONTROL

Continued

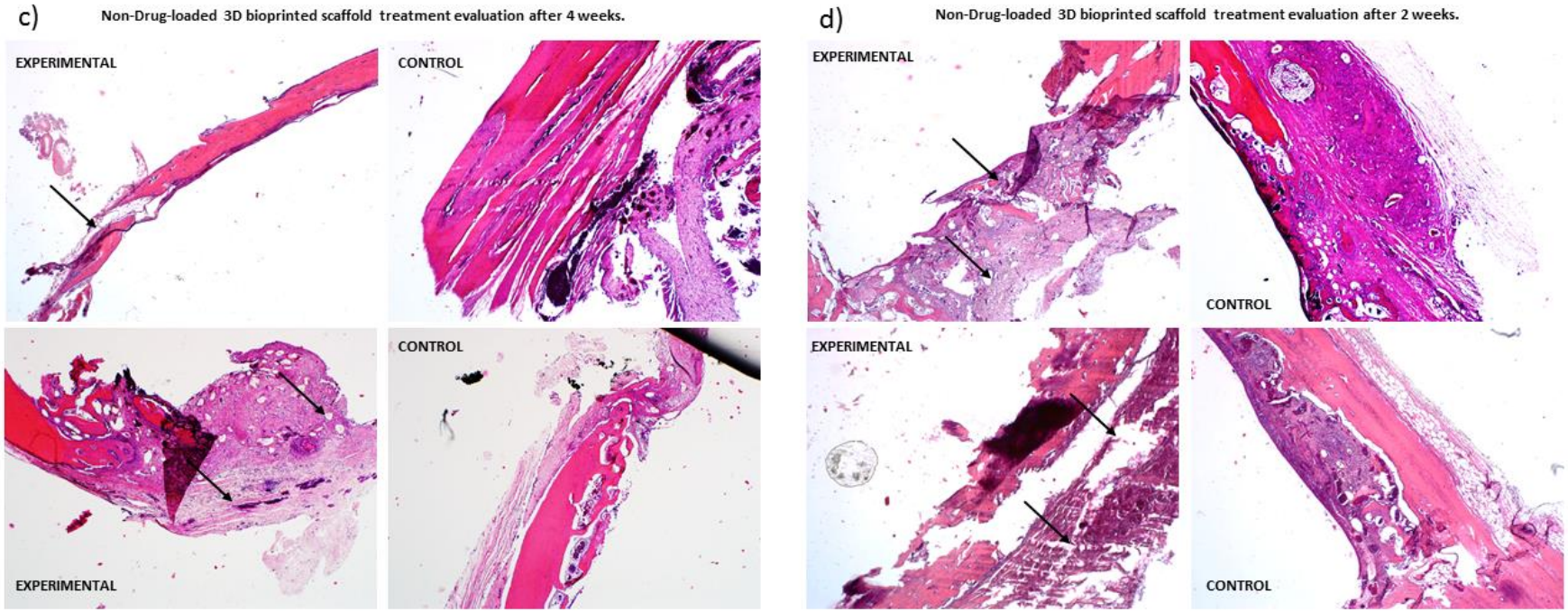


Figure 5.7: Histological evaluation of the nasal bone induced fracture after treatment with; a) 3D scaffold loaded with simvastatin after 4-week evaluation illustrating prominent osteoblastic activity (arrows) ; b) 3D scaffold loaded with simvastatin after 2-week evaluation with mild periosteal reactions and peripheral new bone formation (arrows); c) 3D scaffold loaded with no simvastatin after 4-week evaluation with new bone formation noted on the periphery with osteoblastic activity (arrows), d) 3D scaffold loaded with no simvastatin after 2-week evaluation reflecting osteoblastic activity and surrounding granulation tissue (arrows). All samples were evaluated using the control, as described in Figure 5.2.

It can be concluded that the nasal bones treated with the 3D bioprinted scaffold demonstrated greater evidence of healing and new bone formation, in comparison to the control, where healing appeared to be far less progressive. Treatment with simvastatin revealed substantial bone growth and proliferation, compared to unloaded simvastatin 3D bioprinted scaffolds, which displayed a slower rate of bone growth with greater inflammatory cells present. It was also determined that all control areas of nasal deformation displayed higher necrotic cell appearances, thus using the rabbit's natural immune cascade to fight off foreign body markers, with no supportive therapeutics. Results of bone healing and osteoblast activity was superior in the 3D bioprinted scaffold with simvastatin over 4 weeks, proving the concept of bone regeneration and healing.

5.4. Concluding Remarks

A tailor designed 3D bioprinted pseudo-bone drug delivery scaffold was designed for the purpose of bone healing and regeneration. The 3D bioprinted scaffold was evaluated for its physicomechanical, cell viability and *in vivo* potential to promote bone growth and healing. Due to the porous nature of the 3D bioprinted scaffold, the strain distribution experienced by the scaffold ranged up to 13.2% over 60sec, with a young's modulus of 26.5Mpa, ideal for bone implantable therapeutics. Over days 20 and 30 respectively, cells were clearly seen to have spread with greater density of the 3D scaffold surface area, observing filopodias extending around the entire scaffold architecture and attached 3-dimensionally to the scaffold. At day 30, it was clearly observed that cells utilized the larger surface area of the scaffold, reaching confluence and covering almost the entire surface of the 3D bioprinted scaffold. *In vivo* studies confirmed that the nasal bones, after being induced with a nasal fracture and treated with the 3D bioprinted scaffold, demonstrated greater evidence of healing, new bone formation and mild secondary inflammation, in comparison to the control, where healing appeared to be far less progressive. Treatment with simvastatin revealed substantial bone growth and proliferation, compared to unloaded simvastatin 3D bioprinted scaffolds which displayed a slower rate of bone growth with greater inflammatory cell markers present.

5.5. References

Alam, S.; Ueki, K.; Nakagawa, K.; Marukawa, K.; Hashiba, Y.; Yamamoto, E.; Sakulsak, N.; Iseki, S. Statin-Induced Bone Morphogenetic Protein (BMP) 2 Expression During Bone Regeneration:

An Immunohistochemical Study. *Oral Surgery, Oral Medicine, Oral Pathology, Oral Radiology, and Endodontology* 2009, *107*, 22-29.

Aljohani, W.; Ullah, M.; Zhang, X.; Yang, G. Bioprinting And Its Applications In Tissue Engineering And Regenerative Medicine. *International Journal of Biological Macromolecules*2018, *107*, 261-275.

Ashman, O.; Phillips, A. Treatment Of Non-Unions With Bone Defects: Which Option And Why?. *Injury* 2013, *44*, S43-S45.

Beger, B.; Blatt, S.; Pabst, A.; Hansen, T.; Goetz, H.; Al-Nawas, B.; Ziebart, T. Biofunctionalization Of Synthetic Bone Substitutes With Angiogenic Stem Cells: Influence On Regeneration Of Critical-Size Bone Defects In An In Vivo Murine Model. *Journal of Cranio-Maxillofacial Surgery* 2018, *46*, 1601-1608.

Brydone, A.; Meek, D.; Maclaine, S. Bone Grafting, Orthopaedic Biomaterials, And The Clinical Need For Bone Engineering. *Proceedings of the Institution of Mechanical Engineers, Part H: Journal of Engineering in Medicine* 2010, *224*, 1329-1343.

Curry, A.; Pensa, N.; Barlow, A.; Bellis, S. Taking Cues From The Extracellular Matrix To Design Bone-Mimetic Regenerative Scaffolds. *Matrix Biology* 2016, *52-54*, 397-412.

Elsalanty, M.; Genecov, D. Bone Grafts In Craniofacial Surgery. *Craniomaxillofacial Trauma and Reconstruction* 2009, *2*, 125-134.

Gruskin, E.; Doll, B.; Futrell, F.; Schmitz, J.; Hollinger, J. Demineralized Bone Matrix In Bone Repair: History And Use. *Advanced Drug Delivery Reviews* 2012, *64*, 1063-1077.

He, B.; Zhao, J.; Ou, Y.; Jiang, D. Biofunctionalized Peptide Nanofiber-Based Composite Scaffolds For Bone Regeneration. *Materials Science and Engineering: C* 2018, *90*, 728-738.

Kondiah, P.; Choonara, Y.; Kondiah, P.; Kumar, P.; Marimuthu, T.; du Toit, L.; Pillay, V. Development Of An Injectable Pseudo-Bone Thermo-Gel For Application In Small Bone Fractures. *International Journal of Pharmaceutics* 2017, *520*, 39-48.

Li, Z.; Jia, S.; Xiong, Z.; Long, Q.; Yan, S.; Hao, F.; Liu, J.; Yuan, Z. 3D-Printed Scaffolds With Calcified Layer For Osteochondral Tissue Engineering. *Journal of Bioscience and Bioengineering* 2018, *126*, 389-396.

Luo, Y.; Li, Y.; Qin, X.; Wa, Q. 3D Printing Of Concentrated Alginate/Gelatin Scaffolds With Homogeneous Nano Apatite Coating For Bone Tissue Engineering. *Materials & Design*2018, *146*, 12-19.

Martin, V.; Bettencourt, A. Bone Regeneration: Biomaterials As Local Delivery Systems With Improved Osteoinductive Properties. *Materials Science and Engineering: C* 2018, *82*, 363-371.

Moraschini, V.; Almeida, D.; Calasans-Maia, J.; Diuana Calasans-Maia, M. The Ability Of Topical And Systemic Statins To Increase Osteogenesis Around Dental Implants: A Systematic Review Of Histomorphometric Outcomes In Animal Studies. *International Journal of Oral and Maxillofacial Surgery* 2018, *47*, 1070-1078.

Roseti, L.; Parisi, V.; Petretta, M.; Cavallo, C.; Desando, G.; Bartolotti, I.; Grigolo, B. Scaffolds For Bone Tissue Engineering: State Of The Art And New Perspectives. *Materials Science and Engineering: C* 2017, *78*, 1246-1262.

Saletta, J.; Garcia, J.; Caramês, J.; Schliephake, H.; da Silva Marques, D. Quality Assessment Of Systematic Reviews On Vertical Bone Regeneration. *International Journal of Oral and Maxillofacial Surgery* 2018.

Su, W.; Wang, Y.; Chou, C. Optimal Fluid Flow Enhanced Mineralization Of MG-63 Cells In Porous Chitosan Scaffold. *Journal of the Taiwan Institute of Chemical Engineers* 2014, *45*, 1111-1118.

Thaller, P.; Fürmetz, J.; Wolf, F.; Eilers, T.; Mutschler, W. Limb Lengthening With Fully Implantable Magnetically Actuated Mechanical Nails (PHENIX®)—Preliminary Results. *Injury* 2014, *45*, S60-S65.

Turnbull, G.; Clarke, J.; Picard, F.; Riches, P.; Jia, L.; Han, F.; Li, B.; Shu, W. 3D Bioactive Composite Scaffolds For Bone Tissue Engineering. *Bioactive Materials* 2018, *3*, 278-314.

Wang, W.; Yeung, K. Bone Grafts And Biomaterials Substitutes For Bone Defect Repair: A Review. *Bioactive Materials* 2017, *2*, 224-247.

Xia, Y.; Sun, J.; Zhao, L.; Zhang, F.; Liang, X.; Guo, Y.; Weir, M.; Reynolds, M.; Gu, N.; Xu, H. Magnetic Field And Nano-Scaffolds With Stem Cells To Enhance Bone Regeneration. *Biomaterials* 2018, *183*, 151-170.

Xie, R.; Hu, J.; Hoffmann, O.; Zhang, Y.; Ng, F.; Qin, T.; Guo, X. Self-Fitting Shape Memory Polymer Foam Inducing Bone Regeneration: A Rabbit Femoral Defect Study. *Biochimica et Biophysica Acta (BBA) - General Subjects* 2018, *1862*, 936-945.

CHAPTER 6
CONCLUSION AND FUTURE RECOMMENDATIONS

6.1 Conclusion

The study of novel 3D bioprinted scaffolds encompasses a great deal of innovative research, striving for significant bone healing and repair, displaying an unprecedented potential for a new era of 3D printed scaffolds in the field of bone tissue engineering. A 3D bioprinted pseudo-bone drug delivery scaffold was developed to exhibit the morphology, matrix hardness as well as the matrix resilience of healthy human bone. The 3D bioprinted scaffold was designed using CAD software. MATLAB® software and ANN were used for optimization of the bioink formulation. Polypropylene fumarate (PPF), free radical polymerised polyethylene glycol- polycaprolactone (PEG-PCL-PEG) and pluronic (PF127) were utilized for developing the 3D bioprinted scaffold. Simvastatin was incorporated into the 3D bioprinted scaffolds to promote further bone healing and repair properties. The ANN-optimised 3D bioprinted scaffold displayed remarkable properties as a controlled release platform, exhibiting drug release over 20 days. The 3D bioprinted scaffold further exhibited formation of a pseudo-bone matrix using a human clavicle bone model, which was induced with a butterfly fracture. The strength of the pseudo-bone matrix was assessed to be as strong as original bone, having a 99% MH and 98% MR property, to healthy human clavicle bones.

Physicomechanical, cell viability studies using MG-63 cells and *in vivo* studies utilizing a rabbit model were also undertaken. A young's modulus of 26,5 Mpa and the strain distribution experienced by the scaffold ranged up to 13.2% over 60 sec owing to the porous nature of the 3D bioprinted scaffold. *In vivo* studies established that after the nasal bones were induced with a critical-sized bone defect, and treated with the 3D bioprinted scaffold, there was substantial bone healing and new bone formation. Treatment with simvastatin revealed considerable bone growth and proliferation, compared to unloaded simvastatin 3D printed scaffolds, which exhibited a slower rate of bone growth with greater inflammatory cells present. It can be concluded that the nasal bones treated with the 3D bioprinted scaffold demonstrated greater evidence of healing and new bone formation, in comparison to the control, where healing appeared to be far less progressive.

6.2 Future Outlook and Recommendations

A great emphasis has been given to the development of tough and durable 3D printed scaffolds which will be able to sustain loading *in vivo* for moderate and high load-bearing applications, although the mechanical design requirements for bioresorbable scaffolds differ considerably depending on the functional requirements of the bone it is replacing. Natural bone obtains its distinctive amalgamation of mechanical properties from an architectural design that extends from nanoscale to macroscopic dimensions, with accurately and carefully engineered interfaces. The bone's fracture resistance stems from toughening mechanisms at these dimensions. The smallest length-scales determine the bone's intrinsic fracture resistance by encouraging plasticity as well as impacting on bone strength. The larger-scales extrinsically strengthen bone by protecting the growing crack. Thus far, there are no synthetic biomaterials with such a structure. However, these unique mechanical properties could be achieved through combining mechanisms acting at various length scales.

Much has been done to manipulate the mechanical properties, such as strength, toughness and stiffness, of 3D printed scaffolds through inventing hydrogels and nanostructures, e.g., nanoparticles or nanofibre reinforcements in polymer matrices, to imitate the bone's natural makeup. It was established that Synthetic whitlockite (WH: $Ca_{18}Mg_2(HPO_4)_2(PO_4)_{12}$) nanoparticles can recapitulate early-stage of bone regeneration. This can be achieved by prohibiting osteoclast activity, stimulating osteogenic differentiation, and transforming into mechanically enhanced hydroxyapatite (HAP)-neo bone tissues by the continuous supply of PO_{34} and Mg_2þ under physiological conditions. Based on structural analysis, the dynamic phase transformation from WH to HAP contributed as a crucial factor for bone regeneration. Nevertheless, it was noted that although the incorporation of hydrogel and nanoscale reinforcement increases the strength, the toughness drops drastically. Therefore, the formulation of stronger and tougher 3 D printed scaffold constituents entails the combination of a hierarchical design incorporating many length-scales to produce strength, i.e., to mimic composite deformation of hydrogels and nanocrystals of hyaluronic acid and collagen, together with the micro-level structures to produce toughness, e.g., to mimic osteons and cement lines.

3D printed scaffolds could play a more active role in the regeneration process of bone, which need many biological events in which growth factors supply signals to initiate healing. Bone development *in vivo* particularly involves the release of chemicals, such as growth factors, at

crucial time points to trigger osteoinduction and thus bone regeneration could be markedly increased by the confined delivery of suitable growth factors, such as TGF-β, BMPs, IGF, or FGF. Drug release spatio-temporal profiles could be formulated to resemble signaling *in vivo* if the signaling for osteoinduction could be specified. The four fundamental questions that should direct the design of chemical release tools are: what to release, when, where and how much.

Another drug delivery alternative is the utilization of polymer-based 3D printed scaffolds with various chemicals contained within the polymer. The use of glass-based scaffolds, e.g., Bioglass®, for sustained release of ions is an appealing modification of this approach. Bioactive glass can chemically bond to bone, whilst degrading in the body in a very controlled fashion. Many bioactive glasses have been formulated with various degradation rates while targeting multiple applications, as the glass composition can be effortlessly altered and several different ions could be integrated. Examples of these include implant coatings, 3D printed scaffold fabrication and bone fillers. The release of Si from bioactive glasses could be advantageous. The release of other ions from the glass *in vivo* could be employed to assist in angiogenesis, e.g., Cu^{2+}, as well as differentiation towards osteoblastic lineages, e.g., Sr. Various glass constituents could be used to manipulate the release rates.

Research was carried out on novel polyvinyl alcohol-bioglass $45S_5$ based composite nanofibrous membranes as bone scaffolds. Composite nanofibrous membranes based on sol-gel derived bioglass (BG) and magnetic bioglass (MBG) blended with polyvinyl alcohol (PVA), were electrospun and evaluated. These membranes were amorphous in structure with negligible crystalline precipitates. These membranes possessed a biodegradable nature. The composites displayed increased tensile strength, greater proliferation of human osteosarcoma MG63 cells and increased alkaline phosphatase enzyme activity than the bare PVA membrane. It was thus proved that these composites possessed substantial potential in bone tissue engineering. Nonetheless, the effect of pH changes prompted by the degradation of glass, the ideal release rates, as well as the role of glass surface roughness should be studied systematically.

In summary, new design concepts and formulation approaches are desperately required to produce novel 3D printed scaffolds for bone regeneration and repair. Specifically, more research is needed in the field of bone tissue engineering to discover the relationships that connect composition and material architecture at multiple-length scales with macroscopic mechanical behavior and the potential for osteogenesis. The results of this research could be utilized to

fabricate new systems that have the capability to manipulate chemistry and cellular responses. This knowledge will also serve to conduct systematic studies on surface roughness and drug delivery profiles. The great possibilities opened by the increasing emphasis on hydrogels and nanotechnology in the field of bone tissue engineering now permit the modification of 3D printed scaffold chemistry with a revolutionary degree of control. The physicochemical environment could be monitored and manipulated to observe the key cellular events at the molecular level. The results of such bone tissue engineering could create an ideal bone scaffold that could be used in the treatment of bone defects. The goal is to produce “active” 3D printed scaffolds that are explicitly fabricated for bone regeneration that will provisionally substitute for natural tissues, while interacting with their surroundings, responding to environmental changes, as well as actively direct cellular events. These scaffolds will combine with bone tissue while they are actively absorbed, with controlled osteogenic activity, which will take advantage of the biological principles of bone repair and regeneration. As a result, these capabilities will produce faster bone formation, increased healing time and speedy recovery to function.

7. Appendices

7.1. Animal Ethics Clearance Certificate



STRICTLY CONFIDENTIAL

ANIMAL ETHICS SCREENING COMMITTEE (AESC)

CLEARANCE CERTIFICATE NO. 2017/11/75/D

APPLICANT: Ms P Kondiah

SCHOOL: Pharmacy and Pharmacology
DEPARTMENT:
LOCATION:

PROJECT TITLE: In vivo bone regeneration assessment of implantable 3D printed drug delivery scaffold in New Zealand White rabbits

Number and Species

24+1(for pilot study) Total=25X 1.5kg-2.5kg male and female White New Zealand rabbits

Approval was given for the use of animals for the project described above at an AESC meeting held on 2017/11/28. This approval remains valid until 2020/02/06.
Unreported changes to the application may invalidate the clearance given by the AESC
An annual progress report must be provided

The use of these animals is subject to AESC guidelines for the use and care of animals, is limited to the procedures described in the application form and is subject to any additional conditions listed below:

Signed: _____ (Chairperson, AESC) Date: 13th February 2018

I am satisfied that the persons listed in this application are competent to perform the procedures therein, in terms of Section 23 (1) (c) of the Veterinary and Para-Veterinary Professions Act (19 of 1982)

Signed: _____ (Registered Veterinarian) Date: 12 February 2018

cc: Supervisor: Professor V Pillay
Director: CAS

Works 2000/Iain0015/AESCCert.wps

7.2 International Published Review Paper

molecules

MDPI

Review

A Review of Injectable Polymeric Hydrogel Systems for Application in Bone Tissue Engineering

Pariksha J. Kondiah, Yahya E. Choonara, Pierre P. D. Kondiah, Thashree Marimuthu, Pradeep Kumar, Lisa C. du Toit and Viness Pillay *

Wits Advanced Drug Delivery Platform Research Unit, Department of Pharmacy and Pharmacology, School of Therapeutic Sciences, Faculty of Health Sciences, University of the Witwatersrand, Johannesburg, 7 York Road, Parktown 2193, South Africa; 549348@students.wits.ac.za (P.J.K.); yahya.choonara@wits.ac.za (Y.E.C.); pierre.kondiah@wits.ac.za (P.P.D.K.); thashree.marimuthu@wits.ac.za (T.M.); pradeep.kumar@wits.ac.za (P.K.); lisa.dutoit@wits.ac.za (L.C.d.T.)
* Correspondence: viness.pillay@wits.ac.za; Tel.: +27-11-717-2274

Academic Editor: Derek J. McPhee
Received: 19 September 2016; Accepted: 16 November 2016; Published: 21 November 2016

Abstract: Biodegradable, stimuli-responsive polymers are essential platforms in the field of drug delivery and injectable biomaterials for application of bone tissue engineering. Various thermo-responsive hydrogels display water-based homogenous properties to encapsulate, manipulate and transfer its contents to the surrounding tissue, in the least invasive manner. The success of bioengineered injectable tissue modified delivery systems depends significantly on their chemical, physical and biological properties. Irrespective of shape and defect geometry, injectable therapy has an unparalleled advantage in which intricate therapy sites can be effortlessly targeted with minimally invasive procedures. Using material testing, it was found that properties of stimuli-responsive hydrogel systems enhance cellular responses and cell distribution at any site prior to the transitional phase leading to gelation. The substantially hydrated nature allows significant simulation of the extracellular matrix (ECM), due to its similar structural properties. Significant current research strategies have been identified and reported to date by various institutions, with particular attention to thermo-responsive hydrogel delivery systems, and their pertinent focus for bone tissue engineering. Research on future perspective studies which have been proposed for evaluation, have also been reported in this review, directing considerable attention to the modification of delivering natural and synthetic polymers, to improve their biocompatibility and mechanical properties.

Keywords: biodegradable; thermo-responsive polymers; hydrogels; tissue engineering; drug delivery; stimuli-responsive

7.3 International Published Research Paper 1

International Journal of Pharmaceutics 520 (2017) 39–48

Contents lists available at ScienceDirect

International Journal of Pharmaceutics

journal homepage: www.elsevier.com/locate/ijpharm

Development of an injectable pseudo-bone thermo-gel for application in small bone fractures

Pariksha J. Kondiah, Yahya E. Choonara, Pierre P.D. Kondiah, Pradeep Kumar, Thashree Marimuthu, Lisa C. du Toit, Viness Pillay*

Wits Advanced Drug Delivery Platform Research Unit, Department of Pharmacy and Pharmacology, School of Therapeutic Sciences, Faculty of Health Sciences, University of the Witwatersrand, Johannesburg, 7 York Road, Parktown, 2193, South Africa

ARTICLE INFO

Article history:
Received 29 November 2016
Received in revised form 17 January 2017
Accepted 19 January 2017
Available online 31 January 2017

Keywords:
Pseudo-bone thermo-gel
Controlled drug release
Thermo-responsive
Bone fractures

ABSTRACT

A pseudo-bone thermo-gel was synthesized and evaluated for its physicochemical, mechanical and rheological properties, with its application to treat small bone fractures. The pseudo-bone thermo-gel was proven to have thermo-responsive properties, behaving as a solution in temperatures below 25 °C, and forming a gelling technology when maintained at physiological conditions. Poly propylene fumerate (PPF), Pluronic F127 and PEG-PCL-PEG were strategically blended, obtaining a thermo-responsive delivery system, to mimic the mechanical properties of bone with sufficient matrix hardness and resilience. A Biopharmaceutics Classification System (BCS) class II drug, simvastatin, was loaded in the pseudo-bone thermo-gel, selected for its bone healing properties. *In vitro* release analysis was undertaken on a series of experimental formulations, with the ideal formulations obtaining its maximum controlled drug release profile up to 14 days. *Ex vivo* studies were undertaken on an induced 4 mm diameter butterfly-fractured osteoporotic human clavicle bone samples. X-ray, ultrasound as well as textural analysis, undertaken on the fractured bones before and after treatment displayed significant bone filling, matrix hardening and matrix resilience properties. These characteristics of the pseudo-bone thermo-gel thus proved significant potential for application in small bone fractures.

© 2017 Elsevier B.V. All rights reserved.

1. Introduction

Approximately 2.2 million bone graft surgeries are conducted globally each year. As a result, surgeons are faced with multiple clinical challenges in bone reconstruction. Some of these challenges are defect sizes, anatomic sites, mechanical stresses and available soft tissue cover (Tanga et al., 2016). The gold standard for repairing skeletal defects is autologous bone grafting, however, this method has many disadvantages which include bone graft loss, problems relating to the surgical site, short-term instability in massive defects and autograft failure rates which is greater than 50% in complicated healing environments (Bosco et al., 2016). Due to these shortcomings, the utilization of synthetic implants is becoming increasingly popular. Nevertheless, present day biomaterials were initially fabricated for other engineering approaches, as a result, there may be many limitations such as a foreign-body reaction, infection, as well as extrusion of the implanted biomaterial (Iwase et al., 2016).

Recently, the development of injectable polymeric hydrogels and thermo-gels for the treatment of bone defects are gaining much research popularity. These systems are composed of various polymers that have specific properties that will heal the defected bone and support bone regeneration (Zhao et al., 2016; LogithKumar et al., 2016). To date, injectable thermo-gels in the field of bone tissue engineering has provided numerous advantages over former approaches. Injectable therapy has an unparalleled benefit in which complex defected areas can be effortlessly targeted without invasive methods. It can also increase the physico-mechanical properties of the damaged bone by delivering many drug molecules as well as growth factors to the site of injury (Farokhi et al., 2016).

Due to the thermo-gel possessing water based homogenous properties, it displays a remarkable platform for bone tissue engineering. It has the ability to encapsulate, manipulate and transfer its constituents to the surrounding tissue. Polymeric thermo-gels, loaded with a statin drug, has been known to increase bone repair. The polymeric gel further provides mechanical support at the site of bone injury (Nayef et al., 2016). A thermo-responsive injectable system behaves as a transitional sol-gel

* Corresponding author.
E-mail address: viness.pillay@wits.ac.za (V. Pillay).

http://dx.doi.org/10.1016/j.ijpharm.2017.01.039
0378-5173/© 2017 Elsevier B.V. All rights reserved.

7.4 5th Nano Today Conference, Waikoloa Beach Marriott, Hawaii, USA, December 6th-10th, 2017. Poster presentation.

Development of an injectable tissue engineered thermo-gel drug delivery system for application in small bone fractures

Pariksha J. Kondiah[1], Yahya E. Choonara[1], Pierre P. D. Kondiah[1], Thashree Marimuthu[1], Lisa C. du Toit[1], Pradeep Kumar[1] and Viness Pillay[1]*

[1]Wits Advanced Drug Delivery Platform Research Unit, Department of Pharmacy and Pharmacology, School of Therapeutic Sciences, Faculty of Health Sciences, University of the Witwatersrand, Johannesburg, 7 York Road, Parktown, 2193, South Africa

Introduction:
A pseudo-bone thermo-gel was synthesized and evaluated for its physicochemical, mechanical and rheological properties, with its application to treat small bone fractures. The pseudo-bone thermo-gel was proven to have thermo-responsive properties, behaving as a solution in temperatures below 25°C, and forming a gelling technology when maintained at physiological conditions. Strategic copolymers were designed to mimic the mechanical properties of bone with sufficient matrix hardness and resilience. A Biopharmaceutics Classification System (BCS) class II drug, simvastatin, was loaded in the pseudo-bone thermo-gel, selected for its bone healing properties.

Methods:
Free radical polymerization was undertaken to synthesize the copolymeric injectable delivery system, employing various chemical, rheological and mechanical evaluation on the thermo-gel. FTIR, visco-elastic evaluation, *in vitro* release and human bone *ex vivo* studies were undertaken to determine the characteristic nature of the thermo-gel.

Results:
In vitro release analysis was undertaken on a series of experimental formulations, with the ideal formulations obtaining its maximum controlled drug release profile up to 14 days. *Ex vivo* studies were undertaken on an induced 4mm diameter butterfly-fractured osteoporotic human clavicle bone samples. X-ray, ultrasound as well as textural analysis, undertaken on the fractured bones before and after treatment displayed significant bone filling, matrix hardening and matrix resilience properties.

Discussion:
These characteristics of the pseudo-bone thermo-gel thus proved significant potential for application in small bone fractures. Results displayed significant bone filling, matrix hardening and matrix resilience properties, similar to the original density of the bone. It can thus be concluded that the developed pseudo-bone thermo-gel has significant potential for *in vivo* evaluation, with promising therapeutic benefits for treating small bone fractures.

7.5 7th International Conference on Mechanics of Biomaterials and Tissues, Waikoloa Hawaii, USA, 10-14th December 2017. Oral presentation.

Design and evaluation of a 3D bioprinted implantable drug delivery scaffold for application in bone tissue engineering

Pariksha J. Kondiah[1], Yahya E. Choonara[1], Pierre P. D. Kondiah[1], Thashree Marimuthu[1], Lisa C. du Toit[1], Pradeep Kumar[1] and Viness Pillay[1]*

[1]Wits Advanced Drug Delivery Platform Research Unit, Department of Pharmacy and Pharmacology, School of Therapeutic Sciences, Faculty of Health Sciences, University of the Witwatersrand, Johannesburg, 7 York Road, Parktown, 2193, South Africa

Introduction:
A 3D bioprinted nano-particulate drug delivery scaffold was synthesised and optimized as a thermo-responsive implantable technology, possessing similar matrix hardness and resilience properties as healthy bone tissue, once incorporated in situ. The 3D bioprinted scaffold was developed using computer aided design (CAD) software, with further optimization of the designed formulations, employing MATLAB® programing and artificial neural networks.

Methods:
3D bioprinting was undertaken to design an implantable drug delivery scaffold for controlled release of loaded drug. Morphological, artificial neural network studies, in vitro release and optimization studies were undertaken on the implantable scaffold. The prepared formulations were synthesised and polymerically blended to obtain a stimuli-responsive implant. TGA was also undertaken to determine the degree of thermodegradation in the implantable system. Biomaterial testing was employed using a BioTester 5000 Cell scale system, evaluating the tensile strength and viscoelastic nature of the implant.

Results:
The designed scaffold displayed significant bone filling and matrix hardening properties. The 3D bioprinted scaffold demonstrated remarkable properties as a controlled release platform, biodegrading gradually over 20 days and releasing its loaded contents in a sustained manner, allowing contact adhesion between fractured/damaged bone and formation of artificial bone matrix within these sites. SEM analysis confirmed the programmed architecture of the scaffold, with precise pore dimensions for cell biocompatibility.

Discussion:
It was confirmed that the 3D bioprinted drug delivery scaffold has great potential for application in bone fractures, due to its physicochemical and phsicomechanical properties. In vitro release further confirmed gradual biodegradation of the scaffold, with ideal bone matrix hardness and resilience to healthy bone tissue. The elastic nature of the scaffold displayed promising properties for resistance of internal stresses that can be experienced in situ, once implanted. It can thus be confirmed that 3D Bioprinting has significant value in advanced biomaterial design, with optimum properties for site specific controlled drug delivery.